An Investigation of the Air-Side Forced Convection Heat Transfer from Saw-Tooth Shaped, Multi-Layer, Wire-On-Tube Condensers

J. M. S. Lum and A. M. Clausing

ACRC TR-127 August 1997

For additional information:

Air Conditioning and Refrigeration Center
University of Illinois
Mechanical & Industrial Engineering Dept.
1206 West Green Street
Urbana, IL 61801

(217) 333-3115

Prepared as part of ACRC Project 67
Optimization of the Performance of Wire and Tube Condensers
A. M. Clausing, Principal Investigator

The Air Conditioning and Refrigeration Center was founded in 1988 with a grant from the estate of Richard W. Kritzer, the founder of Peerless of America Inc. A State of Illinois Technology Challenge Grant helped build the laboratory facilities. The ACRC receives continuing support from the Richard W. Kritzer Endowment and the National Science Foundation. The following organizations have also become sponsors of the Center.

Amana Refrigeration, Inc.
Brazeway, Inc.
Carrier Corporation
Caterpillar, Inc.
Copeland Corporation
Dayton Thermal Products
Delphi Harrison Thermal Systems
Eaton Corporation
Ford Motor Company
Frigidaire Company
General Electric Company
Hydro Aluminum Adrian, Inc.
Indiana Tube Corporation
Lennox International, Inc.
Modine Manufacturing Co.
Peerless of America, Inc.
Redwood Microsystems, Inc.
The Trane Company
Whirlpool Corporation
York International, Inc.

For additional information:

Air Conditioning & Refrigeration Center
Mechanical & Industrial Engineering Dept.
University of Illinois
1206 West Green Street
Urbana IL 61801

217 333 3115

AN INVESTIGATION OF THE AIR-SIDE FORCED CONVECTION HEAT TRANSFER FROM SAW-TOOTH SHAPED, MULTI-LAYER, WIRE-ON-TUBE CONDENSERS

James Marn Sung Lum, M.S.
Department of Mechanical and Industrial Engineering
University of Illinois at Urbana-Champaign, 1997
Arthur M. Clausing, Advisor

ABSTRACT

This investigation focuses on determining the relative air-side heat transfer performance of several wire-on-tube condensers with multiple layers at high angles-of-attack with respect to a forced air flow. During each experiment, a wind tunnel containing a variable height test section was used to draw air, with free stream velocities ranging from 0.2 m/s to 2.0 m/s (0.66 ft/s to 6.56 ft/s), through the wire and tube matrix of a multi-layer condenser. The total heat transfer rate from each condenser layer was determined by performing an overall energy balance on the fluid (water for purposes of this study) flowing through the serpentine tube of the condenser. The contribution of radiation to the overall heat transfer rate was estimated and accounted for, as were the influences of the fin efficiency of the condenser wires and the thermal constriction resistance resulting from heat flow to locations on the tube surface at which wires are welded. Over the course of the study, influences of the free stream air velocity, condenser angle-of-attack ($45° \leq \alpha \leq 90°$), condenser orientation ($\psi = 0$ for air flow normal to the wires of the condenser and $\psi = \pi/2$ for air flow normal to the serpentine tube), and geometric differences between condensers ($D_w \equiv$ wire diameter, $S_w \equiv$ wire spacing, $S_t \equiv$ tube spacing, and $S_L \equiv$ layer spacing) on the air-side convection heat transfer performance were examined. In addition, alternative condenser designs such as (i) staggered-wire condenser layers, (ii) one-sided condenser layers, and (iii) staggered-tube condensers were also studied.

TABLE OF CONTENTS

TABLE OF CONTENTS (cont.)

LIST OF TABLES

LIST OF TABLES (cont.)

LIST OF FIGURES

LIST OF FIGURES (cont.)

LIST OF FIGURES (cont.)

NOMENCLATURE (cont.)

t	tube
tot	total
w	wire
wbase	wire base
1, 2, ...	condenser layer number

NOMENCLATURE

Roman Symbols (Dimensional Parameters)

A	surface area [m^2]
c_p	constant pressure specific heat [J/kg•K]
D	diameter [m]
g	gravitational acceleration [9.81 m/s^2]
h	convection heat transfer coefficient [W/m^2•K]
$\bar{h}$	average convection heat transfer coefficient [W/m^2•K]
k	thermal conductivity [W/m•K]
L	length [m]
$\dot{m}$	mass flow rate [kg/s]
N	number (i.e. quantity)
Q	energy transfer [J]
q	heat transfer rate [W]
R	thermal resistance [K/W]
S	centerline-to-centerline spacing [m]
T	temperature [K]
V	velocity [m/s]

Roman Symbols (Dimensionless Parameters)

C_D	drag coefficient, $\Delta p/(^1/_2 \bullet \rho \bullet V^2)$
D_t^*	dimensionless tube diameter, D_t/D_w
f	friction factor
Gr	Grashof number, $g \bullet \beta \bullet (T_w - T_a) \bullet D^3/\nu^2$
L_t^*	dimensionless tube length, L_t/D_w
L_w^*	dimensionless wire length, L_w/D_w
m	fin parameter, $(h \bullet S_t^2/k \bullet D_w)^{1/2}$
Nu	Nusselt number, $h \bullet D/k$
Pr	Prandtl number, $\nu \bullet \rho \bullet c_p/k$
Ra	Rayleigh number, $Gr \bullet Pr$
Ri	Richardson number, Gr/Re^2
Re	Reynolds number, $V \bullet D/\nu$
S_t^*	dimensionless centerline-to-centerline tube spacing, S_t/D_w
S_w^*	dimensionless centerline-to-centerline wire spacing, S_w/D_w

NOMENCLATURE (cont.)

Greek Symbols

α	angle-of-attack measured from a horizontal datum [deg]
β	volumetric coefficient of expansion [K^{-1}]
Δ	difference
δ	thickness [m]
ε	total, hemispherical emissivity
η	fin efficiency
ν	kinematic viscosity [m^2/s]
ρ	density [kg/m^3]
σ	Stefan-Boltzmann constant [5.67×10^{-8} $W/m^2 \cdot K^4$]
ψ	yaw angle [rad] where $\psi = 0$: air flow $\perp$ to wires $\psi = \pi/2$: air flow $\perp$ to tubes

Subscripts

a	air
$\alpha = 0°$	horizontally oriented
$\alpha = 90°$	vertically oriented
amb	ambient condition
bare	beneath the paint
char	characteristic
conv	convection heat transfer
cond	conduction heat transfer
eff	effective
i	inner surface
in	inlet
int	associated with the convection heat transfer within the condenser tube
max	maximum
meas	measured quantity
out	outlet
p	paint
r	refrigerant (water)
rad	radiation heat transfer
surr	surrounding

1. INTRODUCTION

Wire-on-tube condensers are typically used to dissipate the energy, in the form of heat, removed from both the freezer and fresh food compartments of household refrigerators. Although some condensers are designed to be cooled by natural convection, the condensers found in most modern refrigerators are subjected to forced air flows which are drawn over the condensers by fans.

As their name suggests, wire-on-tube condensers are made up of steel tubing and wires. They are fabricated by first bending the tubing into parallel passes, thereby forming a planar serpentine. Wires are then spot welded to each side of the serpentine such that they are perpendicular to the tube passes of the serpentine. These wires act as extended surfaces, or fins, for the condenser, providing secondary surfaces through which additional energy can be transferred to the surroundings from the refrigerant flowing within the serpentine. After the wires and tubing are assembled together, black paint is applied to the outer surfaces of the condenser. This prevents rust from forming on the condenser and also increases the emissivity, ε, of its outer surfaces, allowing the condenser to discharge a greater amount of energy through radiation heat transfer with its surroundings.

The overall effectiveness of a wire-on-tube condenser (or any heat exchanger) is determined primarily by the rate at which it can transfer energy from the refrigerant flowing within it to its environment. This heat transfer rate is governed by the temperatures of both the refrigerant, T_r, and the condenser's environment, T_a (for purposes of convection heat transfer) and T_{surr} (for purposes of radiation heat transfer), each of which may be difficult to adjust, in addition to the thermal resistance which obstructs heat flow between the refrigerant and the condenser's environment.

The thermal resistance between the refrigerant and the environment of the condenser can be divided into several smaller resistances, the largest of which is the external, or "air-side", resistance which obstructs heat flow from the outer surfaces of the condenser to the surrounding air. In a previous study performed by Admiraal and Bullard (1993) the air-side thermal resistance of a refrigerator wire-on-tube condenser was shown to account for over 95% of the total resistance in the portion of the condenser containing two-phase refrigerant. In addition, this resistance contribution also ranged from 42% to 63% and from 55% to 75% of the total resistance for the subcooled and superheated regions, respectively.

Since the air-side thermal resistance accounts for such an overwhelming portion of the total resistance, it is obvious that the performance of a wire-on-tube condenser can most readily be increased by decreasing the resistance between the outer surfaces of the condenser and the surrounding air. This can be accomplished by increasing either the outer surface area of the

condenser (A_w and/or A_t) or the air-side convection heat transfer coefficient associated with the condenser, h. The size and, as a result, surface area of the condenser is often dictated by economic and spatial limitations. In light of this fact, the current study focuses on increasing the relative heat transfer performance of wire-on-tube condensers through increasing the air-side convection heat transfer coefficients associated with the condensers.

Wire-on-tube condensers cooled by forced convection are usually located in the lower portions of refrigerators (beneath the fresh food compartments), where they are almost always suspended horizontally within horizontal air flows, as shown in Fig. 1.1a. However, experimental results from Hoke (1995) and Swofford (1995) clearly indicate that the air-side convection heat transfer coefficient of a wire-on-tube condenser is significantly increased as the angle-of-attack between the plane of the condenser and an air flow is increased. Data obtained from condensers tested at $\alpha = 0°$ and $\alpha = 90°$ show that the convection heat transfer performance of a condenser is increased by at least 160% when α is increased from 0° to 90°. As a result, it would appear that a wire-on-tube condenser's performance would be greatly enhanced if it (or parts of it) were oriented nearly perpendicular to the air flow in which it is placed. Due to the dimensional restrictions which are associated with a refrigerator, a wire-on-tube condenser of this type might take the form of that shown in Fig. 1.1b, where the condenser has been folded up into a saw-tooth shaped multi-layer configuration and placed at the rear of the refrigerator next to the compressor.

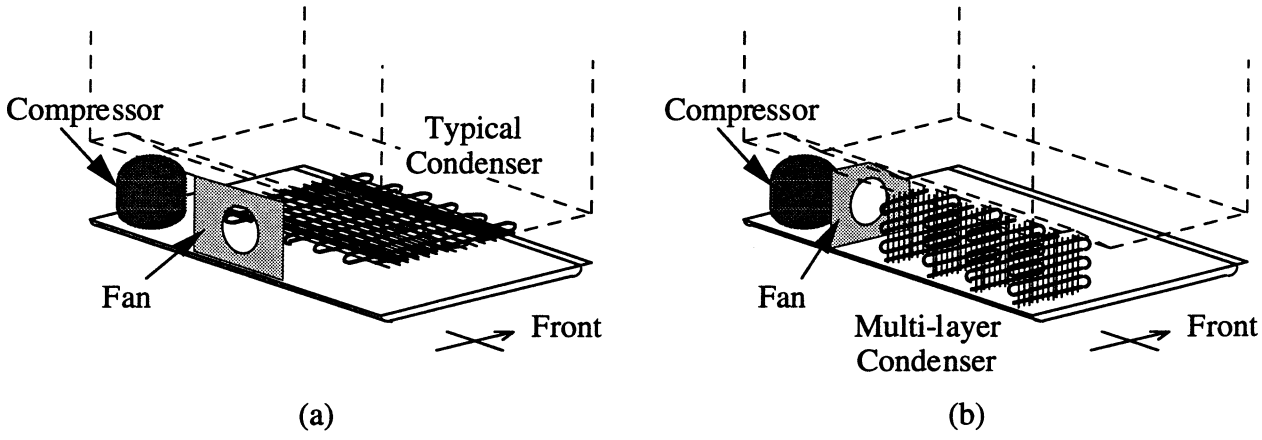

Figure 1.1 Lower portions of refrigerators with (a) a typical condenser and (b) a multi-layer condenser

This investigation attempts to not only quantify the relative air-side heat transfer performance of wire-on-tube condensers at high angles-of-attack with respect to a forced air flow, but also to determine the interaction between multiple condenser layers placed in close proximity of one another as shown in Fig. 1.1b. Influential parameters such as the free stream

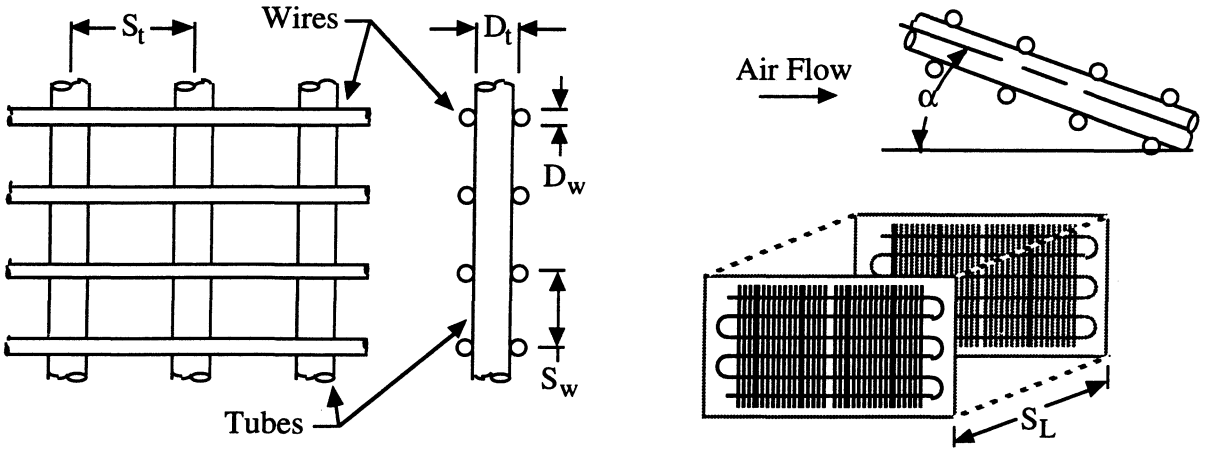

Figure 1.2 Nomenclature definitions for several of the parameters studied

air velocity (V), condenser angle-of-attack (α), condenser orientation (ψ), and condenser geometry (i.e. $D_w \equiv$ wire diameter, $S_w \equiv$ wire spacing, $S_t \equiv$ tube spacing, and $S_L \equiv$ layer spacing) are each considered when examining performance. The definitions of several of these parameters are shown in Fig. 1.2. In addition, the effect of the relative locations of certain geometric elements within a particular multi-layer wire-on-tube condenser has also been studied. In doing so, alternative condenser designs such as (i) staggered-wire condenser layers, (ii) one-sided condenser layers, and (iii) staggered-tube condensers were developed and tested.

Due to the nature of the investigation, condenser coils possessing large gaps in their wire mats, as shown in Fig. 1.3, were assumed to be unsuitable for testing. As a result, only four different wire-on-tube condensers obtained from two manufacturers were tested during this

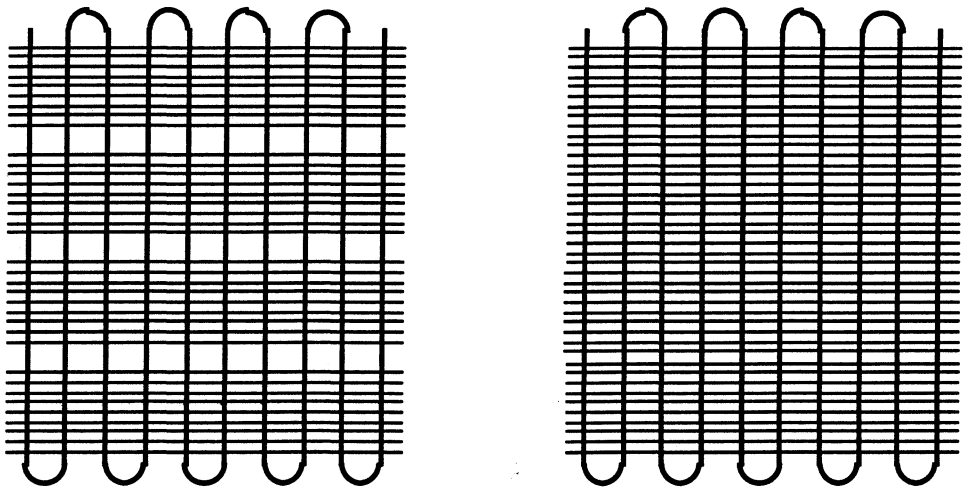

Figure 1.3 Condenser coil suitability based on the presence of large wire gaps

investigation. In most instances only one of the three major geometric parameters (i.e. D_w, S_w, and S_t) was varied between condenser coils. This allowed the effect of each geometric parameter to be studied individually, while also giving some variation between condensers, thereby increasing the utility of the results.

2. LITERATURE REVIEW

To date, only a few studies pertaining to wire-on-tube condensers have been performed. Of these, an overwhelming majority involve the testing and analysis of wire-on-tube condensers cooled by natural convection and radiation. Since most modern refrigerator condensers are now exposed to forced convection air flows generated by fans, the applicability of much of the previous research is extremely limited.

Research involving wire-on-tube condensers first appeared in publication as a series of M.S. Theses by Rudy (1956), Howard (1956), and Carley (1956). Working concurrently, each of the authors focused on determining the influence of a single (or in the case of Rudy, two) geometric parameter(s) on the heat transfer performance of wire-on-tube condensers subjected to natural convection and radiation.

Experiments performed by Rudy focused on studying the effects of D_w and S_w on the heat transfer rate from wire-on-tube condensers tested in horizontal ($\alpha = 0°$) and vertical ($\alpha = 90°$) orientations. Plots appearing in his thesis clearly indicate that the air-side thermal resistance ($R_a = {}^1/_{hA}$) decreases with increasing D_w and decreasing S_w when the condenser is subjected to both natural convection and radiation. Unfortunately, since Rudy was unable to determine an effective outer surface area for each of the condensers tested, the air-side convection heat transfer coefficients associated with the data that he obtained could not be estimated.

Howard's experiments focused on determining the effect of S_t on the heat transfer rate from wire-on-tube condensers tested in a horizontal position. As shown by the data presented for condensers with two different S_w, the heat transfer rate per tube pass increases with increasing S_t when the condenser is exposed to natural convection and radiation. As in the case of Rudy, Howard was also unable to determine an effective outer surface area for each condenser. As a result, the air-side convection heat transfer coefficients associated with Howard's data were also left undetermined.

The effect of D_t on the heat transfer rate from horizontally oriented wire-on-tube condensers subjected to natural convection and radiation was the focus of Carley's experiments. His results indicate that the air-side thermal resistance decreases with increasing D_t. Unlike Rudy and Howard, Carley attempted to determine the air-side convection heat transfer coefficients associated with the condensers that he tested. Assuming an effective outer surface area of $(A_t + \eta_w A_w)$, he found that the air-side convection heat transfer coefficients (assuming $h = h_t = h_w$) associated with the wire-on-tube condensers decrease with increasing D_t.

Data obtained from the three previous sources were referenced by Witzell and Fontaine (1957a) in a journal article correlating the effects of the geometry of horizontally oriented wire-

on-tube condensers on heat transfer (natural convection only) performance. Since the Prandtl numbers, Pr, associated with the data examined were nearly constant, Witzell and Fontaine found that the heat transfer performance of horizontally oriented wire-on-tube condensers cooled by natural convection are governed by

$$Nu = 0.4724\ Gr^{0.2215} \tag{2.1}$$

where the characteristic dimension used in determining the Nusselt and Grashof numbers, Nu and Gr, are based on the area-weighted average of the condenser tube and wire diameters, D_{char}, as follows:

$$D_{char} = \frac{A_t D_t + A_w D_w}{A_t + A_w} \tag{2.2}$$

Witzell and Fontaine (1957b) detailed the use of their correlation as a design tool for wire-on-tube condensers which are exposed to natural convection and radiation. Due to the experimental origin of the correlation, Witzell and Fontaine warn that extrapolation from the following geometric limitations may produce questionable results:

1. Only horizontally oriented wire-on-tube condensers may be considered.
2. The outer dimensions of the condenser should be 610 mm x 914 mm (24 in x 36 in) with the larger dimension along the length of the wires.
3. $0.88\ mm \le D_w \le 2.32\ mm$ $(0.0348\ in \le D_w \le 0.0915\ in)$
   $4.23\ mm \le S_w \le 25.4\ mm$ $(0.167\ in \le S_w \le 1\ in)$
   $4.76\ mm \le D_t \le 15.9\ mm$ $(0.188\ in \le D_t \le 0.625\ in)$
   $25.4\ mm \le S_t \le 102\ mm$ $(1\ in \le S_t \le 4\ in)$

Papanek (1958) presented data in the form of an M.S. Thesis detailing the effect of α (measured from a horizontal datum) on the convection heat transfer coefficients associated with wire-on-tube condensers subjected to both natural convection and radiation. During each experiment, the wires of the condenser were kept in a horizontal orientation while the tube passes were rotated to various angles ($\psi = 0$). Studying condensers with four different S_w, Papanek found (i) that h (assuming $h = h_t = h_w$ and $A_{eff} = A_t + \eta_w A_w$) for natural convection decreases with increasing α and (ii) that the angular dependence of h increases as S_w decreases.

As in the case of Witzell and Fontaine (1957a), Papanek also attempted to correlate the effects of wire-on-tube condenser geometry on heat transfer (natural convection only) performance. Using the characteristic dimension defined by Eq. (2.2), he determined that the Nusselt-Grashof relations for wire-on-tube condensers subjected to natural convection are

$$(Nu)_{\alpha=0^\circ} = 0.2714\,Gr^{0.307} \qquad (Nu)_{\alpha=90^\circ} = 0.0188\,Gr^{0.7556} \qquad (2.3a\ \&\ b)$$

where the subscripts $\alpha = 0°$ and $\alpha = 90°$ correspond to condensers placed in horizontal and vertical orientations, respectively.

Witzell, Fontaine, and Papanek (1959) recorrelated the data presented in the previous source by assuming a characteristic dimension of

$$D_{char}^{-1/4} = \frac{A_t D_t^{-1/4} + \eta_w A_w D_w^{-1/4}}{A_t + A_w} \qquad (2.4)$$

Using this new characteristic dimension, the Nusselt-Grashof correlations for wire-on-tube condensers subjected to natural convection were recalculated to be

$$(Nu)_{\alpha=0^\circ} = 0.905\,Gr^{0.176}\left[\frac{S_w - D_w}{S_w}\right]^{1.2} \qquad (Nu)_{\alpha=90^\circ} = 0.034\,Gr^{0.726} \qquad (2.5a\ \&\ b)$$

where the subscripts $\alpha = 0°$ and $\alpha = 90°$ again correspond to condensers placed in horizontal and vertical orientations, respectively.

A study performed by Cyphers, Cess, and Somers (1959) also attempted to quantify the effect of α (also measured from a horizontal datum) on the convection heat transfer coefficients associated with wire-on-tube condensers subjected to both natural convection and radiation. Both the case where the wires of the condenser were kept horizontal while the tube passes were rotated ($\psi = 0$) and the case where the wires were rotated while the condenser tube passes were kept horizontal ($\psi = \pi/2$) were examined. Defining an average convection heat transfer coefficient, $\bar{h}$, as

$$q = \bar{h}\left(A_t + A_w\right)\left(\bar{T}_t - T_a\right) \qquad (2.6)$$

where $\bar{T}_t$ is the average outer surface temperature of the condenser tube passes, $\bar{h}$ for natural convection was found to decrease with increasing α for both the $\psi = 0$ and $\psi = \pi/2$ cases.

The data obtained from the $\psi = \pi/2$ case were also used to estimate the convection heat transfer coefficients associated with the condenser wires, h_w, for $0° \le \alpha \le 90°$. Using the relation

$$\bar{h} = h_t \frac{A_t}{A_t + A_w} + h_w \frac{A_w}{A_t + A_w} - h_{rad} \qquad (2.7)$$

where h_{rad} is the average radiation heat transfer coefficient, Cyphers, Cess, and Somers calculated h_w as a function of α and compared the results to the theoretically determined heat

transfer coefficients for natural convection heat transfer from an infinite yawed cylinder. As shown by this comparison, the estimated h_w are approximately equal to the h_w determined using the theoretical Nusselt-Grashof relation

$$Nu = \frac{2}{\ln\left[1 + 5\left(Gr \cos\alpha\right)^{-1/4}\right]} \tag{2.8}$$

for the entire range of α.

In addition to determining the dependence of $\bar{h}$ on α, Cyphers, Cess, and Somers performed experiments to determine the effect of the presence of confining walls on the $\bar{h}$ associated with wire-on-tube condensers subjected to both natural convection and radiation. During each of these experiments, a pair of vertical walls were positioned with each on either side of the condenser. The distance between the walls was varied during the investigation, while the condenser was kept either in a vertical position or tilted (i.e. α was varied) such that the edges of the condenser were in contact with the confining walls. In general, the data indicate that $\bar{h}$ decreases as the spacing between the walls decreases for both of the conditions where the condenser was kept vertical and when it was angled with respect to the walls.

Collicott, Fontaine, and Witzell (1963) presented the results of a study aimed at determining the effective radiation view factors associated with wire-on-tube condensers. In the study, several wire-on-tube condensers were tested in an evacuated chamber ($p \leq 10^{-3}$ mm Hg) in an effort to eliminate the contribution of convection to the overall heat transfer rates. By defining an effective radiation view factor, F_{eff}, as

$$q_{rad} = F_{eff}\, \varepsilon_{eff}\, \sigma \left(A_t + A_w\right)\left(\bar{T}_t - T_{surr}\right) \tag{2.9}$$

where q_{rad} is the radiation heat transfer rate from a condenser, ε_{eff} is an effective emissivity, and T_{surr} is the temperature of the environment, Collicott, Fontaine, and Witzell were able to determine the F_{eff} associated with wire-on-tube condensers as a function of the ratios D_t/S_t and D_w/S_w. In general, F_{eff} appears to decrease with increasing values of D_w/S_w. A similar conclusion can not be drawn between F_{eff} and D_t/S_t.

Collicott, Fontaine, and Witzell recognized the fact that their experimentally determined F_{eff} were not actual view factors. That is, the F_{eff} that they determined were dependent on the temperature distribution within the condenser wires in addition to the geometry of the wire-on-tube condenser. As a result, they stress that the reported F_{eff} should ideally be used under conditions which yield temperature distributions similar to those experienced by the specimens that were tested in the evacuated chamber (i.e. conditions involving very little convection heat transfer). Conditions under which the fin efficiencies of the condenser wires, η_w, are low should

result in temperature distributions which are extremely dissimilar to those of the test conditions, artificially causing F_{eff} to overestimate the actual radiation view factor. Collicott, Fontaine, and Witzell also point out, however, that in cases where the increased heat transfer rate resulting from natural convection does not drastically alter the temperature distribution within the wires of the condenser (i.e. $\eta_w \sim 1.0$), the application of the experimentally determined F_{eff} to conditions involving both natural convection and radiation should provide satisfactory results.

Collicott, Fontaine, and Witzell used the experimentally determined values of F_{eff} to approximate and remove q_{rad} from the overall heat transfer rate from several wire-on-tube condensers at various α subjected to both natural convection and radiation. Nusselt numbers were then calculated from these values of q_{conv} using both Eq. (2.2) and (2.6), and compared to the theoretical Nu for isothermal horizontal cylinders (cooled by natural convection) with identical D_{char} given by the equation

$$Nu = 0.11\,(Gr\,Pr)^{1/3} + (Gr\,Pr)^{0.1} \tag{2.10}$$

As shown in the plots presented, the ratio of the Nu of a wire-on-tube condenser to that of an isothermal horizontal cylinder with identical D_{char} increases (to a maximum of 1.0) with increasing values of D_t/S_t and decreases with increasing α.

The first known studies involving wire-on-tube condensers exposed to forced convection and radiation were published by Hoke (1995) and Swofford (1995) in the form of a pair of M.S. Theses, which were later reprinted in a technical report by Hoke, Swofford, and Clausing (1995). Their investigations focused on determining how the relative convection heat transfer performance of several wire-on-tube condensers vary as a function of (i) the free stream velocity of the forced convection flows to which the condensers are exposed, (ii) the α of the condensers for both the $\psi = 0$ (where $|\alpha| \leq 20°$) and $\psi = \pi/2$ (where $|\alpha| \leq 40°$) cases, and (iii) the variation in the wire and tube geometry (D_w, S_w, D_t, and S_t).

Hoke and Swofford performed their experiments in a wind tunnel (see Chapter 3 - Experimental Apparatus & Instrumentation) capable of attaining free stream air velocities of up to 2.0 m/s (6.56 ft/s). The dimensions of the wind tunnel test section were chosen to be 305 mm (12 in) high and 914 mm (36 in) wide in order to allow the wire-on-tube condensers to be rotated at the various α necessary for their experiments. Both Hoke and Swofford acknowledge that the dimensions of the test section used are in no way similar to those available in a household refrigerator and, as such, may have resulted in slight discrepancies between the data obtained from their experiments and the convection heat transfer performance of a wire-on-tube condenser placed in an actual refrigerator. In addition, the condensers tested in the wind tunnel were subjected to velocity profiles which were spatially uniform over the cross-sectional face of the

wind tunnel test section. Since it is known that the wire-on-tube condensers in actual refrigerators experience highly non-uniform air flows, additional discrepancies may also have been introduced in this manner. It is important to note, however, that although their results may not exactly predict the relative heat transfer performance of wire-on-tube condensers cooled within the tightly confined, highly non-uniform, forced convection air flows produced beneath refrigerators, the findings of Hoke and Swofford (i) present a close approximation of an actual wire-on-tube condenser's performance and (ii) allow the effects of V, α, ψ, and geometry on condenser heat transfer performance to be readily assessed.

The convection heat transfer coefficient associated with the wires of a wire-on-tube condenser, h_w, defined as

$$h_w = \frac{q_{conv}}{\left(\frac{A_t}{\sqrt{D_t^*}} + \eta_w A_w\right)\left(\overline{T}_t - T_a\right)} \tag{2.11}$$

where D_t^* is the dimensionless tube diameter ($D_t^* = {}^{Dt}/_{Dw}$), was used as a measure of each condenser's heat transfer performance. Since h_w is also used as a measure of performance in the current investigation, the development of a similar heat transfer coefficient definition will be presented in further detail in Chapter 4 - Data Reduction.

As expected, the h_w associated with wire-on-tube condensers were generally found to increase with increasing V and increasing α for both the $\psi = 0$ and $\psi = {}^{\pi}/_{2}$ cases. Exceptions to this conclusion, however, were observed in cases involving horizontal condensers exposed to air flows with free stream velocities below 0.5 m/s (1.64 ft/s). Under these conditions it is believed that the buoyancy forces interact with the inertial forces of the forced convection flow to produce h_w which are, in some cases, lower than those associated with wire-on-tube condensers exposed to only natural convection (V = 0) and radiation. Note that, in addition to finding a direct relationship between h_w and both V and α, the h_w for the $\psi = 0$ case were also found to be slightly higher than those of the $\psi = {}^{\pi}/_{2}$ case for most α.

The dependence of h_w on the actual wire and tube geometry of the condenser was determined by examining seven different wire-on-tube condensers obtained from four refrigerator manufacturers. These condensers were each subjected to the same set of forced convection tests for both the cases of $\psi = 0$ and $\psi = {}^{\pi}/_{2}$. The data obtained were then used in calculating Nu_w, which were later examined in detail. For the data involving $Re_w > 50$ and $2.8 \leq S_w^* \leq 4.4$, the Nusselt-Reynolds relation associated with wire-on-tube condensers was found to be

$$Nu_w = C\,Re_w^n \left[0.985 - 98.5 \exp\left(-2.32\, S_w^*\right)\right] \tag{2.12}$$

where S_w^* is the dimensionless wire spacing ($S_w^* = {}^{Sw}/_{Dw}$) and both C and n are constants determined from curve fits of the data. In the case of $\psi = 0$,

$$C = 0.274 - 0.247 \cos\left(|\alpha| - 4.87\right) \exp\left[-0.00234\,(\alpha + 0.902)^2\right] \tag{2.13a}$$

$$n = 0.585 - 0.249 \cos\left(|\alpha| + 20.0\right) \exp\left[-0.00441\,(\alpha + 1.66)^2\right] \tag{2.13b}$$

For the case of $\psi = {}^{\pi}/_{2}$,

$$C = 0.263 - 0.235 \cos(\alpha) \exp\left(-0.00289\,\alpha^2\right) \tag{2.14a}$$

$$n = 0.55 + 0.269 \cos(\alpha) \exp\left(-0.00597\,\alpha^2\right) \tag{2.14b}$$

In addition to examining the effects of V, α, ψ, and condenser geometry on the h_w associated with wire-on-tube condensers exposed to both forced convection and radiation, Hoke performed a series of experiments to determine (i) the forced convection heat transfer coefficients associated with a condenser without wires (i.e. an unpainted serpentine tube) at various α for both the $\psi = 0$ and $\psi = {}^{\pi}/_{2}$ cases and (ii) the effect of L_w on the h_w associated with wire-on-tube condensers exposed to forced convection and radiation at various α (for the $\psi = {}^{\pi}/_{2}$ case only). Careful examination of the data obtained from these tests reveal that, in general, (i) the h associated with a wireless condenser oriented at $\alpha > 20°$ and $\psi = {}^{\pi}/_{2}$ is approximately equal to that predicted for a cylinder in cross flow using correlations developed by Hilpert (1933) and Zhukauskas (1972) and (ii) the relative convection heat transfer performance of a wire-on-tube condenser oriented between $\alpha = -5°$ and $\alpha = 0°$ decreases with increasing length, L_w.

Swofford also performed additional experiments aimed at studying the effect of α on the h_w associated with a wire-on-tube condenser subjected to either natural or forced convection coupled with radiation. In each of these tests, Swofford used a small-sized wire-on-tube condenser with outer dimensions 283 mm x 279 mm (11.1 in x 11 in). This allowed the range of α tested to be increased such that $0° \le \alpha \le 90°$ for both the $\psi = 0$ and $\psi = {}^{\pi}/_{2}$ cases. Plots appearing in his thesis clearly show that (i) the h_w associated with a condenser exposed to natural convection and radiation decreases with increasing α for both the $\psi = 0$ and $\psi = {}^{\pi}/_{2}$ cases and (ii) the h_w associated with a condenser exposed to forced convection and radiation increases with increasing α for both the $\psi = 0$ and $\psi = {}^{\pi}/_{2}$ cases, reaching a maximum which is at least 250% that associated with a horizontal condenser at $\alpha = 90°$. Note that h_w for the $\psi = 0$ case was again

found to be slightly higher than that of the $\psi = \pi/2$ case for most α for a wire-on-tube condenser exposed to forced convection and radiation.

Hoke, Clausing, and Swofford (1997) summarized the major findings of Hoke (1995) and Swofford (1995) in a technical article focusing on the effects of V, α, ψ, and condenser geometry on the relative heat transfer performance associated with wire-on-tube condensers exposed to both forced convection and radiation. The development and utility of the definition of h_w is discussed as are general conclusions which can be drawn from the data. Hoke, Clausing, and Swofford highlight both the extremely strong dependence of h_w on α and the accuracy of Eq. (2.12), (2.13), and (2.14) in predicting h_w.

3. EXPERIMENTAL APPARATUS & INSTRUMENTATION

Much of the equipment used in this investigation was developed for use in the research conducted by Hoke (1995), Swofford (1995), and Rasmussen (1997). Previously used testing apparatus such as (i) an induced flow wind tunnel, (ii) a variable height wind tunnel test section, and (iii) a temperature regulated water circulation system were each utilized in the experiments of the current investigation. In addition, several multi-layer condenser support frames have since been constructed, and new instrumentation designed to acquire temperature data utilizing both absolute and differential thermopiles has been installed. Each of these, including the previously developed equipment, is discussed in detail in the following sections.

3.1 Wind Tunnel

The wind tunnel used to produce the forced air flows in which the wire-on-tube condensers of this investigation were tested was designed and built by Hoke (1995). Shown in Fig. 3.1, the wind tunnel consists of several sections, each of which performs a different and distinct function. During operation, air is pulled into the wind tunnel through an opening at the front of the flow conditioning section. The air then flows through the test section in which the condensers are mounted and exits through a duct at the rear of the flow exhaust section.

The flow conditioning section, shown in Fig. 3.2, acts as a sieve between the ambient air and the air to which the condenser mounted in the test section is exposed. As can be seen, air is

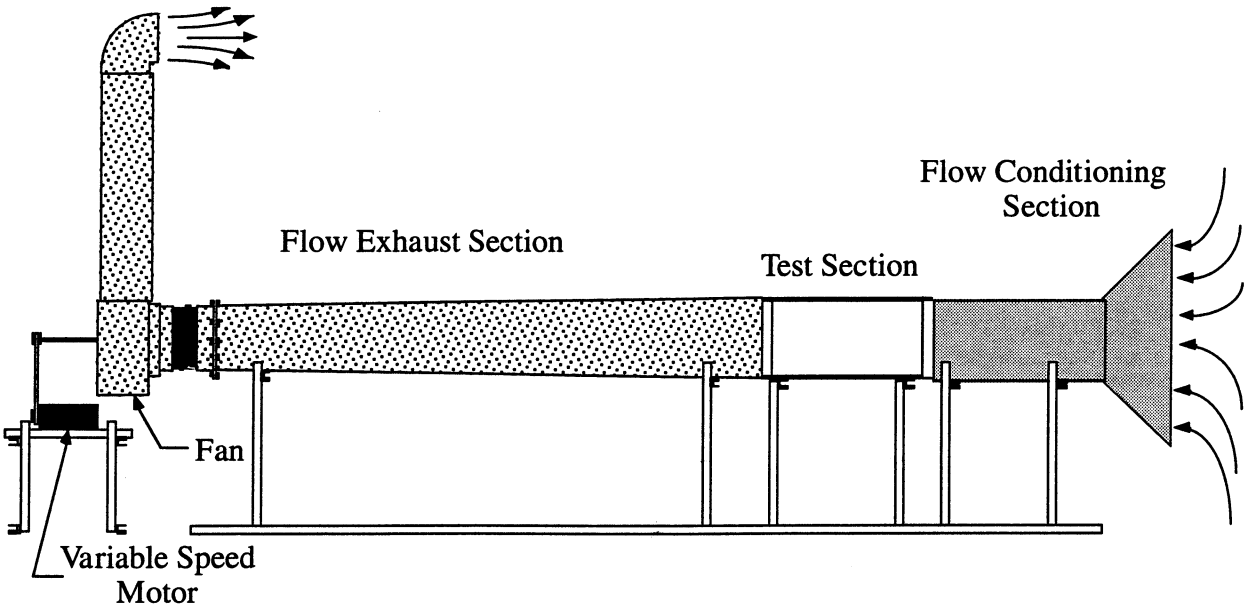

Figure 3.1 Wind tunnel used to induce an air flow over the condenser (Scale = 3:100)

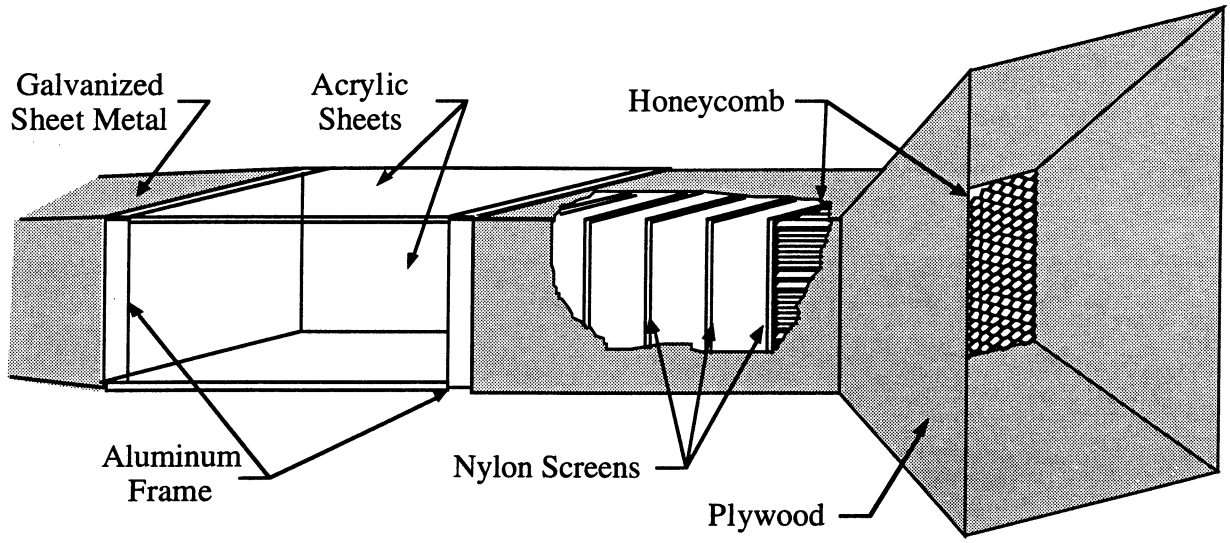

Figure 3.2 Cut-away view of the wind tunnel flow conditioning section (Scale = 64:1000)

first drawn into the plywood hull of the flow conditioning section through a 152 mm (6 in) long piece of aluminum, hexagonal core honeycomb. This causes the path of the air flow to straighten, reducing any turbulence and vortices (or swirls) which may have resulted from ambient instabilities. The air then flows through a series of five nylon screens, which helps to further reduce turbulence and produces a much more spatially uniform flow.

The test section, made from 12.7 mm (0.5 in) thick acrylic sheets supported by an aluminum frame, houses the test specimen (i.e. condenser) during each experiment. The internal dimensions of the test section are as follows: 305 mm (12 in) high, 914 mm (36 in) wide, and 762 mm (30 in) long. During operation, free stream air velocities of up to 2.0 m/s (6.56 ft/s) can be generated within the test section. Both the spatial uniformity over the entire cross-sectional face of the test section and the transient unsteadiness of the air flow produced have been estimated to be less than 2.5% of the free stream air velocity, using a TSI IFA 100 hot wire anemometer. In addition, the turbulence at V = 2.0 m/s (6.56 ft/s) has been measured to be less than 1%.

The flow exhaust section, which houses the fan, produces the driving potential for the air flow. Air enters the flow exhaust section through a 2.44 m (8 ft) long converging, rectangular-to-round, galvanized sheet metal duct. The air is then channeled from the circular exit of duct, measuring 254 mm (10 in) in diameter, into a 203 mm (8 in) long flexible piece before being pulled through a backward inclined centrifugal fan. The fan, powered by a 560 W ($^3/_4$ hp) variable speed DC motor, is ultimately responsible for producing the driving potential of the air flow. The air then exits from the wind tunnel via a series of rectangular and circular ducts leading from the fan casing.

3.2 Variable Height Wind Tunnel Test Section

In an effort to better simulate the tightly confined, forced convection air flow experienced by a condenser situated beneath a refrigerator fresh food compartment, a variable height test section was developed by Rasmussen (1997) for use in conjunction with the wind tunnel mentioned in Section 3.1 - Wind Tunnel. This variable height test section was designed to fit within the original 305 mm x 914 mm x 762 mm (12 in x 36 in x 30 in) wind tunnel test section and is made up of four individual panels.

The top and bottom panels each consist of a 6.35 mm (0.25 in) thick sheet of acrylic bonded to four slotted acrylic tabs and attached in a plane with a thin sheet of flexible polycarbonate. When used to assemble the variable height test section, the slotted acrylic tabs of the top and bottom panels are bolted to both side panels (also made of acrylic), forming a rectangular-shaped duct. The far edges of the polycarbonate sheets of the top and bottom panels are then gently bent and locked down into position such that they are flush against the top and bottom corners of the acrylic side panels. The assembled variable height test section appears much like that shown in Fig. 3.3.

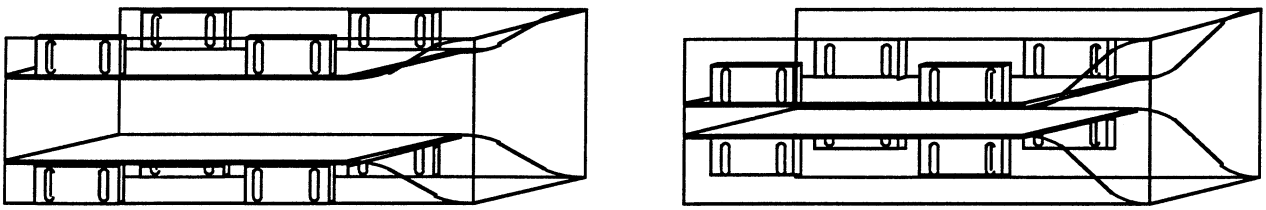

(a) (b)

Figure 3.3 Variable height wind tunnel test section set at (a) maximum height and (b) minimum height (Scale = 72:1000)

During testing, the variable height test section is situated within the original wind tunnel test section with its side nearest to the polycarbonate sheets facing the flow conditioning section of the wind tunnel (see Section 3.1 - Wind Tunnel). Foam and acrylic barriers are used to block regions of the test and flow conditioning sections of the wind tunnel which extend beyond the width of the variable height test section. The use of barriers accounts for the difference in width between the inside of the wind tunnel and that of the variable height test section and forces the air flow generated by the wind tunnel to pass entirely through the variable height test section.

As it enters the variable height test section, air is channeled through the path formed by the polycarbonate sheets. The curved form of the polycarbonate sheets act to produce a smooth contraction between the height of the original wind tunnel test section and that of the new test section. The acrylic portions of the top and bottom panels, along with the side panels, define the

rigid boundaries of the new test section.

The height of the variable height test section is determined by how the acrylic portions of the top and bottom panels are situated with respect to one another and the side panels before they are locked into place. Slots located in the acrylic tabs of the top and bottom panels allow the height of the test section to be continuously adjusted from 50.8 mm (2 in) to 152 mm (6 in). Figures 3.3a & b illustrate the variable height test section at its maximum and minimum heights, respectively.

Unlike its height, the other dimensions of the variable height test section are not flexible. The width of the test section is determined solely by the width of the top and bottom panels used. In order to accommodate different sized condensers, two sets of top and bottom panels were constructed, one set with a width of 406 mm (16 in) and another set with a width of 762 mm (30 in). The length of the test section (acrylic portion only) measures 622 mm (24.5 in). Acrylic extensions to the rear of the variable height test section have been built and used, when necessary, to accommodate condensers requiring greater lengths.

3.3 Multi-layer Condensers and Support Frames

One of the goals of this investigation was to study the interaction between individual layers of a multi-layer wire-on-tube condenser. To do this, several sets of nearly identical single layer condensers, the geometry of which have been listed in Table 3.1, were prepared and tested with the layers of a particular set placed in series with one another. During each experiment, the layers of a particular condenser set were connected through the use of mixing cups attached (using plastic-welding epoxy) to Tygon™ tubing, as shown in Fig. 3.4. This union of the individual condenser layers results in the creation of a "pseudo" multi-layer condenser.

As can be seen in Fig. 3.4a, the mixing cups used in linking the individual condenser layers are composed of two 12.7 mm x 6.35 mm (0.5 in x 0.25 in) brass couplings soldered to an interconnecting 12.7 mm (0.5 in) O.D. copper tube. This particular geometric configuration creates a sudden expansion followed by a sudden contraction, which causes fluid flowing through a particular mixing cup to achieve a much more spatially uniform temperature profile. A series of copper-constantan (type T) stainless steel sheathed thermocouple probes have also been inserted into and secured to each mixing cup using epoxy (see Fig. 3.4b). When properly connected, these thermocouple probes allow the absolute temperature of the fluid flowing within the mixing cup, as well as the differential temperature between the fluid flowing within two consecutive mixing cups, to be accurately measured. Adhesive foam placed around the entire outer surface of each mixing cup and portions of the Tygon™ tubing serves to insulate the fluid flowing through the mixing cups from influences outside the mixing cups.

The individual layers of the multi-layer condensers were oriented with respect to one

Table 3.1 Geometry of the multi-layer condenser layers

Variable	Units	Coil 6	Coil 8	Coil 9	Coil 10
D_w	mm (in)	1.38 (0.0542)	1.58 (0.0621)	1.57 (0.0618)	1.58 (0.0620)
δp_w	mm (in)	0.02 (0.0006)	0.01 (0.0005)	0.01 (0.0004)	0.01 (0.0005)
S_w	mm (in)	6.07 (0.239)	6.34 (0.250)	6.35 (0.250)	5.08 (0.200)
N_w	wires	66	150	60	204
L_w	mm (in)	150 (5.91)	148 (5.82)	151 (5.96)	152 (5.99)
D_t	mm (in)	4.80 (0.189)	4.80 (0.189)	4.83 (0.190)	4.85 (0.191)
δp_t	mm (in)	0.02 (0.0008)	0.02 (0.0007)	0.03 (0.0013)	0.04 (0.0017)
$D_{t,i}$	mm (in)	3.34 (0.132)	3.34 (0.132)	3.34 (0.132)	3.34 (0.132)
S_t	mm (in)	25.4 (1)	50.8 (2)	31.8 (1.25)	31.8 (1.25)
N_t	tubes	6	3	5	5
‡ L_t	mm (in)	202 (7.97)	471 (18.53)	186 (7.31)	515 (20.28)

‡ Excludes tube portions which are not directly exposed to forced convection

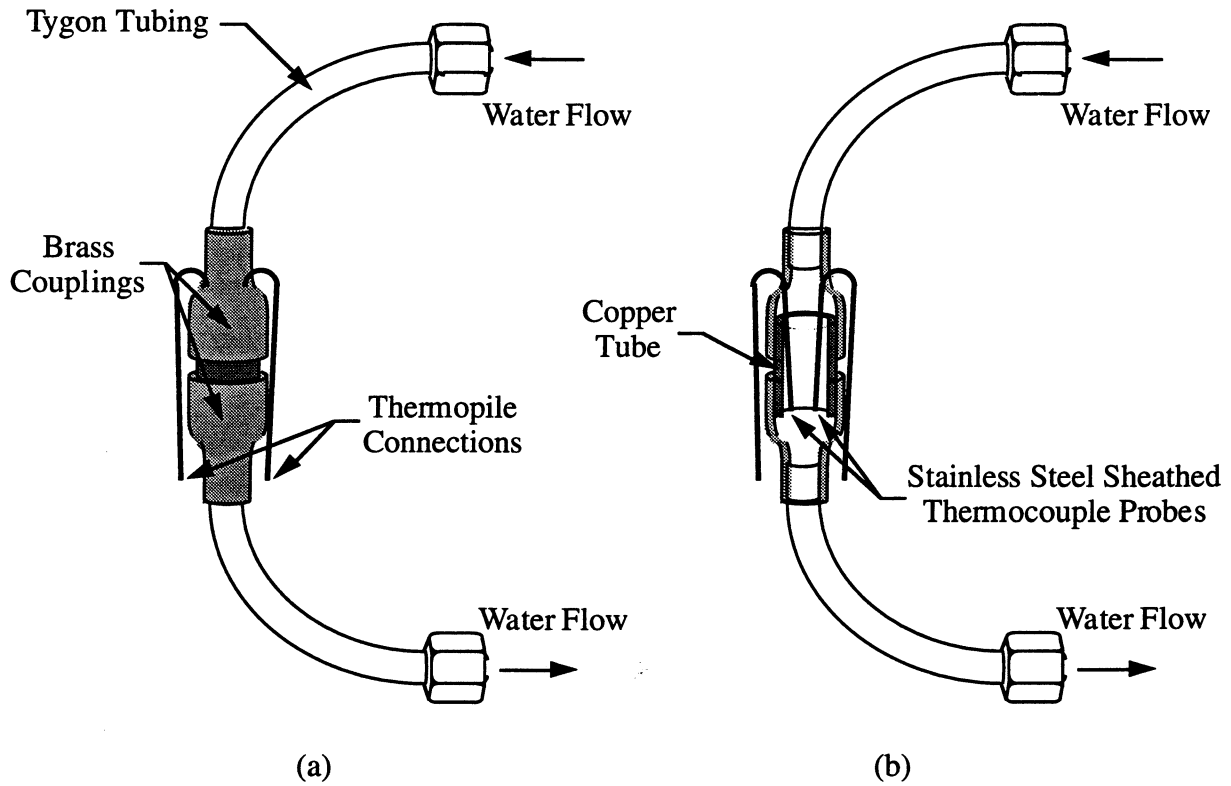

Figure 3.4 (a) Exterior and (b) interior views of the mixing cups

another through the use of a series of support frames, as shown in Fig. 3.5 and 3.6. These support frames, made primarily of plywood and foam, provided both structural support and form to each set of condenser layers, allowing the layers of the multi-layer condensers to be fixed into a desired geometric configuration (i.e. a set of desired S_L, α, and ψ).

The variable S_L condenser support frame, shown in Fig. 3.5, allowed the centerline-to-centerline distance between consecutive vertical ($\alpha = 90°$) condenser layers to be adjusted. As can be seen in Fig. 3.5a, the variable S_L condenser support frame consists of a series of foam-lined, plywood and acrylic pieces held together by four threaded nylon rods and a set of metal fasteners. Each of the plywood and acrylic pieces, excluding the pair of plywood contours located at the front of the frame, were designed to be slightly under 152 mm (6 in) in height in order to be used in conjunction with the variable height test section (see Section 3.2 - Variable Height Wind Tunnel Test Section) set at its maximum height. The plywood contours, on-the-other-hand, were designed to match the curved shape formed by the polycarbonate sheets of the fully assembled variable height test section.

When assembling a multi-layer wire-on-tube condenser using the variable S_L support frame, the nylon rods (assuming that nuts and washers are already in place) are first threaded through slots located in the pair of L-shaped plywood pieces at the back of the frame. They are then threaded through holes in a pair of acrylic guides (not shown in Fig. 3.5a) and passed through the tube bends of a condenser layer from the condenser set being investigated. A pair of acrylic guides (again not shown in Fig. 3.5a) are then added to the frame, followed by a pair of plywood spacers. At this time, additional plywood spacers may be threaded onto the rods (two pairs of spacers are shown in Fig. 3.5a) or another condenser layer sandwiched between acrylic guides may instead be added to the frame. By varying the number of pairs of plywood spacers employed between each set of consecutive condenser layers, the S_L of the multi-layer condenser can be varied incrementally. Over the course of the study, nine different S_L were investigated, ranging from 16.3 mm (0.642 in) to 76.1 mm (2.99 in), in increments of 7.47 mm (0.294 in). After including a sufficient number of condenser layers and plywood spacers, a pair of L-shaped plywood pieces are threaded onto the rods, followed by a set of washers and wing-nuts. The variable S_L condenser support frame is then completed by attaching the pair of plywood contours to the front of the entire assemblage.

A fully assembled multi-layer wire-on-tube condenser using the variable S_L support frame is shown in Fig. 3.5b. Note that although the multi-layer condenser shown has only two layers, any number of condenser layers may be tested in this manner. The use of foam, threaded nylon rods, and acrylic guides in assembling the variable S_L support frame serves to minimize any conduction heat transfer that may occur between portions of the multi-layer condenser and the variable S_L condenser support frame.

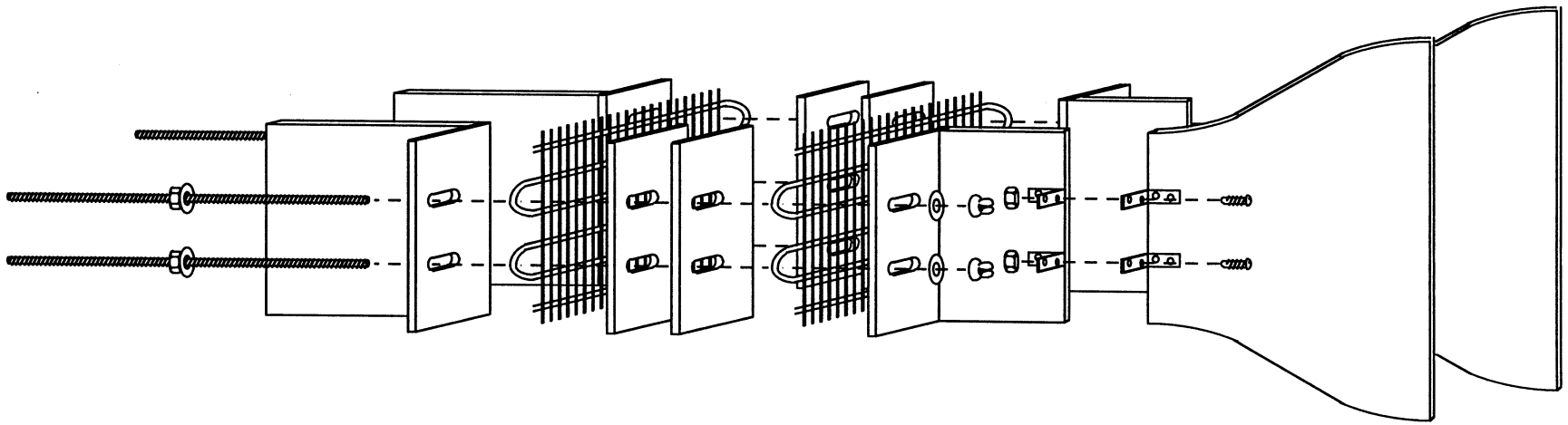

(a)

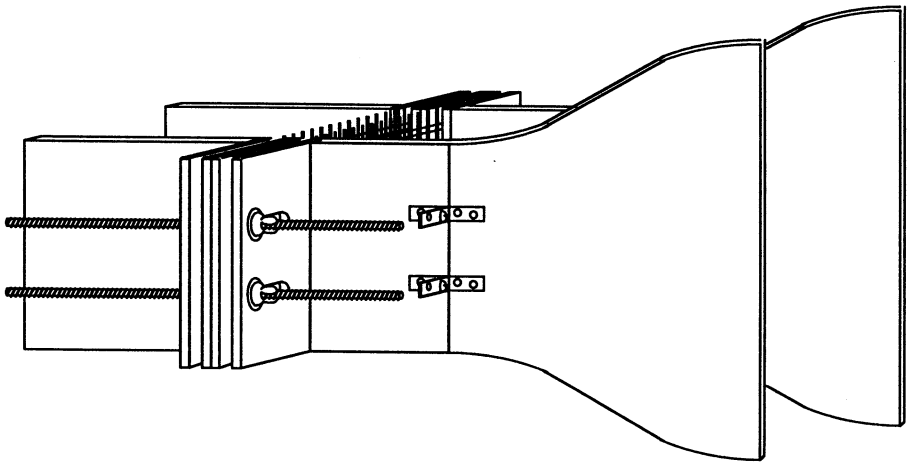

(b)

Figure 3.5 Variable S_L condenser support frame shown (a) in an exploded view and (b) fully assembled (Scale = 18:100)

In an effort to examine the forced convection heat transfer performance of multi-layer wire-on-tube condensers with layers at various α (with $|\alpha|$ uniform over an entire multi-layer condenser for a particular experiment), a series of α condenser support frames were also designed and constructed to be used in conjunction with the variable height test section (again, see Section 3.2 - Variable Height Wind Tunnel Test Section).

These support frames, a couple of which are shown in Fig. 3.6, consist of a pair of plywood contours designed to match the consolidation of both the curved shape formed by the polycarbonate sheets and the straight form of the rigid acrylic portions of the fully assembled variable height test section. Slots cut from each of the plywood contours, at pre-determined locations along the lengths of the contours, allow condenser layers to be oriented at certain angles with respect to the air flow when their tube bends are slid into the slots. As can be seen, sets designed to accommodate both the $\psi = 0$ (see Fig. 3.6a) and $\psi = \pi/2$ (see Fig. 3.6b) cases at a variety of α (45°, 60°, and 75°) were constructed.

Note that in the constructing these α condenser support frames, the effects of the buoyancy forces were assumed to be negligible with respect to the inertial forces of the forced convection flow generated during each experiment. That is, it was assumed that the heat transfer performance of a particular condenser oriented at $\alpha = \alpha_1$ would be approximately equal to that of the same condenser oriented at $\alpha = -\alpha_1$. Experimental data obtained by Hoke (1995) and Swofford (1995) clearly indicate that the + or - sign associated with α has a negligible effect on h_w for condensers oriented at $|\alpha| \geq 20°$, for both the $\psi = 0$ and $\psi = \pi/2$ cases. Since this study focuses on condensers oriented at $|\alpha| \geq 45°$, the assumption that the buoyant forces pose negligible effects on h_w is a valid one. A direct extension of this assumption is the supposition that condensers may be rotated about a vertical, as opposed to a horizontal, axis in determining α without bearing any consequence to h_w. As can be seen in Fig. 3.6a, the sets of α support frames designed to accommodate the $\psi = 0$ case make use of this extended assumption.

Due to the large extent of the information required to describe the dimensions which are relevant to each α condenser support frame, tables containing this material have been presented in Appendix A: Dimensions Related to α Support Frame Condensers. The corresponding figure (see Fig. A.1) attempts to illustrate the definitions of each of the major table headings. As can be seen, both the columns containing the height and width of the new test section are self-explanatory. Entries under the heading "axial length between slots" correspond to the distance along the length of the contours between the locations at which each of a pair of slots intended for a particular condenser layer are situated. This distance, along with the width of the new test section, determines the α of the condenser layer placed within the slots. Note that the height of the new test section (i.e. the straight portions of each set of α support frames) was designed so as to ensure that a distance of no more than 2 mm (0.079 in) would exist between the top and

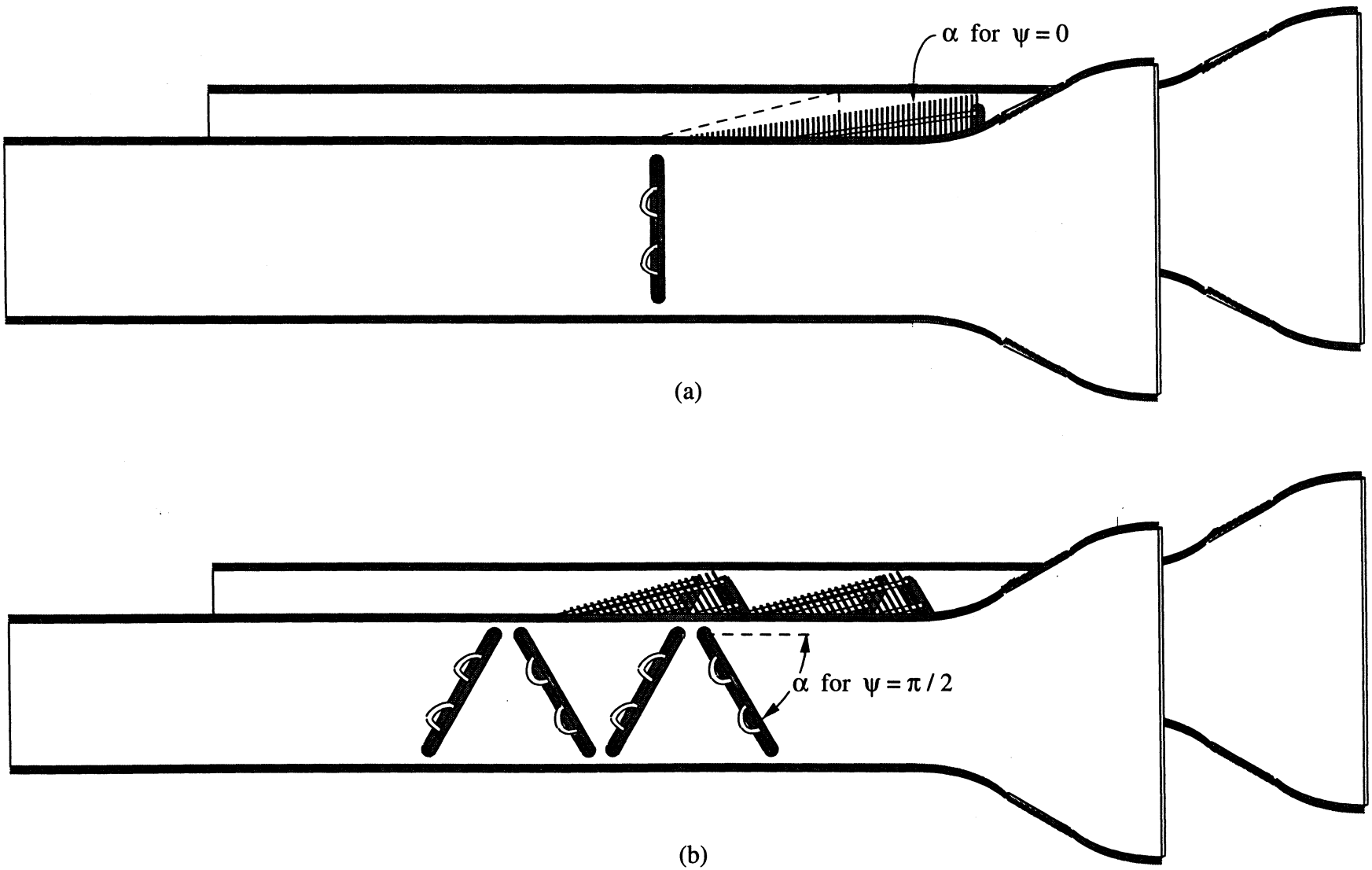

Figure 3.6 Typical α condenser support frames for the (a) $\psi = 0$ case and (b) $\psi = \pi/2$ case (Scale = 18:100)

condenser layer (oriented at a particular α) and the top and bottom inner surfaces of the variable height test section.

During testing, each of the multi-layer wire-on-tube condensers formed using either the variable S_L support frame or an α support frame is situated within both the variable height test section and the original wind tunnel test section (see Section 3.1 - Wind Tunnel). The same foam and acrylic barriers that were used to account for the difference in width between the inside of the wind tunnel and that of the variable height test section are, in this case, used to block the regions of the test and flow conditioning sections of the wind tunnel and the variable height test section which extended beyond the width of the condenser support frame. This forces the air flow generated by the wind tunnel to pass entirely through the volume defined by both the variable height test section and the condenser support frame.

As can be seen in Fig. 3.5 and 3.6, the tube bends of the multi-layer condensers formed using the support frames are not directly exposed to the forced convection air flows. That is, the bends of each condenser layer are either recessed within foam and plywood (as in Fig. 3.5) or they are isolated within still air by foam-lined walls (as in Fig. 3.6). Whichever the case, it is clear that a multi-layer condenser support frame not only provides structural support and form to each set of condenser layers, but also serves to force the air flow to which the condenser is subjected to be drawn through the wire and tube matrix of the condenser. This may at first seem trivial, however, the true impact of this can be seen when considering the following:

Although the wire-on-tube condensers located in actual refrigerators and those tested using the variable height test section are subjected to tightly confined, forced convection air flows, it is still likely that much of the air flow to which a particular condenser is subjected may not pass through the wire and tube matrix of the condenser. Rather, much of the air may flow around and/or through the tube bends of the condenser, effectively bypassing the wire and tube matrix of the condenser. This results in a decrease in the air velocity (from that measured upstream of the condenser) actually experienced by the wires and tube passes of the condenser, which would ultimately be reflected as a decrease in the measured h_w.

By employing a set of support frames during each experiment, the air is no longer able to flow around and/or through the tube bends of the condenser (which are either recessed within foam and plywood or isolated within still air). As a result, the wires and tube passes of the condenser experience air velocities which are comparable to that measured upstream of the condenser.

3.4 Temperature Regulated Water Circulation System

A circulation system, similar to that shown in Fig. 3.7, was used to supply water at a given temperature to each of the condensers involved in the current study. Developed by

Swofford (1995), the system consists primarily of a preheating section and an accurate temperature regulation section. Together these sections allow the water passing through the system and the water entering into each of the condensers to be adjusted to and maintained at a desired temperature.

Note that during each of the experiments water is circulated through the condensers instead of refrigerant due to the following factors:

1. The thermophysical properties of water are accurately known.
2. The thermal resistance associated with water flowing through the condenser tube passes is relatively small and can easily be accounted for.
3. The consequences from leaks in the circulation system are minimal, since water is much easier to clean up than refrigerant and does not pose any health related problems.
4. Water is inexpensive.

It is important to note that, although the internal thermal resistance (between the fluid and the inner walls of the condenser) associated with water flowing within a condenser is not identical to that associated with a two-phase refrigerant flowing within the same condenser, the air-side convection heat transfer performance measured from each case will be approximately the same, assuming identical test conditions. This is a direct result of the fact that the calculation of h_w requires that the thermal resistance contribution associated with the air-side convection heat

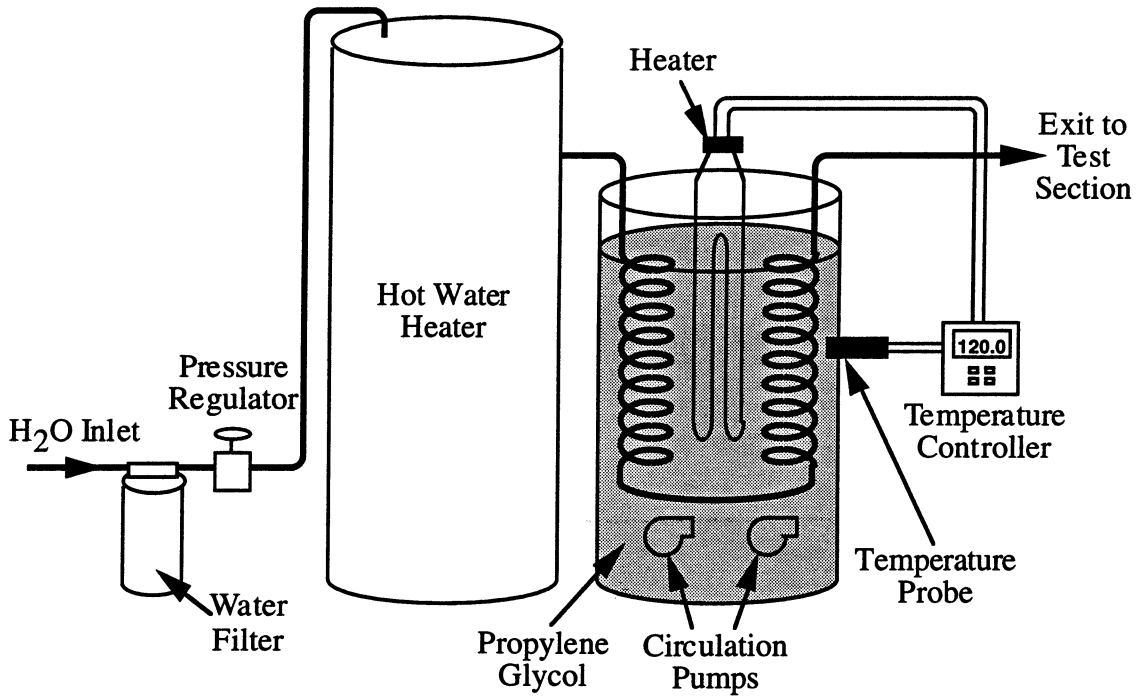

Figure 3.7 Temperature regulated circulation system used to supply water to the condensers

transfer first be isolated from the total thermal resistance. This ultimately means that, assuming that the internal thermal resistance can be accurately determined and that there exists a finite temperature drop across the inlet and the outlet of the condenser, almost any fluid can be substituted for the refrigerant in the condenser.

During each experiment, water from the city water supply is allowed to enter the circulation system. It is first passed through a water purifier to filter out impurities that may be present. The water then passes through a pressure regulator and enters a domestic hot water heater, where it is preheated to a temperature of 322.1 ± 5.6 K (120 ± 10 °F). Upon exiting the hot water heater, it is routed through a pair of plate-fin evaporator coils situated within an isothermal bath. While traveling through the bath, the water participates in heat transfer with the propylene glycol of the bath (heat exchanger effectiveness is ~ 0.99), causing the water to exit the bath at a temperature approximately equal to that of the propylene glycol. Lastly, the water is channeled through insulated tubing to the wind tunnel test section (see Section 3.1 - Wind Tunnel), where it is passed through the condenser being investigated.

The isothermal bath used to accurately regulate the temperature of the water supplied to the condensers contains forty-two gallons of propylene glycol (which is used because of its good thermophysical properties and its non-corrosive nature) and is maintained at a nearly constant, nearly spatially uniform temperature. A 610 mm (24 in) stainless steel sheathed thermocouple probe inserted into the propylene glycol of the bath is used to monitor the bath temperature. When the temperature of the bath decreases to 0.06 °C (0.1 °F) below the desired temperature, a 4 kW (13.7 kBtu/hr) heater is activated. The heater is then allowed to warm the bath until the temperature of the propylene glycol exceeds the desired temperature by 0.06 °C (0.1 °F), at which time the heater is again deactivated. A pair of 14.9 W ($^1/_{50}$ hp) immersion pumps located within the bath are used to mix the propylene glycol in order to minimize stratification.

3.5 Experimental Set-up

In preparation for each experiment, the single or multi-layer wire-on-tube condenser under investigation is positioned within the wind tunnel test section (see Section 3.1 - Wind Tunnel) at a desired α and ψ. For purposes of this investigation, this positioning involves first inserting the condenser within a set of multi-layer condenser support frames (see Section 3.3 - Multi-layer Condensers and Support Frames) and then placing both the condenser and the support frame within the variable height test section (see Section 3.2 - Variable Height Wind Tunnel Test Section). Assuming that the correct support frame is used, the condenser should already be positioned with both the desired α and the desired ψ.

After the mixing cups are used to connect the layers, only a pair openings in the resulting multi-layer condenser, an inlet and an outlet, remain. The inlet, usually the opening furthest

from the front of the wind tunnel (for the case of a counter flow heat exchanger), is attached to the insulated tubing leading from the isothermal bath of the water circulation system (see Section 3.4 - Temperature Regulated Water Circulation System). The outlet is connected to a disposal tube which leads away from the test section and to a plastic bucket where the water passing through the condenser can be weighed.

3.6 Data Acquisition System

Over the course of a particular experiment, several measurements are obtained and recorded. These measurements include the following:

1. The free stream air velocity (V)
2. The absolute air temperature upstream of the condenser ($T_{a,in}$)
3. The absolute water temperatures at the condenser's inlet and outlet ($T_{r,in}$ and $T_{r,out}$)
4. Differences in the water temperature for consecutive mixing cups ($\Delta T_{r,1}$, $\Delta T_{r,2}$, etc.)
5. The mass flow rate of the water flowing through the condenser ($\dot{m}_r$)
6. The pressure drop across the entire multi-layer condenser (Δp)

Note that none of the measurements listed above are obtained directly from a single meter reading. Each involves some form of mathematical manipulation in order to acquire the desired information from one or more meter readings.

The free stream air velocity is obtained by measuring the velocity directly upstream of the condenser. This measurement is made using a TSI 8355 Air Velocity Meter. Calibrated prior to use, the meter bears an absolute uncertainty of ± 0.03 m/s (0.1 ft/s). The measured velocity, V_{meas}, is read directly from the meter display and is adjusted to account for existing ambient conditions using the equation

$$V = V_{meas}\left(\frac{T_{a,in}}{294.25\ K}\right)\left(\frac{760\ mm\ Hg}{p_{amb}}\right) \tag{3.1}$$

where p_{amb} is the ambient pressure.

Copper-constantan (type T) thermocouple junctions located within the flow conditioning section of the wind tunnel (see Section 3.1 - Wind Tunnel) are used to measure $T_{a,in}$. The reference junction of each of these thermocouples has been carefully sealed within a Kay Instruments ICE POINT reference to ensure that each thermocouple is referenced to 0.0 °C (32 °F). The emf generated by the differences in the temperatures between the junctions of the thermocouples are read directly from a Fluke digital voltmeter with a resolution of 1 μV.

The thermocouples have each been calibrated using an isothermal bath much like that mentioned in Section 3.4 - Temperature Regulated Water Circulation System and a thermometer with 0.05 K (0.09 °F) resolution. The calibration curves obtained for each of the five thermocouples used are shown in Fig. 3.8. Although the temperature-microvolt relation for each thermocouple was approximately the same, a separate calibration curve for each was determined in order to minimize the uncertainty in the measurements. These relations are as follows:

$$T_{air,a} = 273.85 + (2.4538 \bullet 10^{-2})\,(\mu V) + (3.4176 \bullet 10^{-7})\,(\mu V)^2 - (2.286 \bullet 10^{-10})\,(\mu V)^3 \quad (3.2a)$$

$$T_{air,b} = 274.05 + (2.4457 \bullet 10^{-2})\,(\mu V) + (5.3761 \bullet 10^{-7})\,(\mu V)^2 - (2.972 \bullet 10^{-10})\,(\mu V)^3 \quad (3.2b)$$

$$T_{air,c} = 273.48 + (2.5189 \bullet 10^{-2})\,(\mu V) - (5.288 \bullet 10^{-8})\,(\mu V)^2 - (1.485 \bullet 10^{-10})\,(\mu V)^3 \quad (3.2c)$$

$$T_{air,d} = 274.43 + (2.3134 \bullet 10^{-2})\,(\mu V) + (1.3742 \bullet 10^{-6})\,(\mu V)^2 - (4.686 \bullet 10^{-10})\,(\mu V)^3 \quad (3.2d)$$

$$T_{air,e} = 274.68 + (2.2947 \bullet 10^{-2})\,(\mu V) + (1.4870 \bullet 10^{-6})\,(\mu V)^2 - (4.958 \bullet 10^{-10})\,(\mu V)^3 \quad (3.2e)$$

where μV corresponds to the voltmeter reading in microvolts and the resulting T_{air} are in units of K. The precision limits associated with these thermocouples range anywhere from 0.04 K (0.06 °F) to 0.06 K (0.11 °F). For each thermocouple, three separate readings are averaged to determine the measured air temperature, resulting in an absolute uncertainty of approximately ± 0.07 K (0.12 °F) for each measurement. A total of four of these averaged temperatures are then also averaged to obtain the value of $T_{a,in}$. Assuming that the air temperature is spatially uniform, the absolute uncertainty of the resulting quantity is estimated to be ± 0.06 K (0.10 °F).

The absolute temperatures of the water flowing through the inlet and outlet of the condenser are measured in much the same way as $T_{a,in}$. Thermopiles, composed of a total of four thermocouple junctions (as opposed to two in the case of a standard thermocouple), are used to measure both $T_{r,in}$ and $T_{r,out}$. The use of four thermocouple junctions instead of two allows the temperatures to be measured with a much greater resolution, nearly doubling the number of μV corresponding to 1 K.

A pair of 1.02 mm (0.040 in) diameter stainless steel sheathed thermocouple probes (which serve as two of the four junctions), embedded within each of the mixing cups at the both the inlet and the outlet of the condenser, allow the absolute temperature of the water flowing within the mixing cups to be determined. As in the case of the thermocouples used in measuring $T_{a,in}$, a Kay Instruments ICE POINT reference is used to ensure that the thermopiles are referenced to 0.0 °C (32 °F). Unlike the thermocouples, however, two reference junctions are sealed within the ICE POINT reference. The emf generated by the differences in the

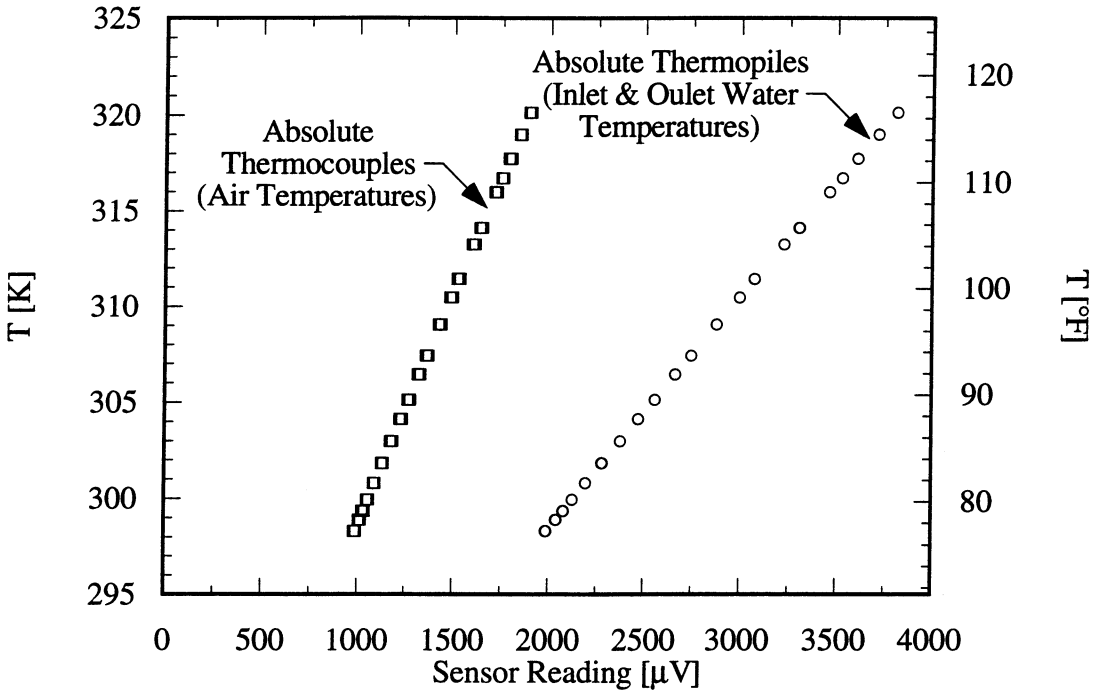

Figure 3.8 Calibration curves used for the absolute thermocouples and thermopiles

temperatures between the mixing cups and the ICE POINT reference are also read directly from the same Fluke digital voltmeter with a resolution of 1 μV.

Both of the absolute thermopiles have been calibrated using the same isothermal bath and thermometer used in calibrating the air thermocouples. The calibration curves obtained for both thermopiles are also shown in Fig. 3.8. Again, although the temperature-microvolt relations for both thermopiles were approximately the same, a separate calibration curve for each was determined in order to minimize the uncertainty associated with $T_{r,in}$ and $T_{r,out}$. These temperature-microvolt relations are as follows:

$$T_{r,in} = 275.01 + (1.0987 \bullet 10^{-2})\,(\mu V) + (5.1466 \bullet 10^{-7})\,(\mu V)^2 - (7.67 \bullet 10^{-11})\,(\mu V)^3 \qquad (3.3a)$$

$$T_{r,out} = 275.20 + (1.0711 \bullet 10^{-2})\,(\mu V) + (6.2852 \bullet 10^{-7})\,(\mu V)^2 - (9.10 \bullet 10^{-11})\,(\mu V)^3 \qquad (3.3b)$$

where again μV corresponds to the voltmeter reading in microvolts and the resulting $T_{r,in}$ and $T_{r,out}$ are in units of K.

In an effort to reduce the error in readings which may result from conduction along the axis of a particular thermocouple probe, each probe was inserted at least 25.4 mm (1 in) into its corresponding mixing cup. In addition, three separate temperature readings from each

thermopile were averaged to determine $T_{r,in}$ and $T_{r,out}$. The absolute uncertainty resulting from these measurement is estimated to be ± 0.07 K (0.12 °F).

Differences in temperature between the water flowing through consecutive mixing cups was measured using differential thermopiles. Like the absolute thermopiles, these thermopiles are composed of four thermocouple junctions. The differential thermopiles, however, are not referenced using an ICE point reference. Instead all four of the thermocouple junctions of each differential thermopile are situated within a pair of consecutive mixing cups (two in each) in the form of 1.02 mm (0.040 in) diameter stainless steel sheathed thermocouple probes. Again, the emf generated by the differences in the temperatures between water flowing through the consecutive mixing cups are read directly from the same Fluke digital voltmeter.

The calibration of the differential thermopiles was also performed using the same isothermal bath and thermometer used in calibrating the air thermocouples. The temperature-microvolt behavior obtained for each of the differential thermopiles are shown in Fig. 3.9. Note that $\delta T/\delta_{(volts)}$ has been plotted as a function of T (as opposed to T as a function of the sensor reading) since, due to the nature of the differential thermopiles, knowledge of $\delta T/\delta_{(volts)}$ is much more useful than that of the absolute temperature. Note also that the scale of the y axis shown in Fig. 3.9 ranges from 0.010 K/μV (0.018 °F/μV) to 0.013 K/μV (0.023 °F/μV). This causes any differences between the curves shown to appear somewhat accentuated. In actuality, the curves

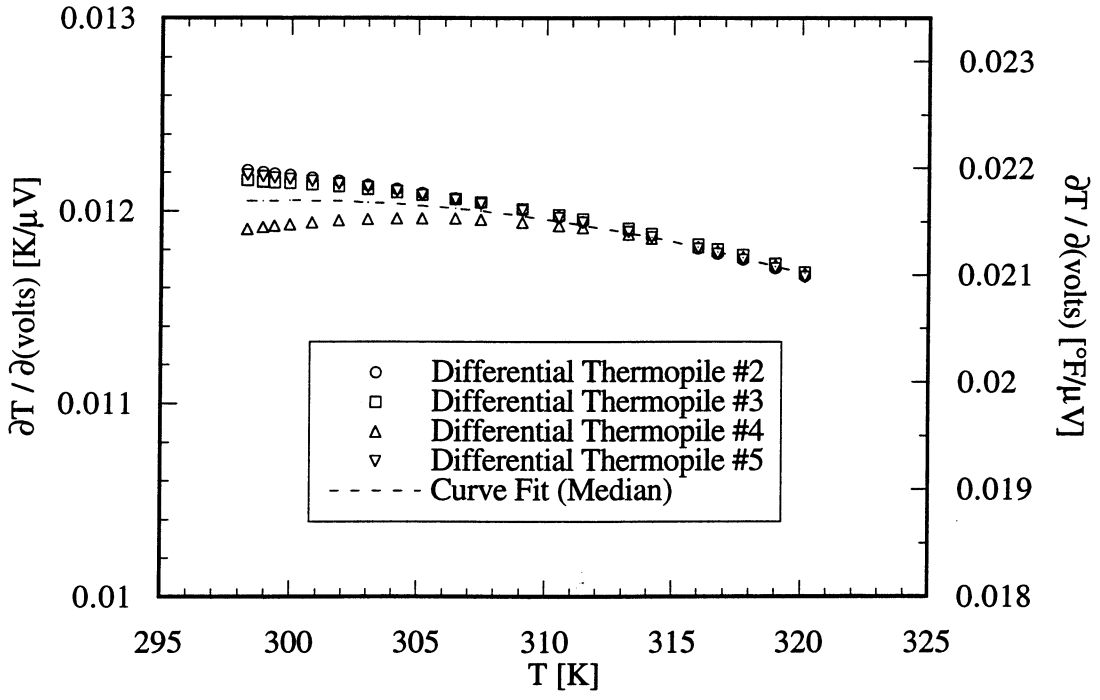

Figure 3.9 Calibration curve used for the differential thermopiles

are nearly identical. This, along with the fact that the ΔT_r measured by these thermopiles is equivalent to the integral of $\delta T/\delta(\text{volts})$ with respect to the voltage (which is related to the area beneath the curves in Fig. 3.9), indicates that a single calibration curve could be used without incurring any significant errors. This $\delta T/\delta(\text{volts})$-temperature relation, based on the median curve fit of the temperature-microvolt behavior of the thermopiles is given by

$$\frac{\partial T}{\partial(\text{volts})} = -0.152 + (1.338 \bullet 10^{-3})\, T - (3.452 \bullet 10^{-6})\, T^2 + (2.72 \bullet 10^{-9})\, T^3 \qquad (3.4)$$

where T is in units of K.

As was the case with the absolute thermopiles, the stainless steel sheathed thermocouple probes of the differential thermopiles were each embedded at least 25.4 mm (1 in) into their corresponding mixing cups, helping to minimize the error in readings due to conduction along the axis of each thermocouple probe. For each thermopile, three separate readings were averaged to determine ΔT_r, resulting in an absolute uncertainty of approximately ± 0.06 K (0.11 °F).

The mass flow rate of the water flowing through the condenser (which is held constant during each experiment) was determined by measuring the amount of time required for a certain amount of water, supplied from the outlet of the condenser, to accumulate within a plastic bucket. A standard stopwatch, bearing an absolute uncertainty between ± 0.0063 s and ± 0.0088 s, was used to record the amount of time that elapsed between when the water was first allowed to enter the bucket and when the water was no longer allowed to accumulate. A Scientech SG 5000 Electronic Balance, located beneath the bucket, was used to measure the mass of the water that had accumulated. The balance, calibrated using a 2000 ± 0.005 g Electronic Balance Calibration Mass, has an absolute uncertainty of ± 0.10 g (0.00022 lb_m).

The mass flow rate of the water flowing through the condenser, $\dot{m}_r$, was calculated by dividing the mass of the water measured by the amount of time required for it to accumulate. The absolute uncertainty of this quantity calculated from the uncertainties associated with both the stopwatch and the balance, assuming reasonable operator biases of ± 0.03 s and ± 8.00 g (0.018 lb_m), is ± 0.05 g/s (0.397 lb_m/hr). The precision limit due solely to the unsteadiness of the water flow rate, however, has been measured to be ± 0.27 g/s (2.14 lb_m/hr). As a result, the absolute uncertainty associated with the measurement of $\dot{m}_r$ should actually be on the order of ± 0.27 g/s (2.14 lb_m/hr).

An Omega PX653 Pressure Transducer was used to measure the pressure drop across the entire multi-layer condenser, Δp, during each experiment. Pressure taps located both upstream and downstream of the condenser were connected to the transducer through a network of Tygon™ tubing. An Omega digital voltmeter with a 1 mV resolution was used to display the

output supplied by the pressure transducer.

Calibration data for the pressure transducer was supplied by the manufacturer, resulting in a calibration curve shown in Fig. 3.10. Note that although a total of five calibration points, ranging from 0 to 24.9 Pa (0.1 in H_20), were supplied by the manufacturer, the two highest points were neglected in favor of the lower three since all of the measured Δp were lower than the third highest point, 12.5 Pa (0.05 in H_2O). The Δp-voltage relation for this curve is given by

$$\Delta p = -9.64 + 11.155\,(\text{volts}) - 1.25\,(\text{volts})^2 \tag{3.5}$$

where Δp is in units of Pa. Although the manufacturer specifications indicate that the absolute uncertainty of the Δp measured by the pressure transducer should be approximately $\pm$ 0.065 Pa (0.0003 in H_2O), the actual uncertainty is expected to be somewhat higher. This is due to the fact that (i) the pressure taps may not be exactly perpendicular to the walls of the test section and (ii) minute leaks may exist at the interface of the variable height test section and the wind tunnel.

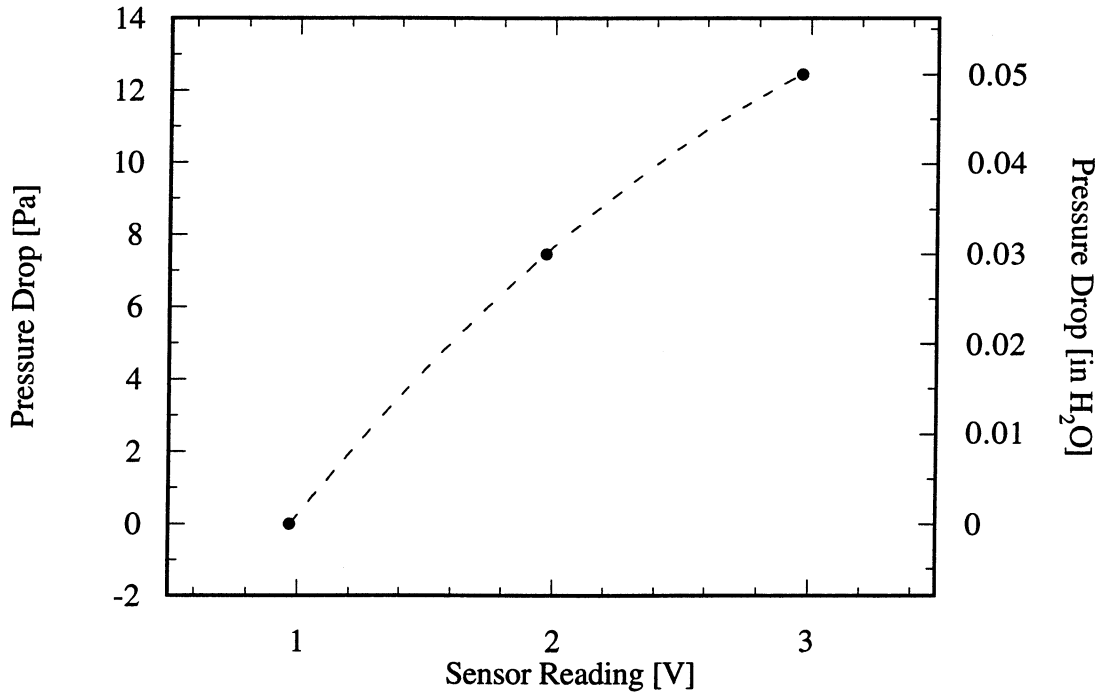

Figure 3.10 Calibration curve used for differential pressure measurements

4. DATA REDUCTION

The transfer of energy in the form of heat from a particular wire-on-tube condenser to its environment represents a very complex and challenging problem. Some of the major complications which result from an analysis of this type of condenser include:

1. The existence of highly non-isothermal surfaces such as those belonging to the wires of the condenser. The average temperature of these non-isothermal wire surfaces must be properly accounted for by determining the fin efficiency, η_w, associated with the condenser wires for each air velocity to which the wire-on-tube condenser is exposed.

2. The presence of both tube passes and wires in the geometry of the condenser, which allow energy to be dissipated from the condenser through multiple heat paths.

3. The existence of an intricate condenser geometry, which makes the accurate determination of both the convection heat transfer coefficients and the radiation exchange factors (i.e. view factors) extremely difficult.

These complexities, together, make the task of obtaining useful information from experimental measurements seem almost insurmountable. In addition, the serpentine tube of a particular wire-on-tube condenser may also not be bent within a single plane like those found in typical household refrigerators. Instead, the serpentine tube (and, as a result, the overall geometry of the condenser) may be bent or formed into a series of layers, as in the case of a multi-layer condenser. In these instances, the heat exchanger type (e.g. counter or parallel flow) serves to further complicate the task of determining meaningful results.

The following sections outline the method used in determining a measure of performance for each condenser evaluated in the current study. A FORTRAN program utilizing the procedures and equations discussed was developed and used to determine the relative performance of each layer of a particular condenser from the experimental measurements acquired during each test. The source code for this data reduction program, along with a simplified program flow chart (see Fig. B1), have been provided in Appendix B: Data Reduction Program for Multi-layer Wire-on-Tube Condensers.

4.1 Analysis of the Heat Transfer Problem

As in the case with any highly complex problem, the process of reducing the experimental measurements acquired during each test into a meaningful measure of condenser performance can most readily be accomplished by first attempting to segment the heat transfer problem into several smaller, more manageable tasks. Quantities associated with these smaller tasks can then be systematically determined and combined to find an overall solution to the original problem.

Before discussing the division of the heat transfer problem into smaller tasks, it is important to note that several quantities vital to the overall solution of the problem can be calculated directly from the measured quantities: V, $T_{a,in}$, $T_{r,in}$ and $T_{r,out}$, ΔT_r across each condenser layer, and $\dot{m}_r$. In the case of multi-layer condensers, the total heat transfer rate from a particular condenser layer, q_{tot}, can be determined by performing an overall energy balance on the fluid flowing through the serpentine tube of the condenser layer. This can be accomplished for each layer of the condenser by using the equation

$$q_{tot} = \dot{m}_r \, c_{p,r} \, \Delta T_r \tag{4.1}$$

where $c_{p,r}$ is the specific heat of water (the fluid used in the current investigation) and ΔT_r is the difference in water temperature across the condenser layer being evaluated.

The absolute temperature of the air to which each layer of a multi-layer condenser is exposed can also be determined directly from the experimental data obtained. Assuming that the air experienced by a particular condenser layer is spatially uniform in temperature and that it is thoroughly mixed between each layer, the temperature of the air directly downstream of a condenser layer (and, as a result, directly upstream of the successive condenser layer) can be determined by performing an overall energy balance on the air flowing over the condenser. The resulting equation for this can be mathematically manipulated to the yield the relation

$$[T_a]_{k+1} = [T_a]_k + \frac{q_{tot}}{\dot{m}_a \, c_{p,a}} \tag{4.2}$$

where $\dot{m}_a$ is the mass flow rate of the air (which is directly related V), $c_{p,a}$ is the specific heat of air, and $[T_a]_{k+1}$ and $[T_a]_k$ are the temperatures of the air directly downstream and upstream of the k^{th} condenser layer, respectively. Note that the labeling convention used in the current study numbers each layer of a multi-layer condenser in ascending order from upstream to downstream of the condenser. Figure 4.1 illustrates this index notation for multi-layer condensers used as both counter flow and parallel flow heat exchangers.

With q_{tot}, $[T_a]_{k+1}$, and $[T_a]_k$ already determined for each layer of a particular multi-layer wire-on-tube condenser, the process of determining the performance of each condenser layer based on experimental data can be initiated by first considering the total thermal resistance between the fluid flowing within a particular condenser layer and the layer's environment, R_{tot}. This resistance, which is directly related to the temperature difference between the fluid flowing within the layer and the layer's environment and inversely proportional to q_{tot}, can be used as a reference in determining the relative importance of some of the thermal resistances from which R_{tot} is composed.

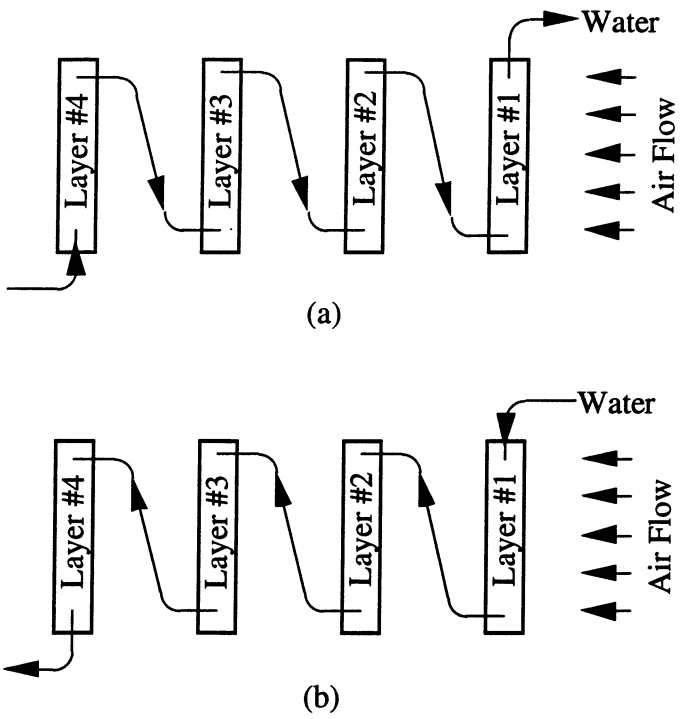

Figure 4.1 Index notation used in labeling the layers of multi-layer condensers in (a) counter flow and (b) parallel flow

Energy dissipated from the fluid flowing within a particular condenser layer is transferred through convection heat transfer to the inner surface of the condenser tube. The corresponding thermal resistance, R_{int}, can be used, along with R_{tot}, $[T_a]_k$, and $[T_r]_{k+1/2}$ (the average temperature of the fluid flowing through the k^{th} layer) to estimate the average surface temperature of the inside of the condenser tube.

The energy passing from the condenser fluid to the inner surface of the condenser tube is also conducted through the wall of the condenser tube. Since (i) wires are welded at discrete locations with a spacing of S_w along the outer surface of the condenser tube and (ii) a majority of the energy is expected to be dissipated from the condenser through the wires, the conduction occurring through the condenser tube wall cannot be accurately evaluated by assuming purely radial (i.e. one-dimensional) heat flow. Instead all three dimensions, radial, circumferential, and axial, must be considered when evaluating the conduction heat transfer rates.

Assuming that the thermal conductivity of the steel condenser tube is uniform along the entire layer, the governing equation for three-dimensional conduction heat transfer within the wall of the condenser tube takes the form of

$$\frac{1}{r}\frac{\partial}{\partial r}\left(r\frac{\partial T}{\partial r}\right)+\frac{1}{r^2}\frac{\partial^2 T}{\partial \phi^2}+\frac{\partial^2 T}{\partial z^2}=0 \qquad (4.3)$$

where r, ϕ, and z correspond to locations in the radial, circumferential, and axial directions, respectively. In order to simplify the analysis, the heat transfer rates in the radial direction and both the circumferential and axial directions together can be assumed to be independent of one another. That is, the magnitude of q_r is assumed to have no effect on the calculation of $q_\phi + q_z$ and, similarly, the magnitude of $q_\phi + q_z$ is assumed to have no effect on the calculation of q_r. Consequently, the governing equation shown in Eq. (4.3) can be separated into two distinct equations

$$\frac{\partial}{\partial r}\left(r\frac{\partial T}{\partial r}\right)=0 \qquad\qquad \frac{1}{r^2}\frac{\partial^2 T}{\partial \phi^2}+\frac{\partial^2 T}{\partial z^2}=0 \qquad\qquad (4.4a \text{ \& } b)$$

where Eq. (4.4a) and (4.4b) correspond to the heat flux component in the radial direction and both the circumferential and axial directions together, respectively.

In choosing to solve Eq. (4.4), a thermal resistance associated with the radial conduction through the wall of the condenser tube, $R_{cond,t}$, can be calculated and used, much like R_{int}, to estimate the average temperature of the outer surface of the condenser tube, $\overline{T}_t$. Once the $\overline{T}_t$ for each layer of a multi-layer condenser is known, the radiation heat transfer rate and, as a result, the convection heat transfer rate, from the tube passes and wires of the condenser can be estimated. Effective wire surface temperatures can be approximated by evaluating the effect of the circumferential and axial conduction within the condenser tube (see Section 4.4 - Effect of Thermal Constriction) and by accounting for the fin efficiency of the wires, η_w.

By now it should be clear that each condenser layer has multiple paths through which energy from the fluid flowing within it can be dissipated. In general, the rate at which the energy flows (i.e. the heat transfer rate) is greatest through the path which affords the lowest thermal resistance. The air-side thermal resistances, composed of resistances associated with the convection and radiation heat transfer rates from the tube passes ($R_{conv,t}$ and $R_{rad,t}$) and wires ($R_{conv,w}$ and $R_{rad,w}$), together account for the largest portion of R_{tot} (Admiraal and Bullard, 1993). Unfortunately, due to the composition of wire-on-tube condensers, all of the energy leaving a particular condenser must flow through one of these air-side thermal resistances.

In an earlier study, Hoke (1995) and Swofford (1995) determined that the air-side convection heat transfer performance of a wire-on-tube condenser can be increased significantly by increasing α of the condenser. This increase in performance corresponds to a decrease in either one or both of the air-side convection resistances ($R_{conv,t}$ and $R_{conv,w}$), ultimately increasing the rate at which energy can be dissipated from the condenser. Since (i) the air-side radiation resistances ($R_{rad,t}$ and $R_{rad,w}$) were found to be approximately the same under most circumstances and (ii) the air-side convection and radiation resistances exist in a parallel

relationship which allows the total heat transfer rate to be changed significantly without altering either $R_{rad,t}$ and $R_{rad,w}$, it can easily be concluded that a sensible measure of the heat transfer performance of a particular wire-on-tube condenser should be based primarily on the air-side convection heat transfer performance of the condenser.

4.2 Air-side Convection Heat Transfer Coefficient

The key to successfully determining a useful measure of performance for each wire-on-tube condenser from the experimental measurements lies in the proper definition of the air-side convection coefficients, h_t and h_w, which are associated with the convection heat transfer between the outer surfaces of the condenser tube passes and wires, respectively, and the air to which the condenser is exposed. This is due primarily to the fact that (i) the air-side convection heat transfer rate can be drastically increased by altering such parameters as V, α, ψ, and the geometry of the condenser (while the radiation heat transfer rate is nearly constant under most circumstances) and (ii) the overall size of a particular condenser is often limited by economics and the availability of space within the refrigerator. As will be shown in the following text, h_t and h_w are interdependent and their exact relationship may be approximated with little consequence. As a result, the heat transfer coefficient associated with the condenser wires, h_w, may be used, instead of both h_t and h_w, as the primary measure of heat transfer performance for wire-on-tube condensers.

Assuming that (i) the outer surface temperature, $\overline{T}_t$, across the tube passes of a particular condenser layer is uniform (i.e. ignoring the effects of circumferential and axial conduction on $\overline{T}_t$), (ii) the temperature of the air to which the condenser is exposed is also spatially uniform, and (iii) the extent to which the boundary layers of the condenser tube passes and the wires interact can be ignored, the total convection heat transfer rate from a particular wire-on-tube condenser layer can be determined using the relation

$$q_{conv} = A_t\, h_t \left(\overline{T}_t - [T_a]_k\right) + A_w\, h_w \left(\overline{T}_w - [T_a]_k\right) \tag{4.5}$$

where $\overline{T}_w$ is the average surface temperature of the condenser wires.

Note that, at this point, assuming that q_{conv} can be accurately obtained from q_{tot}, Eq. (4.5) has a total of three undefined values: h_t, h_w, and $\overline{T}_w$. As mentioned previously, however, h_t and h_w are interdependent and, as a result, h_t need not be found. Furthermore, as the primary measure of heat transfer performance for wire-on-tube condensers, h_w should be the only unknown in Eq. (4.5). Consequently, the average surface temperature of the condenser wires, $\overline{T}_w$, must somehow be related to quantities which are either known or can be determined from what is known.

resulting log-mean temperature difference, ΔT_{lm}, between the outer surface temperatures of the condenser tube and the surrounding air can be calculated using

$$\Delta T_{lm} = \frac{\left(T_{t,in} - [T_a]_k\right) - \left(T_{t,out} - [T_a]_k\right)}{\ln\left(\frac{T_{t,in} - [T_a]_k}{T_{t,out} - [T_a]_k}\right)} \tag{4.14}$$

where $T_{t,in}$ and $T_{t,out}$ are the outer surface temperatures at the inlet and outlet of the serpentine tube of the condenser layer, respectively. Equation (4.13) can then be adjusted to account for the non-uniformity of the condenser tube outer surface temperature by replacing the temperature difference ($\overline{T}_t$ - $[T_a]_k$) with ΔT_{lm} as follows:

$$h_w \equiv \frac{q_{conv}}{\left(\frac{A_t}{\sqrt{D_t^*}} + \eta_c\, \eta_w\, A_w\right) \Delta T_{lm}} \tag{4.15}$$

In addition to neglecting the possibility of differences in the outer surface temperatures between consecutive the tube passes in the development of Eq. (4.13), the effect of circumferential and axial conduction on $\overline{T}_t$ was also ignored. This allowed the regions around each wire and tube interface to be spatially uniform in temperature. It is important to note, however, that q_w is expected to be significantly higher than q_t. As a result, by ignoring that the effects of the circumferential and axial conduction on $\overline{T}_t$, the resulting error should be negligible.

4.3 Internal Convection and Radial Tube Conduction

The thermal resistances associated with (i) the convection heat transfer between the fluid flowing within the condenser and the inner surface of the condenser tube, R_{int}, and (ii) the conduction heat transfer occurring radially through the wall of the condenser tube, $R_{cond,t}$, can each be determined without the use of significant assumptions. Although both of these resistances are relatively small in magnitude, the calculation and removal of their effects plays a role in normalizing the experimental results to account for variations in such variables as $\dot{m}_r$, $D_{t,i}$, and the outer diameter of the condenser tube beneath the paint, $D_{t,bare}$.

The resistance R_{int} can be determined by assuming that (i) the fluid flow within the condenser tube passes is fully developed both hydrodynamically and thermally, (ii) the fluid flow is turbulent ($Re_{D_{t,i}} > 2300$), (iii) the inner surface of the condenser tube is smooth, and (iv) either the heat flux or the temperature is nearly uniform across the entire inner surface of each

A relation between $\overline{T}_w$ and the temperature at the base of each of the condenser wires, T_{wbase}, can be determined by examining the definition of the fin efficiency of the condenser wires given by

$$\eta_w \equiv \frac{\tanh(m)}{m} = \frac{\overline{T}_w - [T_a]_k}{T_{wbase} - [T_a]_k} \tag{4.6}$$

where m is the dimensionless fin parameter associated with each condenser wire. The square of this parameter, m^2, is equal to the ratio of the internal axial resistance associated with the conduction heat transfer within the condenser wires and the external resistance associated with the convection heat transfer between the wire surfaces and the surrounding air. This ratio, m^2, is

$$m^2 \approx \frac{h_w S_t^2}{k_s D_{w,bare}} \tag{4.7}$$

where $D_{w,bare}$ is the condenser wire diameter beneath the paint (i.e. $D_{w,bare} = D_w - 2 \bullet \delta_{p,w}$) and k_s is the thermal conductivity of the steel condenser wires.

The substitution of Eq. (4.6) into Eq. (4.5) yields the relation

$$q_{conv} = A_t\, h_t \left(\overline{T}_t - [T_a]_k\right) + \eta_w\, A_w\, h_w \left(T_{wbase} - [T_a]_k\right) \tag{4.8}$$

Again the relation has two undetermined quantities (since h_t and h_w are related), h_w and T_{wbase}. However, if an effective thermal constriction efficiency, η_c, which accounts for the circumferential and axial conduction within the condenser tube to the locations at which the wires are welded, is defined as

$$\eta_c = \frac{T_{wbase} - [T_a]_k}{\overline{T}_t - [T_a]_k} \tag{4.9}$$

then Eq. (4.8) can be rewritten as

$$q_{conv} = \left(A_t\, h_t + \eta_c\, \eta_w\, A_w\, h_w\right)\left(\overline{T}_t - [T_a]_k\right) \tag{4.10}$$

where η_c is dependent on the convection heat transfer coefficient of the fluid within the condenser tube, h_r, as well as the geometry of the condenser (see Section 4.4 - Effect of Thermal Constriction).

Assuming that h_w, is constant over the surface area of all of the wires of a particular

condenser layer. Under these assumptions, a local Nusselt number, Nu_r, associated with the fluid flowing through each condenser layer can be computed using a correlation proposed by Gnielinski (Gnielinski, 1976). This relation, which is valid for conditions where $2300 < Re_{D_{t,i}} < 5 \cdot 10^6$ and $0.5 < Pr_r < 2000$, takes the form of

$$Nu_r = \frac{\left(f/8\right)\left(Re_{D_{t,i}} - 1000\right)^{Pr_r}}{1 + 12.7\left(f/8\right)^{1/2}\left(Pr_r^{2/3} - 1\right)} \tag{4.16}$$

where $Re_{D_{t,i}}$ and Pr_r are the Reynolds number (with characteristic dimension $D_{t,i}$) and Prandtl number associated with the fluid flowing through the condenser, respectively, and f is the friction factor which, in the case of smooth tubes, can be expressed as

$$f = \left[0.79 \ln\left(Re_{D_{t,i}}\right) - 1.64\right]^{-2} \tag{4.17}$$

Once the Nu_r associated with each condenser layer has been determined, the convection heat transfer coefficient corresponding to each can be calculated using

$$h_r = \frac{Nu_r \, k_r}{D_{t,i}} \tag{4.18}$$

where k_r is the thermal conductivity of the condenser fluid (i.e. water). These values of h_r can then in turn be used in determining the R_{int} associated with each layer using the relation

$$R_{int} = \frac{1}{h_r \, A_{t,i}} \tag{4.19}$$

where $A_{t,i}$ is the internal surface area of the tube passes of a particular condenser layer.

The resistance obstructing the axial heat flow through the wall of the condenser tube, $R_{cond,t}$, can be determined by examining the heat flow between two concentric cylinders. Assuming uniform heat fluxes and temperatures across both the inner and outer surfaces of the condenser tube, $R_{cond,t}$ can be calculated using

$$R_{cond,t} = \frac{D_{t,i} \ln\left[D_{t,bare}/D_{t,i}\right]}{2 \, A_{t,i} \, k_s} \tag{4.20}$$

where k_s is the thermal conductivity of the steel condenser tube.

4.4 Effect of Thermal Constriction

The thermal constriction arises from the fact that a portion of the total energy being transferred from the fluid flowing within the condenser tube is dissipated through the wires of the wire-on-tube condenser. To do this, the energy must first be conducted from the inner surface of the condenser tube to the locations along the outer surface of the condenser tube on to which the wires are welded. This conduction from a relatively large area to a much smaller area results in the formation of temperature gradients (in the circumferential and axial directions) around each weld, causing the additional thermal resistance to be created.

In evaluating the effect of the thermal constriction, it is important to first note that the geometry of a typical wire-on-tube condenser (excluding the tube bends of the condenser) can be thought of as being composed of a series of identical pieces, with each piece consisting of portions of a single condenser tube pass and a single wire, as shown in Fig. 4.2a. As can be seen, the boundaries of the highlighted piece's domain occur midway between consecutive condenser wires and consecutive condenser tubes.

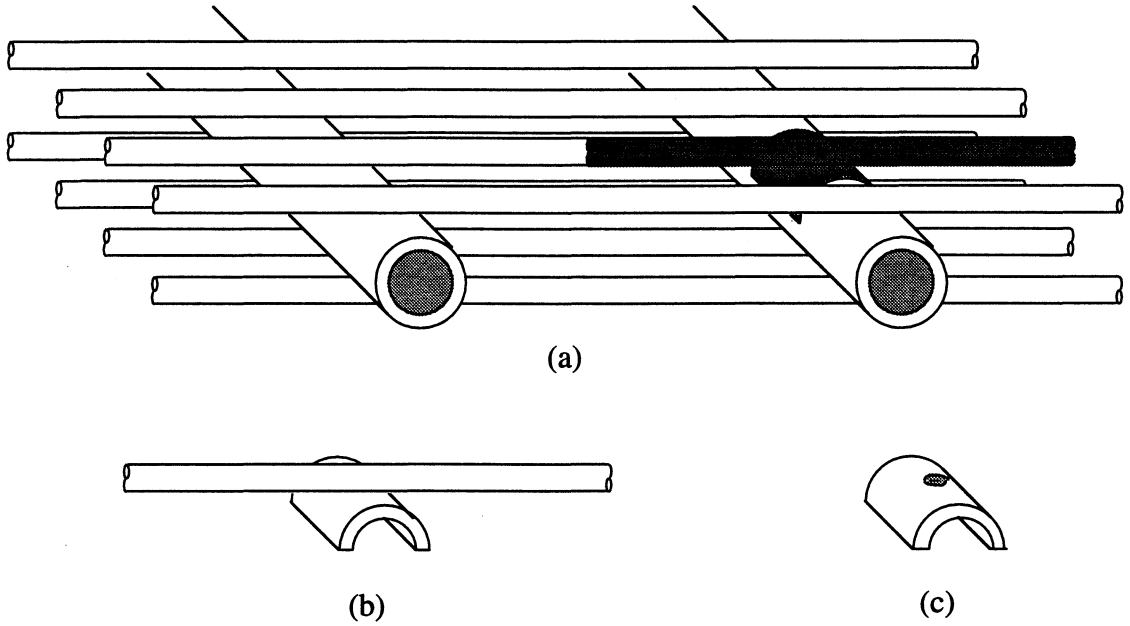

Figure 4.2 Illustrations of (a) the repetitive nature of the geometry of a typical wire-on-tube condenser, (b) a representative portion of the condenser, and (c) a representative wireless condenser portion

Assuming that the heat fluxes and temperatures are nearly the same for each piece of the condenser, an analysis of the entire wire-on-tube condenser may be performed by evaluating a single portion of the condenser, much like that shown in Fig. 4.2b. If the temperature, T_{wbase}, is also assumed to be spatially uniform across the entire weld spot, then the presence of the wire

segment becomes inconsequential to the analysis of the effects of thermal constriction within the condenser tube. As a result, the wire segment may be removed, as shown in Fig. 4.2c.

By further assuming that the effects of thermal constriction are independent of radial location within the condenser tube, the problem may be treated as being two-dimensional. This allows the rounded domain of the condenser tube piece to be represented as a rectangular region with side dimensions $\pi D_t/2$ and S_w. Figure 4.3 shows a flattened view of the condenser portion and the corresponding weld spot area associated with each of the wire-on-tube condensers involved in the current study. Due to the presence of symmetry, only a quarter of each of the portions shown will actually be used to evaluate the effects of the thermal constriction. These quarter portions, along with the isotherms (lines of constant temperature) and adiabats (heat flow lines) associated with the thermal constriction around each weld, are also shown in Fig. 4.3.

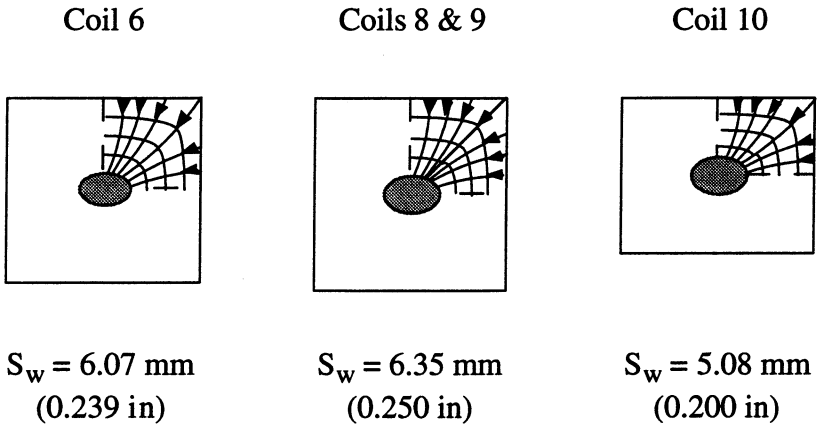

Figure 4.3 Flattened views of the representative wireless portion of each condenser tested (see Table 3.1) and the thermal constriction that occurs within the each portion

As is the case with energy transfer involving any extended surface, the convection heat transfer rate (assuming $q_{conv} >> q_{rad}$) to and from the condenser tube portion is critical in determining the fin efficiency, η_t, with which the tube portion participates in convection heat transfer with its environment. This problem is compounded, however, by the fact that the condenser tube has two fluids with which it participates in convection heat transfer, the condenser fluid (i.e. water for purposes of this study) flowing within the tube and the air flowing around the tube's exterior. Since the heat transfer rate between the inside of the condenser tube and the condenser fluid is much greater than that between the outer surface of the condenser tube and the surrounding air, the latter heat transfer rate can, at this point, be assumed to be negligible. The fin efficiency of the condenser tube, η_t, can then be easily defined as

$$\eta_t = \frac{T_r - \overline{T}_t}{T_r - T_{wbase}} \tag{4.21}$$

Based on the definition of η_t given in Eq. (4.21), a FORTRAN program utilizing the finite-volume method of discretization was written and used to numerically determine an explicit function defining η_t in terms h_r for each of the condensers involved in the current study. When executed, the program subjects the entire domain of a particular condenser portion (see Fig 4.3) to convection heat transfer with the condenser fluid using a specified h_r. The nodes corresponding to the weld spot are held at a constant temperature T_{wbase} throughout the analysis, while conduction heat transfer is allowed to occur between nodes within the domain. In addition, the boundaries of the domain are treated as being adiabatic. This forces any energy leaving the domain through conduction heat transfer to pass through one of the nodes corresponding to the weld spot.

Approximate dimensions for the weld spot associated with each of the condensers were determined by averaging the measurements obtained from at least twenty different wire samples belonging to each of the condensers tested. These measurements were then inputted into the program along with the overall dimensions, $\pi D_t/4$ and $S_w/2$, associated with the rectangular portions of each condenser tube section. The source code for the finite-volume program is shown in Appendix C: Program Used to Evaluate the Fin Efficiency of the Condenser Tube Passes, along with an illustration of the relative sizes of the weld spot and nodes used in discretizing the domain for each of the wire-on-tube condensers tested.

The η_t-h_r relations determined using this procedure for the wire-on-tube condensers involved in the current study are as follows:

$$\eta_{t,coil\ 6} = 1 - (9.8263 \bullet 10^{-5})\, h_r + (8.461 \bullet 10^{-9})\, h_r^2 - (3.5651 \bullet 10^{-13})\, h_r^3 \tag{4.22a}$$

$$\eta_{t,coil\ 8\&9} = 1 - (1.0135 \bullet 10^{-4})\, h_r + (8.9264 \bullet 10^{-9})\, h_r^2 - (3.8074 \bullet 10^{-13})\, h_r^3 \tag{4.22b}$$

$$\eta_{t,coil\ 10} = 1 - (7.9181 \bullet 10^{-5})\, h_r + (5.908 \bullet 10^{-9})\, h_r^2 - (2.2998 \bullet 10^{-13})\, h_r^3 \tag{4.22c}$$

where $\eta_{t,coil\ 6}$, $\eta_{t,coil\ 8\&9}$, and $\eta_{t,coil\ 10}$, are the η_t corresponding to Coil 6, Coils 8 and 9, and Coil 10 (see Table 3.1), respectively, and h_r is in terms of W/m^2-K.

Although the convection heat transfer occurring between the outer surface of the condenser tube and the surrounding air was ignored in developing Eq. (4.22), its existence can be reintroduced into the overall thermal constriction analysis by determining an effective heat transfer coefficient which accounts of the combined effect of the both the internal (between the condenser fluid and the inner tube surface) and external (between the outer tube surface and the

air) convection heat transfer rates. This effective heat transfer coefficient, $h_{r,eff}$, is defined as

$$h_{r,eff}\, A_{t,i} \left(T_r - \overline{T}_t\right) = q_{conv,tot} - q_{conv,t} \tag{4.23}$$

where $q_{conv,tot}$ and $q_{conv,t}$ are equal to the internal and external heat transfer rates, respectively. Equation (4.23) can be simplified to express $h_{r,eff}$ explicitly as

$$h_{r,eff} = \frac{q_{conv,tot} - q_{conv,t}}{A_{t,i} \left(T_r - \overline{T}_t\right)} \tag{4.24}$$

Note that $q_{conv,tot}$ and $q_{conv,t}$ are not totally independent. By performing an overall energy balance on the condenser tube, an equation relating the internal and external heat transfer rates can be expressed as

$$q_{conv,tot} = q_{conv,t} + q_{conv,w} = h_r\, A_{t,i} \left(T_r - \overline{T}_t\right) \tag{4.25}$$

where $q_{conv,w}$ can be thought of as being the portion of energy transferred from the condenser fluid that is not dissipated from the outer tube surface of the wire-on-tube condenser. Using Eq. (4.25), Eq. (4.24) can be mathematically manipulated as follows:

$$h_{r,eff} = \frac{h_r\, A_{t,i} \left(T_r - \overline{T}_t\right) - q_{conv,t}}{A_{t,i} \left(T_r - \overline{T}_t\right)}$$

$$= h_r - \frac{\left(q_{conv,tot} - q_{conv,w}\right)}{A_{t,i} \left(T_r - \overline{T}_t\right)}$$

$$= h_r - \frac{h_r\, A_{t,i} \left(T_r - \overline{T}_t\right)}{A_{t,i} \left(T_r - \overline{T}_t\right)} + \frac{q_{conv,w}}{A_{t,i} \left(T_r - \overline{T}_t\right)}$$

$$= \frac{q_{conv,w}}{A_{t,i} \left(T_r - \overline{T}_t\right)} \tag{4.26}$$

As can be seen, Eq. (4.26) does not express $h_{r,eff}$ in terms of h_r. However, by multiplying both the numerator and denominator of Eq. (4.26) by h_r, it can easily be seen that

$$h_{r,eff} = \left(\frac{h_r}{h_r}\right)\left(\frac{q_{conv,w}}{A_{t,i} \left(T_r - \overline{T}_t\right)}\right) = h_r \left(\frac{q_{conv,w}}{q_{conv,tot}}\right) \tag{4.27}$$

where the ratio $q_{conv,w}/q_{conv,tot}$ can be approximated by manipulating the definition of h_w, given by

Eq. (4.15), as follows:

$$\frac{q_{conv,w}}{q_{conv,tot}} \approx \frac{h_w\,\eta_c\,\eta_w\,A_w\,\Delta T_{lm}}{h_w\left(\frac{A_t}{\sqrt{D_t^*}}+\eta_c\,\eta_w\,A_w\right)\Delta T_{lm}} = \frac{\eta_c\,\eta_w\,A_w}{\left(\frac{A_t}{\sqrt{D_t^*}}+\eta_c\,\eta_w\,A_w\right)} \tag{4.28}$$

Since $h_{r,eff}$, defined by Eq. (4.27) and (4.28), is based on the same temperature difference, $(T_r - \overline{T}_t)$, as is h_r, it should be clear that h_r can simply be replaced by $h_{r,eff}$ to account for the combined effect of the both the internal and external convection heat transfer rates. That is, $h_{r,eff}$ should be substituted in place of h_r in Eq. (4.22) in order to determine η_t.

In order to determine the effect of η_t on the heat transfer rate from a particular wire-on-tube condenser layer, a relation between η_t and effective thermal constriction efficiency, η_c, must also be established. To do this, it is important to note that an explicit relation for T_{wbase} can be formed by rearranging Eq. (4.21) as

$$T_{wbase} = T_r + \frac{\overline{T}_t - T_r}{\eta_t} \tag{4.29}$$

By substituting Eq. (4.29) into Eq. (4.9) and performing a few mathematical operations, an explicit η_c-η_t relation can be established as follows:

$$\eta_c = \frac{\left(T_r + \frac{\overline{T}_t - T_r}{\eta_t}\right) - [T_a]_k}{\overline{T}_t - [T_a]_k}$$

$$= \frac{\eta_t\left(T_r - [T_a]_k\right) + \overline{T}_t - T_r}{\eta_t\left(\overline{T}_t - [T_a]_k\right)}$$

$$= 1 + \frac{\eta_t\,T_r + \overline{T}_t - T_r - \eta_t\,\overline{T}_t}{\eta_t\left(\overline{T}_t - [T_a]_k\right)}$$

$$= 1 + \frac{(1-\eta_t)\left(\overline{T}_t - T_r\right)}{\eta_t\left(\overline{T}_t - [T_a]_k\right)} \tag{4.30}$$

4.5 Effect of Paint Thickness

As is the case with both R_{int} and $R_{cond,t}$, the thermal resistance associated with the paint

covering the outer surfaces of a particular wire-on-tube condenser is expected to be small in magnitude relative to the air-side thermal resistances. Unlike R_{int} and $R_{cond,t}$, however, the existence of paint on the condenser also affects the fin efficiency of the condenser wires, η_w, in addition to increasing the overall thermal resistance. As a result, the accurate determination of the effects of the thermal resistance associated with the paint may be of importance when factoring out the influences of the thickness of the paint covering the condenser from the heat transfer performance of wire-on-tube condensers.

Assuming that both the thickness, $\delta_{p,w}$, and thermal conductivity, k_p, of the paint on the condenser wires can be determined with reasonable accuracy, an effective heat transfer coefficient can be defined to account for the additional thermal resistance resulting from the presence of the paint. This effective heat transfer coefficient, $h_{w,eff}$, can be expressed as

$$\frac{1}{h_{w,eff}\,\pi\,D_{w,bare}\,S_t} = \frac{1}{h_w\,\pi\,D_w\,S_t} + \frac{\ln\left[D_w/D_{w,bare}\right]}{2\,\pi\,k_p\,S_t} \tag{4.31}$$

Equation (4.31) can then subsequently be mathematically manipulated to reveal an explicit relation for $h_{w,eff}$ as follows:

$$\frac{1}{h_{w,eff}} = \frac{D_{w,bare}}{h_w\,D_w} + \frac{D_{w,bare}\,\ln\left[D_w/D_{w,bare}\right]}{2\,k_p}$$

$$h_{w,eff} = \frac{1}{\dfrac{D_{w,bare}}{h_w\,D_w} + \dfrac{D_{w,bare}\,\ln\left[D_w/D_{w,bare}\right]}{2\,k_p}}$$

$$= \frac{2\,h_w\left(D_w/D_{w,bare}\right)k_p}{2\,k_p + h_w\,D_w\,\ln\left[D_w/D_{w,bare}\right]} \tag{4.32}$$

In deriving Eq. (4.32), it was assumed that both $\delta_{p,w}$ and k_p could be determined with reasonable accuracy. However, (i) the average absolute uncertainty in the measurement of $\delta_{p,w}$ is approximately 81% of the magnitude of $\delta_{p,w}$ for each of the condensers involved in the current study and (ii) k_p has been estimated by two separate sources to be 0.167 W/m-K (0.0965 Btu/hr-ft-°F) and 0.470 W/m-K (0.272 Btu/hr-ft-°F). Consequently, any attempt at using Eq. (4.32) to account for the presence of the paint might actually serve to increase the overall

uncertainty of the h_w calculated.

The true effect of the presence of paint on the heat transfer performance of wire-on-tube condensers is evidenced by examining the relation for calculating the total convection heat transfer rate(see Eq. (4.5)). In order to be more accurate, this relation should actually read

$$q_{conv} = A_t\ h_t \left(\overline{T}_t - [T_a]_k\right) + A_{w,bare}\ h_{w,eff} \left(\overline{T}_w - [T_a]_k\right) \tag{4.33}$$

where $A_{w,bare}$ is the surface area of the bare wires (i.e. the surface area of the condenser wires beneath the paint). However, assuming (i) that $\delta_{p,w}$ for a particular condenser is equal to 0.013 mm (0.0005 in), the average $\delta_{p,w}$ measured from the condensers involved in the current study, and (ii) that k_p = 0.167 W/m-K (0.0965 Btu/hr-ft-°F), the quantity $A_w h_w$ over-predicts $A_{w,bare}h_{w,eff}$ by less than 1.1%. Performing the same analysis using k_p = 0.470 W/m-K (0.272 Btu/hr-ft-°F) and the same $\delta_{p,w}$ reveals that $A_w h_w$ over-predicts $A_{w,bare}h_{w,eff}$ by less than 0.4%. Without knowing the true values of $\delta_{p,w}$ and k_p, it is virtually impossible to draw any conclusions about the effect of the thickness of the paint covering the condensers other than the following:

1. The effect of paint on the convection heat transfer performance of a particular wire-on-tube condenser is ~ 1%, provided that $\delta_{p,w}$ is < 0.03 mm (0.0012 in) and k_p is not significantly lower than 0.167 W/m-K (0.0965 Btu/hr-ft-°F).

2. In general (dependent on k_p), the quantity $A_w h_w$ over-predicts $A_{w,bare}h_{w,eff}$. This is due primarily to the fact that $h \propto D^{-n}$, where n is nearly $^1/_2$, and $A \propto D$. The resulting product, Ah, should be proportional to a positive value which is less than $^1/_2$, assuming again that k_p is not significantly lower than 0.167 W/m-K (0.0965 Btu/hr-ft-°F).

3. The changes in $\overline{T}_w$ and $\overline{T}_t$ resulting from the presence of paint on the condensers are extremely small and should have an affect on h_w which opposes that caused by changes in the product of A and h.

4.6 Radiation Heat Transfer

As mentioned previously, the air-side thermal resistances ($R_{conv,t}$, $R_{conv,w}$, $R_{rad,t}$ and $R_{rad,w}$) together account for the largest portion of the total thermal resistance (Admiraal and Bullard, 1993). However, due to the fact that (i) the air-side convection and radiation resistances exist in a parallel relationship and (ii) both $R_{conv,t}$ and $R_{conv,w}$ are highly dependent on parameters such as V, α, ψ and condenser geometry, the ability of $R_{rad,t}$ and $R_{rad,w}$ to affect the magnitude of the total heat transfer rate, q_{tot}, from a particular condenser layer is somewhat limited. Despite of this, the total radiation heat transfer rate, q_{rad}, must be calculated and subtracted from q_{tot} in order to determine the value of q_{conv} needed to evaluate condenser performance.

When evaluating the magnitude of q_{rad}, it is convenient to assume that the tube passes of each condenser layer are at a uniform temperature and that they participate in energy transfer with the surroundings as a single node, or unit. The wires of each condenser layer can similarly be treated as a single node with a uniform temperature. Although the surrounding surfaces which make up the condenser's environment are not nearly as uniform in temperature as the condenser tube passes and wires, they can also be treated as a single node with an infinite thermal capacity (i.e. the temperature of the surroundings is unaffected by the energy transferred to the surroundings). The temperature of this surrounding node, however, can be adjusted to reflect the different temperatures experienced by the various condenser layers. This temperature, T_{surr}, can be determined for each condenser layer using the equation

$$T_{surr} \approx \frac{[T_a]_k + [T_a]_{k+1}}{2} \tag{4.34}$$

where $[T_a]_k$ and $[T_a]_{k+1}$ are used in determining T_{surr} since the surrounding surfaces to which radiation from the condenser is transferred are likely to be similar in temperature to the air to which they are exposed.

The radiation view factor between each pair of nodes, F_{jk}, which denotes the fraction of energy in the form of radiation leaving surface j which is intercepted by surface k, can be calculated by first assuming that each of the surfaces is a diffuse emitter and reflector. That is, the radiative properties (i.e. such as the emissivity, ε) of each surface are assumed to be independent of the angle at which energy transfer occurs. In addition, the surfaces are assumed to have uniform radiosities, causing the amount of radiant energy leaving a particular surface to be spatially uniform over the entire surface. Under these assumptions, the radiation view factors corresponding to each pair of nodes were calculated using several published relations. Each of these relations, along with a few descriptive illustrations, have been presented in Appendix D: Radiation View Factor Equations.

The total radiation heat transfer rate from each condenser layer, q_{rad}, can be calculated by evaluating the radiosity, J, associated with each node. This can readily be done by performing a radiation energy balance at the surface of each node as follows:

$$\left(\sigma T_j^4 - J_j\right)\left(\frac{\varepsilon_j}{1-\varepsilon_j}\right) = \sum_{k=1}^{N}\left(J_j - J_k\right) F_{jk} \tag{4.35}$$

where j and k are the indices corresponding to the surface under examination and all of the other surfaces, respectively, N is the total number of nodes, and σ is the Stefan-Boltzmann constant. In addition to being diffuse (i.e. independent of the angle at which energy transfer occurs), the

emissivity, ε, in Eq. (4.35) is also assumed to be independent of the wavelength of the energy being transferred (i.e. the surface is gray).

Note that the use of Eq. (4.35) in the evaluation of the radiosity for each node yields a set of N simultaneous equations with N unknown radiosities. These equations can be solved by first rearranging them as follows:

$$\left(\sigma T_j^4 - J_j\right)\left(\frac{\varepsilon_j}{1-\varepsilon_j}\right) = \sum_{k=1}^{N} J_j F_{jk} - \sum_{k=1}^{N-1} J_k F_{jk} - \sigma T_{surr}^4 F_{j-surr}$$

$$= J_j - \sum_{k=1}^{N-1} J_k F_{jk} - \sigma T_{surr}^4 F_{j-surr}$$

$$J_j\left(\frac{1}{1-\varepsilon_j}\right) - \sum_{k=1}^{N-1} J_k F_{jk} = \sigma T_j^4\left(\frac{\varepsilon_j}{1-\varepsilon_j}\right) + \sigma T_{surr}^4 F_{j-surr} \qquad (4.36)$$

As can be seen, Eq. (4.36) now appears in the form of $[A]\bullet\{x\} = \{b\}$, which can easily be solved through matrix solution methods such as Gauss-Jordan Elimination.

Upon determining the radiosities associated with each node, the total radiation heat transfer rate from each condenser layer can be calculated using the equation

$$q_{rad} = \left(\sigma \overline{T}_t^4 - J_t\right)\frac{\varepsilon_p A_t}{\left(1-\varepsilon_p\right)} + \left(\sigma \overline{T}_w^4 - J_w\right)\frac{\varepsilon_p A_w}{\left(1-\varepsilon_p\right)} \qquad (4.37)$$

where J_t and J_w are the radiosities associated with the tube passes and wires of the condenser layer and ε_p is the total, hemispherical emissivity of the paint covering the surfaces of the condenser ($\varepsilon_p \sim 0.95$).

4.7 Heat Losses from Non-Exposed Surfaces

Much of the discussion concerning data reduction thus far applies exclusively to the portions of the wire-on-tube condensers that are exposed to forced convection air flows. However, due to that fact that each of the multi-layer condensers involved in the current study were formed using one of the condenser support frames (see Chapter 3 - Experimental Apparatus & Instrumentation), the tube bends of each condenser layer were shielded from the forced convection air flows. In light of this fact, it would be prudent to account for the energy dissipated form these non-exposed surfaces by using the relation

$$q_{tot} = q_{conv} + q_{rad} + q_{conv,ne} + q_{rad,ne} \qquad (4.38)$$

where $q_{conv,ne}$ and $q_{rad,ne}$ are the portions of the total energy dissipated from the condenser which leave through convection and radiation heat transfer between the non-exposed surfaces of the condenser and the environment around the condenser.

Because the tube bends of each condenser layer are not uniformly angled with respect to the vertically acting buoyant forces (i.e. the angle varies along the length of the tube bend), it is difficult to find a single relation that will accurately describe the heat transfer interaction due exclusively to natural convection from the non-exposed condenser tube surfaces. However, since the convection heat transfer coefficient, $h_{t,ne}$, is not expected to change significantly over the surface area of an entire tube bend and the non-exposed portion of the condenser tube surfaces accounts for only a small fraction of the total condenser surface area, an equation corresponding to natural convection heat transfer between a long horizontal cylinder and the surrounding air can be used in estimating an average heat transfer coefficient associated natural convection from the non-exposed condenser tube surfaces. This relation, developed by Churchill and Chu (1975), is valid for conditions where $10^{-5} < Ra_D < 10^{12}$ and takes the form of

$$h_{t,ne} = \left(\frac{k_a}{D_t}\right)\left\{0.60 + \frac{0.387\ Ra_{D_t}^{1/6}}{\left[1+(0.559/Pr_a)^{9/16}\right]^{8/27}}\right\}^2 \tag{4.39}$$

where D_t and $\overline{T}_t$ are used in calculating the Rayleigh number, Ra_{D_t}. Upon determining $h_{t,ne}$, the total convection heat transfer rate from the non-exposed surfaces of the condenser to the surrounding air can be calculated using

$$q_{conv,ne} = h_{t,ne}\ A_{t,ne}\left(\overline{T}_t - [T_a]_k\right) \tag{4.40}$$

where $A_{t,ne}$ is the surface area of the non-exposed surface of the condenser tube bends. Note that $[T_a]_k$ is used in Eq. (4.40) as a representative temperature for the surrounding air. This is due primarily to the assumption that the air surrounding the tube bends of a particular condenser layer is unaffected by the energy dissipated from adjacent condenser layers. As a result, the temperature of the air surrounding the tube bends should be approximately the same as that measured upstream of the entire condenser, $[T_a]_k$.

Assuming that all of the energy dissipated in the form of radiation from the tube bends is transferred to the condenser's surroundings, the total radiation heat transfer rate from the non-exposed surfaces of the condenser can be approximated using the equation

$$q_{rad,ne} \approx \sigma\ \varepsilon_p\ A_{t,ne}\left(\overline{T}_t^4 - [T_a]_k\right) \tag{4.41}$$

Note that $[T_a]_k$ is also used in Eq. (4.41) as a representative temperature for the condenser's surroundings. This is justified since a majority of the temperatures of surfaces surrounding the condenser are, for the most part, unaffected by the energy dissipated from the condenser.

5. EXPERIMENTAL RESULTS & DISCUSSION

Both (i) the air-side convection coefficient associated with the wires of each condenser layer, h_w, and (ii) the pressure drop across the entire multi-layer condenser, Δp, are extremely critical in evaluating the performance of a particular multi-layer wire-on-tube condenser. The former, h_w, gives some indication as to the relative rate at which energy can be dissipated from a particular condenser layer through convection heat transfer, while the latter specifies the extent to which the air flow is inhibited. Both the h_w and Δp for multi-layer wire-on-tube condensers are displayed graphically and discussed in the following sections.

Note that the experimental data pertaining to the current study were obtained from condensers that were tested in either (i) the original 305 mm (12 in) high and 914 mm (36 in) wide wind tunnel test section or (ii) the combination of the variable height test section and one of the condenser support frames. For naming purposes, condensers exposed to air flows within the original test section will, hereafter, be referred to as being "unconfined". This is due to the fact that the cross-sectional area of the original test section is significantly greater than the projected frontal areas which are occupied by the wire and tube matrix of the condensers themselves. The air flows to which unconfined condensers are subjected are, therefore, not constrained to pass through the condenser wire and tube matrices (i.e. a portion of the air is allowed to flow around and/or through the tube bends of the condensers).

Condensers situated within the combination of the variable height test section and one of the condenser support frames will be referred to as being "confined" for the remainder of the text, since the air flows to which they are subjected are confined to the regions occupied by the wire and tube matrix of the condensers. Due to the fact that a majority of the experimental data was obtained from confined condensers, data from plots within this section and the appendices should be assumed to be obtained from confined condensers, unless otherwise specified.

For the convenience of the reader, tables containing the raw data (i.e. V, $T_{a,in}$, $T_{r,in}$ and $T_{r,out}$, ΔT across each condenser layer, $\dot{m}_r$, and Δp) and the h_w for each condenser layer have been provided in Appendix F: Tabular Data for a majority of the experiments involved in the current study. By supplying the raw data in addition to the h_w for each condenser layer, the reader is given the option of recalculating the h_w, should the need or desire arise.

5.1 Verification of the Experimental Data

Before attempting to present any experimental results which are of significance to the performance of multi-layer wire-on-tube condensers exposed to both forced convection and radiation, it may be prudent to first examine the validity of the data acquisition and reduction methods used in determining h_w. Both (i) the long-term repeatability of the data obtained from

the apparatus discussed in Chapter 3 - Experimental Apparatus & Instrumentation and (ii) the comparison of the experimentally determined h_w to previously published results are of particular interest and should serve to establish the credibility of the h_w and Δp obtained.

Swofford (1995) presented heat transfer data obtained from an unconfined single layer condenser (Coil 6) oriented at $\alpha = 90°$ and $\psi = \pi/2$. A similar unconfined condenser (also Coil 6) has since been tested with the same α and ψ using the apparatus of the current investigation. The raw data from both of these cases were then reduced using the method outlined in Chapter 4 - Data Reduction (i.e. Swofford's data was rereduced since η_c was originally not accounted for) and are presented together in Fig. 5.1. As expected, the h_w determined from both data sources are nearly identical, with each set of data following the relation $h_w \propto V^n$ where n ~0.5 (i.e. n = 0.466 for a cylinder in cross flow). The average deviation between the h_w of the two sources at a particular V is approximately 2.7%.

Although the wind tunnel and temperature regulated water circulation system used by Swofford were also used in the experiments of the current investigation, the instrumentation used to acquire the temperature data was not common to both investigations. As a result, a possible explanation for the difference in the calculated h_w could be a direct result of the differences in the accuracies of the instrumentation used by Swofford and that of the current investigation. However, since the deviations appear to be fairly small, especially when $V \geq 0.75$ m/s (2.46 ft/s),

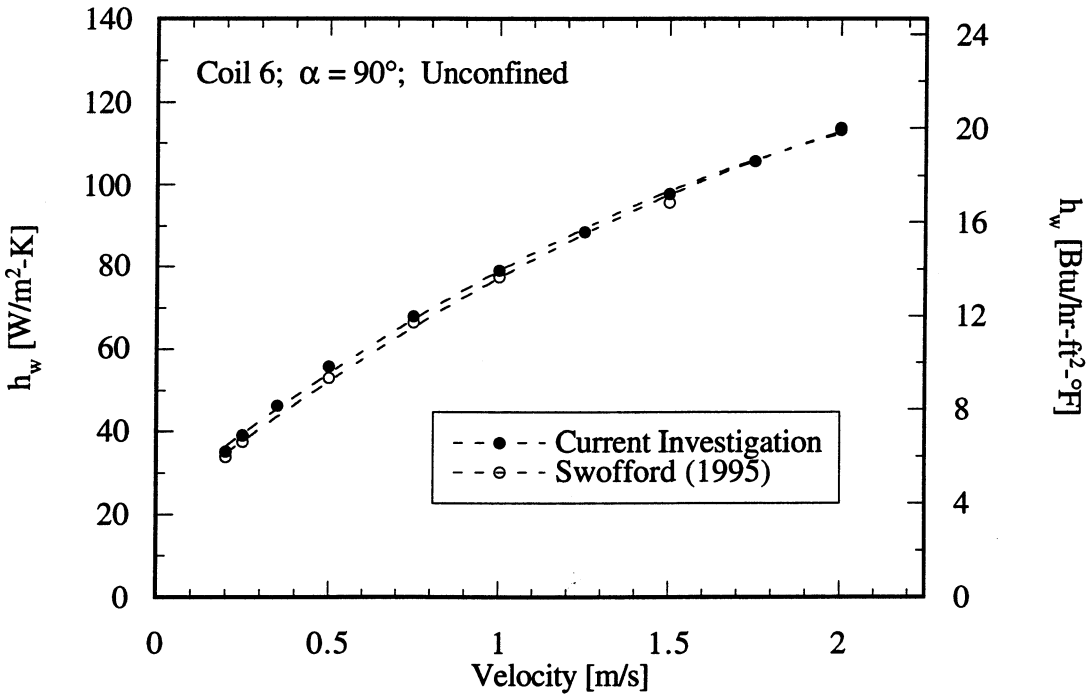

Figure 5.1 Comparison of recently obtained data to that presented by Swofford (1995)

the accuracy of the raw data obtained in the current investigation should be comparable to that associated with the raw data obtained by Swofford.

The long-term repeatability of the h_w obtained in the current investigation is shown in Fig. 5.2 for two different confined single layer condensers, Coils 6 and 8, tested over the course of several months. As can be seen, the data sets for each of the condensers seem to be extremely repeatable, with the deviations between the h_w associated with Coils 6 and 8 averaging 2.1% and 2.3%, respectively. In addition, the h_w for each condenser also appears to follow the $h_w \propto V^n$ relation where n ranges from 0.53 to 0.54. Differences between the magnitudes of the h_w of the two condensers are due strictly to differences in the wire and tube geometry of the condensers and will be discussed in further detail in Section 5.4 - Accounting for Geometric Differences Between Condensers.

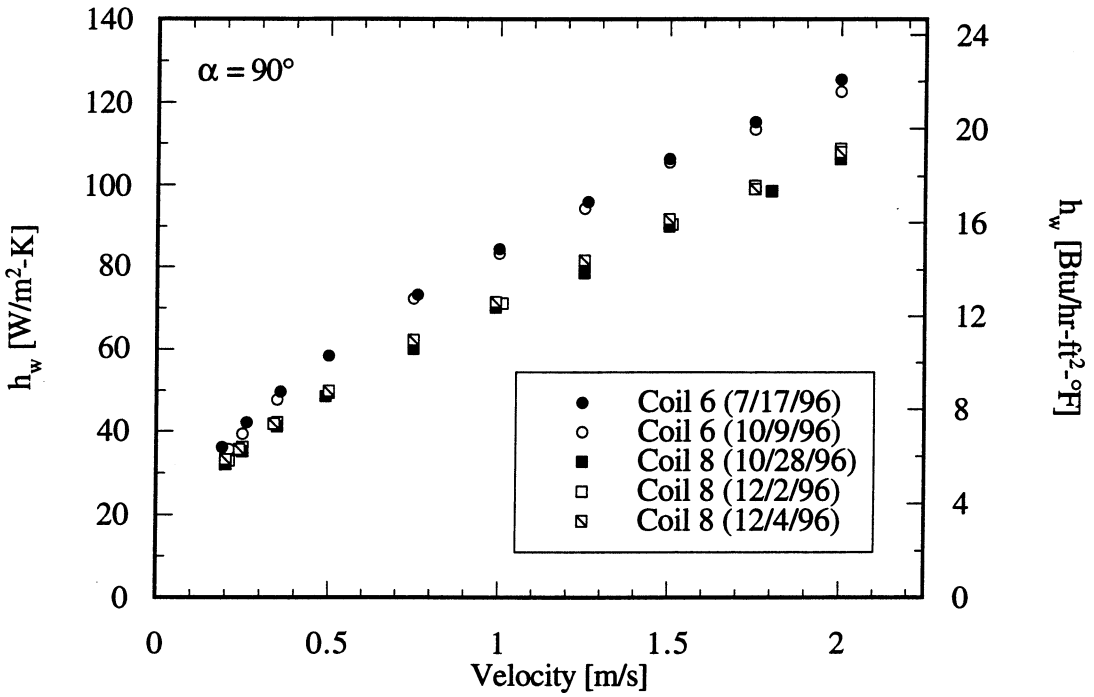

Figure 5.2 Repeatability of the dependence of h_w on V for condensers at $\alpha = 90°$

The repeatability of the Δp measurements can be seen by examining data obtained from both a single layer and a two layer condenser (both Coil 6) over the course of several days (see Fig. 5.3). The average deviation in the Δp measurements from the single layer condenser is nearly 15.1%, while that from the two layer condenser appears to be only 3.1%. This large difference in the average deviation cannot reasonably be explained and, as a result, must offer some insight into the true level of uncertainty in the measurement of Δp. Note, however, that

although the Δp measurements obtained from the single layer condenser deviate an average of 15.1% from one another, the actual difference between the measurements is ≤ 0.309 Pa (0.0012 in H_2O). Since it is known that the condenser fans used in household refrigerators are capable of producing $\Delta p = 10$ Pa (0.04 in H_2O), an uncertainty in the measurement of Δp across the condenser on the order of 0.309 Pa (0.0012 in H_2O) should be easily tolerated.

In addition to illustrating the repeatability of the Δp measurements, Fig. 5.3 also indicates that the Δp from both the single and two layer condensers follow a $\Delta p \propto V^n$ relation where n is slightly less than 2 (i.e. n = 1.8 and 1.7 for the single and two layer condensers, respectively). This Δp-velocity relation is consistent with the fact that $\Delta p \propto V^2 C_D$ where, for a cylinder in cross flow, $C_D \propto Re^{-2/3}$ (White, 1991).

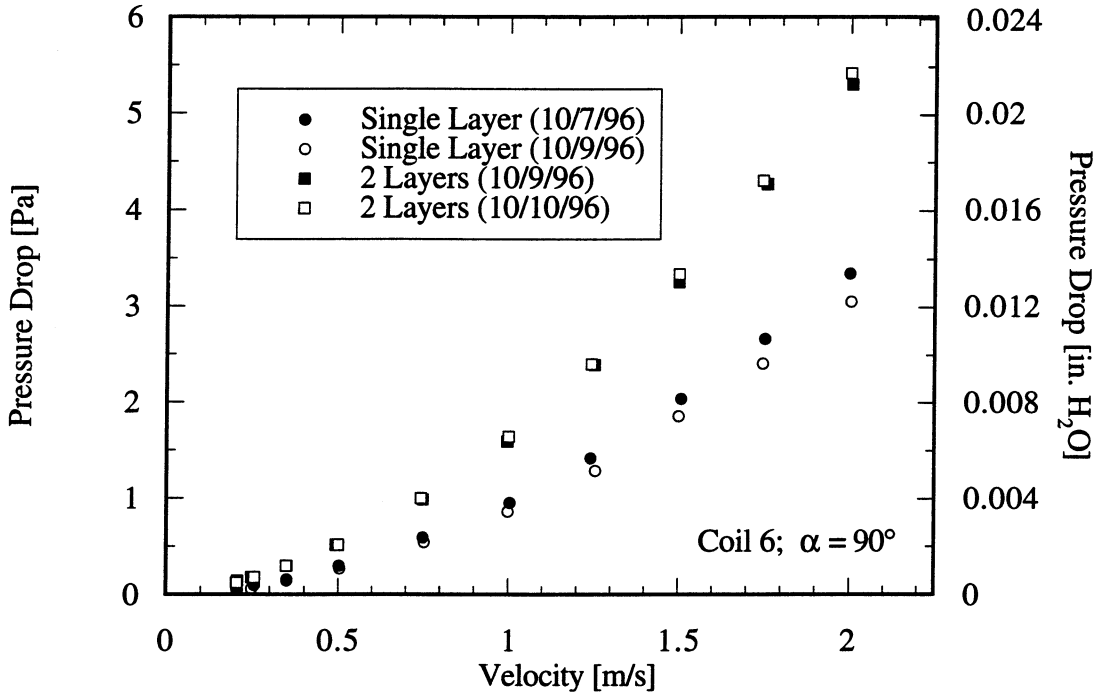

Figure 5.3 Repeatability of the dependence of Δp on V for condensers at $\alpha = 90°$

When oriented vertically (i.e. $\alpha = 90°$) within the wind tunnel test section, both the wires and the tube passes of a particular condenser are situated normal to the horizontally directed air flow. As a result, the convection heat transfer coefficients associated with the wires, h_w, and the tube passes, h_t, should behave similarly to that of cylinders in a cross flow. To confirm this, both the h_w and h_t associated with a confined single layer condenser (Coil 6) are shown in Fig. 5.4 along with the heat transfer coefficients predicted using the correlation developed by Hilpert (1933) for convection heat transfer from a single cylinder in a cross flow (assuming the

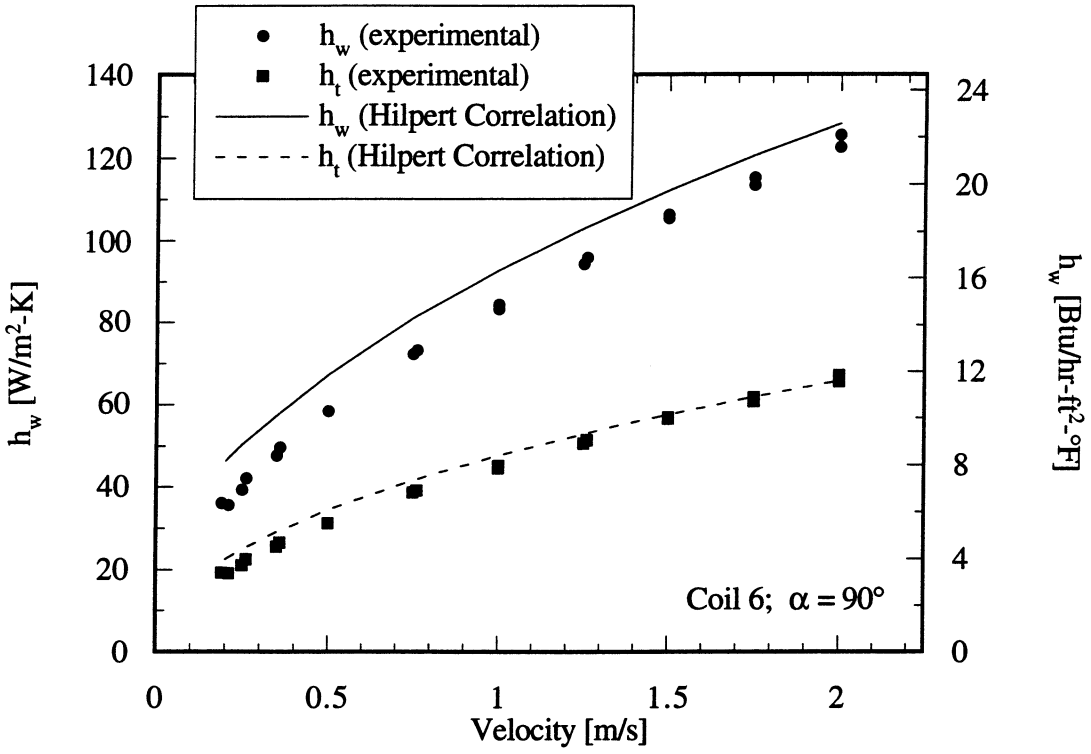

Figure 5.4 Comparison of experimental h_w and h_t to those predicted by the Hilpert Correlation

same D_w and D_t). As can be seen, the experimental and predicted h_t are nearly identical, while the experimental h_w appear to be slightly lower than those predicted by Hilpert's correlation. This difference in the h_w can be readily explained by considering the fact that the experimental h_w are heat transfer coefficients averaged over the wires located on both sides of the condenser tube passes. At $\alpha = 90°$, certain regions of the condenser wires fall directly downstream of the

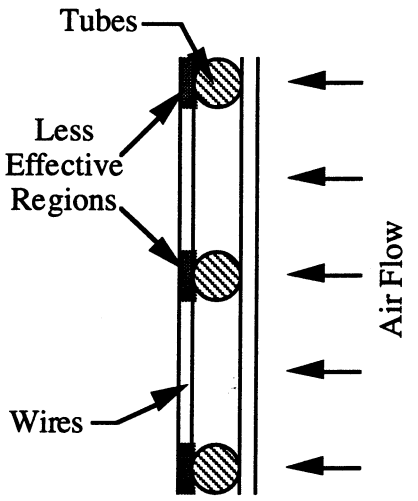

Figure 5.5 Wire regions directly downstream of the tube passes

condenser tube passes, as shown in Fig. 5.5. As a result, these regions experience air temperatures that are significantly higher than those experienced by the rest of the wires. This causes the convection heat transfer rate from the downstream wire regions to decrease, thereby decreasing the average h_w.

5.2 Effect of the Number and Spacing of Condenser Layers on Performance

The h_w as a function of V associated with each layer of a particular confined four-layer wire-on-tube condenser (Coil 6) at $\alpha = 90°$ are shown in Fig. 5.6. As can be seen, the h_w of individual condenser layers appear to be nearly independent of layer placement within the multi-layer condenser. That is, the h_w associated with the first layer are nearly the same as those of the second layer, and so on. The average absolute deviation between the h_w associated with each layer is approximately 3.9%, while the average RMS deviation is slightly higher at 4.7%.

The data shown in Fig. 5.6 were obtained from a condenser placed in an overall counter flow configuration (i.e. with the condenser fluid flowing in the opposite direction of the air flow). Further experiments involving multi-layer condensers placed in overall parallel flow configurations (i.e. with the condenser fluid flowing in the same direction as the air) also indicate that the h_w for individual layers are nearly independent of layer placement. In addition, multi-layer condensers with both two and three layers were also tested at $\alpha = 90°$, with the centerline-

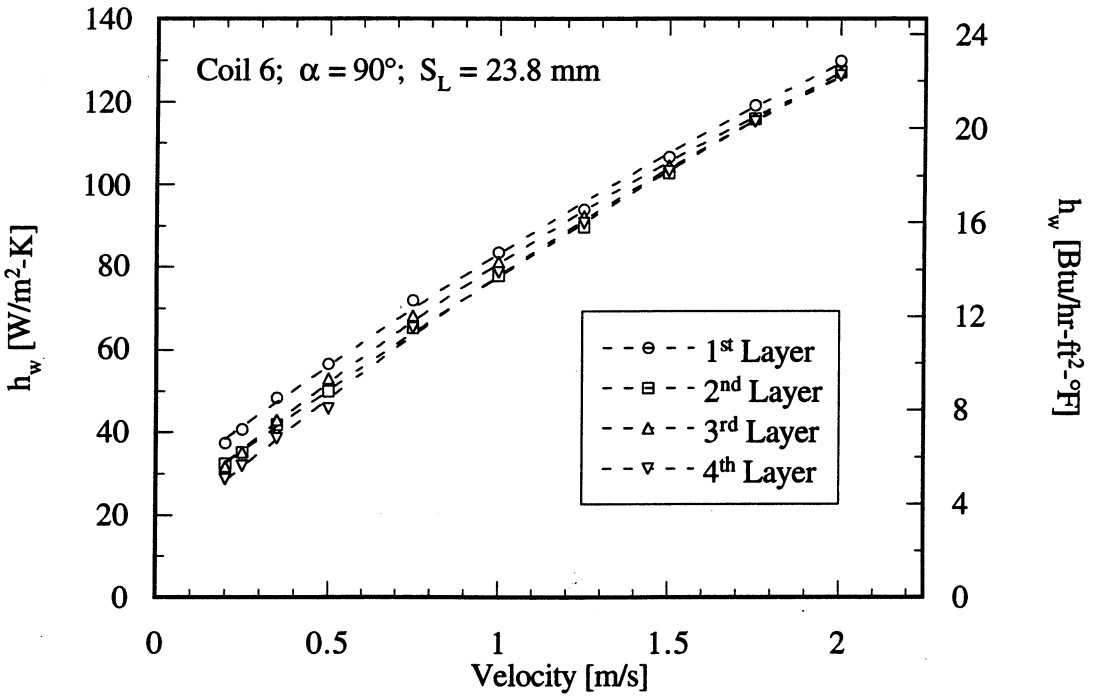

Figure 5.6 h_w vs. V for each layer of a four-layer condenser at $\alpha = 90°$

to-centerline spacing between condenser layers, S_L, kept constant at 23.8 mm (0.937 in). As anticipated, the h_w obtained from these experiments were nearly identical to those obtained from the four-layer condenser. This verifies the expectation that the presence of downstream condenser layers has no effect on the h_w associated with condenser layers upstream. This finding, along with the fact that h_w is nearly independent of layer placement implies that the heat transfer performance of multi-layer condensers can be studied without considering the differences between both (i) the h_w associated with the individual layers of a particular multi-layer condenser and (ii) the h_w associated with multi-layer condensers with different N_L.

The Δp obtained from several confined multi-layer condensers (each Coil 6) with each composed of a different number of condenser layers ($1 \leq N_L \leq 4$) at $\alpha = 90°$ are shown in Fig. 5.7. As can be seen, Δp appears to be almost linearly dependent on N_L, since the differences between the Δp associated with the three- and four-layer condensers are approximately the same as the differences between the Δp associated with the two- and three-layer condensers, and so on. This $\Delta p \propto N_L$ relation further reinforces the fact that the performance of multi-layer condensers can be evaluated without considering N_L, allowing the Δp (in addition to the N_L independent h_w) obtained from multi-layer condensers with a particular N_L to be applied to condensers composed of any N_L (given the same wire and tube geometry).

Note that the magnitudes of the Δp shown in Fig. 5.7, at V as high as 2.0 m/s (6.56 ft/s),

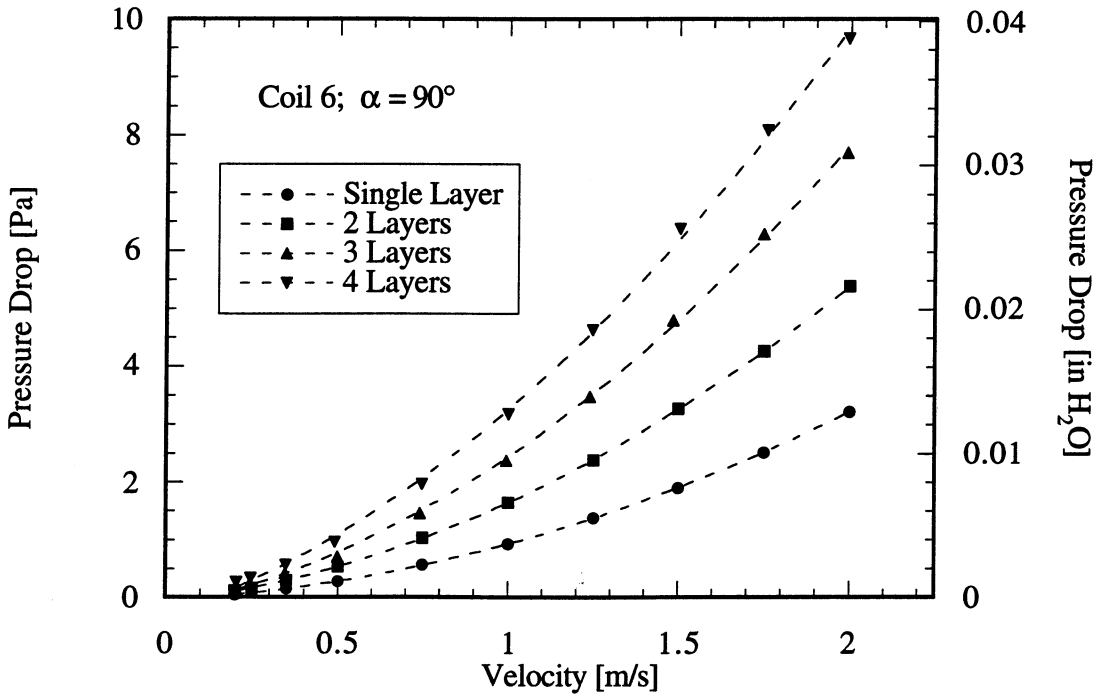

Figure 5.7 Δp vs. V for multi-layer condensers with $\alpha = 90°$ and varying N_L

are each less than the $\Delta p = 10$ Pa (0.040 in H_2O) that household refrigerator condenser fans are capable of producing. This comparison indicates that multi-layer condensers with at least four layers at $\alpha = 90°$ are compatible for use within current household refrigerators.

The effect of the centerline-to-centerline spacing, S_L, between consecutive condenser layers on the h_w associated with each layer of a confined two-layer wire-on-tube condenser was determined by examining condensers (each Coil 6) with nine different S_L, ranging from 16.3 mm (0.642 in) to 76.1 mm (2.99 in). As expected, the h_w associated with the first layer of each condenser were nearly identical, with an average absolute deviation of 1.3% and an average RMS deviation of 1.6%. The h_w associated with the second layer of each condenser varied slightly, however, with the average absolute and average RMS deviations increasing to 2.8% and 3.4%, respectively.

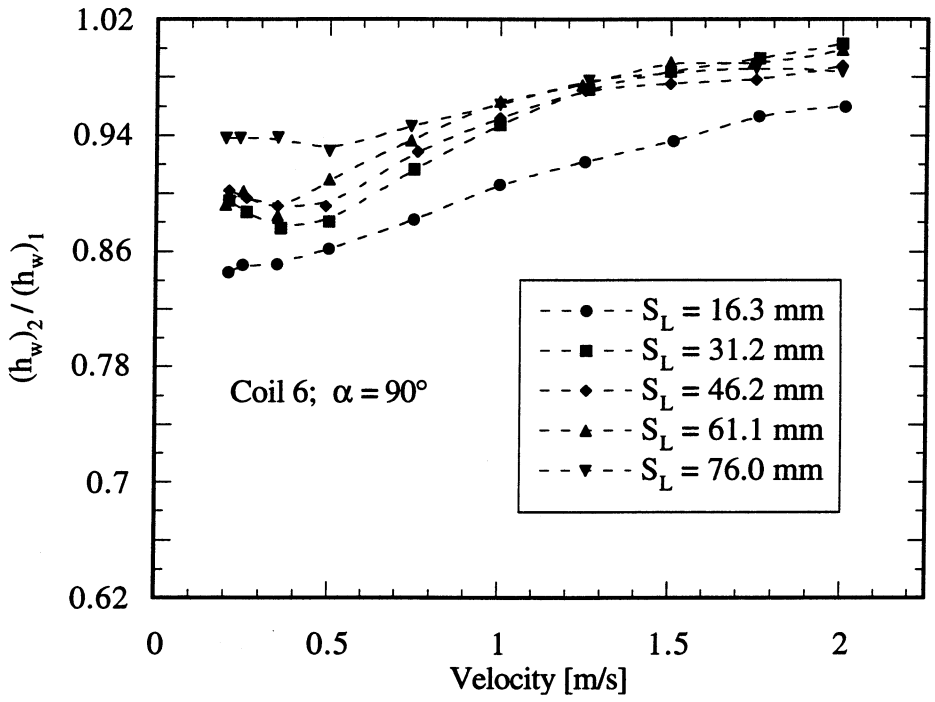

Figure 5.8 Effect of V on the ratio $^{(hw)2}/_{(hw)1}$ for two-layer condensers at $\alpha = 90°$

Figure 5.8 shows the ratio of the h_w associated with the second layer of a confined two-layer wire-on-tube condenser (Coil 6) to those of the first layer, $^{(hw)2}/_{(hw)1}$, as a function of V for several S_L. In each case, $^{(hw)2}/_{(hw)1}$ appears to be lowest when $V \leq 0.5$ m/s (1.64 ft/s) and increases with increasing V to about 1.0 (for certain S_L, $^{(hw)2}/_{(hw)1}$ actually exceeds 1.0). Most of the $^{(hw)2}/_{(hw)1}$ shown for $V \geq 0.5$ m/s (1.64 ft/s) appear to fall between 0.9 and 1.0, indicating that neither V nor S_L have a significant effect on $^{(hw)2}/_{(hw)1}$.

It is important to note that although some of the differences in the $(h_w)_2/(h_w)_1$ data shown in Fig. 5.8 appear to be dramatic, the y-axis scale only spans from 0.62 to 1.02. This causes differences in the data to appear exaggerated (by approximately 250%), allowing small differences in the data to be observed.

The same set of experimental data used in Fig. 5.8 are also presented in Fig. 5.9, with $(h_w)_2/(h_w)_1$ plotted as a function of S_L for several V. In general, $(h_w)_2/(h_w)_1$ increases with increasing S_L, and the rate at which $(h_w)_2/(h_w)_1$ increases seems decrease with increasing V. Again, the y-axis scale used in Fig. 5.9 (which also spans from 0.62 to 1.02) exaggerates the differences in the magnitudes of $(h_w)_2/(h_w)_1$. The rate of change of $(h_w)_2/(h_w)_1$ with S_L is actually minimal for $S_L \geq 31.2$ mm (1.23 in). The implies that the S_L of a particular multi-layer wire-on-tube condenser should have little effect on the h_w associated with downstream condenser layers, provided that $S_L \geq 31.2$ mm (1.23 in).

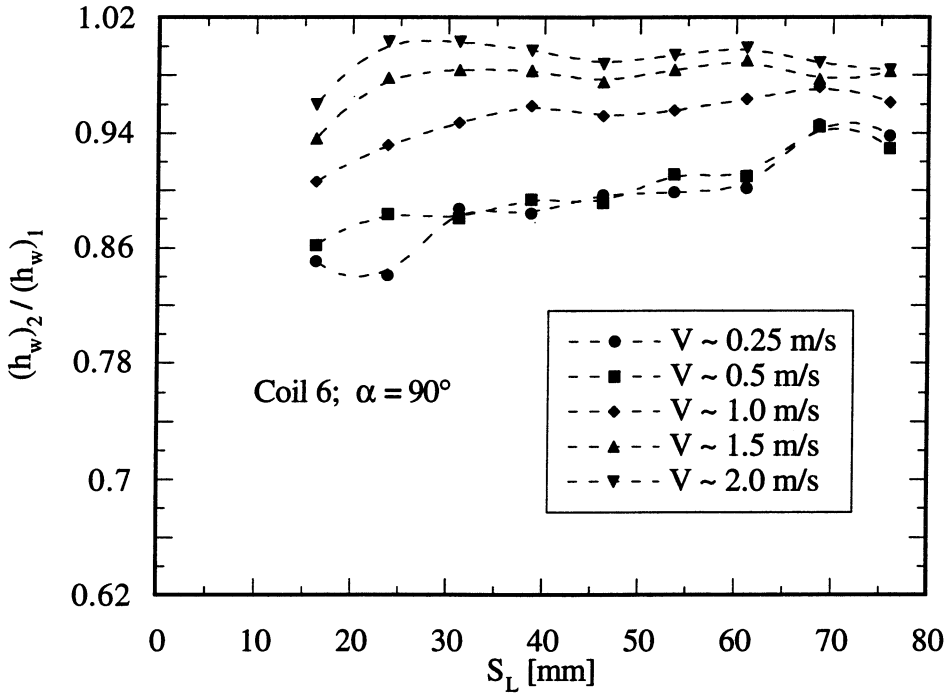

Figure 5.9 Effect of S_L on the ratio $(h_w)_2/(h_w)_1$ for two-layer condensers at $\alpha = 90°$

5.3 Effect of Angle-of-Attack and Orientation on Condenser Performance

Previously published results of Hoke (1995) and Swofford (1995) indicate that the h_w associated with unconfined single layer condensers are highly dependent on both α and ψ. Unfortunately, since each of the multi-layer wire-on-tube condensers involved in the current investigation are composed of condenser layers which are confined, trends observed between h_w

and both α and ψ by Hoke and Swofford are of limited utility. As a result, a series of experiments have since been performed to determine the effects of α and ψ on both the h_w and Δp associated with confined condensers.

Due to the fact that h_w is nearly independent of layer placement (see Section 5.2 - Effect of the Number and Spacing of Condenser Layers on Performance), only the h_w averaged over all of the layers of each condenser will be considered for the remainder of this section and in the following two sections. In addition, since h_w and N_L are also independent of one another, N_L is inconsequential to the determination of the condenser averaged h_w and, as a result, may not be specified on certain data plots.

Since the dependence of h_w and Δp on α and ψ are similar for condensers with different wire and tube geometries, only the data obtained from Coil 6 are presented graphically in this section. Matching plots illustrating the α and ψ dependence of the h_w and Δp obtained from Coils 8, 9, and 10 can be found in Appendix G: Additional Heat Transfer & Pressure Drop Plots.

The h_w as a function of α for a particular confined, multi-layer, wire-on-tube condenser, Coil 6, are shown (as solid symbols) for several different V in Fig. 5.10, for the case where the air flow is perpendicular to the condenser wires ($\psi = 0$). For comparison purposes, the h_w vs. α ($\psi = 0$) obtained by Swofford from an unconfined single layer condenser (also Coil 6) are also shown (as open symbols) in Fig. 5.10. As expected, the h_w associated with the confined condenser are greater than those associated with the unconfined condenser for almost any combination of V and α shown. The difference between the h_w reaches a maximum at $V = 2.0$ m/s (6.56 ft/s) and $\alpha = 45°$, where the confined condenser performs up to 23% better than the unconfined condenser.

The h_w associated with the confined condenser (Coil 6) decreases with increasing α. This is contrary to the direct relationship between h_w and α shown at $\psi = 0$ for the unconfined condenser. Both this discrepancy and the increase in performance between confined and unconfined condensers can be explained by the fact that the air velocities experienced by the condensers are not equal to V. That is, the wire and tube matrix of a particular confined condenser actually occupies a large portion of the cross-sectional area of the test section in which the condenser is situated. Since the flow area in the vicinity of the confined condenser is significantly lower than that upstream of the condenser, the air velocity in the vicinity of the condenser must increase (due to conservation of mass). The velocity experienced by the wire and tube matrix of a particular unconfined condenser, on-the-other-hand, is actually lower than V since some of the air is allowed to flow around and/or through the tube bends of the condenser.

The same inverse relationship between h_w and α is also observed for Coils 8, 9, and 10 at $\psi = 0$ (see Fig. G.1, G.8, and G.15). Unfortunately, since no corresponding experimental h_w data are available for unconfined condensers within the desired α range, comparisons of the confined

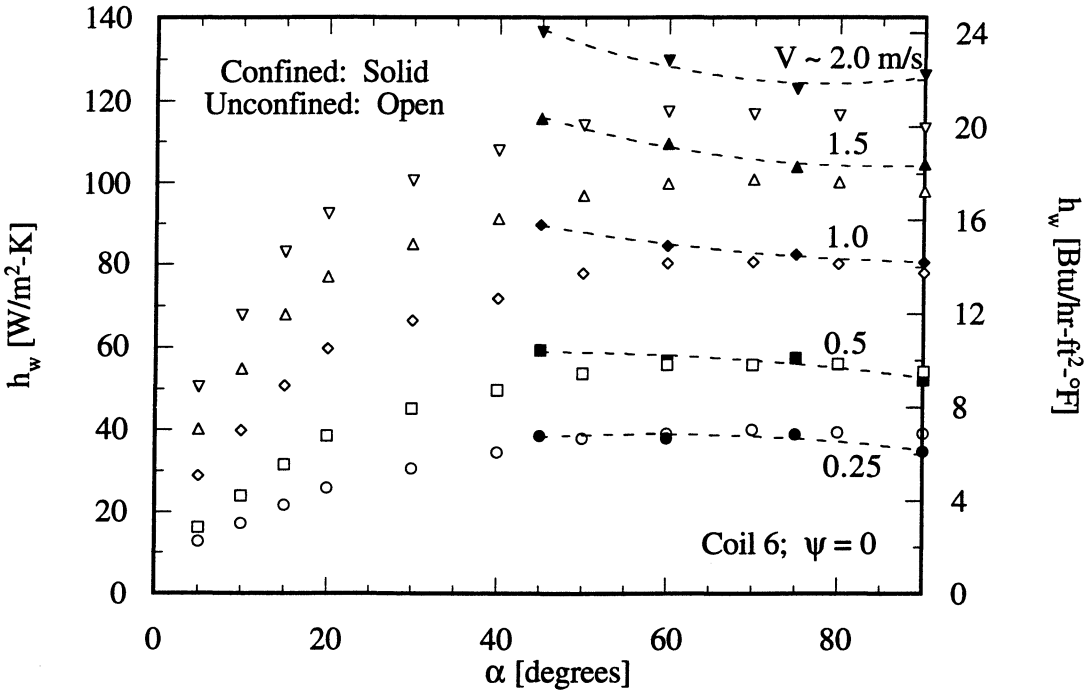

Figure 5.10 Effect of confinement on h_w for a condenser with air flow $\perp$ to the wires

and unconfined performance of these condensers cannot be made.

Both the Nu_w and $Re_{w,max}$ associated with the experimental data were calculated for each of the confined condensers at $\psi = 0$. For each dimensionless parameter, the D_w associated with the condenser involved in the particular experiment was used as the characteristic length. In order to account for the effect of the increase in velocity near the condenser, $Re_{w,max}$ is based on the maximum fluid velocity, V_{max}, where V_{max} is defined the average velocity of the air passing through the minimum flow area. The minimum flow area was determined by subtracting the frontal projected area of a single set of wires (i.e. the wires on one side of a condenser layer) and the tube passes of a particular condenser layer from the cross-sectional area of the test section. The resulting explicit relation for V_{max} in terms of V is

$$V_{max} = \left(\frac{H_{duct}}{H_{duct} - N_t D_t}\right)\left(\frac{W_{duct}}{W_{duct} - (1/2)N_w D_w}\right)V \qquad (5.1)$$

where H_{duct} and W_{duct} are the height and width of the test section, respectively. Ratios of V_{max} over V have been provided in Table 5.1 for Coils 6, 8, 9, and 10 at various α ($\psi = 0$).

As is done in the case of fluid flow over tube banks, only a single set of wires was used in

Table 5.1 V_{max}/V for Condensers at $\psi = 0$

α [degrees]	Coil 6	Coil 8	Coil 9	Coil 10
45	1.754	1.704	1.772	2.102
60	1.652	1.552	1.665	1.849
75	1.601	1.492	1.606	1.752
90	1.586	1.474	1.592	1.728

the calculation of V_{max} instead of both wire sets. This is due primarily to the fact that local regions of the air stream are required to simultaneously flow around both a single set of wires and the tube passes of a particular condenser in the regions where the wires and tube passes are welded together. As a result, V_{max} is influenced by the presence of a single set of wires and the tube passes.

The Nu_w and $Re_{w,max}$ corresponding to the data in Fig. 5.10 are shown in Fig. 5.11 for various α. As can be seen, the Nu_w-$Re_{w,max}$ relations associated with Coil 6 appear to be at each α. This is not surprising, since the wires of the condensers, which account for both an overwhelming majority of the surface area and a significant portion of the convection heat

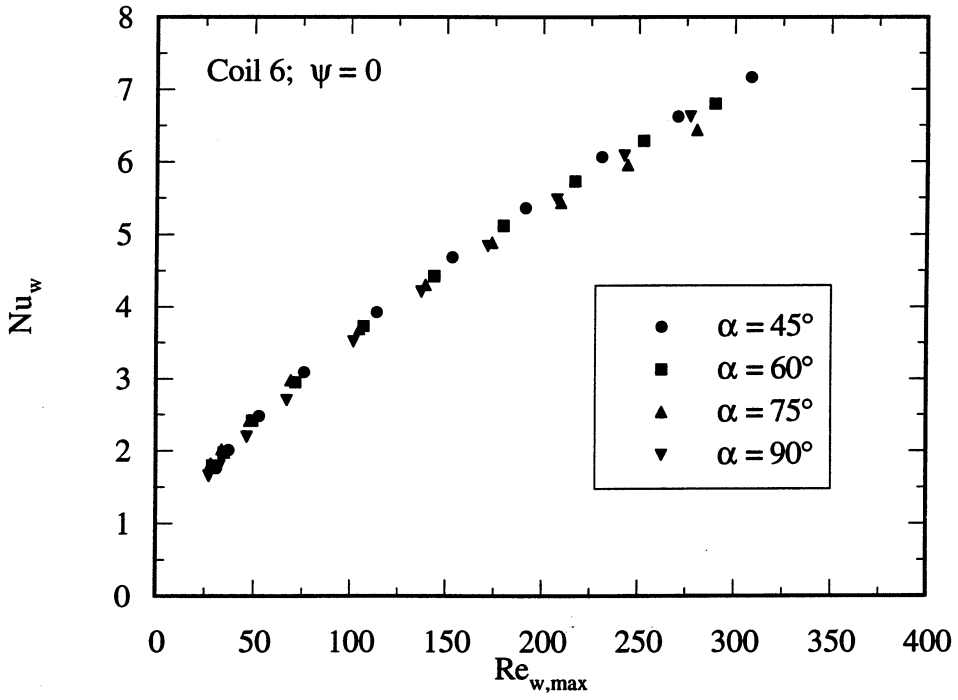

Figure 5.11 Nu_w vs. $Re_{w,max}$ for Coil 6 with air flow ⊥ to the wires

transfer rate, are, at all times, perpendicular to the air flow when $\psi = 0$. As a result, the Nu_w-$Re_{w,max}$ relations for condensers at $\psi = 0$ should be similar, regardless of α.

The corresponding Nu_w and $Re_{w,max}$ obtained from confined condensers (Coils 8, 9, and 10) at $\psi = 0$ (see Fig. G.2, G.9, and G.16) reveal that the Nu_w-$Re_{w,max}$ relations are not independent of α for all wire and tube geometries. The Nu_w of Coils 8 and 9 appear to be inversely related to α, increasing slightly with decreasing α. The Nu_w of Coil 10, on-the-other-hand, appear to be even less dependent of α than those of Coil 6. Upon close inspection of the wire and tube geometries, both Coils 8 and 9 are found to have the largest centerline-to-centerline spacing between consecutive wires, S_w (Coils 8 and 9) = 6.34 mm (0.250 in), while Coil 10 has the smallest, S_w (Coil 10) = 5.08 mm (0.200 in). Although a logical explanation cannot be offered at this time to support this positive correlation between S_w and the degree to which Nu_w is influenced by α ($\psi = 0$), it is important to note that only four different wire and tube geometries have been examined in the current investigation, two of which have identical S_w. Consequently, further testing of geometries which span a wider range of S_w is necessary in order to determine the influence of S_w.

The pressure drops, Δp, per condenser layer obtained from Coil 6 are shown as a function of α ($\psi = 0$) in Fig. 5.12 for various V. As can be seen, the Δp obtained at $\alpha < 90°$ are

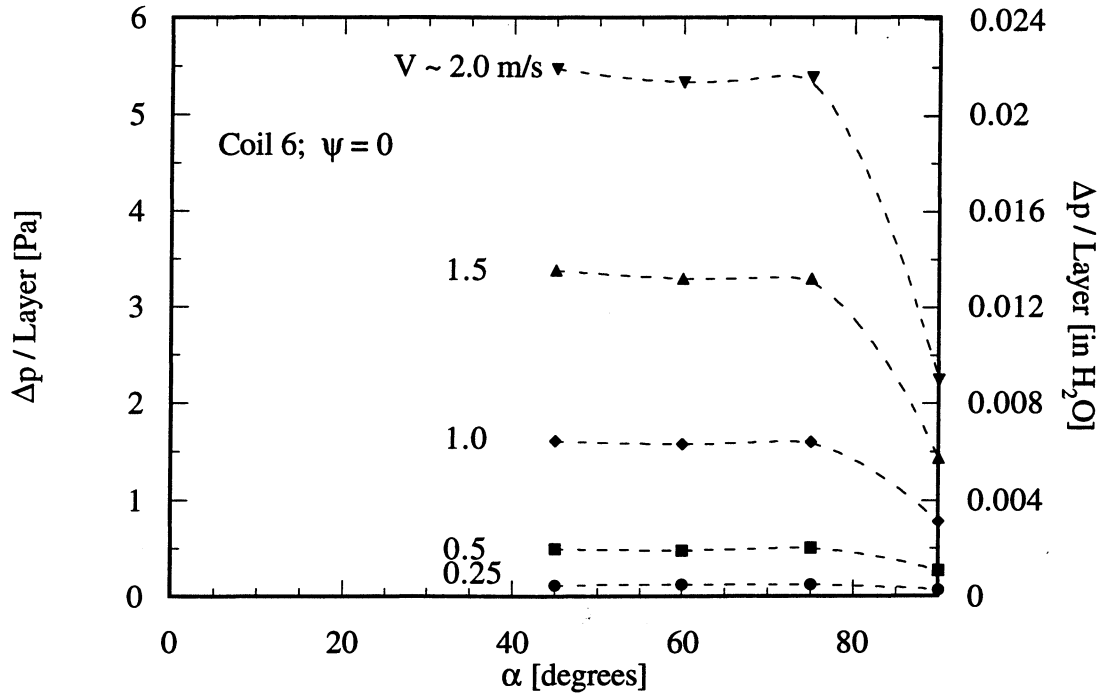

Figure 5.12 Δp per layer vs. α for Coil 6 with air flow $\perp$ to the wires

significantly greater than those obtained at $\alpha = 90°$. The Δp is greatest at V = 2.0 m/s (6.56 ft/s) and $\alpha = 45°$, where it is 145% greater than the Δp obtained from Coil 6 at V = 2.0 m/s (6.56 ft/s) and $\alpha = 90°$.

Similar findings about the α dependence ($\psi = 0$) of the Δp per condenser layer have also been observed for Coils 8, 9, and 10 (see Fig. G.3, G.10, and G.17). A key difference that exists amongst the Δp data associated with each of the condensers (Coils 6, 8, 9, and 10) is that of the α at which Δp is greatest. In the case of Coil 6, the maximum Δp occurs at $\alpha = 45°$, while for Coils 8, 9, and 10, the maximum Δp occur at $\alpha = 60°$.

This variation in the α ($\psi = 0$) at which the Δp per condenser layer reaches a maximum might be explained by noting that Δp is a function of several quantities which include:

1. The velocity of the air, V_{max}, to which the wire and tube matrix of the condenser is exposed. The magnitude of V_{max} increases with decreasing α and is also dependent on the wire and tube geometry of the condenser.

2. The drag coefficient, C_D, associated with the combination of the wires and tube passes of the condenser. Although an exact method for determining the C_D associated with flow through wire-on-tube condensers has yet to be determined, it can clearly be concluded that the magnitude of C_D is lower for condensers at α where one set of condenser wires (i.e. the wires on one side of the condenser layer) falls in-line along the path of the air flow with the other set of wires. Cross-sectional views of each condenser are shown in Fig. 5.13 for various α ($\psi = 0$). As can be seen, for certain condenser-α combinations, the wires of on one side of the condenser fall in-line with the other wires, decreasing both C_D and Δp.

The fact that Δp is a function of several quantities, which are each dependent on vastly different parameters, should account for the fact that a variation in the α ($\psi = 0$) at which Δp is greatest exists. However, without first acquiring a greater knowledge of the C_D associated with each condenser at each α, any attempt at explaining the exact reasons for each of the variations in the Δp data would be pointless.

The h_w associated with a particular confined, multi-layer, wire-on-tube condenser (Coil 6) are shown (as solid symbols) for several different V in Fig. 5.14 as a function of α, for the case where the air flow is perpendicular to the condenser tube passes, $\psi = \pi/2$. As in the case of Fig. 5.10, the h_w vs. α ($\psi = \pi/2$) obtained by Swofford from an unconfined single layer condenser (also Coil 6) are also shown (as open symbols), in Fig. 5.14, for comparison purposes. Again, the h_w associated with the confined condenser are greater than those associated with the unconfined condenser for almost any combination of V and α ($\psi = \pi/2$) shown. The difference between the h_w also reaches a maximum at V = 2.0 m/s (6.56 ft/s) and $\alpha = 45°$ ($\psi = \pi/2$), where the h_w associated with the confined condenser is 11% greater than that of the unconfined condenser. As in the case where $\psi = 0$, this increase in performance between confined and unconfined condensers at $\psi = \pi/2$ can also be explained by noting that the air velocity

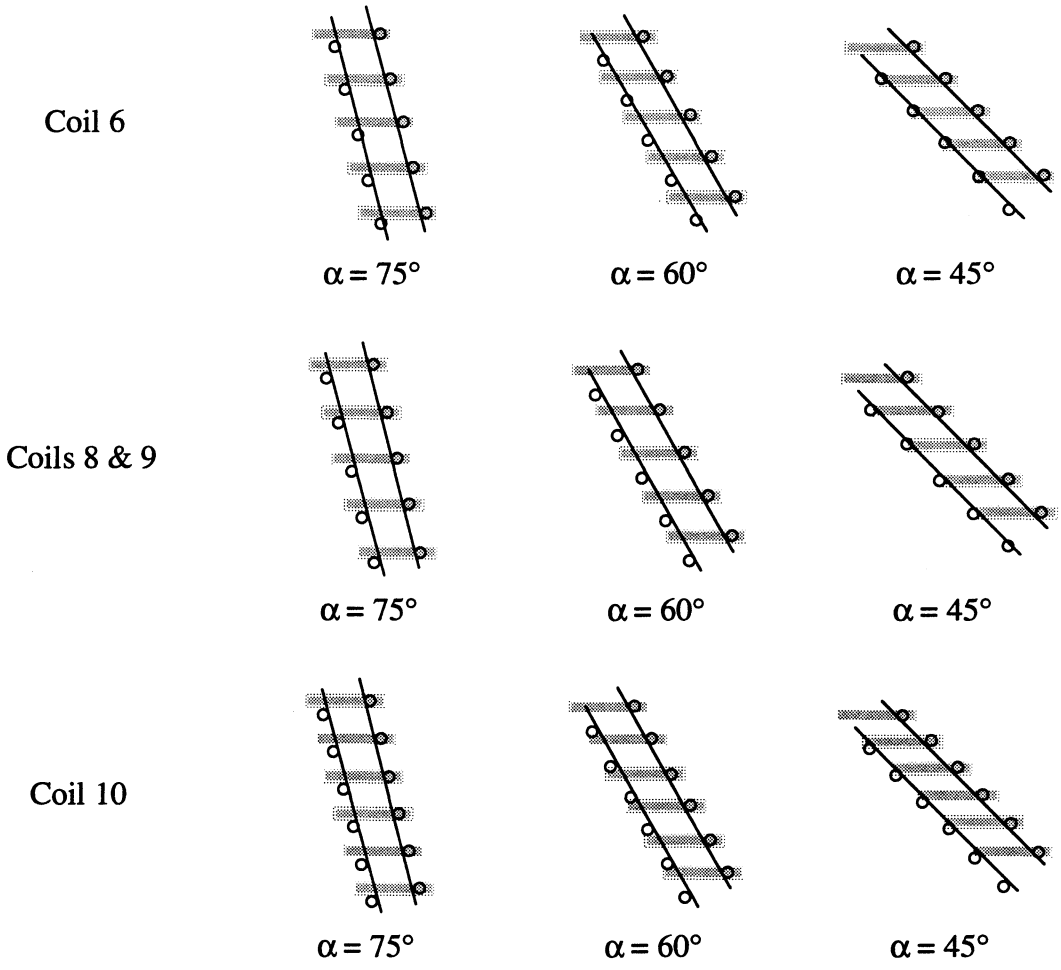

Figure 5.13 Cross-sectional views of each condenser for various α with air flow $\perp$ to the wires

experienced by the condensers is not equal to V.

Unlike the case where $\psi = 0$, the h_w associated with Coil 6 at $\psi = \pi/2$ appear to increase with increasing α. This agrees with the trend observed for h_w and α shown for the unconfined condenser at $\psi = \pi/2$. Similar direct relationships between h_w and α are also observed for Coils 8, 9, and 10 at $\psi = \pi/2$ (see Fig. G.4, G.11, and G.18). Again, since no corresponding experimental h_w data are available for unconfined condensers (Coils 8, 9, and 10) within the desired α range, comparisons of the confined and unconfined performance of these condensers cannot be made.

The Nu_w and $Re_{w,max}$ corresponding to the experimental h_w data ($\psi = \pi/2$) are also calculated using D_w as the characteristic length and velocity V_{max}. Ratios of V_{max} over V are shown in Table 5.2 for Coils 6, 8, 9, and 10 at various α. Figure 5.15 shows Nu_w as a function of $Re_{w,max}$ for a particular confined multi-layer condenser (Coil 6) for various α at $\psi = \pi/2$. As can be seen, the Nu_w vs. $Re_{w,max}$ data for each α do not follow a single Nu_w-$Re_{w,max}$ relation as

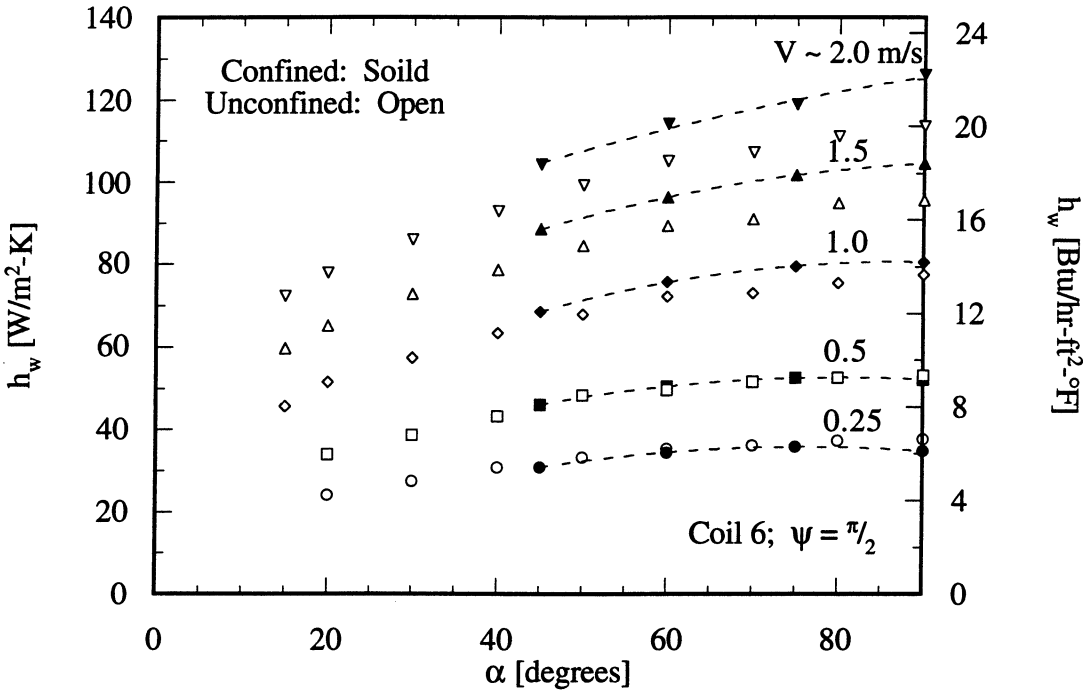

Figure 5.14 Effect of confinement on h_w for a condenser with air flow $\perp$ to the tube passes

did the Nu_w vs. $Re_{w,max}$ data associated with a few of the condensers at $\psi = 0$. This variation amongst the Nu_w-$Re_{w,max}$ relationships associated with condensers at different α ($\psi = \pi/2$) can be attributed to the fact that the wires of these condensers are not all at the same angle with respect to the air flow. The resulting Nu_w-$Re_{w,max}$ relations should, therefore, be different for condensers at different α. Corresponding plots of the Nu_w vs. $Re_{w,max}$ data obtained from Coils 8, 9, and 10 at $\psi = \pi/2$ (see Fig. G.5, G.12, and G.19) also indicate that the Nu_w-$Re_{w,max}$ relations for confined condensers vary as a function of α when $\psi = \pi/2$.

The pressure drops, Δp, per condenser layer obtained from Coil 6 at $\psi = \pi/2$ are shown in Fig. 5.16 as a function of α for various V. As can be seen, the Δp obtained from the condensers

Table 5.2 V_{max}/V for Condensers at $\psi = \pi/2$

α [degrees]	Coil 6	Coil 8	Coil 9	Coil 10
45	1.739	1.536	1.711	1.858
60	1.643	1.499	1.636	1.775
75	1.600	1.481	1.602	1.738
90	1.586	1.474	1.592	1.728

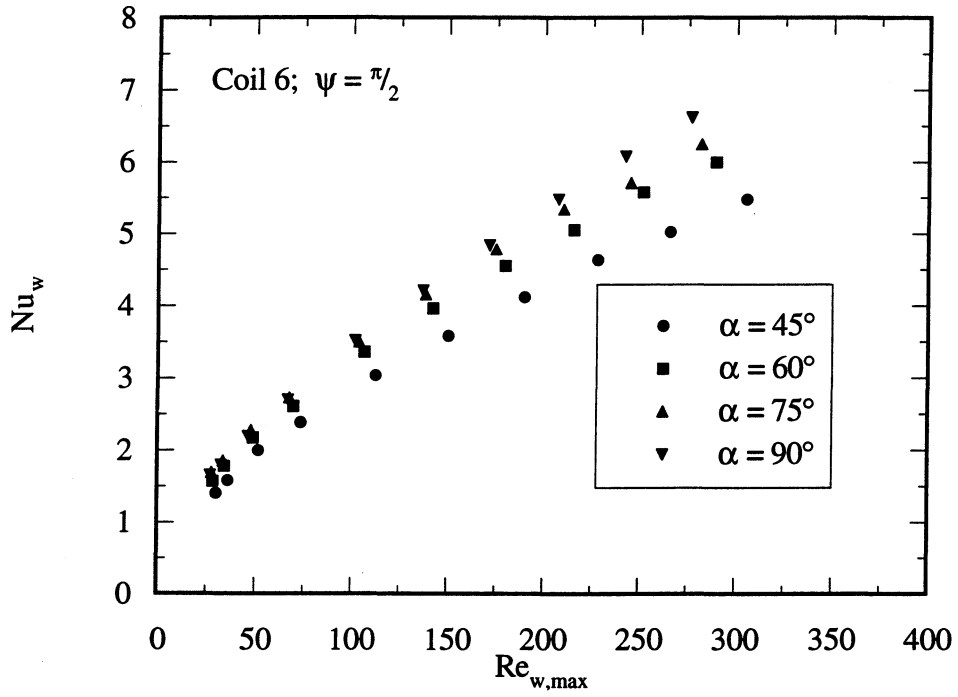

Figure 5.15 Nu_w vs. $Re_{w,max}$ for Coil 6 with air flow ⊥ to the tube passes

at $\alpha < 90°$ are 2.8% to 32.6% lower in magnitude to those obtained from the condenser at $\alpha = 90°$. In addition, the magnitudes of the Δp shown in Fig. 5.16 are each less than the Δp that household refrigerator condenser fans are capable of producing, $\Delta p = 10$ Pa (0.040 in H_2O). Consequently, as in the case of condensers at $\alpha = 90°$, this comparison indicates that multi-layer condensers with at least four layers at $\psi = \pi/2$ are compatible for use within current household refrigerators. Figures G.6, G.13, and G.20 each indicate similar results concerning the α dependence ($\psi = \pi/2$) of the Δp per condenser layer for Coil 8, 9, and 10.

By examining the h_w vs. α data from both Fig. 5.10 and 5.14, one might conclude that multi-layer condensers situated with their wires perpendicular to the air flow (i.e. $\psi = 0$) perform significantly better (i.e. have higher h_w) than those situated with their tube passes perpendicular to the air flow (i.e. $\psi = \pi/2$). This is true only if the h_w of the $\psi = 0$ and $\psi = \pi/2$ cases are compared at the same V and α. However, the magnitude of V is highly dependent on the Δp associated with the air flowing through the condensers. Figure 5.17 shows the ratios of the h_w associated with both of the $\psi = 0$ and the $\psi = \pi/2$ cases, $(h_w)_{\psi=0}/(h_w)_{\psi=\pi/2}$, in addition to the ratios of the Δp obtained from both the ψ orientations, $(\Delta p)_{\psi=0}/(\Delta p)_{\psi=\pi/2}$, for Coil 6, as functions of α for various V. As can be seen, the h_w at $\psi = 0$ are greater than those at $\psi = \pi/2$ by as much as 31%. The ratios of the Δp, however, are much larger in magnitude, with the Δp obtained at $\psi = 0$

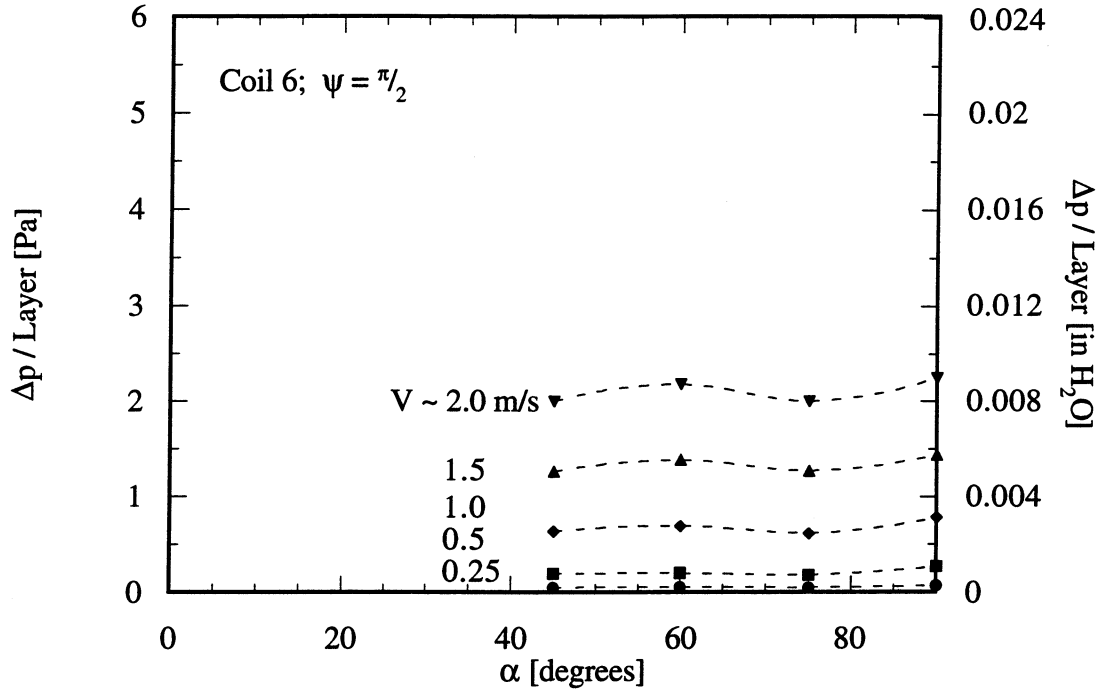

Figure 5.16 Δp per layer vs. α for Coil 6 with air flow ⊥ to the tube passes

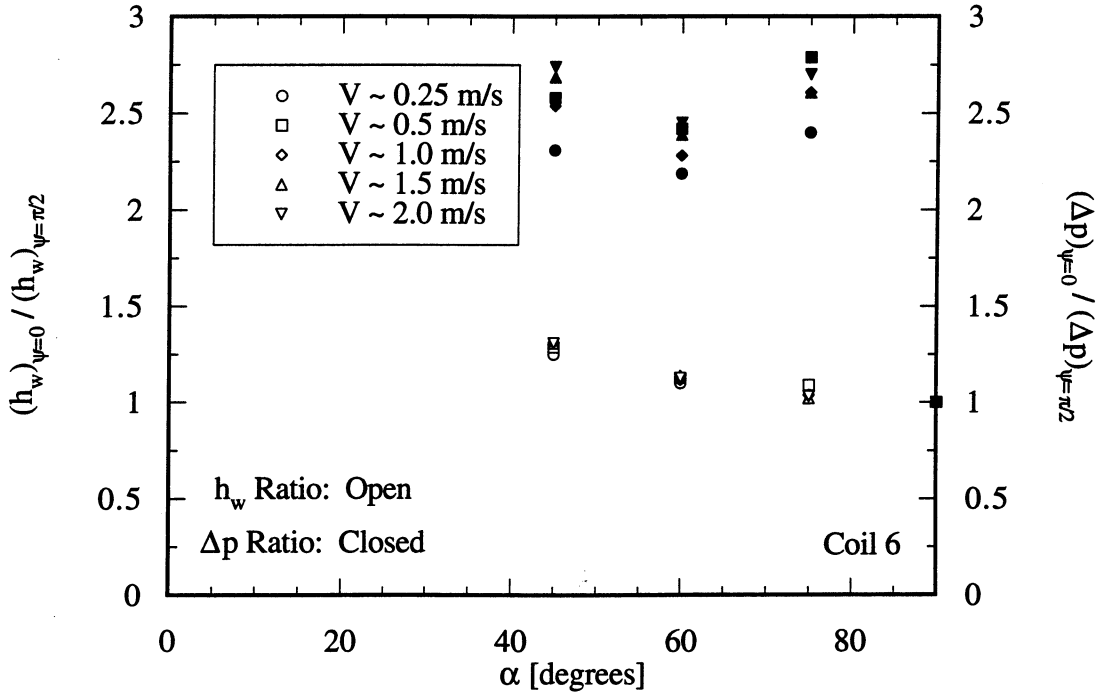

Figure 5.17 Comparison of the h_w and Δp per layer of Coil 6 at $\psi = 0$ and $\psi = \pi/2$

greater than those obtained at $\psi = \pi/2$ by up to 179%. Corresponding plots involving Coils 8, 9, and 10 (see Fig. G.7, G.14, and G.21) also display the same trends, with the percent difference in the h_w associated with both ψ orientations always significantly lower than the percent difference in the Δp obtained from both the ψ orientations. Each of these plots comparing the relative performance of condensers at different ψ illustrate that although the h_w associated with the $\psi = 0$ case are greater than those associated with the $\psi = \pi/2$ case (at the same V and α), condensers situated at $\psi = \pi/2$ actually have a better overall performance than those situated at $\psi = 0$.

5.4 Accounting for Geometric Differences Between Condensers

One of the major complications currently preventing the performance of wire-on-tube condensers from being optimized is the fact that these condensers have several different geometric parameters (i.e. D_w, S_w, D_t, and S_t), each of which has the potential to alter the condenser's relative performance. Note, however, that only a few of these parameters are of particular interest to the current investigation. Since the outer diameter of the condenser tube passes, D_t, is approximately the same for the condensers found in most household refrigerators, there is no immediate need to study D_t extensively. In addition, a large portion of the effects of the centerline-to-centerline spacing between consecutive condenser tube passes, S_t, on the heat transfer performance of condensers are accounted for through the use of η_w in the definition of h_w. As a result, it is hypothesized that the remaining influence of S_t on h_w is small. The effects of the two remaining parameters, D_w and S_w, on both h_w and Δp can be gauged by examining the data obtained from condensers composed of four different wire and tube geometries. Each condenser was subjected to the same set of experiments over the course of the investigation in order to yield comparable data.

The trends in both the h_w and Δp data as functions of V and condenser geometry appear to be similar for condensers at different α and ψ. As a result, only the data obtained from condensers at $\alpha = 90°$ are presented graphically in this section. Matching plots of data obtained from condensers at various α and ψ can be found in Appendix G: Additional Heat Transfer & Pressure Drop Plots.

Figure 5.18 shows the h_w vs. V data for confined condensers composed of various wire and tube geometries at $\alpha = 90°$. As can be seen, there is a considerable difference between the h_w vs. V data obtained from each condenser. The h_w vs. V data at various α for both the $\psi = 0$ and $\psi = \pi/2$ cases (see Fig. G.22, G.26, G.30, G.34, G.38, and G.42) also show considerable difference between the h_w vs. V data obtained from each condenser.

In general, Coil 8 appears to have the lowest h_w at any given V. For cases where either $\psi = \pi/2$ (at any α) or $\alpha = 90°$, Coil 6 has the highest h_w at any given V, followed by Coil 10 and then Coil 9. When $\psi = 0$, the order in which the magnitudes of the h_w appear (at a particular α)

is dependent on α. For the case where $\alpha = 75°$and $\psi = 0$, Coil 6 has the highest h_w, while Coils 9 and 10 yield h_w which are nearly identical to one another. When $\alpha = 45°$ or 60° (and $\psi = 0$), however, Coil 9 has the highest h_w, followed by Coil 6 and then Coil 10.

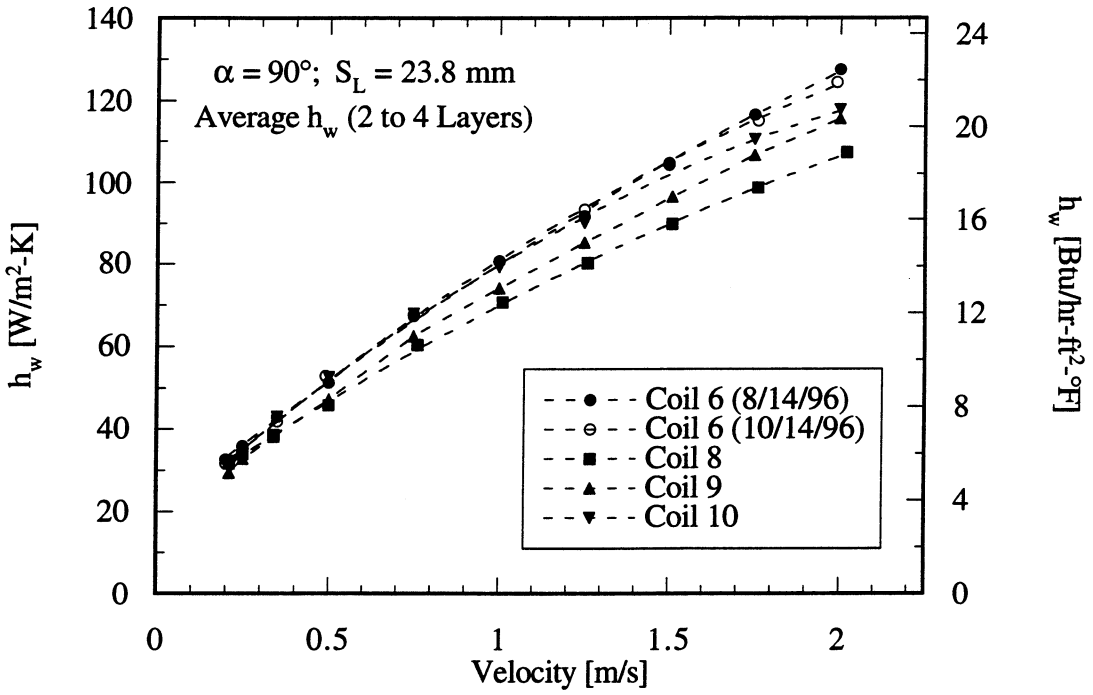

Figure 5.18 h_w vs. V for condensers at $\alpha = 90°$

The Nu_w and $Re_{w,max}$ corresponding to the experimental h_w data at $\alpha = 90$ are shown in Fig. 5.19 for confined condensers composed of various wire and tube geometries. Again, D_w was used as the characteristic length and V_{max} was used in the calculation of $Re_{w,max}$. Similar Nu_w vs. $Re_{w,max}$ plots are shown in Fig. G.23, G.27, G.31, G.35, G.39, and G.43 for data obtained from confined condensers at various α for both the $\psi = 0$ and $\psi = \pi/2$ cases. As can be seen, most of the Nu_w-$Re_{w,max}$ relations appear to be independent of the wire and tube geometry of the condensers. Exceptions to this rule, however, exist in the $\psi = 0$ data obtained at $\alpha = 45°$ and $\alpha = 60°$. For these cases, the degree of the scatter in the Nu_w vs. $Re_{w,max}$ data appears to increase with decreasing α.

This same relation between Nu_w and α was also observed earlier in the Section 5.3 - Effect of Angle-of-Attack and Orientation on Condenser Performance in the case of $\psi = 0$, where the degree to which α influences Nu_w was hypothesized to be dependent on S_w. However, it was noted that only four different wire and tube geometries (two of which have identical S_w) have been examined in the current investigation. As a result, further testing is advised before

establishing any sort of correlation between S_w and the degree to which Nu_w is influenced by α ($\psi = 0$). In addition, since the degree to which the data is scattered only appears to be of significance when $\alpha = 45°$ and $\psi = 0$ (i.e. the degree of scatter in Fig. G.27 appears to be small), the differences in the Nu_w-$Re_{w,max}$ relations associated with the data obtained from condenser at $\psi = 0$ may possibly be overlooked if the case where $\alpha = 45°$ is evaluated separately from the remaining data.

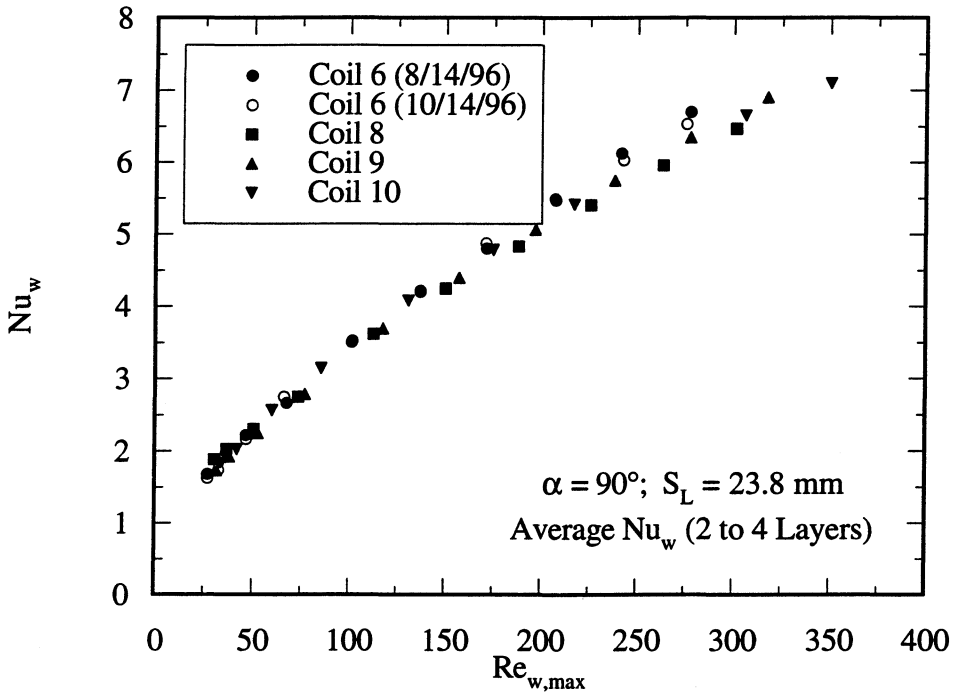

Figure 5.19 Nu_w vs. $Re_{w,max}$ for condensers at $\alpha = 90°$

The Δp per condenser layer are shown in Fig. 5.20 as a function of V for confined condensers composed of various wire and tube geometries at $\alpha = 90°$. As can be seen, for any V, Coil 10 yields the highest Δp, followed by Coil 9 and then Coil 6. Coil 8 appears to yield the lowest Δp. This same order in which the magnitudes of the Δp appear is identical for the Δp per layer vs. V data obtained from confined condensers at various α and both ψ (see Fig. G.24, G.28, G.32, G.36, G.40, and G.44).

The order in which the magnitudes of the Δp appear also seems to be identical to the order in which the magnitudes of V_{max}/V appear for both the $\psi = 0$ and $\psi = \pi/2$ cases (see Tables 1 and 2). That is, the V_{max}/V associated with Coil 10 is always the highest at any combination of α and ψ, followed by those associated with Coil 9, those associated with Coil 6, and then those

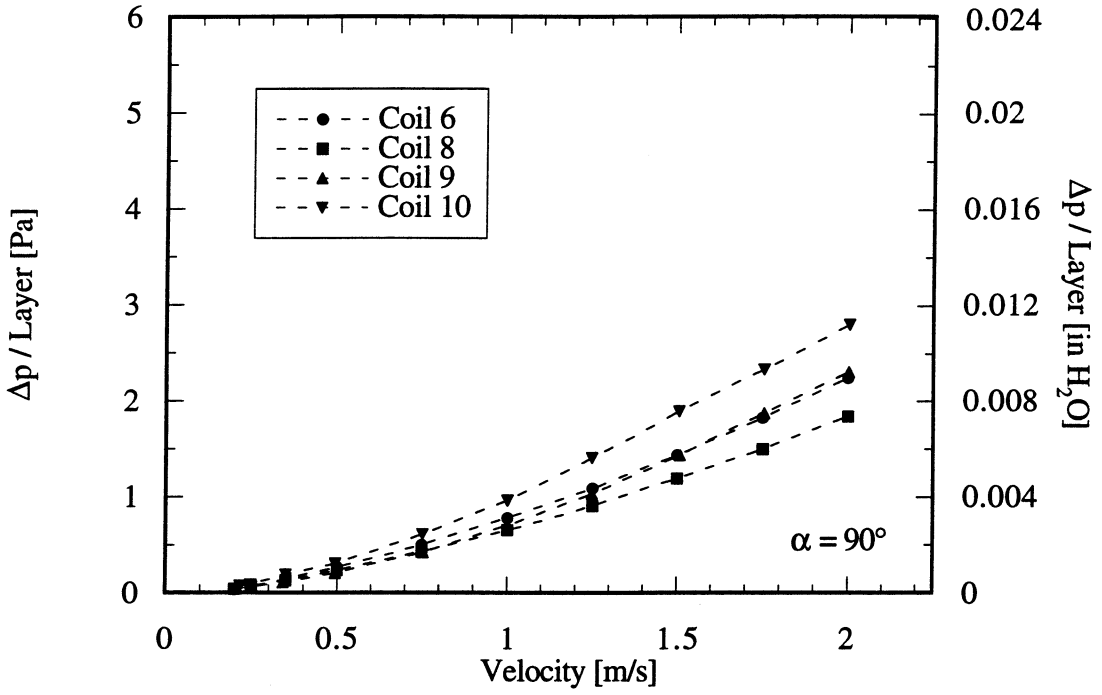

Figure 5.20 Δp per layer vs. V for condensers at $\alpha = 90°$

associated with Coil 8. This is not surprising, since it is known that $\Delta p \propto V^n$, where V_{max} is used in place of V.

The Δp per condenser layer as a function of V_{max} are shown in Fig. 5.21 for Coils 6, 8, 9, and 10 at $\alpha = 90$. As can be seen, the data associated with each wire and tube geometry follow identical Δp-V_{max} relations. Similar observations can also be made concerning the Δp vs. V_{max} data at various α and both ψ (see Fig. G.25, G.29, G.33, G.37, G.41, and G.45). Once again, however, this trend is violated by the Δp vs. V_{max} data obtained from confined condensers at $\alpha = 45°$ and $\psi = 0$. However, as in the case with the Nu_w vs. $Re_{w,max}$ data, the Δp-V_{max} relations associated with the data obtained from confined condensers may be treated as being independent of wire and tube geometry if the $\alpha = 45°$ and $\psi = 0$ case is evaluated separately from the remaining data.

5.5 Correlation of the Data Obtained from Confined Wire-on-Tube Condensers

In correlating the data obtained, it is clear that $Re_{w,max}$ has the largest effect on Nu_w. Data plots from each of the condensers at various α and both ψ suggest that the relation between Nu_w and $Re_{w,max}$ is of the form

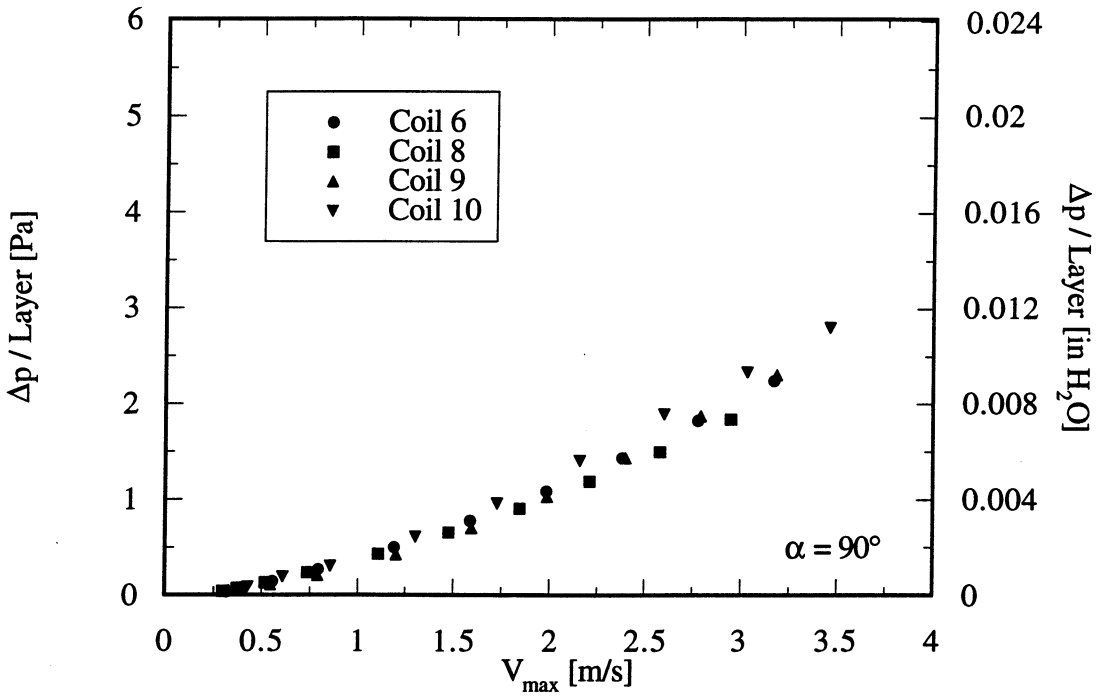

Figure 5.21 Δp per layer vs. V_{max} for condensers at $\alpha = 90°$

$$Nu_w = C\, Re_{w,max}^{n} \tag{5.2}$$

where both C and n are either constants or functions of variables other than $Re_{w,max}$. Curve-fits (i.e. least-squares) of the Nu_w vs. $Re_{w,max}$ data reveal that the exponent n in Eq. (5.2) is nearly constant for all α, ψ, and condenser (wire and tube) geometries. As a result, Eq. (5.2) can be rewritten as

$$Nu_w = C\, Re_{w,max}^{0.5744} \tag{5.3}$$

where the exponent n in Eq. (5.2) has been replaced by a value which is indicative of each of the Nu_w-$Re_{w,max}$ curve fits. Although the exponent n is nearly independent of α, ψ, and condenser geometry, the coefficient C is a function of one or more of these parameters.

Plots of the Nu_w obtained from confined condensers composed of various wire and tube geometries as a function of $Re_{w,max}$ show that the relationships between Nu_w and $Re_{w,max}$ are nearly independent of the condenser wire and tube geometry for both the $\psi = 0$ and $\psi = \pi/2$ cases (see Section 5.4 - Accounting for Geometric Differences Between Condensers). Although exceptions to this generalization were observed within the data sets obtained at $\alpha = 45°$ and $\alpha = 60°$ for the case where $\psi = 0$, the degree of scatter within the Nu_w vs. $Re_{w,max}$ data is modest

and decreases as α increases. As a result, any effects of the condenser wire and tube geometry on Nu_w which may exist (for $\alpha \leq 60°$ and $\psi = 0$) will be ignored for purposes of correlating the data.

Data obtained from Coils 6 and 10 show no dependence between Nu_w and α when $\psi = 0$ (see Section 5.3 - Effect of Angle-of-Attack and Orientation on Condenser Performance). Coils 8 and 9, however, show that Nu_w increases slightly with decreasing α ($\psi = 0$). Although it is hypothesized that the degree to which α influences Nu_w is directly related to S_w, the exact influence of this variable cannot be deduced since too few condensers with different S_w were tested. As a result, a correlation between S_w and the degree to which Nu_w is influenced by α ($\psi = 0$) cannot be positively established. Since (i) Nu_w is independent of α for Coils 6 and 10 and (ii) a direct relationship between S_w and the degree to which Nu_w is influenced by α cannot be supported at this time, the coefficient C in Eq. (5.3) is assumed to be independent of α when $\psi = 0$. A least-squares curve-fit of all of the data obtained from confined condenser at various α ($\psi = 0$) and condenser geometries yields the following:

$$C = 0.2591 \qquad \text{for } \psi = 0,\ 45° \leq \alpha \leq 90° \qquad (5.4)$$

In the case where $\psi = \pi/2$, the Nu_w vs. $Re_{w,max}$ data obtained from confined condensers composed of various wire and tube geometries clearly show a direct relationship between Nu_w and α. Individual curve-fits at each α reveal that

$$C = 0.502 \sin(\alpha) \exp\left(-1.014\,\alpha + 0.3775\,\alpha^2\right) \qquad \text{for } \psi = \pi/2,\ 45° \leq \alpha \leq 90° \qquad (5.5)$$

where α is in terms of radians.

The differences between the values of the Nu_w obtained experimentally from various α, ψ, and condenser geometries ($Nu_{w,exp}$) and those ($Nu_{w,corr}$) determined using Eq. (5.3), (5.4), and (5.5) are shown in Fig. 5.22 as a function of $Re_{w,max}$. As can be seen, most $Nu_{w,corr}$ lie within 10% of the experimentally determined Nu_w. The average absolute deviation of the predicted Nu_w is approximately 3.7%, while the RMS deviation is only 4.8%.

Values of $Nu_{w,corr}$ have also been plotted in Fig. 5.23 as a function of their corresponding $Nu_{w,exp}$. As can be seen, Eq. (5.3), (5.4), and (5.5) do an excellent job of predicting Nu_w, as is clearly evidenced by the fact that all of data points are tightly clustered near the path defined by $Nu_{w,corr} = Nu_{w,exp}$.

Although the Δp obtained from confined condensers were presented in previous sections as functions of V and V_{max}, it may actually be useful to correlate the Δp data in terms of nondimensional groups. That is, a correlation of the Δp data should be developed in terms of C_D and $Re_{w,max}$.

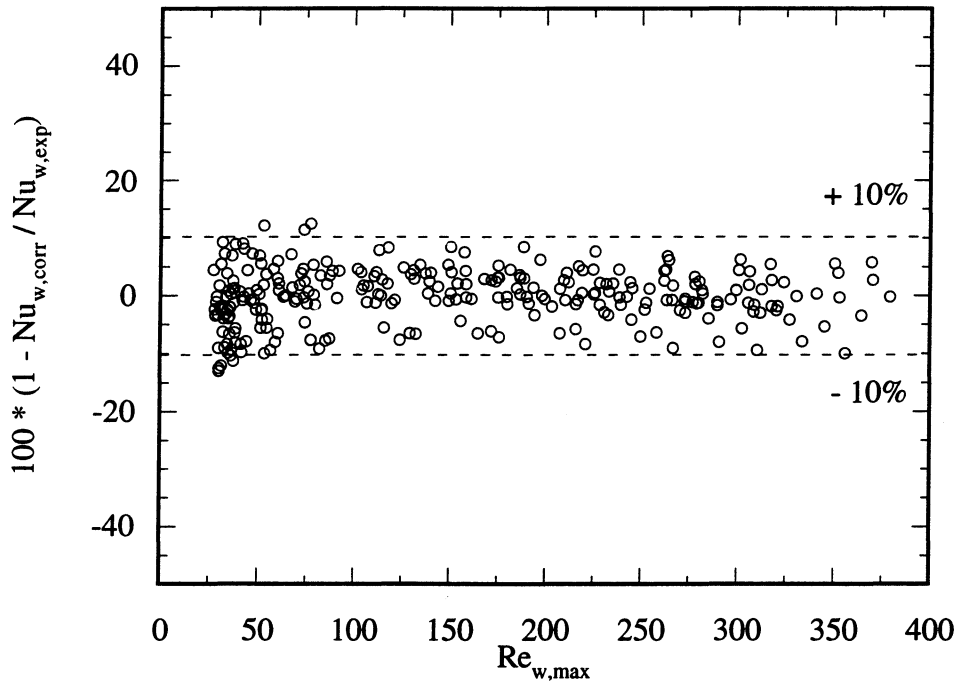

Figure 5.22 Difference between the experimental Nu_w and those predicted by the correlation

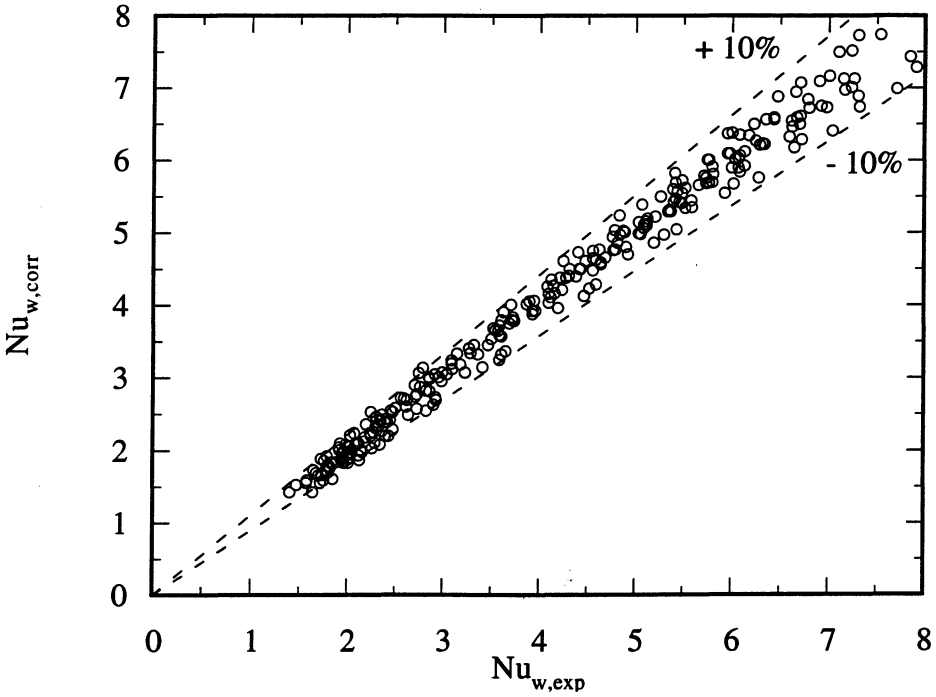

Figure 5.23 Comparison of the experimental Nu_w and those predicted by the correlation

The C_D associated with wire-on-tube condensers at various α is highly dependent on the locations of the wires on one side of the condenser with respect to those on the other side of the condenser when $\psi = 0$ (see Fig. 5.13). The magnitude of C_D is lower at α where one set of condenser wires falls in-line along the path of the air flow with the other set of wires. As a result, much more data (than is currently available) would be required in order to develop a correlation between the C_D and $Re_{w,max}$ associated with wire-on-tube condensers at $\psi = 0$.

A correlation between the C_D and $Re_{w,max}$ associated with wire-on-tube condensers at $\psi = \pi/2$, however, can be developed. Since the tube passes of the condensers are perpendicular to the air flow when $\psi = \pi/2$, the wires located on one side of the condenser are always in-line along the path of the air flow with the those on the other side of condenser. As a result, the C_D associated with a particular condenser should not change suddenly as α is adjusted between 45° and 90°.

Due to the fact that the geometry of a wire-on-tube condenser involves a series of cylindrical bodies, many of which are at high angles with respect to the air flow, one might expect the C_D-$Re_{w,max}$ relation of these condensers to be similar to that of a cylinder in cross flow. One such C_D-Re correlation, developed by White (1991), appears in the form of

$$C_D = D_1 + D_2 \, Re_{w,max}^{-D_3} \tag{5.6}$$

where D_1, D_2, and D_3 are each either a constant or a function of variables other than $Re_{w,max}$ (note that White uses all constants). As was the case with the Nu_w vs. $Re_{w,max}$ data, least-squares curve-fits of the C_D vs. $Re_{w,max}$ data show that the exponent D_3 in Eq. (5.6) is nearly constant for all α ($\psi = \pi/2$ only) and condenser geometries. Consequently, Eq. (5.6) can be rewritten as

$$C_D = D_1 + D_2 \, Re_{w,max}^{-0.06533} \tag{5.7}$$

Although C_D is not expected to change suddenly as α ($\psi = \pi/2$) is adjusted, the C_D vs. $Re_{w,max}$ data obtained from confined condensers composed of various wire and tube geometries clearly indicate that C_D is dependent on α. Individual curve-fits of the C_D at each α reveal that

$$D_1 = -0.7856 \sin(\alpha) \exp(1.177\,\alpha - 0.3229\,\alpha^2) \qquad \text{for } \psi = \pi/2,\ 45° \le \alpha \le 90° \tag{5.8}$$

$$D_2 = 2.451 \sin(\alpha) \exp(0.2858\,\alpha) \qquad \text{for } \psi = \pi/2,\ 45° \le \alpha \le 90° \tag{5.9}$$

where again α is in terms of radians.

Figure 5.24 shows the differences between the values of the C_D obtained experimentally ($C_{D,exp}$) from condensers at various α ($\psi = \pi/2$ only) composed of various wire and tube geometries and those ($C_{D,corr}$) determined using Eq. (5.7), (5.8), and (5.9) as a function of $Re_{w,max}$. As can be seen, many of the values of $C_{D,corr}$ are within 15% of the experimentally determined C_D. Both the average absolute deviation (8.4%) and the RMS deviation (10.7%) of the predicted C_D are slightly worse than those of the predicted Nu_w.

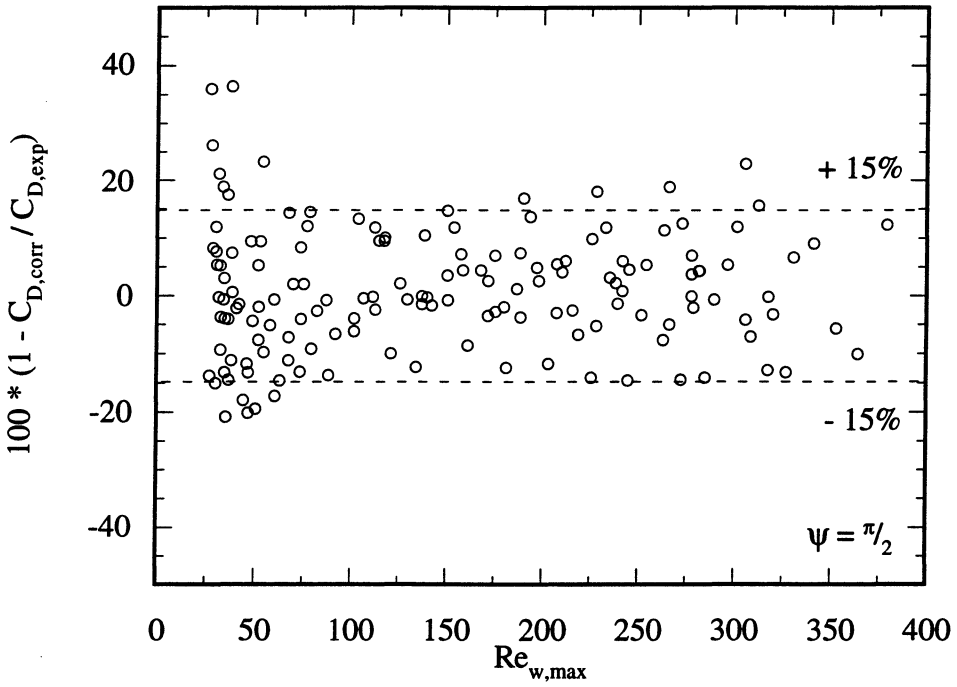

Figure 5.24 Difference between the experimental C_D and those predicted by the correlation

Values of $C_{D,corr}$ have also been plotted in Fig. 5.25 as a function of their corresponding $C_{D,exp}$. As can be seen, Eq. (5.7), (5.8), and (5.9) do not predicted C_D from $Re_{w,max}$ as well as Eq. (5.3), (5.4), and (5.5) predicted Nu_w from $Re_{w,max}$. However, most of the data points in Fig. 5.25 are clustered around the path defined by $C_{D,corr} = C_{D,exp}$, indicating that the correlation is fairly accurate.

5.6 Effect of the Relative Locations of Condenser Wires and Tubes Passes

As shown in the case of the Δp data obtained from condensers at various α with $\psi = 0$, the relative location of certain geometric elements within a particular multi-layer wire-on-tube condenser can have an effect on the condenser's performance (see Section 5.3 - Effect of Angle-of-Attack and Orientation on Condenser Performance). In light of this fact, experiments

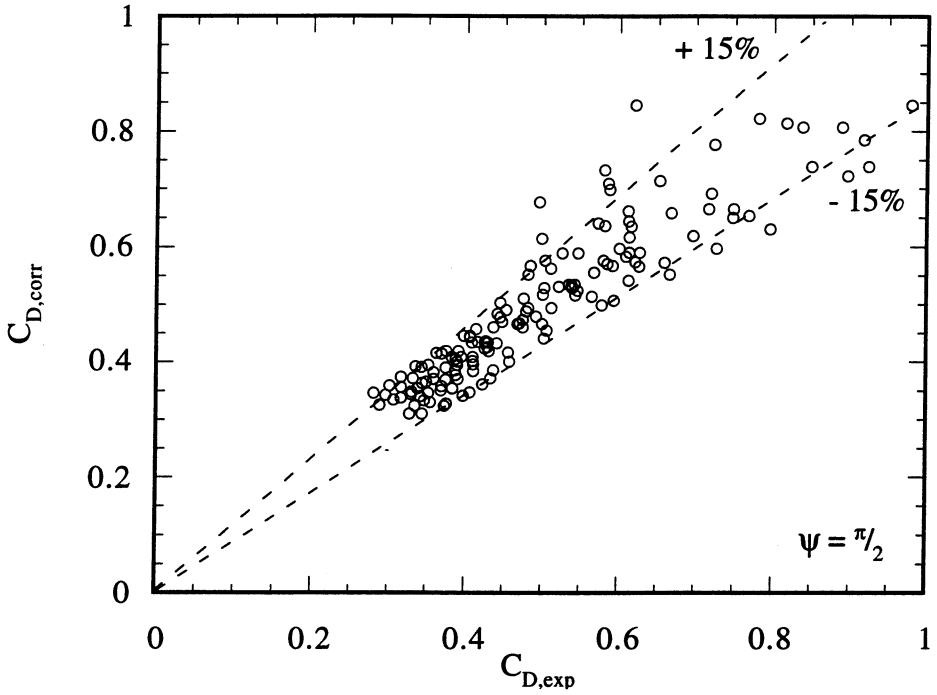

Figure 5.25 Comparison of the experimental C_D and those predicted by the correlation

involving several alternative condenser designs have been performed. These alternative designs were each constructed by either modifying the individual layers, as in the case of the "staggered-wire" and "one-sided" condenser layers (see Fig. 5.26a), or by off-setting the vertical placement of consecutive condenser layers, as in the case of the staggered-tube condenser (see Fig. 5.26b). During testing, each of the designs was subjected to forced convection air flows within a confined space, similar to those experienced by condensers involved in other portions of the

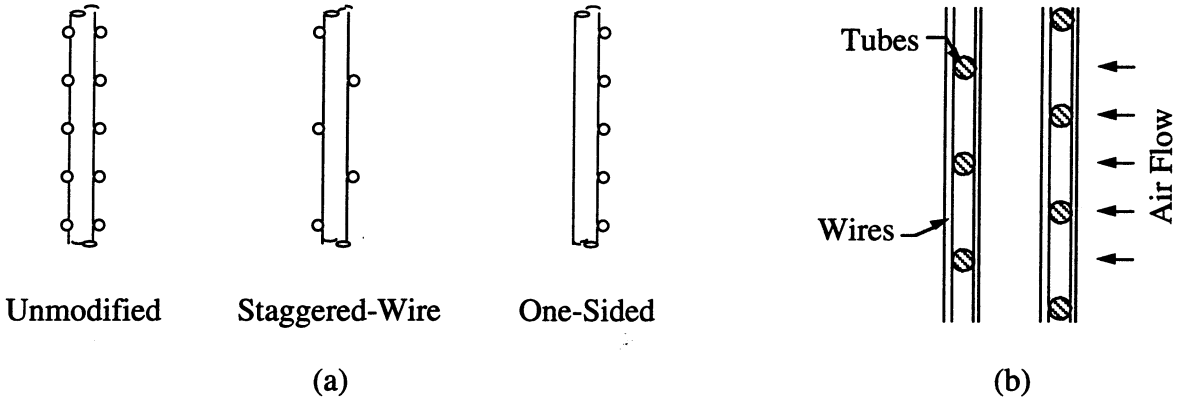

Figure 5.26 Alternative condenser designs which include (a) staggered-wire and one-sided condenser layers and (b) staggered-tube condenser

investigation. Raw data enabling the calculation of both h_w and Δp were recorded.

Figure 5.27 shows the ratios of both the h_w and the Δp associated with modified and unmodified condenser layers at $\alpha = 90°$. As can be seen, the h_w obtained from both the staggered-wire and the one-sided condenser layers are higher than those of the unmodified layer (Coil 6). The difference in performance (over the unmodified layer) ranges from as high as 15.6% at V = 0.2 m/s (0.66 ft/s) to 4.6% at V = 2.0 m/s (6.56 ft/s) for the staggered-wire condenser layer. The h_w of the one-sided layer are slightly higher than those of the staggered-wire layer, ranging anywhere from 5.9% to 20.5% higher than those of the unmodified condenser layer. It is hypothesized that these differences in performance are a result of the fact that none of the wires on either the staggered-wire or one-sided layer are in tandem with other wires within the layer. As a result, a much larger portion of the condenser wires on the staggered-wire and one-sided layers experience lower air temperatures than those of the unmodified layer. This causes the h_w associated with the modified layers to be higher.

As can also be seen in Fig. 5.27, the Δp per layer obtained from the staggered-wire and the one-sided condenser layers are lower than those of the unmodified layer by nearly 40%. This is due to the fact that the staggered-wire and the one-sided condenser layers both have 50% fewer wires than the unmodified layer.

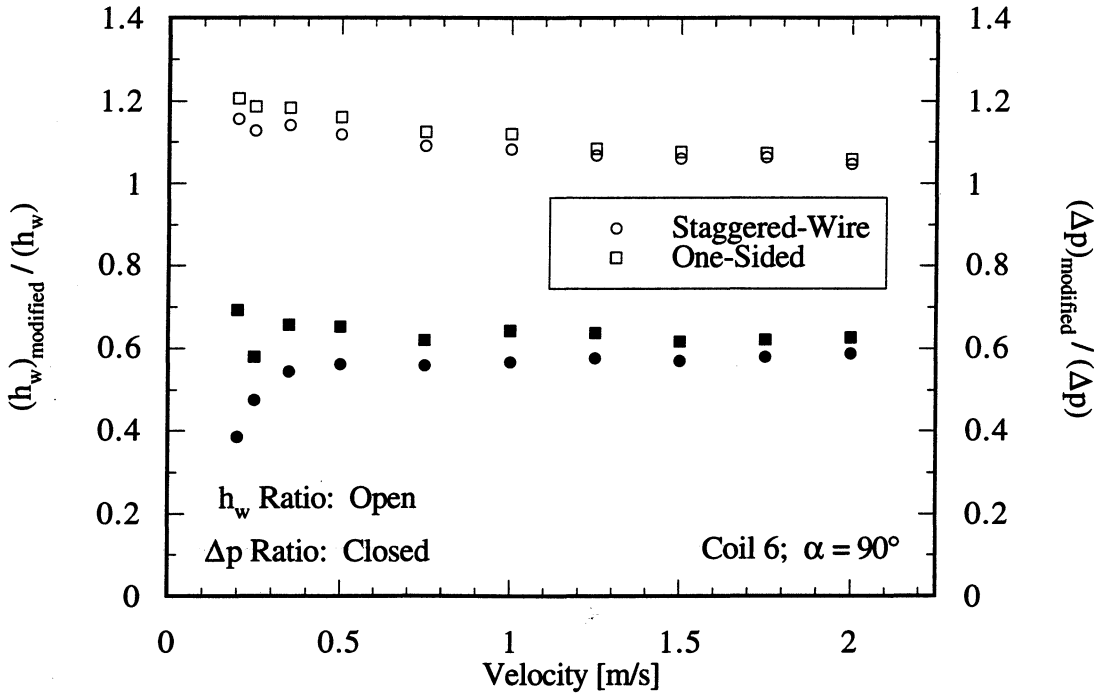

Figure 5.27 Comparison of the h_w and Δp per layer of modified and unmodified layers

The ratios of the h_w associated with the second condenser layer to those of the first layer are shown in Fig. 5.28 for two confined staggered-tube condensers. As can be seen, the h_w associated with the second layer of are greater than those of the first layer by up to 9.7% at V = 2.0 m/s (6.56 ft/s). This difference in performance is a result of the fact that the tube passes of the second layer are no longer situated within the wake of the tube passes of the first layer. Consequently, the h_w of the second layer (calculated by assuming that the air is well-mixed between consecutive condenser layers) is higher.

Figure 5.28 also shows the ratios of the Δp per layer associated with staggered-tube and standard multi-layer wire-on-tube condensers. As can be seen, the Δp obtained from the staggered-tube condensers are significantly lower than those of a standard condenser at $V \leq 0.75$ m/s. However, the ratio of the Δp increases as V increases, until the Δp of the staggered-tube condensers are higher than those of a standard condenser.

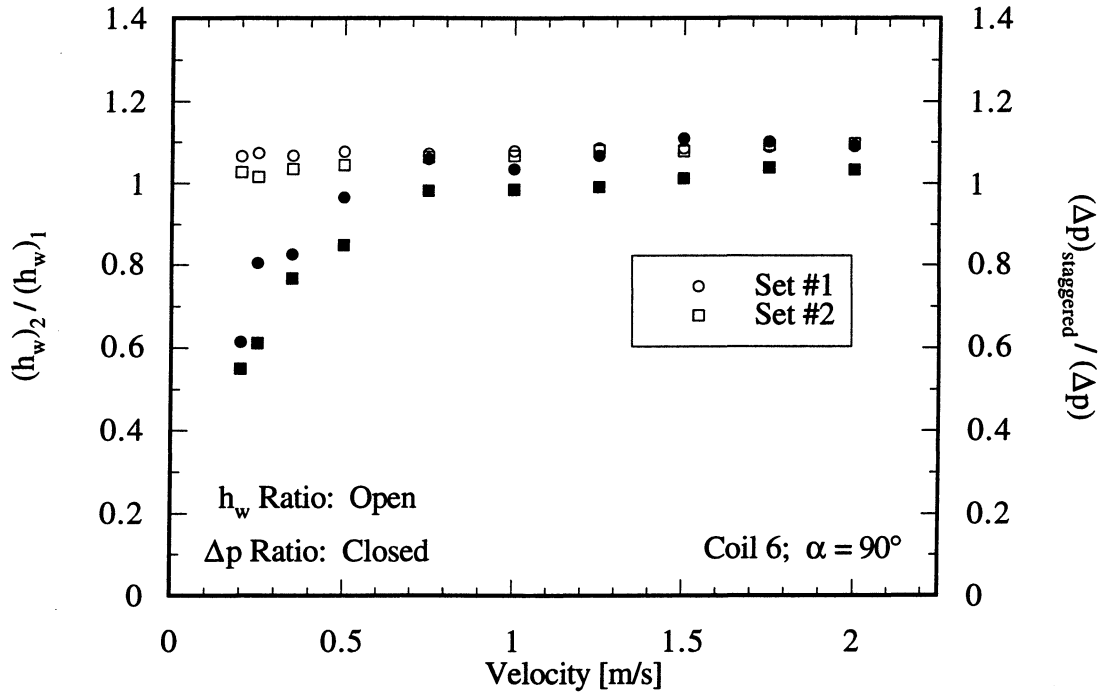

Figure 5.28 Comparison of the h_w and Δp per layer of condensers with staggered tubes

6. CONCLUSIONS

The following conclusions may be drawn from the data obtained during the current investigation. Note that these conclusions are only applicable for confined, saw-tooth shaped, wire-on-tube condensers with wire and tube geometries similar to those studied:

$$1.38 \text{ mm } (0.0542 \text{ in}) \leq D_w \leq 1.58 \text{ mm } (0.0621 \text{ in})$$
$$5.08 \text{ mm } (0.200 \text{ in}) \leq S_w \leq 6.35 \text{ mm } (0.250 \text{ in})$$
$$4.80 \text{ mm } (0.189 \text{ in}) \leq D_t \leq 4.85 \text{ mm } (0.191 \text{ in})$$
$$25.4 \text{ mm } (1 \text{ in}) \leq S_t \leq 50.8 \text{ mm } (2 \text{ in})$$

In addition, each of these condensers were exposed to forced convection flows with $Re_{w,max} \leq 420$ and $45° \leq \alpha \leq 90°$. Extrapolation from these limits could invalidate some of the conclusions.

1) The h_w associated with downstream condenser layers is nearly independent of S_L when $S_L \geq 31.2$ mm (1.23 in). This, along with the fact that h_w is independent of both N_L and placement within a particular multi-layer condenser, allows multi-layer condensers to be designed and evaluated based primarily on the performance of single layer condensers with identical wire and tube geometries.

2) h_w is highly dependent on α. For the case where $\psi = \pi/2$, h_w increases as α increases. This implies that condensers with this orientation should be designed such that they have large angles-of-attack.

3) The Δp associated with multi-layer condensers is linearly dependent on the N_L. This simplifies the design process for multi-layer condensers, since the Δp for a particular multi-layer condenser can easily be predicted from that of an identically oriented single layer condenser with the same wire and tube geometry.

4) The Δp per layer associated with condensers at $\psi = 0$ are significantly higher than those of condensers at $\psi = \pi/2$. Furthermore, the percent differences between the Δp are much greater than the percent difference in h_w obtained from the two ψ orientations (where the h_w are slightly higher for $\psi = 0$). As a result, the design and use of multi-layer condensers at $\psi = 0$ is not advised.

5) Equations (5.3), (5.4), and (5.5) do an excellent job of correlating the Nu_w data obtained from the condensers studied for both the $\psi = 0$ and $\psi = \pi/2$ cases. Almost all of the predicted Nusselt numbers lie within 10% of the experimentally determined values. The average absolute and RMS deviations are 3.7% and 4.8%, respectively.

6) The C_D associated with wire-on-tube condensers at $\psi = \pi/2$ can be predicted with reasonable accuracy using Eq. (5.7), (5.8), and (5.9). The average absolute and RMS deviations associated with the C_D correlation are 8.4% and 10.7%, respectively.

REFERENCES

Admiraal, D.M., and C.W. Bullard, 1993, "Heat Transfer in Refrigerator Condensers and Evaporators," ACRC TR-48, Air Conditioning and Refrigeration Center, University of Illinois at Urbana-Champaign, pp. 34-35.

Carley, H. J., 1956, "A Study of Wire and Tube Heat Exchangers," M.S. Thesis, Purdue University, Dept. of Mechanical Engineering, Lafayette, Indiana.

Churchill, S.W., and H.H.S. Chu, 1975, "Correlating Equations for Laminar and Turbulent Free Convection from a Horizontal Cylinder," *International Journal of Heat and Mass Transfer*, Vol. 18, No. 1049.

Collicott, H.E., W.E. Fontaine, and O.W. Witzell, 1963, "Radiation and Free Convection Heat Transfer from Wire and Tube Heat Exchangers," *ASHRAE Journal,* Vol. 5, pp. 79-83.

Cyphers, J. A., R. D. Cess, and E. V. Somers, 1959, "Heat Transfer Character of Wire-and-Tube Heat Exchangers," *ASHRAE Journal,* Vol. 1, pp. 86-90 & 110.

Feingold, A., 1966, "Radiant-Interchange Configuration Factors Between Various Selected Plane Surfaces," *Proceedings of the Royal Society Discussion Meeting, London*, Ser. A, Vol. 292, No. 1428, pp. 51-60.

Gnielinski, V., 1976, "Single Correlation for Calculating Average Heat and Mass Transfer Coefficients to Single Bodies in Laminar and Turbulent Flow," *International Chemical Engineering*, Vol. 16, No. 359.

Hoke, J. L., 1995, "Experimental Investigation of the Convective Heat Transfer Coefficient of Refrigerator Condenser Coils in Forced Convection," M.S. Thesis, University of Illinois, Dept. of Mechanical Engineering, Urbana, Illinois.

Hoke, J. L., T. D. Swofford, and A. M. Clausing, 1995, "An Experimental Investigation of the Air-Side Convective Heat Transfer Coefficient on Wire and Tube Refrigerator Condenser Coils," ACRC TR-86, Air Conditioning and Refrigeration Center, University of Illinois at Urbana-Champaign.

Hoke, J. L., A. M. Clausing and T. D. Swofford, 1997, "An Experimental Investigation of Convective Heat Transfer From Wire-On-Tube Heat Exchangers, *ASME J. of Heat Transfer*, Vol. 119, pp. 348-356.

Hilpert, R., 1933, "Wärmeabgabe von geheizten Drähten und Rohren im Lufstrom," *Forsch. Gebiete Ingenieurw.*, Vol. 4, No. 215.

Howard, W. H., 1956, "A Study of Wire and Tube Heat Exchangers," M.S. Thesis, Purdue University, Dept. of Mechanical Engineering, Lafayette, Indiana.

Howell, J.R., 1982, *A Catalog of Radiation Configuration Factors*, New York: McGraw-Hill, Inc.

Incropera, F. P., and D. P. DeWitt, 1990, *Fundamentals of Heat and Mass Transfer*, 3rd ed., New York: John Wiley & Sons.

REFERENCES (cont.)

Morgan, V.T., 1975, "The Overall Convective Heat Transfer from Smooth Circular Cylinders," in T. F. Irvine and J. P. Hartnett, Jr., Eds., *Advances in Heat Transfer*, Academic Press, New York, Vol. 11, pp. 199-264.

Papanek, W. J., 1958, "Convective Film Coefficients for a Wire and Tube Heat Exchanger," M.S. Thesis, Purdue University, Dept. of Mechanical Engineering, Lafayette, Indiana.

Rasmussen, R.L., 1997, "An Experimental Investigation of the Air-Side Heat Transfer Characteristics of Heat Exchangers," M.S. Thesis, University of Illinois, Dept. of Mechanical Engineering, Urbana, Illinois.

Rudy, W. J., 1956, "A Study of Wire and Tube Heat Exchangers," M.S. Thesis, Purdue University, Dept. of Mechanical Engineering, Lafayette, Indiana.

Swofford, T. D., 1995, "An Experimental Investigation of Natural and Forced Convection Heat Transfer from Wire and Tube Condensers," M.S. Thesis, University of Illinois, Dept. of Mechanical Engineering, Urbana, Illinois.

White, F.M., 1991, *Viscous Fluid Flow*, New York: McGraw-Hill, Inc., pp. 181-183.

Witzell, O.W., and W.E. Fontaine, 1957a, "Design of Wire and Tube Condensers," *Refrigerating Engineering,* Vol. 65, pp. 41-44.

Witzell, O.W., and W.E. Fontaine, 1957b, "What are the Heat Transfer Characteristics of Wire and Tube Condensers?" *Refrigerating Engineering,* Vol. 65, pp. 33-37 & 127.

Witzell, O.W., W.E. Fontaine, and W. J. Papanek, 1959, "Convective Films Evaluated for Wire and Tube Heat Exchangers," *ASHRAE Journal,* Vol. 1, pp. 35-37 & 127.

Zhukauskas, A., 1972, "Heat Transfer from Tubes in Cross Flow," in J. P. Hartnett and T. F. Irvine, Jr., Eds., *Advances in Heat Transfer*, Vol. 8, Academic Press, New York.

APPENDIX A: CONDENSER SUPPORT FRAME DIMENSIONS

Table A.1 Dimensions pertinent to the α condenser support frames used with Coil 6

Frame		Units	Height of New Test Section	Width of New Test Section	Axial Length Between Slots
ψ	α				
0	45°	mm (in)	152.4 (6.0)	147.6 (5.81)	147.6 (5.81)
0	60°	mm (in)	152.4 (6.0)	178.6 (7.03)	106.4 (4.19)
0	75°	mm (in)	152.4 (6.0)	196.9 (7.75)	58.74 (2.313)
$\pi/2$	45°	mm (in)	111.1 (4.38)	202.4 (7.97)	---
$\pi/2$	60°	mm (in)	133.4 (5.25)	202.4 (7.97)	---
$\pi/2$	75°	mm (in)	147.6 (5.81)	202.4 (7.97)	---
0 or $\pi/2$	90°	mm (in)	152.4 (6.0)	202.4 (7.97)	---

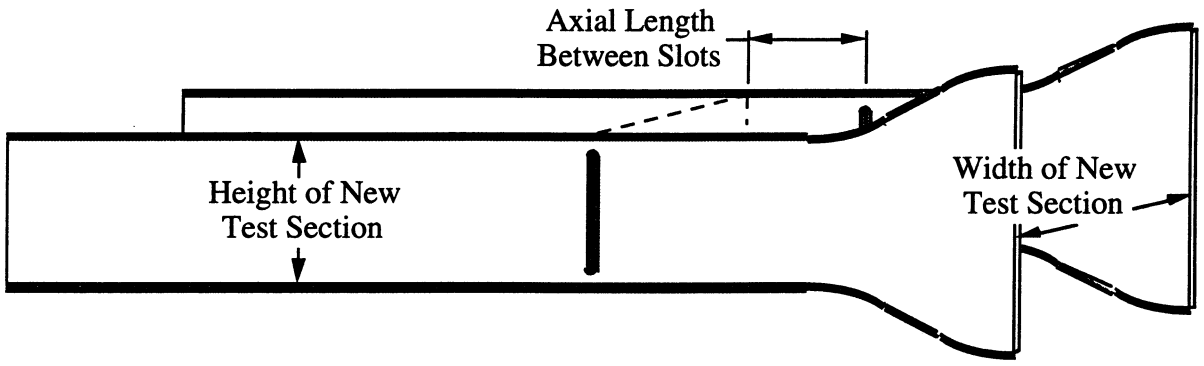

Figure A.1 Schematic illustrating the dimensions pertinent to multi-layer condensers constructed using α condenser support frames (Scale = 12:100)

Table A.2 Dimensions pertinent to the α condenser support frames used with Coil 8

Frame		Units	Height of New Test Section	Width of New Test Section	Axial Length Between Slots
ψ	α				
0	45°	mm (in)	152.4 (6.0)	337.3 (13.28)	337.3 (13.28)
0	60°	mm (in)	152.4 (6.0)	411.2 (16.19)	240.5 (9.47)
0	75°	mm (in)	152.4 (6.0)	456.4 (17.97)	127.8 (5.03)
$\pi/2$	45°	mm (in)	111.1 (4.38)	470.7 (18.53)	---
$\pi/2$	60°	mm (in)	133.4 (5.25)	470.7 (18.53)	---
$\pi/2$	75°	mm (in)	147.6 (5.81)	470.7 (18.53)	---
0 or $\pi/2$	90°	mm (in)	152.4 (6.0)	470.7 (18.53)	---

Table A.3 Dimensions pertinent to the α condenser support frames used with Coil 9

Frame		Units	Height of New Test Section	Width of New Test Section	Axial Length Between Slots
ψ	α				
0	45°	mm (in)	152.4 (6.0)	135.7 (5.34)	135.7 (5.34)
0	60°	mm (in)	152.4 (6.0)	164.3 (6.47)	98.43 (3.875)
0	75°	mm (in)	152.4 (6.0)	181.0 (7.13)	53.98 (2.125)
$\pi/2$	45°	mm (in)	111.1 (4.38)	185.7 (7.31)	---
$\pi/2$	60°	mm (in)	133.4 (5.25)	185.7 (7.31)	---
$\pi/2$	75°	mm (in)	147.6 (5.81)	185.7 (7.31)	---
0 or $\pi/2$	90°	mm (in)	152.4 (6.0)	185.7 (7.31)	---

Table A.4 Dimensions pertinent to the α condenser support frames used with Coil 10

Frame		Units	Height of New Test Section	Width of New Test Section	Axial Length Between Slots
ψ	α				
0	45°	mm (in)	152.4 (6.0)	369.1 (14.53)	369.1 (14.53)
0	60°	mm (in)	152.4 (6.0)	449.3 (17.69)	263.5 (10.38)
0	75°	mm (in)	152.4 (6.0)	499.3 (19.66)	139.7 (5.50)
$\pi/2$	45°	mm (in)	111.1 (4.38)	515.1 (20.28)	---
$\pi/2$	60°	mm (in)	133.4 (5.25)	515.1 (20.28)	---
$\pi/2$	75°	mm (in)	147.6 (5.81)	515.1 (20.28)	---
0 or $\pi/2$	90°	mm (in)	152.4 (6.0)	515.1 (20.28)	---

APPENDIX B: DATA REDUCTION PROGRAM FOR MULTI-LAYER WIRE-ON-TUBE CONDENSERS

```
      program multilayer
c ***************************************************************************
c  This program determines the approximate air-side convection heat transfer
c  coefficient associated with individual passes of a multi-layer wire-on-
c  tube condenser.  The multi-layer configuration under investigation
c  consists of several single layer wire-on-tube condensers (each at high
c  angles-of-attack with respect to the air flow) situated in a series.
c  Experimental data is obtained by subjecting the condenser to forced
c  convection at various air flow rates.  The effectiveness of each
c  condenser layer is determined by assuming that (i) the air is well-mixed
c  between condenser layers and that (ii) the ratio of the thermal masses of
c  the refrigerant and the air is zero.  Test velocities, inlet air
c  temperatures, both inlet & outlet refrigerant (water) temperatures, and
c  temperature differences across each layer are read from input files along
c  with the overall geometry of the multi-layer condenser.  Note that the
c  program has been written to analyze a counterflow heat exchanger.  As a
c  result, individual passes are numbered from the downstream to upstream of
c  the air.  Note, however, that the condenser layers are numbered from
c  upstream to downstream with respect to the air flow (opposite of the
c  program) for purposes of output.
c ***************************************************************************

      implicit none
      integer coil, NL, psi, NW, NT, i, j, k, l
      real SL, theta, DW, PW, SW, XLWS(6), AWS(6)
      real DT, PT, DTI, ST, XLTS, ATS, ATIS, Hduct, Wduct
      character datafile*18

c  coil     -- set of condenser layers used
c  NL       -- number of layers in the multi-layer condenser
c  SL       -- center-to-center spacing [m] between consectutive condenser
c              layers
c  theta    -- angle of inclination [rad] with respect to the air flow
c  psi      -- yaw angle where:  0 = perpendicular to wires
c                                1 = perpendicular to tube passes
c  DW       -- diameter [m] of the wires (including the paint thickness)
c  PW       -- thickness [m] of the paint covering the wires
c  SW       -- center-to-center spacing [m] between consecutive wires
c  NW       -- number of exposed wires on each condenser layer
c  XLWS(i)  -- length [m] of the wires on layer i
c  AWS(i)   -- surface area [m^2] of the exposed wires of layer i
c              (neglect weld area effects)
c  DT       -- outer diameter [m] of the tube passes (including the paint
c              thickness)
c  PT       -- thickness [m] of the paint covering the tube passes
c  DTI      -- inner diameter [m] of the tube passes
c  ST       -- center-to-center spacing [m] between consecutive tube passes
c  NT       -- number of tube passes in each condenser layer
c  XLTS     -- length [m] of the exposed tube passes
c  ATS      -- outer surface area [m^2] of the exposed tube passes per layer
c              (neglect weld area effects)
c  ATIS     -- inner surface area [m^2] of the tube passes per layer
c  Hduct    -- height [m] of the variable height test section during testing
c  Wduct    -- width [m] of the variable height test section during testing
```

```
      integer NVA, IER
      real VA(20), Vmax, MdotA, Tair(0:6,20), Tinput
      real RHOA, XMUA, XKA, CPA, PRA, GRB, c1(6), eta(6), eta_c(6)
      real heff, hw(6,20), mconv, etaconv(6,20), Nu_w(6,20), Re_w(6,20)

c  NVA       -- number of velocity conditions
c  VA(j)     -- air velocity [m/s] during velocity condition j
c  Vmax      -- air velocity [m/s] based on the minimum flow area
c  MdotA     -- mass flow rate [kg/s] of air over the condenser
c  Tair(i,j)-- temperature [K] of the air upstream of condenser layer i
c              during velocity condition j
c  Tinput    -- temperature input [K] used in subroutine GASPT
c  RHOA      -- density [kg/m^3] of air
c  XMUA      -- viscosity [kg/m-s] of air
c  XKA       -- thermal conductivity [W/m-K] of air
c  CPA       -- specific heat [J/kg-K] of air
c  PRA       -- Prandtl number of air
c  c1(i)     -- ratio of the total heat transfer coefficients of the tube
c               passes and wires of layer i (used in calculating combined
c               mode fin efficiency; also sqrt(DW/DT) adjusted for paint
c               thickness)
c  eta(i)    -- combined mode fin efficiency of wires on condenser layer i
c  heff      -- effective convection coefficient [W/m^2-K] which includes the
c               resistance due to the paint covering the wires
c  hw(i,j)   -- convection coefficient [W/m^2-K] of condenser layer i during
c               velocity condition j which accounts for the resistance due to
c               the paint covering the wires
c  mconv     -- actual fin parameter of the condenser wires
c  etaconv(i,j)-- actual fin efficiency of wires on condenser layer i during
c               velocity conditon j
c  Nu_w(i,j)-- Nusselt number associated with air flow over the wires of
c               condenser layer i during velocity condition j
c  Re_w(i,j)-- Reynolds number based on the minimum flow area associated
c               with air flow over the wires of condenser layer i during
c               velocity condition j

      real Mdot(20), Tref(0:6,20), CPR, HR, XKS, vf(13,13), fractionQw

c  Mdot(j)   -- mass flow rate [kg/s] of the refrigerant in the condenser
c               during velocity condition j
c  Tref(i,j)-- temperature [K] of the refrigerant measured by thermocouple
c               set i during velocity condition j
c  CPR       -- specific heat [J/kg-K] of the refrigerant
c  HR        -- convection coefficient [W/m^2-K] for the refrigerant flow in
c               the condenser tube
c  XKS       -- thermal conductivity [W/m-K] of steel
c  vf(i,j)   -- view factor matrix
c  fractionQw-- approximate fraction of the total energy leaving the
c               condenser through the wires

      real Q(6,20), Qradw(6), Qradt(6), Qconv(6,20), Qconvtot, Qne
      real lmtd(6), T1, T2, Twire(6), Ttube(6), Tsurr(6)
      real R_int, R_condt, R_tube(6,20), R_total(6,20)

c  Q(i,j)    -- total heat transfer rate [W] of condenser layer i during
c               velocity condition j
c  Qradw(i)  -- radiation heat transfer rate [W] from the wires associated
c               with condenser layer i
```

```
c  Qradt(i) -- radiation heat transfer rate [W] from the tube passes
c              associated with condenser layer i
c  Qconv(i,j)-- forced convection heat transfer rate [W] of condenser layer
c              i during velocity condition j
c  Qne       -- combined natural convection and radiation heat transfer rate
c              from non-exposed surfaces
c  lmtd(i)   -- log-mean temperature difference [K] associated with condenser
c              layer i
c  T1        -- tube surface temperature [K] at inlet of condenser layer
c  T2        -- tube surface temperature [K] at outlet of condenser layer
c  Twire(i)  -- average wire surface temperature [K] of condenser layer i
c  Ttube(i)  -- average tube surface temperature [K] of condenser layer i
c  Tsurr     -- approximate effective temperature [K] of the surroundings
c  R_int     -- thermal resistance [K/W] between the refrigerant flow and
c              the inner tube wall
c  R_condt   -- thermal resistance associated with axial conduction through
c              the tube wall
c  R_tube(i,j)-- total thermal resistance [K/W] between the refrigerant flow
c              and the outer tube surface of condenser layer i during
c              velocity condition j
c  R_total(i,j)-- total thermal resistance [K/W] between the refrigerant
c              flow and the air flow of condenser layer i during velocity
c              condition j

      CPR = 4180.
      XKS = 60.5

c
c *** Read the data obtained and the geometry of the condenser from an
c *** existing input file.  In addition, calculate the view factors between
c *** condenser layer elements.
c
      call input(coil,NL,SL,theta,psi,DW,PW,SW,NW,XLWS,AWS,DT,PT,DTI,ST,NT,
     + XLTS,ATS,ATIS,Hduct,Wduct,NVA,VA,Tair,Mdot,Tref,datafile)
c
      call viewfactor(NL,SL,theta,psi,DW,SW,NW,XLWS,DT,ST,NT,XLTS,vf)

c
c *** Determine the thermal resistance associated with axial conduction
c *** through the tube wall
c
      R_condt = DTI * log((DT-2.*PT)/DTI) / (2.*ATIS*XKS)

c
c *** Calculate the mass flow rate of the air
c
      do 80 j=1,NVA
        Tinput = Tair(NL,j)
        call gaspt(1,Tinput,RHOA,XMUA,XKA,CPA,GRB,PRA,IER)
        MdotA = RHOA * VA(j) * Hduct * Wduct

c
c *** Calculate the total heat transfer rate from each condenser layer
c
        do 20 i=1,NL
          Q(i,j) = Mdot(j) * CPR * abs(Tref(i-1,j)-Tref(i,j))
          Qconv(i,j) = Q(i,j)
          c1(i) = sqrt(DW/DT)
```

```
          eta(i) = 1.
          eta_c(i) = 1.
          Ttube(i) = Tref(i,j)
   20   continue

c
c *** Calculate the effective air temperature to which each condenser layer
c *** is exposed.  Assume that the air is thoroughly mixed between condenser
c *** layers.
c
        do 60 k=1,100
          Qconvtot = 0.
          do 30 i=NL,1,-1
            Qconvtot = Qconvtot + Qconv(i,j)
            Tair(i-1,j) = Tair(i,j) + Qconv(i,j) / (MdotA*CPA)
            lmtd(i) = (Tref(i-1,j)-Tref(i,j))
     +              / log((Tref(i-1,j)-Tair(i,j))/(Tref(i,j)-Tair(i,j)))
            R_total(i,j) = lmtd(i) / Q(i,j)
   30     continue

c
c *** Determines the internal thermal resistance using the Gnielinski
c *** Correlation
c
          do 40 i=1,NL
            call internal(i,j,DTI,ST,NT,ATIS,Mdot,Tref,HR,R_int)
            R_tube(i,j) = R_int + R_condt

c
c *** Determine the resistance resulting from thermal constriction around
c *** each of the spot welds
c
            call spotweld(i,j,coil,DW,AWS,DT,ATS,Tair,eta,eta_c,Tref,HR,
     + Ttube,fractionQw)

c
c *** Estimate the fin efficiency of the condenser wires to account for the
c *** thermal constriction resistance resulting from the spot welds
c
            T1 = Tref(i-1,j) - (Tref(i-1,j)-Tair(i,j)) * (R_int+R_condt)
     +          / R_total(i,j)
            T2 = Tref(i,j) - (Tref(i,j)-Tair(i,j)) * (R_int+R_condt)
     +          / R_total(i,j)
            lmtd(i) = (T1-T2) / log((T1-Tair(i,j))/(T2-Tair(i,j)))
            call find_eta(i,j,DW,PW,AWS,DT,PT,ST,ATS,c1,eta,eta_c,XKS,Q,
     + lmtd)

c
c *** Estimate the temperatures at the painted surfaces of the tube passes
c *** and wires of each condenser layer and the temperatures of the
c *** surroundings seen by each condenser layer
c
            Ttube(i) = (T1+T2) / 2.
            Twire(i) = Tair(i,j) + eta_c(i) * eta(i) * (Ttube(i)-Tair(i,j))
            Tsurr(i) = (Tair(i,j)+Tair(i-1,j)) / 2
            if (i.eq.1) Tsurr(i) = Tsurr(i) + (Tair(NL,j)-Tair(i-1,j)) / 2
   40     continue
```

```
c
c *** Determine the radiation heat transfer rate
c
          call radiation(NL,AWS,ATS,Qradw,Qradt,Twire,Ttube,Tsurr,vf)

c
c *** Determine the combined natural convection and radiation heat transfer
c *** rate from non-exposed surfaces and the forced convection heat transfer
c *** rate from exposed surfaces
c
          do 50 i=1,NL
            call nonexpose(i,j,coil,NL,NW,AWS,NT,DT,ST,XLTS,Tair,Qne,Ttube)
            Qconv(i,j) = Q(i,j) - Qradt(i) - Qradw(i) - Qne
            Qconvtot = Qconvtot - Qconv(i,j)
            call find_c(i,j,DW,AWS,DT,ATS,Tair,c1,Qconv,Qradw,Qradt,Twire,
     + Ttube)
   50     continue
          if (Qconvtot.lt.0.0001) goto 70
   60   continue

c
c *** Find the hw and the fin efficiency of the wires due to convection heat
c *** transfer only for each condenser layer
c
   70   do 80 i=1,NL
          hw(i,j) = Qconv(i,j)
     +              / ((ATS*sqrt(DW/DT)+eta_c(i)*eta(i)*AWS(i))*lmtd(i))
          write(*,*) i, j, hw(i,j)
          mconv = sqrt(hw(i,j)*ST**2./(XKS*(DW-2.*PW)))
          etaconv(i,j) = tanh(mconv) / mconv

c
c *** Find the Nusselt and Reynolds (based on the minimum flow area) numbers
c *** associated with the wires and tube passes of each condenser layer
c
          Tinput = 0.5 * Twire(i) + 0.5 * Tair(i,j)
          call gaspt(1,Tinput,RHOA,XMUA,XKA,CPA,GRB,PRA,IER)
          Nu_w(i,j) = hw(i,j) * DW / XKA
c
          Vmax = VA(j) * (Wduct/(Wduct-real(NW/2)*DW))
     +          * (Hduct/(Hduct-real(NT)*DT))
          Re_w(i,j) = RHOA * Vmax * DW / XMUA
   80 continue

c
c *** Write the reduced data to output files
c
c     call output(coil,NL,SL,theta,psi,NVA,VA,hw,etaconv,Nu_w,Re_w,Q,
c    + Qconv,R_tube,R_total,datafile)

      end


      subroutine input(coil,NL,SL,theta,psi,DW,PW,SW,NW,XLWS,AWS,DT,PT,DTI,
     + ST,NT,XLTS,ATS,ATIS,Hduct,Wduct,NVA,VA,Tair,Mdot,Tref,datafile)
c ***************************************************************************
c  This subroutine reads the measurements obtained during each experiment
c  and the geometry of the condenser from an existing input file
```

```
c ************************************************************************

      implicit none
      integer coil, NL, psi, NW, NT, NVA, i, j
      real SL, theta, DW, PW, SW, XLWS(6), AWS(6)
      real DT, PT, DTI, ST, XLTS, ATS, ATIS, Hduct, Wduct
      real VA(20), Mdot(20), Tair(0:6,20), Tref(0:6,20)
      real DWP, DTP, pi
      character openfile*24, datafile*18, name(39)*18

c  DWP      -- diameter [m] of the wires (excluding paint thickness)
c  DTP      -- diameter [m] of the tube passes (excluding paint thickness)

      data (name(i),i=1,39) / '( 6/1CF/Single /1)', '( 6/2PF/16.3 mm/1)',
     + '( 6/2PF/23.8 mm/1)', '( 6/2PF/31.2 mm/1)', '( 6/2PF/38.7 mm/1)',
     + '( 6/2PF/46.2 mm/1)', '( 6/2PF/53.6 mm/1)', '( 6/2PF/61.1 mm/1)',
     + '( 6/2PF/68.6 mm/1)', '( 6/2PF/76.0 mm/1)', '( 6/4CF/23.8 mm/1)',
     + '( 6/1CF/45 deg /0)', '( 6/1CF/60 deg /0)', '( 6/1CF/75 deg /0)',
     + '( 6/4CF/45 deg /1)', '( 6/4CF/60 deg /1)', '( 6/4CF/75 deg /1)',
     + '( 8/1CF/Single /1)', '( 8/2CF/23.8 mm/1)', '( 8/1CF/45 deg /0)',
     + '( 8/1CF/60 deg /0)', '( 8/1CF/75 deg /0)', '( 8/4CF/45 deg /1)',
     + '( 8/4CF/60 deg /1)', '( 8/4CF/75 deg /1)', '( 9/3CF/23.8 mm/1)',
     + '( 9/1CF/45 deg /0)', '( 9/1CF/60 deg /0)', '( 9/1CF/75 deg /0)',
     + '( 9/3CF/45 deg /1)', '( 9/3CF/60 deg /1)', '( 9/3CF/75 deg /1)',
     + '(10/4CF/23.8 mm/1)', '(10/1CF/45 deg /0)', '(10/1CF/60 deg /0)',
     + '(10/1CF/75 deg /0)', '(10/4CF/45 deg /1)', '(10/4CF/60 deg /1)',
     + '(10/4CF/75 deg /1)' /

      pi = 3.141592654

      openfile(1:6) = 'input '

c
c *** Inquire as to which data file should be opened
c
      write(*,*) 'Select which data file should be opened'
      write(*,*)
      do 10 i=1,37,2
   10   write(*,20) i, name(i), i+1, name(i+1)
   20   format(2(8x,i2,' -- input ',a18))
      write(*,30) 39, name(39)
   30 format(8x,i2,' -- input ',a18)
c
      read(*,*) j
      if ((j.ge.1).and.(j.le.39)) then
        datafile = name(j)
        openfile(7:24) = datafile
      else
        write(*,*) 'Unavailable data file selected'
        stop
      endif

c
c *** Read the data obtained and the geometry of the condenser from the
c *** existing input file
c
      open(15,file=openfile,status='old')
        do 40 i=1,6
```

```
   40     read(15,*)
          read(15,*) coil, NL, SL, theta, psi, NW, (XLWS(i),i=1,6), NT, XLTS,
     +               Hduct, Wduct, NVA
          read(15,*)
          read(15,*)
          do 50 j=1,NVA
   50     read(15,*) VA(j), (Tref(i,j),i=0,NL), Tair(NL,j), Mdot(j)
       close(15)

c
c *** Initialize parameters not read from input files
c
      if (coil.eq.6) then
        DW = 0.00138
        PW = 0.000015
        SW = 0.00607
        DT = 0.00480
        PT = 0.000020
        DTI = 0.00334
        ST = 0.0254
      elseif (coil.eq.8) then
        DW = 0.00158
        PW = 0.000014
        SW = 0.00634
        DT = 0.00480
        PT = 0.000018
        DTI = 0.00334
        ST = 0.0508
      elseif (coil.eq.9) then
        DW = 0.00157
        PW = 0.000010
        SW = 0.00635
        DT = 0.00483
        PT = 0.000033
        DTI = 0.00334
        ST = 0.03175
      elseif (coil.eq.10) then
        DW = 0.00158
        PW = 0.000013
        SW = 0.00508
        DT = 0.00485
        PT = 0.000043
        DTI = 0.00334
        ST = 0.03175
      else
        write(*,*) 'Unavailable condenser selected'
        stop
      endif

c
c *** Calculate the exposed wire and tube surface areas per condenser layer.
c *** Note that if the condenser was not tested in the variable height test
c *** section, the tube bends must be included in area calculations.
c
      do 60 i=1,NL
        AWS(i) = 0.
        if (i.le.NL) AWS(i) = real(NW) * pi * DW * XLWS(i)
   60 continue
```

```
      ATS = real(NT) * pi * DT * XLTS
      ATIS = real(NT) * pi * DTI * XLTS
      if (SL.gt.10.) then
        ATS = ATS + real(NT-1) * pi**2. * DT * (ST/2.)
        ATIS = ATIS + real(NT-1) * pi**2. * DTI * (ST/2.)
      endif

      return
      end


      subroutine viewfactor(NL,SL,theta,psi,DW,SW,NW,XLWS,DT,ST,NT,XLTS,vf)
c ***************************************************************************
c  This subroutine calculates the view factors between elements of
c  individual multi-layer condenser layers. The wires and tube passes are
c  each assumed to be uniform in temperature along each layer.
c ***************************************************************************

      implicit none
      integer NL, psi, NW, NT, i, j, k, l
      real SL, theta, DW, SW, XLWS(6), avg_XLWS, DT, ST, XLTS, pi
      real fww, fws1, fwt, fws, ftt, fts1, ftw, fts, fs1w, fs1t
      real x, y, flayer, flayerww, flayerwt, flayerws1
      real flayertt, flayertw, flayerts1, tau, vf(13,13)
      real N, phi

c  fww      -- view factor between consecutive wires within the same layer
c  fws1     -- view factor from the condenser wires to an imaginary surface
c  fwt      -- view factor from the condenser wires to the tube passes of
c              the same layer
c  fws      -- view factor from the condenser wires to the surroundings
c  ftt      -- view factor between consecutive tube passes within the same
c              layer
c  fts1     -- view factor from the condenser tube passes to an imaginary
c              surface
c  ftw      -- view factor from the condenser tube passes to the wires of
c              the same layer
c  fts      -- view factor from the condenser tube passes to the
c              surroundings
c  fs1w     -- view factor from an imaginary surface to the condenser wires
c  fs1t     -- view factor from an imaginary surface to the condenser tube
c              passes
c  x        -- ratio of the height of the imaginary surfaces to the distance
c              between them
c  y        -- ratio of the width of the imaginary surfaces to the distance
c              between them
c  flayer   -- view factor between the surfaces tangent to consecutive
c              condenser layers
c  flayerww -- view factor between the wires of consecutive condenser layers
c  flayerwt -- view factor from the wires of one pass to the tube passes of
c              a consecutive layer
c  flayertt -- view factor between the tube passes of consecutive condenser
c              layers
c  flayertw -- view factor from the tube passes of one layer to the wires of
c              a consecutive layer
c  tau      -- effective transmissivity through a condenser layer

      pi = 3.141592654
```

```
c
      avg_XLWS = 0.
      do 10 i=1,NL
   10   avg_XLWS = avg_XLWS + XLWS(i) / real(NL)

c
c *** Calculate the view factors between consecutive wires and consecutive
c *** tube passes within the same layer
c
      fww = (((SW/DW)**2.-1.)**0.5+asin(DW/SW)-(SW/DW)) / pi
      ftt = (((ST/DT)**2.-1.)**0.5+asin(DT/ST)-(ST/DT)) / pi

c
c *** Calculate the view factors between the wires & an imaginary surface
c *** and the tube passes & the same surface.  Take the surface to be a
c *** plane which separates the wires from the tube passes.
c
      fws1 = (1.-2.*fww) / 2.
      fs1w = fws1 * (pi*DW) / SW
c
      fts1 = (1.-2.*ftt) / 2.
      fs1t = fts1 * (pi*DT) / ST

c
c *** Calculate the view factors between the wires and the tube passes of
c *** the same layer
c
      fwt = fws1 * fs1t
      ftw = 2. * fts1 * fs1w

c
c *** Calculate the view factors between the wires & the surroundings and
c *** the tube passes & the surroundings.  Account for interaction between
c *** wires on opposite sides of the tube passes of the same layer.
c
      fws = 1. - 2. * fww - fws1 * (1.-fs1t) * fs1w - fwt
      fts = 1. - 2. * ftt - ftw

c
c *** If the condenser layers are vertical, then calculate the view factor
c *** between parallel imaginary sufaces.  Take these surfaces to be planes
c *** running tangent to each of the layers.
c
      if (NL.eq.1) then
        flayer = 0.
      elseif ((theta.gt.1.53).and.(theta.lt.1.61)) then
        x = avg_XLWS / (SL-DT-2.*DW)
        y = XLTS / (SL-DT-2.*DW)
        flayer = (0.5*log((1.+x**2.)*(1.+y**2.)/(1.+x**2.+y**2.))
     +          + x * (1.+y**2.)**0.5 * atan(x/(1.+y**2.)**0.5)
     +          + y * (1.+x**2.)**0.5 * atan(y/(1.+x**2.)**0.5)
     +          - x * atan(x) - y * atan(y)) * 2. / (pi*x*y)

c
c *** If the condenser layers are inclined, then calculate the view factor
c *** between two rectangles with one common edge and included angle of phi.
c *** Take these surfaces to be planes running tangent to each of the
c *** layers.
```

```
c
      else
        if (psi.eq.0) then
          N = XLTS / avg_XLWS
        else
          N = avg_XLWS / XLTS
        endif
c
        phi = pi - 2. * theta
        call anglevf(N,N,phi,flayer,pi)
      endif

c
c *** Calculate the view factors between elements of consecutive condenser
c *** layers and the effective transmissivity of a condenser layer
c
      flayerww = (fws/2.) * flayer * (fs1w+(1.-fs1w)*(1.-fs1t)*fs1w)
      flayerwt = (fws/2.) * flayer * (1.-fs1w) * fs1t
      flayerws1 = (fws/2.) * flayer * (1.-fs1w)**2 * (1.-fs1t)
c
      flayertt = (fts/2.) * flayer * (1.-fs1w) * fs1t
      flayertw = (fts/2.) * flayer * (fs1w+(1.-fs1w)*(1.-fs1t)*fs1w)
      flayerts1 = (fts/2.) * flayer * (1.-fs1w)**2 * (1.-fs1t)
c
      tau = (1.-fs1w)**2. * (1.-fs1t)

c
c *** Calculate the view factor between the tube passes of each of the
c *** layers
c
      do 20 i=1,NL
        do 20 j=1,NL
          if (i.eq.j) then
            vf(i,j) = ((real(NT)-1.)/real(NT)) * 2. * ftt
          else
            vf(i,j) = flayertt * (flayer*tau)**(abs(i-j)-1.)

c --- staggered tube
c           if (i.eq.2) vf(i,j) = 1.05115046 * vf(i,j)
c           if (i.eq.1) vf(i,j) = 0.87595872 * vf(i,j)

c           if (i.eq.1) vf(i,j) = (fts/2.) * flayer * fs1t
c                                                   [for 2 layer one-sided coils]
c           if (i.eq.2) vf(i,j) = (0.5-ftt) * flayer * (1.-fs1w) * fs1t
c                                                   [for 2 layer one-sided coils]

          endif
   20 continue

c
c *** Calculate the view factor between the wires of each of the layers
c
      do 30 i=NL+1,2*NL
        do 30 j=NL+1,2*NL
          if (i.eq.j) then
            vf(i,j) = ((real(NW)-2.)/real(NW))
     +                * (2.*fww+fws1*(1.-fs1t)*fs1w)
c    +                * (2.*fww)                    [for one-sided coils]
```

```
          else
            vf(i,j) = flayerww * (flayer*tau)**(abs(i-j)-1.)

c --- staggered tube
c           if (i.eq.2) vf(i,j) = 1.05115046 * vf(i,j)
c           if (i.eq.1) vf(i,j) = 0.87595872 * vf(i,j)

c           if (i.eq.1) vf(i,j) = (0.5-fww) * flayer * (1.-fs1t) * fs1w
c                                                    [for 2 layer one-sided coils]
c           if (i.eq.2) vf(i,j) = (0.5-fww-fws1*(1.-fs1t)*fs1w-fwt) * flayer
c    +                           * fs1w              [for 2 layer one-sided coils]
          endif
   30 continue

c
c *** Calculate the view factors between the wires and tube passes of each
c *** of the layers
c
      do 40 i=1,NL
        do 40 j=NL+1,2*NL
          if (i.eq.(j-NL)) then
c           vf(i,j) = ftw / 2.                     [for one-sided coil only]
            vf(i,j) = ftw
          else
            vf(i,j) = flayertw * (flayer*tau)**(abs(i-j+NL)-1.)

c --- staggered tube
c           if (i.eq.2) vf(i,j) = 1.05115046 * vf(i,j)
c           if (i.eq.1) vf(i,j) = 0.87595872 * vf(i,j)

c           if (i.eq.1) vf(i,j) = (fts/2.) * flayer * (1.-fs1t) * fs1w
c                                                    [for 2 layer one-sided coils]
c           if (i.eq.2) vf(i,j) = (0.5-ftt) * flayer * fs1w
c                                                    [for 2 layer one-sided coils]
          endif
   40 continue
c
      do 50 i=NL+1,2*NL
        do 50 j=1,NL
          if ((i-NL).eq.j) then
            vf(i,j) = fwt
          else
            vf(i,j) = flayerwt * (flayer*tau)**(abs(i-j-NL)-1.)

c --- staggered tube
c           if (i.eq.2) vf(i,j) = 1.05115046 * vf(i,j)
c           if (i.eq.1) vf(i,j) = 0.87595872 * vf(i,j)

c           if (i.eq.1) vf(i,j) = (0.5-fww) * flayer * fs1t
c                                                    [for 2 layer one-sided coils]
c           if (i.eq.2) vf(i,j) = (0.5-fww-fws1*(1.-fs1t)*fs1w-fwt) * flayer
c    +                           * (1.-fs1w) * fs1t
c                                                    [for 2 layer one-sided coils]
          endif
   50 continue

c
c *** Calculate the view factors between the condenser layers and the
```

```
c *** surroundings
c
      do 60 i=1,2*NL
        vf(i,2*NL+1) = 1.
        do 60 j=1,2*NL
          vf(i,2*NL+1) = vf(i,2*NL+1) - vf(i,j)
   60 continue

      return
      end


      subroutine anglevf(L,N,phi,flayer,pi)
c ***********************************************************************
c  This subroutine calculates the view factor between two rectangles with
c  one common edge and included angle of phi
c ***********************************************************************

      implicit none
      integer i, division
      real L, N, phi, flayer, pi
      real s, c, t, lawcos, z, m

      s = sin(phi)
      c = cos(phi)
      t = tan(phi)
      lawcos = N**2. + L**2. - 2. * N * L * cos(phi)
c
      flayer = -(1./4.) * sin(2.*phi) * (N*L*s + (pi/2.-phi)*(N**2.+L**2.)
     +        + L**2.*atan((N-L*c)/(L*s)) + N**2.*atan((L-N*c)/(N*s)))
c
      flayer = flayer + (1./4.) * s**2.
     +        * log(((1.+N**2.)*(1.+L**2.)/(1.+lawcos))**(1./s**2.+1./t**2.)
     +        * (L**2.*(1.+lawcos)/((1.+L**2.)*lawcos))**(L**2.))
c
      flayer = flayer + (1./4.) * N**2. * s**2.
     +        * log((N**2./lawcos) * ((1.+N**2.)/(1.+lawcos))**cos(2.*phi))
c
      flayer = flayer + L * atan(1./L) + N * atan(1./N)
     +        - sqrt(lawcos) * atan(1./sqrt(lawcos))
c
      flayer = flayer + (1./2.) * N * s * sin(2.*phi) * sqrt(1+N**2.*s**2.)
     +        * (atan(N*c/sqrt(1+N**2.*s**2.))
     +        +atan((L-N*c)/sqrt(1+N**2.*s**2.)))
c
      z = 0.
      division = 250
      do 10 i=0,division
        if ((i.eq.0).or.(i.eq.division)) then
          m = 0.5
        else
          m = 1.
        endif
        flayer = flayer + m * (L/real(division)) * c * sqrt(1.+z**2.*s**2.)
     +          * (atan((N-z*c)/sqrt(1.+z**2.*s**2.))
     +          + atan(z*c/sqrt(1.+z**2.*s**2.)))
        z = z + L / real(division)
   10 continue
```

```
c
      flayer = flayer / (pi*L)

      return
      end


      subroutine gaspt(NGAS,T,RHO,XMU,XK,CP,GRB,PR,IER)
c ***********************************************************************
c  Programmed by: A. M. Clausing;  Version: April 1982
c  Properties of gases in SI units (T.gt.0) or English units (T.lt.0)
c  functional representations used are of the form:  Y = A * T**B.
c  Arrays A and B contain the respective constants.
c ***********************************************************************

c  input:
c  NGAS -- type of gas
c              1 = dry air
c              2 = nitrogen
c  T    -- absolute temperature [K] if positive or [R] if negative
c              150 K < T < 2100 K for dry air
c              83 K < T < 450 K for nitrogen
c              ranges are specified in array R

c  output:
c  RHO  -- density [kg/m^3] or [lbm/ft^3]
c  XMU  -- viscosity [kg/m-s] or [lbm/ft-s]
c  XK   -- thermal conductivity [W/m-K] or [BTU/hr-ft-R]
c  CP   -- specific heat [J/kg-K] or [Btu/lbm-R]
c  GRB  -- G * beta / XNU**2 (1/M3-K) OR (1/fT3-R)
c  PR   -- Prandtl number (dimensionless)
c  IER  -- error parameter
c              1 = gas number does not exist - gas is assumed to be air
c              2 = temperature out of range of property subroutine

      dimension A(15,2), B(15,2), R(3,2)
c
      data A / 364.1, .1764E-6, .1423E-3, 990.8, .4178E20, 1.23, 350.6,
     + .4914E-6, .2494E-3, 299.4, .4985E19, .59,3*.0, 432.4, 9.1E-8,
     + 1.239E-4, 1553., 4.379E20, 1.137, 351.6, .18E-6, .221E-3, 1031.,
     + .408E20, .841,3*.0 /
c
      data B / -1.005, .814, .9138, .00316, -4.639, -.09685, -.999, .6429,
     + .8152, .1962, -4.284, .0239, 3*.0, -1.046, .938, .9466, -.079,
     + -5.102, -.0872, -1.005, .8058, .8345, .00239, -4.636, -.02652, 3*.0 /
c
      data R / 150., 400., 2100., 83., 160., 450. /

      IER = 0
      if ((NGAS.gt.0).and.(NGAS.lt.3)) goto 10
      IER = 1
      NGAS = 1
   10 I = 1
      TP = T
      if (T.lt..0) TP = -T / 1.8
      if ((TP.lt.R(1,NGAS)).or.(TP.gt.R(3,NGAS))) IER = 2
      if (TP.gt.R(2,NGAS)) I = 7
```

```
c
c *** Calculate thermophysical gas properties
c
      RHO = A(I,NGAS) * TP**B(I,NGAS)
      XMU = A(I+1,NGAS) * TP**B(I+1,NGAS)
      XK = A(I+2,NGAS) * TP**B(I+2,NGAS)
      CP = A(I+3,NGAS) * TP**B(I+3,NGAS)
      GRB = A(I+4,NGAS) * TP**B(I+4,NGAS)
      PR = A(I+5,NGAS) * TP**B(I+5,NGAS)

c
c *** Convert to English units if desired (ie. T<0)
c
      if (T.gt..0) return
      RHO = RHO / 16.02
      XMU = XMU / 1.488
      XK = XK / 1.731
      CP = CP / 4187.
      GRB = GRB / 63.57

      return
      end


      subroutine internal(i,j,DTI,ST,NT,ATIS,Mdot,Tref,HR,R_int)
c ***************************************************************************
c  This subroutine determines the thermal resistance corresponding to the
c  convection heat transfer between the refrigerant flow and the inner
c  surface of the condenser tube wall.  The Gnielinski Correlation is used
c  to determine the Nusselt number associated with refrigerant flow.
c ***************************************************************************

      implicit none
      integer NT, i, j
      real DTI, ST, ATIS, Mdot(20), Tref(0:6,20), Tinput
      real RHOR, XMUR, XKR, PRR, RER, F, NUR, HR, R_int, Pdrop, pi

c  RHOR     -- density [kg/m^3] of the refrigerant
c  XMUR     -- viscosity [kg/m-s] of the refrigerant
c  XKR      -- thermal conductivity [W/m-K] of the refrigerant
c  PRR      -- Prandtl number of the refrigerant
c  RER      -- Reynolds number associated with the refrigerant flow in the
c              condenser tube
c  F        -- dimensionless friction factor associated with the
c              refrigerant flow in the condenser tube
c  NUR      -- Nusselt number associated with the refrigerant flow in the
c              condenser tube
c  Pdrop    -- internal pressure [Pa] difference between the inlet and the
c              outlet of a particular condenser layer

      RHOR = 989.
      pi = 3.141592654

c
c *** Calculate the thermophysical properties of the refrigerant flowing
c *** through each condenser layer
c
      Tinput = (Tref(i-1,j)+Tref(i,j)) / 2.
```

```
       XMUR = (8.7128*10.**-2.) - (7.4592*10.**-4.) * Tinput
      +       + (2.1577*10.**-6.) * Tinput**2.
      +       - (2.0997*10.**-9.) * Tinput**3.
       XKR = - (2.8155) + (2.6844*10.**-2.) * Tinput
      +      - (7.0477*10.**-5.) * Tinput**2.
      +      + (6.3449*10.**-8.) * Tinput**3.
       PRR = (731.79) - (6.3177) * Tinput
      +      + (1.8383*10.**-2.) * Tinput**2.
      +      - (1.7969*10.**-5.) * Tinput**3.

c
c *** Determine the internal thermal resistance using the Gnielinski
c *** Correlation
c
       RER = 4. * Mdot(j) / (pi*DTI*XMUR)
       if (RER.lt.2300) write(*,*) 'Error - Flow is laminar'
       if (RER.gt.5000000.) write(*,*) 'Error - Correlation limits violated'
       F = (0.79*log(RER)-1.64) **(-2.)
       NUR = (F/8.) * (RER-1000.) * PRR
      +      / (1. + 12.7 * (F/8.)**(1./2.) * (PRR**(2./3.)-1.))
       HR = NUR * XKR / DTI
       R_int = 1. / (HR*ATIS)
c      Pdrop = 8. * (pi*DTI*real(NT)*10.25+real(NT)*pi**2.*DTI*(ST/2.))
c     +        * F * Mdot**2. / (pi**3.*RHOR*DTI**6.)

       return
       end


       subroutine spotweld(i,j,coil,DW,AWS,DT,ATS,Tair,eta,eta_c,Tref,HR,
      + Ttube,fractionQw)
c ***************************************************************************
c  This subroutine determines the resistance resulting from thermal
c  constriction around each of the spot welds
c ***************************************************************************

       implicit none
       integer coil, i, j
       real DW, AWS(6), DT, ATS, Tair(0:6,20), eta(6), eta_c(6)
       real Tref(0:6,20), HR, Ttube(6), fractionQw, eta_t

c
c *** Approximate the fraction of the total energy leaving the condenser
c *** through the wires
c
       fractionQw = eta_c(i) * eta(i) * AWS(i)
      +            / (sqrt(DW/DT)*ATS+eta_c(i)*eta(i)*AWS(i))

c
c *** Determine the fin efficiency of the condenser tube
c
       if (coil.eq.6) then
         eta_t = 1. - (9.8263*10.**(-5.))*(HR*fractionQw)
      +         + (8.461*10.**(-9.))*(HR*fractionQw)**2.
      +         - (3.5651*10.**(-13.))*(HR*fractionQw)**3.
       elseif ((coil.eq.8).or.(coil.eq.9)) then
         eta_t = 1. - (1.0135*10.**(-4.))*(HR*fractionQw)
      +         + (8.9264*10.**(-9.))*(HR*fractionQw)**2.
```

```
     +         - (3.8074*10.**(-13.))*(HR*fractionQw)**3.
      else
        eta_t = 1. - (7.9181*10.**(-5.))*(HR*fractionQw)
     +         + (5.908*10.**(-9.))*(HR*fractionQw)**2.
     +         - (2.2998*10.**(-13.))*(HR*fractionQw)**3.
      endif

c
c *** Determine the effect of fin efficiency of the condenser tube on the
c *** wires of the condenser
c
      eta_c(i) = 1. + (1.-eta_t) * (Ttube(i)-0.5*Tref(i,j)-0.5*Tref(i-1,j))
     +          / (eta_t*(Ttube(i)-Tair(i,j)))

      return
      end


      subroutine find_eta(i,j,DW,PW,AWS,DT,PT,ST,ATS,c1,eta,eta_c,XKS,Q,
     + lmtd)
c ***************************************************************************
c  This subroutine approximates the fin efficiency of the wire of each
c  condenser layer.  Simultaneous equations are solved using a
c  Newton-Raphson procedure.
c ***************************************************************************

      implicit none
      integer i, j, k
      real DW, PW, AWS(6), DT, PT, ST, ATS
      real c1(6), eta(6), eta_c(6), XKS, Q(6,20), lmtd(6)
      real a(3,3), b(3), x(3), xnorm, fnorm

c  a(i,j)  -- Before gaussj subroutine:  Jacobian based on the values of
c               variables at the previous interation
c             After gaussj subroutine:  inverted martix
c  b(i)    -- Before gaussj subroutine:  vector of function values based on
c               the values of variables at the previous interation
c             After gaussj subroutine:  residual vector
c  x(i)    -- solution vector:  x(1) = h; x(2) = eta; x(3) = m
c  xnorm   -- 1-norm value of the x vector residuals
c  fnorm   -- 1-norm value of the function values

c
c *** Assign inital values to h, eta, and m
c
      if (j.eq.1) then
        x(1) = 53.
        x(2) = 0.95
        x(3) = 0.41
      else
        x(2) = eta(i)
        x(1) = Q(i,j) / ((c1(i)*ATS+eta_c(i)*x(2)*AWS(i))*lmtd(i))
        x(3) = sqrt(x(1)*ST**2./(XKS*(DW-2.*PW)))
      endif

c
c *** Iterated to find h, eta, and m
c
```

```
      do 10 k=1,100

c
c *** Calculate the function values of the system based on the values of the
c *** variables at the previous iteration
c
        b(1) = Q(i,j) / ((c1(i)*ATS+eta_c(i)*x(2)*AWS(i))*lmtd(i)) - x(1)
        b(2) = tanh(x(3))/x(3) - x(2)
c       b(2) = (0.8*tanh(x(3))+0.2*tanh(x(3)/1.25)*1.25)/x(3) - x(2)
        b(3) = sqrt(x(1)*ST**2./(XKS*(DW-2.*PW))) - x(3)

c
c *** Calculate the 1-norm value of the function values. If below the
c *** acceptable tolerance, then return an approximate solution vector to
c *** the main program
c
        fnorm = abs(b(1)/100.) + abs(b(2)) + abs(b(3))
        if (fnorm.lt.0.00001) goto 20

c
c *** Calculate the Jacobian of the system based on the values of variables
c *** at the previous interation
c
        a(1,1) = -1.
        a(1,2) = - AWS(i) * Q(i,j)
     +           / ((c1(i)*ATS+eta_c(i)*x(2)*AWS(i))**2.*lmtd(i))
        a(1,3) = 0.
        a(2,1) = 0.
        a(2,2) = -1.
        a(2,3) = (x(3)*(1./cosh(x(3)))**2.-tanh(x(3))) / x(3)**2.
c       a(2,3) = 0.8 * (x(3)*(1./cosh(x(3)))**2.-tanh(x(3)))/x(3)**2.
c    +          + 0.2 * (x(3)/1.25*(1./cosh(x(3)/1.25))**2.
c    +          -tanh(x(3)/1.25))/(x(3)/1.25)**2.
        a(3,1) = 0.5 * sqrt(ST**2./(x(1)*XKS*(DW-2.*PW)))
        a(3,2) = 0.
        a(3,3) = -1.

c
c *** Obtain the solution residuals by Gauss Jordan elimination
c
        call gaussj(a,3,3,b,1,1)

c
c *** Calculate the values of the variables at the current iteration
c
        x(1) = x(1) - b(1)
        x(2) = x(2) - b(2)
        x(3) = x(3) - b(3)

c
c *** Calculate the 1-norm value of the x residuals.  If below the
c *** acceptable tolerance, then return an approximate solution vector to
c *** the main program.
c
        xnorm = abs(b(1)/100.) + abs(b(2)) + abs(b(3))
        if (xnorm.lt.0.001) goto 20
   10 continue
c
```

```
      write(*,*) 'Newton-Raphson failed to converge'
   20 eta(i) = x(2)

      return
      end


      subroutine gaussj(a,n,np,b,m,mp)
c ***********************************************************************
c  This routine yields a linear solution by Gauss-Jordan elimination.
c  a(1:n,1:n) is an input matrix stored in an array of physical dimensions
c  np by np.  b(1:n,1:m) is an input matrix containing the m right-hand side
c  vectors, stored in an array of physical dimensions np by mp.  On output,
c  a(1:n,1:n) is replaced by its matrix inverse, and b(1:n,1:m) is replaced
c  by the corresponding set of solution vectors.  nmax is the largest
c  anticipated value of n.
c
c  Obtained from 'Numerical Recipes'.
c ***********************************************************************

      implicit none
      integer m, mp, n, np, nmax
      real a(np,np), b(np,mp)
      parameter (nmax=50)
      integer i, icol, irow, j, k, l, ll
      integer ipiv(nmax), indxr(nmax), indxc(nmax)
      real big, dum, pivinv
c
c *** nmax is the largest anticipated value of n.  The integer arrays ipiv,
c *** indxr, & indxc are used for bookkeeping on the pivoting.
c

      do 10 j=1,n
        ipiv(j) = 0
   10 continue

c
c *** This is the main loop over the columns to be reduced
c
      do 110 i=1,n
        big = 0.

c
c *** This is the outer loop of the search for a pivot element
c
        do 30 j=1,n
          if (ipiv(j).ne.1) then
            do 20 k=1,n
              if (ipiv(k).eq.0) then
                if (abs(a(j,k)).ge.big) then
                  big = abs(a(j,k))
                  irow = j
                  icol = k
                endif
              elseif (ipiv(k).gt.1) then
                pause 'singular matrix in gaussj'
              endif
   20       continue
```

```
          endif
   30   continue
        ipiv(icol) = ipiv(icol) + 1

c
c *** We now have the pivot element, so we interchange rows, if needed, to
c *** put the pivot element on the diagonal.  The columns are not physically
c *** interchanged, only relabeled:
c ***
c *** indxc(i), the column of the ith pivot element, is the ith column that
c *** is reduced, while indxr(i) is the row in which the pivot element was
c *** originally located.  If indxr(i) not equal to indxc(i) there is an
c *** implied column interchange.  With this form of bookkeeping, the
c *** solution b's will end up in the correct order, and the inverse matrix
c *** will be scrambled by columns.
c
        if (irow.ne.icol) then
          do 40 l=1,n
            dum = a(irow,l)
            a(irow,l) = a(icol,l)
            a(icol,l) = dum
   40     continue
          do 50 l=1,m
            dum = b(irow,l)
            b(irow,l) = b(icol,l)
            b(icol,l) = dum
   50     continue
        endif

c
c *** We are now ready to divide the pivot row by the pivot element, located
c *** at irow and icol
c
        indxr(i) = irow
        indxc(i) = icol
        if (a(icol,icol).eq.0.) pause 'singular matrix in gaussj'
        pivinv = 1./a(icol,icol)
        a(icol,icol) = 1.
        do 60 l=1,n
          a(icol,l) = a(icol,l) * pivinv
   60   continue
        do 70 l=1,m
          b(icol,l) = b(icol,l) * pivinv
   70   continue

c
c *** Next, we reduce all the rows except the pivot row
c
        do 100 ll=1,n
          if (ll.ne.icol) then
            dum = a(ll,icol)
            a(ll,icol) = 0.
            do 80 l=1,n
              a(ll,l) = a(ll,l) - a(icol,l) * dum
   80       continue
            do 90 l=1,m
              b(ll,l) = b(ll,l) - b(icol,l) * dum
   90       continue
```

```
          endif
  100   continue
  110 continue

c
c *** This is the end of the main loop over columns of the reduction.  It
c *** only remains to unscramble the solution in view of the column
c *** interchanges.  We do this by interchanging pairs of columns in the
c *** reverse order that the permutation was built up.
c
      do 130 l=n,1,-1
        if (indxr(l).ne.indxc(l)) then
          do 120 k=1,n
            dum = a(k,indxr(l))
            a(k,indxr(l)) = a(k,indxc(l))
            a(k,indxc(l)) = dum
  120     continue
        endif
  130 continue

      return
      end


      subroutine radiation(NL,AWS,ATS,Qradw,Qradt,Twire,Ttube,Tsurr,vf)
c ***************************************************************************
c  This subroutine determines the radiation heat transfer rate from each
c  condenser layer
c ***************************************************************************

      implicit none
      integer NL, i, j
      real AWS(6), ATS, Qradw(6), Qradt(6), Twire(6), Ttube(6), Tsurr(6)
      real vf(13,13), sigma, epsilon, a(12,12), b(12)

c  sigma   -- Stefan-Boltzmann constant
c  epsilon -- total, hemispherical emissivity of the paint covering the
c             condenser surfaces
c  a(i,j)  -- Before gaussj subroutine:  coefficients of the radiosities of
c               different nodes
c             After gaussj subroutine:  inverted martix
c  b(i)    -- Before gaussj subroutine: vector of the blackbody emissivities
c               of different nodes
c             After gaussj subroutine:  vector of the radiosities of
c               different nodes

      sigma = 5.67*10.**(-8.)
      epsilon = 0.95

c
c *** Set up heat transfer equations
c
      do 10 i=1,2*NL
        if (i.le.NL) then
          b(i) = sigma * Ttube(i)**4. * epsilon / (1.-epsilon)
     +           + sigma * Tsurr(i)**4. * vf(i,2*NL+1)
        else
          b(i) = sigma * Twire(i-NL)**4. * epsilon / (1.-epsilon)
```

```
     +           + sigma * Tsurr(i-NL)**4. * vf(i,2*NL+1)
         endif

c
c *** Obtain the radiosities by Gauss Jordan elimination
c
         do 10 j=1,2*NL
           if (i.eq.j) then
             a(i,j) = 1. / (1.-epsilon) - vf(i,j)
           else
             a(i,j) = -vf(i,j)
           endif
   10 continue
c
      call gaussj(a,2*NL,12,b,1,1)

c
c *** Determine the radiation heat transfer rate
c
      do 20 i=1,NL
        Qradt(i) = (sigma*Ttube(i)**4.-b(i)) * epsilon * ATS / (1.-epsilon)
        Qradw(i) = (sigma*Twire(i)**4.-b(i+NL)) * epsilon * AWS(i)
     +           / (1.-epsilon)

c --- staggered tube
c       if (i.eq.2) Qradt(i) = Qradt(i) * 5. / 6.
c       if (i.eq.2) Qradw(i) = Qradw(i) * 5. / 6.

   20 continue

      return
      end


      subroutine nonexpose(i,j,coil,NL,NW,AWS,NT,DT,ST,XLTS,Tair,Qne,Ttube)
c ***************************************************************************
c  This subroutine estimates the combined natural convection and radiation
c  heat transfer rate from condenser surfaces which are not exposed to the
c  forced convection air flow
c ***************************************************************************

      implicit none
      integer coil, NL, NW, NT, i, j
      real AWS(6), DT, ST, XLTS, A_ne, Tair(0:6,20), Tinput
      real RHOA, XMUA, XKA, CPA, GRB, PRA, IER, Ttube(6)
      real diffusivity, Ra, h_ne, sigma, Qne, pi

      sigma = 5.67 * 10.**(-8.)
      pi = 3.141592654

c
c *** Determine the total area of the non-exposed surfaces
c
      A_ne = real(NT-1) * pi**2. * DT * (ST/2.)
      if (coil.eq.6) then
        A_ne = A_ne + real(NT) * pi * DT * (0.256-XLTS)
     +        + AWS(i) * (66.-real(NW)) / real(NW)
      elseif (coil.eq.8) then
```

```
         A_ne = A_ne + real(NT) * pi * DT * (0.483-XLTS)
     +         + AWS(i) * (150.-real(NW)) / real(NW)
         elseif (coil.eq.9) then
           A_ne = A_ne + real(NT) * pi * DT * (0.203-XLTS)
     +         + AWS(i) * (60.-real(NW)) / real(NW)
         else
           A_ne = A_ne + real(NT) * pi * DT * (0.716-XLTS)
     +         + AWS(i) * (204.-real(NW)) / real(NW)
         endif

c
c *** Estimate natural convection heat transfer rate from non-exposed
c *** surfaces
c
         Tinput = (Ttube(i)+Tair(NL,j)) / 2.
         call gaspt(1,Tinput,RHOA,XMUA,XKA,CPA,GRB,PRA,IER)
c
         diffusivity = XKA / (RHOA*CPA)
         Ra = 9.807 * (Ttube(i)-Tair(i,j)) * DT**3. * RHOA
     +    / (XMUA*diffusivity*Tinput)
         h_ne = (XKA/DT) * (0.6+0.387*Ra**(1./6.)
     +      / (1.+(0.559/PRA)**(9./16.))**(8./27.))**2.
         Qne = h_ne * A_ne * (Ttube(i)-Tair(NL,j))

c
c *** Estimate radiation heat transfer rate from non-exposed surfaces
c
         if (coil.ne.10) then
           Qne = Qne + sigma * 0.95 * A_ne * (Ttube(i)**4.-Tair(NL,j)**4.)
         else
           Qne = Qne + sigma * 0.50 * A_ne * (Ttube(i)**4.-Tair(NL,j)**4.)
         endif

         return
         end


         subroutine find_c(i,j,DW,AWS,DT,ATS,Tair,c1,Qconv,Qradw,Qradt,Twire,
        + Ttube)
c ***********************************************************************
c  This subroutine adjusts the constant c1
c ***********************************************************************

         implicit none
         integer i, j
         real DW, AWS(6), DT, ATS, Tair(0:6,20), c1(6)
         real Qradw(6), Qradt(6), Qconv(6,20), Qconvt, Qconvw
         real Twire(6), Ttube(6), deltaw, deltat

c  Qconvw   -- approximate heat transfer rate due to convection from the
c              wires
c  Qconvt   -- approximate heat transfer rate due to convection from the
c              tube passes

c
c *** Determine the convection heat transfer rates from the wires and tube
c *** passes of each condenser layer
c
```

```
      deltaw = (Twire(i)-Tair(i,j))
      deltat = (Ttube(i)-Tair(i,j))
      Qconvw = Qconv(i,j) / (1.+(ATS/AWS(i))*sqrt(DW/DT)*(deltat/deltaw))
      Qconvt = Qconv(i,j) - Qconvw

c
c *** Determine the ratio of the total heat transfer coefficients of the
c *** wires and tube passes
c
      c1(i) = ((Qradt(i)+Qconvt)/(Qradw(i)+Qconvw)) * (AWS(i)/ATS)
     +       * (deltaw/deltat)

      return
      end


      subroutine output(coil,NL,SL,theta,psi,NVA,VA,hw,etaconv,Nu_w,Re_w,Q,
     + Qconv,R_tube,R_total,datafile)
c ***************************************************************************
c  This subroutine writes the reduced data to output files.  Note that the
c  condenser layers are numbered from upstream to downstream with respect
c  to the air flow (opposite of the program) for purposes of output.
c ***************************************************************************

      implicit none
      integer coil, NL, psi, NVA, i, j
      real SL, theta, VA(20), hw(6,20), etaconv(6,20)
      real Nu_w(6,20), Re_w(6,20)
      real Q(6,20), Qconv(6,20), R_tube(6,20), R_total(6,20)
      character openfile*25, datafile*18, passname(6)*7

      data (passname(i),i=1,6) / 'layer1 ', 'layer2 ', 'layer3 ', 'layer4 ',
     + 'layer5 ', 'layer6 ' /

      do 30 i=1,NL
        openfile(1:7) = passname(NL+1-i)
        openfile(8:25) = datafile
c
        open(i*2+20,file=openfile)
          write(i*2+20,*) 'vel [m/s], layer #, Re_w, Nu_w,',
     +         'h_w [W/m^2-K], eta_w, %R_tube, %Q_rad'
          do 20 j=1,NVA
            write(i*2+20,10) VA(j), NL+1-i, Re_w(i,j), Nu_w(i,j), hw(i,j),
     +           etaconv(i,j), 100.*R_tube(i,j)/R_total(i,j),
     +           100.*(1.-(Qconv(i,j)/Q(i,j)))
   10   format(f4.2,',',i1,',',f5.1,',',f5.3,',',f5.1,',',f5.4,',',f5.2,',',
     + f5.2)
   20   continue
        close(i*2+20)
   30 continue

      return
      end
```

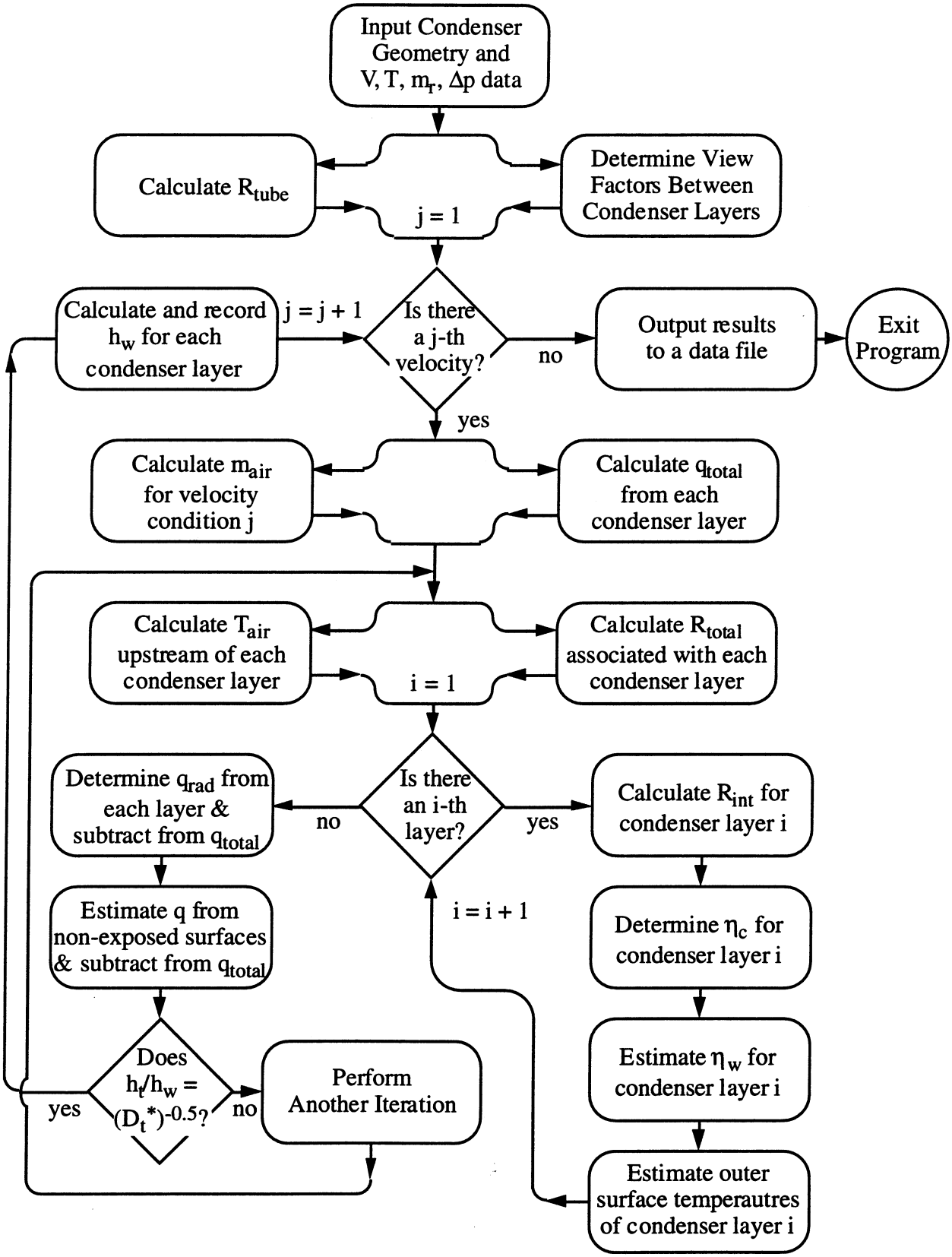

Figure B.1 Flow chart for the multi-layer wire-on-tube condenser data reduction program

APPENDIX C: PROGRAM USED TO EVALUATE THE FIN EFFICIENCY OF THE CONDENSER TUBE PASSES

```
      program constrict
c ***********************************************************************
c   This program simulates the two-dimensional (i.e. axial & azimuthal),
c   steady-state conduction occurring within the serpentine tube of a
c   wire-on-tube condenser.  Since energy is conducted from the entire
c   inner surface of the condenser tube to a much smaller area (i.e. the
c   locations on the outer tube surface at which wires are spot welded),
c   a temperature gradient is formed around each weld spot, causing
c   thermal constriction to occur.  This thermal constriction effect is
c   simulated using equations formulated with the finite volume method
c   of discretization.  User input is read from the file 'constrict.in'
c   and output is written to 'constrict.out'.
c ***********************************************************************

      implicit none
      integer nx, ny, nsy, maxstep, nstart(199), count, i, j, l
      double precision T(0:200,0:200), Told(0:200,0:200)
      double precision dx(0:200), dy(0:200), dz
      double precision k, h, omega, tolerance, error
      double precision aw(199,199), ae(199,199), as(199,199)
      double precision an(199,199), ap(199,199), s(199,199)
      double precision conduction, convection

c   nx          -- number of nodes in x-direction
c   ny          -- number of nodes in y-direction
c   nsy         -- number of nodes in y-direction included in weld spot
c   maxstep     -- maximum number of iterative steps allowed
c   nstart(j)   -- node number of row j above which T can change
c   T(i,j)      -- non-dimensional temperature of node (i,j)
c   Told(i,j)   -- non-dimensional temperature of node (i,j) at previous
c                  iteration
c   dx(i)       -- x-dimension of node column i
c   dy(j)       -- y-dimension of node row j
c   dz          -- z-dimension (thickness) of analysis domain
c   k           -- thermal conductivity [W/m-K] of tube wall
c   h           -- convection coefficient [W/m2-K] associated with
c                  refrigerant flow
c   omega       -- successive over-relaxation factor
c   tolerance   -- size of largest allowable error
c   error       -- average absolute difference between subsequent
c                  temperature solutions
c   aw(i,j)     -- coefficient associated with T(i-1,j)
c   ae(i,j)     -- coefficient associated with T(i+1,j)
c   as(i,j)     -- coefficient associated with T(i,j-1)
c   an(i,j)     -- coefficient associated with T(i,j+1)
c   ap(i,j)     -- coefficient associated with T(i,j)
c   s(i,j)      -- heat transfer source term [W/m3] of node (i,j)

c
c *** Read execution information from existing input file:
c *** 'constrict.in' and initialize arrays
c
      call input(nx,ny,nsy,maxstep,nstart,T,dx,dy,dz,k,h,omega,
     + tolerance,aw,ae,as,an,ap,s)
```

```
      count = 0

c
c *** Print headings for screen output
c
c     write(*,*)
c     write(*,*) 'Iteration  TempError     Qin/Qout'

c
c *** Determine the coefficients of the heat transfer equations due to
c *** conduction through the tube wall and convection with the
c *** refrigerant flow
c
      do 40 l=1,maxstep
        do 20 j=1,ny
          do 10 i=nstart(j),nx
            aw(i,j) = (k/dx(i)) * 2.d0 / (dx(i-1)+dx(i))
            ae(i,j) = (k/dx(i)) * 2.d0 / (dx(i)+dx(i+1))
            as(i,j) = (k/dy(j)) * 2.d0 / (dy(j-1)+dy(j))
            an(i,j) = (k/dy(j)) * 2.d0 / (dy(j)+dy(j+1))
            ap(i,j) = aw(i,j) + ae(i,j) + as(i,j) + an(i,j) + h / dz

c
c *** Update Told by setting Told(i,j) equal to T(i,j)
c
            Told(i,j) = T(i,j)

c
c *** Adjust the temperatures of boundary nodes such that the boundary
c *** appears to be adiabatic
c
            if (j.eq.ny) then
              T(i,0) = T(i,1)
              Told(i,0) = T(i,1)
              T(i,ny+1) = T(i,ny)
              Told(i,ny+1) = T(i,ny)
            endif
   10     continue
c
          if (j.gt.nsy) then
            T(0,j) = T(1,j)
            Told(0,j) = T(1,j)
          else
            T(0,j) = 1.0d0
            Told(0,j) = 1.0d0
          endif
          T(nx+1,j) = T(nx,j)
          Told(nx+1,j) = T(nx,j)
   20   continue

c
c *** Solve the (nx) x (ny) set of simultaneous equations
c
        call gaussseidel(nx,ny,nstart,T,Told,omega,aw,ae,as,an,ap,s)

c
c *** Check to see if existing error is below specified tolerance
c
```

```
         call residual(nx,ny,nstart,T,dx,dy,dz,k,h,error,aw,ae,as,an,ap,
     + s,conduction,convection)
         if (error.lt.tolerance) goto 50
c
         count = count + 1
         if (count.eq.100) then
           write(*,30) l, error, conduction / convection
   30      format(3x,i4,4x,f11.10,4x,f7.6)
           count = 0
         endif
   40 continue
      write(*,*) 'Unable to obtain solution within error limits after',
     + maxstep, 'iterations'

c
c *** Writes execution information and results to output file
c
   50 call output(nx,ny,T,dx,dy,dz,k,h)

      end


      subroutine input(nx,ny,nsy,maxstep,nstart,T,dx,dy,dz,k,h,omega,
     + tolerance,aw,ae,as,an,ap,s)
c **********************************************************************
c   This subroutine reads execution information from existing input
c   file: 'constrict.in' and initializes arrays
c **********************************************************************

      implicit none
      integer nx, ny, nsy, maxstep, nstart(199), i, j
      double precision T(0:200,0:200), dx(0:200), dy(0:200), dz
      double precision dxstd, dystd, k, h, omega, tolerance, factor
      double precision aw(199,199), ae(199,199), as(199,199)
      double precision an(199,199), ap(199,199), s(199,199)

c
c *** Read the execution information from existing input file
c
      open(15,file='constrict.in',status='old')
        read(15,*) nx, ny, nsy, maxstep, dz, k, h, omega, tolerance
        if (nx.gt.199) nx = 199
        if (ny.gt.199) ny = 199
        read(15,*) dxstd, dx(1), dx(nx), dystd, dy(1), dy(ny)
        read(15,*) (nstart(j),j=1,nsy)
      close(15)

c
c *** Initialize nstart and coefficient arrays
c
      factor = 0.3d0 / real(nx)**2.0d0
      do 20 j=1,ny
        if (j.gt.nsy) nstart(j) = 1
        do 10 i=1,nx
          aw(i,j) = 0.0d0
          ae(i,j) = 0.0d0
          as(i,j) = 0.0d0
          an(i,j) = 0.0d0
```

```
          ap(i,j) = 0.0d0
          s(i,j) = 0.0d0

c
c *** Initialize temperature array
c
          if (j.eq.1) T(0,j) = 1.0d0
          if (i.lt.nstart(j)) then
            T(i,j) = 1.0d0
          else
            T(i,j) = 1.0d0 - factor * real(i)**2.0d0
          endif
          if (j.eq.1) T(nx+1,j) = 0.7d0

c
c *** Initialize nodal dimension arrays
c
          if ((j.eq.1).and.((i.ne.1).and.(i.ne.nx))) dx(i) = dxstd
   10   continue
        if ((j.ne.1).and.(j.ne.ny)) dy(j) = dystd
   20 continue

c
c *** Set the dimensions of the boundary nodes such they are comparable
c *** to those of the interior nodes
c
      dx(0) = dxstd
      dx(nx+1) = dxstd
      dy(0) = dystd
      dy(ny+1) = dystd

      return
      end


      subroutine gaussseidel(nx,ny,nstart,T,Told,omega,aw,ae,as,an,ap,s)
c ***********************************************************************
c   This subroutine solves (nx) x (ny) simultaneous equations using the
c   Gauss-Seidel iterative solver
c ***********************************************************************

      implicit none
      integer nx, ny, nstart(199), i, j
      double precision T(0:200,0:200), Told(0:200,0:200), omega
      double precision aw(199,199), ae(199,199), as(199,199)
      double precision an(199,199), ap(199,199), s(199,199)

      do 10 j=1,ny
        do 10 i=nstart(j),nx
   10     T(i,j) = (ae(i,j)*Told(i+1,j)+aw(i,j)*T(i-1,j)+an(i,j)*
     +       Told(i,j+1)+as(i,j)*T(i,j-1)+s(i,j)) * omega / ap(i,j)
     +       + (1.d0-omega) * Told(i,j)

      return
      end


      subroutine residual(nx,ny,nstart,T,dx,dy,dz,k,h,error,aw,ae,as,an,
```

```
     + ap,s,conduction,convection)
c ***********************************************************************
c   This subroutine determines the existing error resulting from the
c   last iteration
c ***********************************************************************

      implicit none
      integer nx, ny, nstart(199), i, j
      double precision T(0:200,0:200), dx(0:200), dy(0:200), dz
      double precision k, h, error, resid
      double precision aw(199,199), ae(199,199), as(199,199)
      double precision an(199,199), ap(199,199), s(199,199)
      double precision conduction, convection

      error = 0.0d0
      conduction = 0.0d0
      convection = 0.0d0
c
      do 10 j=1,ny
        do 10 i=nstart(j),nx
          resid = T(i,j) - (ae(i,j)*T(i+1,j)+aw(i,j)*T(i-1,j)+an(i,j)
     +       *T(i,j+1)+as(i,j)*T(i,j-1)+s(i,j)) / ap(i,j)
          error = error + abs(resid) / (real(nx)*real(ny))
c
          if (i.eq.nstart(j)) conduction = conduction
     +                + aw(i,j) * dx(i) * dy(j) * dz * (T(i-1,j)-T(i,j))
          if ((j.gt.1).and.(i.lt.nstart(j-1))) conduction = conduction
     +                + as(i,j) * dx(i) * dy(j) * dz * (T(i,j-1)-T(i,j))
          convection = convection + h * dx(i) * dy(j) * T(i,j)
   10 continue

      return
      end


      subroutine output(nx,ny,T,dx,dy,dz,k,h)
c ***********************************************************************
c   This subroutine determines eta resulting from thermal constriction
c ***********************************************************************

      implicit none
      integer nx, ny, i, j
      double precision T(0:200,0:200), dx(0:200), dy(0:200), dz
      double precision k, h, eta, area, m

      eta = 0.d0
      area = 0.d0
c
      do 10 j=1,ny
        do 10 i=1,nx
          eta = eta + T(i,j) * dx(i) * dy(j)
          area = area + dx(i) * dy(j)
   10 continue
c
      open(25,file='constrict.out')
      eta = eta / area
      write(25,*) h
      write(25,20) eta
```

```
   20 format('calculated eta = ',f6.4)

c
c *** Determine the efficiency of a standard fin with the same input
c
      m = sqrt(h/(k*dz)) * real(nx) * dx(0)
      write(25,30) tanh(m) / m
   30 format('eta of standard fin = ',f6.4)
      close(25)

      return
      end
```

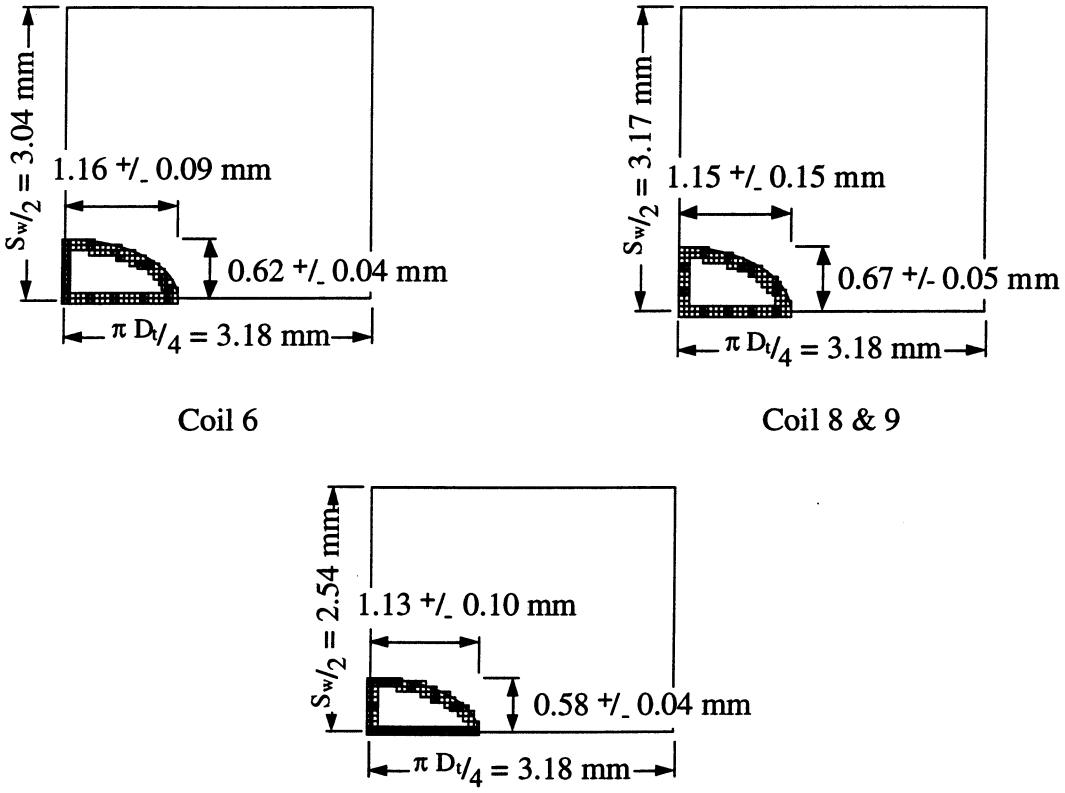

Figure C.1 Relative sizes of the weld spot and nodes used in discretizing the domain for each of the wire-on-tube condensers tested

APPENDIX D: RADIATION VIEW FACTOR EQUATIONS

D.1 Between Consecutive Wires on the Same Side of a Condenser Layer

$$F_{w-w} = \frac{1}{\pi}\left\{\sqrt{\left(S_w/D_w\right)^2 + 1} + \sin^{-1}\left(D_w/S_w\right) - \left(S_w/D_w\right)\right\}$$

D.2 From a Single Wire to an Imaginary Surface Running Tangent Along the Wires

(Note that this is the same as the view factor from all of the wires on one side of a condenser layer together to an imaginary surface running tangent along the wires)

$$F_{w-surf} = \frac{(1 - 2F_{w-w})}{2}$$

D.3 From an Imaginary Surface Running Tangent Along the Wires to All of the Wires on One Side of a Condenser Layer Together

$$F_{surf-w} = F_{w-surf}\left(\frac{A_w}{A_{surf}}\right) = F_{w-surf}\left(\frac{\pi D_w}{S_w}\right)$$

D.4 Between Consecutive Tube Passes of a Condenser Layer

$$F_{t-t} = \frac{1}{\pi}\left\{\sqrt{\left(S_t/D_t\right)+1} + \sin^{-1}\left(D_t/S_t\right) - \left(S_t/D_t\right)\right\}$$

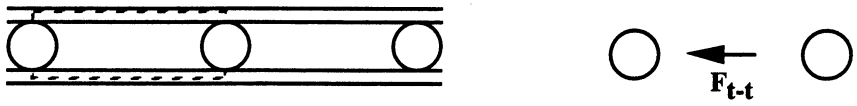

D.5 From a Single Tube to an Imaginary Surface Running Tangent Along the Tube Passes

(Note that this is the same as the view factor from all of the tube passes together to an imaginary surface running tangent along the tube passes)

$$F_{t-surf} = \frac{\left(1 - 2\,F_{t-t}\right)}{2}$$

D.6 From an Imaginary Surface Running Tangent Along the Tube Passes to All of the Tube Passes of a Condenser Layer Together

$$F_{surf-t} = F_{t-surf}\left(\frac{A_t}{A_{surf}}\right) = F_{t-surf}\left(\frac{\pi\,D_t}{S_t}\right)$$

D.7 From All of the Wires on One Side of a Condenser Layer to All of the Tube Passes of the Same Condenser Layer

$$F_{w-t} = \left(F_{w-surf}\right)\left(F_{surf-t}\right)$$

D.8 From All of the Wires on One Side of a Condenser Layer to the Surroundings

(Note that this is the same as view factor from all of the wires on both sides of a condenser layer together to the surroundings)

$$F_{w-surr} = 1 - F_{w-(\text{wires on same side})} - F_{w-(\text{wires on opposite side})} - F_{w-t}$$
$$= 1 - 2F_{w-w} - (F_{w-surf})(1 - F_{surf-t})(F_{surf-w}) - F_{w-t}$$

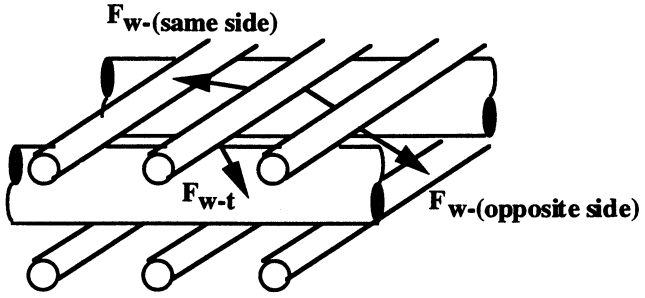

D.9 From All of the Tube Passes of a Condenser Layer to All of the Wires on One Side of the Same Condenser Layer

$$F_{t-w} = 2(F_{t-surf})(F_{surf-w})$$

D.10 From All of the Tube Passes of a Condenser Layer to the Surroundings

$$F_{t-surr} = 1 - 2F_{t-t} - F_{t-w}$$

D.11 From an Imaginary Surface on One Side of a Condenser Layer to an Imaginary Surface on the Other Side of the Same Condenser Layer

(Note that this is the same as the effective transmissivity through a condenser layer)

$$\tau_{eff} = (1 - F_{surf-w})^2 (1 - F_{surf-t})$$

D.12a From an Imaginary Surface Running Tangent Along the Wires of a Condenser Layer to an Imaginary Surface Running Tangent Along the Wires of an Adjacent Condenser Layer (for $\alpha = 90°$ only)

$$F_{layer} = \frac{2}{\pi\, x\, y}\left\{\ln\left[\frac{\left(1+x^2\right)\left(1+y^2\right)}{1+x^2+y^2}\right]^{1/2} - x\tan^{-1}(x) - y\tan^{-1}(y)\right.$$

$$\left. + x\sqrt{1+y^2}\tan^{-1}\left(\frac{x}{\sqrt{1+y^2}}\right) + y\sqrt{1+x^2}\tan^{-1}\left(\frac{y}{\sqrt{1+x^2}}\right)\right\}$$

where $\quad x = \dfrac{L_w}{(S_L - D_t - 2\,D_w)}$

$$y = \frac{L_t}{(S_L - D_t - 2D_w)}$$

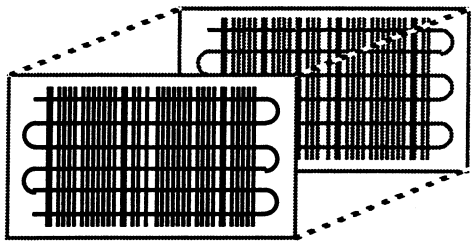

D.12b From an Imaginary Surface Running Tangent Along the Wires of a Condenser Layer to an Imaginary Surface Running Tangent Along the Wires of an Adjacent Condenser Layer (for $\alpha < 90°$)

$$F_{layer} = \frac{1}{\pi L}\left\{-\frac{L^2}{4}\sin 2\Phi\left[\sin\Phi + (\pi - 2\,\Phi) + 2\tan^{-1}\left(\frac{1-\cos\Phi}{\sin\Phi}\right)\right]\right.$$

$$+\frac{1}{4}\sin^2\Phi\ln\left[\left(\frac{1+2\,L^2+L^4}{1+2\,L^2-2\,L^2\cos\Phi}\right)^{\csc^2\Phi\cot^2\Phi}\left(\frac{1+2\,L^2-2\,L^2\cos\Phi}{2+2\,L^2-2\cos\Phi-2\,L^2\cos\Phi}\right)^{L^2}\right]$$

$$+\frac{L^2}{4}\sin^2\Phi\ln\left[\left(\frac{1}{2-2\cos\Phi}\right)\left(\frac{1+L^2}{1+2\,L^2-2\,L^2\cos\Phi}\right)^{\cos 2\Phi}\right]$$

$$+2\,L\tan^{-1}\left(\frac{1}{L}\right) - \sqrt{2\,L^2-2\,L^2\cos\Phi}\,\cot^{-1}\sqrt{2\,L^2-2\,L^2\cos\Phi}$$

$$+\frac{L}{2}\sin\Phi\sin 2\Phi\sqrt{1+L^2\sin^2\Phi}\left[\tan^{-1}\left(\frac{L\cos\Phi}{\sqrt{1+L^2\sin^2\Phi}}\right) + \tan^{-1}\left(\frac{L-L\cos\Phi}{\sqrt{1+L^2\sin^2\Phi}}\right)\right]$$

$$\left. +\cos\Phi\int_0^L\sqrt{1+z^2\sin^2\Phi}\left[\tan^{-1}\left(\frac{z\cos\Phi}{\sqrt{1+z^2\sin^2\Phi}}\right) + \tan^{-1}\left(\frac{L-z\cos\Phi}{\sqrt{1+z^2\sin^2\Phi}}\right)\right]dz\right\}$$

where $\quad L = {}^{L_t}/_{L_w}$ for $\psi = 0$ $\quad$ or $\quad L = {}^{L_w}/_{L_t}$ for $\psi = {}^{\pi}/_{2}$

D.13 From All of the Wires of a Condenser Layer to All of the Wires of an Adjacent Condenser Layer

$$\left(F_{layer}\right)_{w-w} = \left(\frac{F_{w-surr}}{2}\right)\left(F_{layer}\right)\left(F_{surf-(wires\ on\ close\ side)} + F_{surf-(wires\ on\ far\ side)}\right)$$

$$= \left(\frac{F_{w-surr}}{2}\right)\left(F_{layer}\right)\left[F_{surf-w} + \left(1 - F_{surf-w}\right)\left(1 - F_{surf-t}\right) F_{surf-w}\right]$$

D.14 From All of the Wires of a Condenser Layer to All of the Tube Passes of an Adjacent Condenser Layer

$$\left(F_{layer}\right)_{w-t} = \left(\frac{F_{w-surr}}{2}\right)\left(F_{layer}\right)\left(1 - F_{surf-w}\right)\left(F_{surf-t}\right)$$

D.15 From All of the Tube Passes of a Condenser Layer to All of the Tube Passes of an Adjacent Condenser Layer

$$\left(F_{layer}\right)_{t-t} = \left(\frac{F_{t-surr}}{2}\right)\left(F_{layer}\right)\left(1 - F_{surf-w}\right)\left(F_{surf-t}\right)$$

D.16 From All of the Tube Passes of a Condenser Layer to All of the Wires of an Adjacent Condenser Layer

$$\left(F_{layer}\right)_{w-t} = \left(\frac{F_{t-surr}}{2}\right)\left(F_{layer}\right)\left(F_{surf-(wires\ on\ close\ side)} + F_{surf-(wires\ on\ far\ side)}\right)$$

$$= \left(\frac{F_{t-surr}}{2}\right)\left(F_{layer}\right)\left[F_{surf-w} + \left(1 - F_{surf-w}\right)\left(1 - F_{surf-t}\right)F_{surf-w}\right]$$

APPENDIX E: EXPERIMENTAL UNCERTAINTY

Table E.1 Absolute uncertainty associated with condenser geometry

Variable	Range	P (precision limit)	B (bias limit)	U (uncertainty)	% U
D_w	1.37 - 1.58 mm	2.54 μm	2.54 μm	3.59 μm	≤ 0.3 %
D_w ($^w/_o$ paint)	1.36 - 1.56 mm	2.54 μm	2.54 μm	3.59 μm	≤ 0.3 %
S_w	5.08 - 6.35 mm	2.54 μm	2.54 μm	3.59 μm	≤ 0.07 %
L_w	148 - 152 mm	1.6 mm	0.8 mm	1.8 mm	1.2 %
D_t	4.80 - 4.85 mm	2.54 μm	2.54 μm	3.59 μm	≤ 0.07 %
D_t ($^w/_o$ paint)	4.78 - 4.81 mm	2.54 μm	2.54 μm	3.59 μm	≤ 0.07 %
$D_{t,i}$	3.34 mm	2.54 μm	2.54 μm	3.59 μm	≤ 0.1 %
S_t	25.4 - 50.8 mm	2.54 μm	2.54 μm	3.59 μm	≤ 0.01 %
L_t	186 - 515 mm	1.6 mm	0.8 mm	1.8 mm	0.3 - 1.0 %

Table E.2 Absolute uncertainty associated with experimental measurements

Variable	Range	P (precision limit)	B (bias limit)	U (uncertainty)	% U
V	0.2 - 2.0 m/s	0.03 m/s	0.003 m/s	0.03 m/s	1.5 - 15 %
$T_{air,in}$	> 295 K	0.026 K	0.051 K	0.057 K	≤ 0.2 %
$T_{ref,in}$	> 295 K	0.045 K	0.052 K	0.069 K	≤ 0.2 %
$T_{ref,out}$	> 295 K	0.045 K	0.052 K	0.069 K	≤ 0.2 %
$\Delta T_{ref,diff}$	0.96 - 9.51 K	0.026 K	0.055 K	0.061 K	0.6 - 6.3 %
Δm	> 3000 g	8.0 g	0.0050 g	8.0 g	≤ 0.3 %
Δt	> 180 s	0.30 s	0.0065 s	0.30 s	≤ 0.2 %
$\dot{m}_{ref}$	4.6 - 20.8 g/s	0.10 g/s	0.25 g/s	0.27 g/s	1.3 - 5.9 %
H_{duct}	50.8 - 152 mm	1.6 mm	0.8 mm	1.8 mm	1.2 - 3.5 %
W_{duct}	143 - 515 mm	1.6 mm	0.8 mm	1.8 mm	0.3 - 1.3 %
Δp	0.066 - 10.3 Pa	0.020 Pa	0.062 Pa	0.065 Pa	0.6 - 98 %

Table E.3 Absolute uncertainty associated with calculated quantities

Variable	Range	P (precision limit)	B (bias limit)	U (uncertainty)	% U
$c_{p,r}$	4.180 kJ/kg-K	0.001 kJ/kg-K	0.001 kJ/kg-K	0.001 kJ/kg-K	0.03 %
A_w	$\geq$ 0.0427 m^2	0.00046 m^2	0.00024 m^2	0.00052 m^2	$\leq$ 1.2 %
A_t	$\geq$ 0.0141 m^2	0.00014 m^2	0.00007 m^2	0.00016 m^2	$\leq$ 1.1 %
q_{tot}	21.1 W - 344.2 W	0.4 W - 0.7 W	0.9 W - 1.6 W	1.0 W - 1.7 W	0.4 - 8.1 %
ε	0.95	0.05	---	0.05	5.3 %
F_{ij}	0 - 1.0	0.1	---	0.1	$\geq$ 10 %
q_{rad}	3.4 W - 17.6 W	0.7 W - 3.6 W	0.02 W - 0.07 W	0.7 W - 3.6 W	20.7 %
h_w	25.0 W/m^2-K - 136.6 W/m^2-K	1.0 W/m^2-K - 2.8 W/m^2-K	0.2 W/m^2-K - 1.6 W/m^2-K	1.0 W/m^2-K - 3.2 W/m^2-K	2.3 - 12.8 %

APPENDIX F: TABULAR DATA

Both the raw and reduced data associated with each of the condensers involved in the current investigation (Coils 6, 8, 9, and 10) have been provided in tabular form within this appendix. Tables are listed in order of increasing condenser coil numbers (e.g. Coil 6 or Coil 8), ψ, and α.

Note that the heat exchanger configurations (e.g. counter or parallel flow) in which the multi-layer condensers were tested are not explicitly mentioned on any of the tables. Instead the heat exchanger type can be inferred from the order in which the indices of the ΔT table headings appear. Tables in which the indices of the ΔT table headings appear in an increasing order correspond to condensers tested as parallel flow heat exchangers. Conversely, tables in which the indices of the ΔT table headings appear in a decreasing order correspond to condensers tested as counter flow heat exchangers.

Only the h_w averaged over all of the layers of each condenser have been included in the many of the tables (instead of the h_w for each condenser layer). This is due to the fact that h_w has been found to be independent of layer placement, N_L, and S_L (for $S_L > 31.2$ mm). Consequently, the h_w of these condensers are approximately the same for each layer.

Table F.1 Raw and reduced data associated with two-layer condensers (Coil 6; $\alpha = 90°$) with $S_L = 16.3$ mm

V [m/s]	$T_{a,in}$ [K]	$T_{r,in}$ [K]	ΔT_1 [K]	ΔT_2 [K]	$\dot{m}_r$ [kg/s]	$h_{w,1}$ [W/m^2-K]	$h_{w,2}$ [W/m^2-K]
0.21	296.54	319.63	2.14	1.38	0.00476	37	30.9
0.25	296.51	319.67	2.30	1.51	0.00476	40.8	34.7
0.35	296.47	319.68	2.63	1.76	0.00476	49	41.7
0.50	296.50	319.71	2.97	2.03	0.00473	57.9	49.9
0.75	296.53	319.68	3.45	2.40	0.00473	72	63.5
1.00	296.56	319.70	3.82	2.69	0.00473	84.1	76.2
1.25	296.62	319.69	4.14	2.93	0.00472	95	87.6
1.51	296.67	319.64	4.43	3.14	0.00472	106.6	99.8
1.76	296.71	319.63	4.66	3.32	0.00472	116	110.6
2.01	296.72	319.64	4.89	3.47	0.00471	125.4	120.4

Table F.2 Raw and reduced data associated with two-layer condensers (Coil 6; $\alpha = 90°$) with $S_L = 23.8$ mm

V [m/s]	$T_{a,in}$ [K]	$T_{r,in}$ [K]	ΔT_1 [K]	ΔT_2 [K]	$\dot{m}_r$ [kg/s]	$h_{w,1}$ [W/m^2-K]	$h_{w,2}$ [W/m^2-K]
0.21	296.88	319.70	2.13	1.37	0.00461	35.7	29.1
0.25	296.83	319.71	2.30	1.51	0.00461	39.6	33.3
0.35	296.76	319.71	2.62	1.77	0.00461	47.5	40.7
0.49	296.73	319.71	3.00	2.08	0.00460	57.4	50.7
0.75	296.71	319.70	3.49	2.47	0.00460	71.6	65
1.00	296.70	319.67	3.86	2.77	0.00460	83.4	77.7
1.26	296.73	319.67	4.20	3.03	0.00459	94.8	90.7
1.51	296.78	319.66	4.49	3.26	0.00459	105.8	103.5
1.75	296.94	319.64	4.72	3.43	0.00459	116.4	115.8
2.00	296.97	319.63	4.92	3.56	0.00459	125	125.4

Table F.3 Raw and reduced data associated with two-layer condensers (Coil 6; $\alpha = 90°$) with $S_L = 31.2$ mm

V [m/s]	$T_{a,in}$ [K]	$T_{r,in}$ [K]	ΔT_1 [K]	ΔT_2 [K]	$\dot{m}_r$ [kg/s]	$h_{w,1}$ [W/m^2-K]	$h_{w,2}$ [W/m^2-K]
0.21	296.60	319.72	2.15	1.43	0.00488	38.2	33.8
0.26	296.58	319.71	2.33	1.57	0.00488	42.5	37.7
0.36	296.50	319.73	2.62	1.79	0.00488	50.1	43.9
0.50	296.50	319.75	2.97	2.05	0.00488	59.6	52.5
0.75	296.53	319.72	3.41	2.43	0.00487	73.1	67
1.00	296.58	319.72	3.78	2.75	0.00487	85.4	80.9
1.26	296.66	319.72	4.07	2.99	0.00486	96.1	93.4
1.50	296.77	319.74	4.34	3.19	0.00486	107.1	105.4
1.76	296.79	319.67	4.58	3.36	0.00485	116.9	116.1
2.00	296.81	319.69	4.78	3.50	0.00485	125.6	126

Table F.4 Raw and reduced data associated with two-layer condensers (Coil 6; $\alpha = 90°$) with $S_L = 38.7$ mm

V [m/s]	$T_{a,in}$ [K]	$T_{r,in}$ [K]	ΔT_1 [K]	ΔT_2 [K]	$\dot{m}_r$ [kg/s]	$h_{w,1}$ [W/m^2-K]	$h_{w,2}$ [W/m^2-K]
0.20	295.28	319.68	2.14	1.42	0.00483	34.7	29.1
0.26	296.49	319.74	2.35	1.58	0.00483	42.2	37.3
0.35	296.45	319.77	2.63	1.81	0.00484	49.3	43.9
0.50	296.38	319.78	3.01	2.10	0.00484	59.4	53.1
0.75	296.44	319.78	3.48	2.50	0.00483	73.8	68.4
1.01	296.45	319.77	3.84	2.81	0.00483	85.5	82
1.25	296.50	319.73	4.16	3.05	0.00482	97.1	94.3
1.51	296.54	319.71	4.43	3.25	0.00482	107.6	105.8
1.76	296.58	319.69	4.66	3.42	0.00482	117.5	117
2.01	296.62	319.68	4.87	3.55	0.00482	126.8	126.5

Table F.5 Raw and reduced data associated with two-layer condensers (Coil 6; $\alpha = 90°$) with $S_L = 46.2$ mm

V [m/s]	$T_{a,in}$ [K]	$T_{r,in}$ [K]	ΔT_1 [K]	ΔT_2 [K]	$\dot{m}_r$ [kg/s]	$h_{w,1}$ [W/m^2-K]	$h_{w,2}$ [W/m^2-K]
0.21	295.98	319.66	2.26	1.51	0.00474	37.9	33.7
0.26	295.97	319.71	2.47	1.67	0.00474	42.8	38.4
0.35	295.97	319.68	2.74	1.88	0.00474	49.8	44.4
0.49	295.98	319.65	3.09	2.15	0.00471	58.9	52.5
0.76	296.01	319.64	3.62	2.59	0.00471	74.5	69.2
1.00	295.99	319.65	3.97	2.88	0.00471	85.5	81.4
1.25	296.07	319.67	4.30	3.14	0.00471	97	94.2
1.50	296.10	319.63	4.58	3.32	0.00471	107.5	104.9
1.75	296.13	319.64	4.81	3.48	0.00471	116.9	114.4
2.00	296.18	319.61	5.03	3.63	0.00470	126.2	124.7

Table F.6 Raw and reduced data associated with two-layer condensers (Coil 6; $\alpha = 90°$) with $S_L = 53.6$ mm

V [m/s]	$T_{a,in}$ [K]	$T_{r,in}$ [K]	ΔT_1 [K]	ΔT_2 [K]	$\dot{m}_r$ [kg/s]	$h_{w,1}$ [W/m^2-K]	$h_{w,2}$ [W/m^2-K]
0.20	295.60	319.58	2.19	1.49	0.00485	36.8	32.7
0.25	295.53	319.59	2.35	1.62	0.00485	40.4	36.3
0.35	295.48	319.55	2.67	1.86	0.00485	48.3	43.3
0.49	295.51	319.57	3.02	2.15	0.00484	57.5	52.4
0.75	295.51	319.56	3.50	2.54	0.00484	71.2	66.2
0.99	295.50	319.54	3.88	2.85	0.00484	83.2	79.5
1.25	295.52	319.55	4.22	3.09	0.00484	94.5	91.2
1.50	295.56	319.54	4.47	3.30	0.00485	104.3	102.6
1.75	295.57	319.54	4.75	3.49	0.00485	115	113.7
2.00	295.67	319.54	4.95	3.62	0.00485	123.8	123.1

Table F.7 Raw and reduced data associated with two-layer condensers (Coil 6; $\alpha = 90°$) with $S_L = 61.1$ mm

V [m/s]	$T_{a,in}$ [K]	$T_{r,in}$ [K]	ΔT_1 [K]	ΔT_2 [K]	$\dot{m}_r$ [kg/s]	$h_{w,1}$ [W/m^2-K]	$h_{w,2}$ [W/m^2-K]
0.20	295.45	319.49	2.33	1.54	0.00477	39.1	34.5
0.25	295.36	319.51	2.53	1.71	0.00477	43.6	39.3
0.35	295.32	319.51	2.78	1.90	0.00477	49.5	43.8
0.50	295.30	319.54	3.18	2.24	0.00477	59.9	54.5
0.74	295.31	319.54	3.63	2.62	0.00476	72.7	68.1
1.00	295.32	319.52	4.02	2.95	0.00476	84.9	81.8
1.24	295.32	319.52	4.33	3.19	0.00476	95.5	93.1
1.50	295.36	319.50	4.63	3.41	0.00476	106.3	105.3
1.74	295.39	319.48	4.86	3.55	0.00476	115.6	114.4
2.00	295.51	319.49	5.09	3.71	0.00476	125.6	125.5

Table F.8 Raw and reduced data associated with two-layer condensers (Coil 6; $\alpha = 90°$) with $S_L = 68.6$ mm

V [m/s]	$T_{a,in}$ [K]	$T_{r,in}$ [K]	ΔT_1 [K]	ΔT_2 [K]	$\dot{m}_r$ [kg/s]	$h_{w,1}$ [W/m^2-K]	$h_{w,2}$ [W/m^2-K]
0.20	295.52	319.47	2.32	1.61	0.00475	38.9	36.7
0.24	295.53	319.48	2.47	1.73	0.00475	42.4	40.1
0.35	295.52	319.53	2.79	1.99	0.00475	50	47.5
0.49	295.55	319.57	3.14	2.27	0.00474	59.3	56
0.74	295.62	319.58	3.61	2.65	0.00474	73	69.9
1.00	295.75	319.61	3.99	2.94	0.00474	85.1	82.7
1.24	295.74	319.57	4.26	3.14	0.00473	94.1	92.2
1.50	295.77	319.56	4.59	3.35	0.00473	106.8	104.4
1.75	295.82	319.50	4.83	3.50	0.00473	116.6	114.5
2.00	295.85	319.53	5.05	3.65	0.00473	125.6	124.2

Table F.9 Raw and reduced data associated with two-layer condensers (Coil 6; $\alpha = 90°$) with $S_L = 76.0$ mm

V [m/s]	$T_{a,in}$ [K]	$T_{r,in}$ [K]	ΔT_1 [K]	ΔT_2 [K]	$\dot{m}_r$ [kg/s]	$h_{w,1}$ [W/m^2-K]	$h_{w,2}$ [W/m^2-K]
0.20	295.46	319.63	2.31	1.58	0.00485	39	36.1
0.24	295.47	319.67	2.44	1.70	0.00485	42	39.4
0.35	295.46	319.64	2.77	1.97	0.00485	50.3	47.2
0.50	295.47	319.61	3.11	2.23	0.00485	59.6	55.4
0.74	295.54	319.58	3.55	2.59	0.00486	72.9	69
1.00	295.52	319.58	3.95	2.90	0.00486	85.4	82.1
1.26	295.51	319.59	4.26	3.15	0.00486	95.8	93.7
1.50	295.56	319.51	4.54	3.34	0.00485	106.9	105.1
1.75	295.61	319.56	4.80	3.50	0.00485	116.7	115.1
2.00	295.60	319.57	5.01	3.63	0.00485	125.1	123.1

Table F.10 Raw and reduced data associated with Coil 6 at $\alpha = 90°$ (Set #1)

V [m/s]	$T_{a,in}$ [K]	$T_{r,in}$ [K]	ΔT_4 [K]	ΔT_3 [K]	ΔT_2 [K]	ΔT_1 [K]	$\dot{m}_r$ [kg/s]	Avg. h_w [W/m^2-K]	$\Delta p / N_L$ [Pa]
0.20	295.73	319.50	1.17	1.27	1.41	1.81	0.00480	32.6	---
0.25	295.69	319.50	1.33	1.42	1.52	1.89	0.00480	35.8	---
0.35	295.66	319.53	1.65	1.74	1.74	2.05	0.00480	42.9	---
0.50	295.64	319.39	1.99	2.09	1.95	2.16	0.00481	51.3	---
0.75	295.63	319.52	2.71	2.54	2.29	2.34	0.00481	67.7	---
1.00	295.61	319.47	3.20	2.87	2.51	2.42	0.00481	80.5	---
1.25	295.63	319.44	3.59	3.11	2.68	2.47	0.00481	91.7	---
1.50	295.64	319.42	3.96	3.34	2.83	2.52	0.00481	104.3	---
1.75	295.78	319.42	4.27	3.52	2.95	2.55	0.00481	116.6	---
2.00	295.83	319.43	4.56	3.69	3.03	2.56	0.00481	127.6	---

Table F.11 Raw and reduced data associated with Coil 6 at $\alpha = 90°$ (Set #2)

V [m/s]	$T_{a,in}$ [K]	$T_{r,in}$ [K]	ΔT_4 [K]	ΔT_3 [K]	ΔT_2 [K]	ΔT_1 [K]	$\dot{m}_r$ [kg/s]	Avg. h_w [W/m^2-K]	$\Delta p / N_L$ [Pa]
0.20	295.84	319.50	1.02	1.12	1.34	1.72	0.00518	31.6	0.037
0.25	295.77	319.47	1.13	1.22	1.44	1.78	0.00518	33.6	0.072
0.35	295.70	319.51	1.47	1.51	1.70	1.96	0.00518	41.9	0.147
0.49	295.72	319.51	1.92	1.88	1.95	2.11	0.00518	52.9	0.27
0.75	295.69	319.49	2.48	2.35	2.24	2.26	0.00518	67.3	0.504
1.00	295.69	319.46	2.92	2.69	2.47	2.37	0.00518	80.8	0.777
1.25	295.75	319.44	3.31	2.95	2.65	2.43	0.00517	93.3	1.086
1.50	295.78	319.40	3.63	3.19	2.79	2.44	0.00517	104.7	1.433
1.76	295.88	319.40	3.91	3.35	2.89	2.47	0.00517	115.1	1.817
1.99	295.83	319.39	4.15	3.52	2.98	2.49	0.00517	124.4	2.239

Table F.12 Raw and reduced data associated with Coil 6 at $\alpha = 45°$ with air flow $\perp$ to the wires

V [m/s]	$T_{a,in}$ [K]	$T_{r,in}$ [K]	ΔT_1 [K]	$\dot{m}_r$ [kg/s]	Avg. h_w [W/m^2-K]	$\Delta p / N_L$ [Pa]
0.20	295.42	319.76	1.86	0.00560	33.9	0.066
0.24	295.38	319.75	2.03	0.00560	38.6	0.118
0.35	295.40	319.70	2.33	0.00558	47.6	0.257
0.50	295.42	319.71	2.70	0.00558	59.3	0.498
0.74	295.40	319.64	3.14	0.00556	75.2	1.009
1.00	295.41	319.67	3.52	0.00556	89.7	1.610
1.24	295.39	319.67	3.82	0.00556	102.4	2.415
1.50	295.40	319.66	4.11	0.00556	115.8	3.381
1.75	295.41	319.67	4.33	0.00556	126.3	4.369
2.00	295.41	319.62	4.52	0.00556	136.6	5.475

Table F.13 Raw and reduced data associated with Coil 6 at $\alpha = 60°$ with air flow $\perp$ to the wires

V [m/s]	$T_{a,in}$ [K]	$T_{r,in}$ [K]	ΔT_1 [K]	$\dot{m}_r$ [kg/s]	Avg. h_w [W/m^2-K]	$\Delta p / N_L$ [Pa]
0.20	295.69	319.72	1.85	0.00573	34.6	0.083
0.25	295.65	319.73	1.98	0.00573	38	0.127
0.35	295.61	319.75	2.29	0.00570	46.4	0.265
0.50	295.62	319.74	2.62	0.00570	56.7	0.481
0.75	295.58	319.72	3.07	0.00569	71.5	0.975
1.00	295.56	319.73	3.43	0.00569	84.7	1.577
1.25	295.53	319.72	3.78	0.00567	97.8	2.375
1.50	295.53	319.74	4.06	0.00567	109.6	3.297
1.75	295.54	319.69	4.29	0.00566	120	4.280
2.00	295.48	319.69	4.51	0.00566	129.6	5.335

Table F.14 Raw and reduced data associated with Coil 6 at $\alpha = 75°$ with air flow $\perp$ to the wires

V [m/s]	$T_{a,in}$ [K]	$T_{r,in}$ [K]	ΔT_1 [K]	$\dot{m}_r$ [kg/s]	Avg. h_w [W/m^2-K]	$\Delta p / N_L$ [Pa]
0.20	295.86	319.81	1.80	0.00604	35.1	0.083
0.25	295.74	319.83	1.94	0.00604	38.9	0.127
0.35	295.66	319.87	2.21	0.00604	46.5	0.257
0.50	295.62	319.84	2.56	0.00604	57.3	0.507
0.76	295.57	319.86	2.97	0.00603	70.7	1.000
1.00	295.54	319.87	3.30	0.00603	82.5	1.602
1.25	295.51	319.83	3.59	0.00602	93.5	2.399
1.50	295.50	319.84	3.85	0.00602	103.9	3.297
1.74	295.46	319.79	4.08	0.00601	113.8	4.258
2.00	295.43	319.75	4.28	0.00601	122.9	5.384

Table F.15 Raw and reduced data associated with Coil 6 at $\alpha = 45°$ with air flow $\perp$ to the tube passes

V [m/s]	$T_{a,in}$ [K]	$T_{r,in}$ [K]	ΔT_4 [K]	ΔT_3 [K]	ΔT_2 [K]	ΔT_1 [K]	$\dot{m}_r$ [kg/s]	Avg. h_w [W/m^2-K]	$\Delta p / N_L$ [Pa]
0.21	295.37	319.57	0.97	1.05	1.22	1.57	0.00527	27.3	0.040
0.25	295.29	319.51	1.10	1.17	1.33	1.66	0.00527	30.8	0.051
0.35	295.22	319.54	1.43	1.49	1.59	1.86	0.00522	38.6	0.107
0.49	295.17	319.52	1.77	1.77	1.82	2.01	0.00522	46.1	0.193
0.75	295.13	319.49	2.28	2.20	2.12	2.21	0.00519	58.4	0.394
1.00	295.09	319.46	2.69	2.51	2.33	2.32	0.00519	68.6	0.634
1.25	295.09	319.46	3.06	2.79	2.52	2.41	0.00516	78.8	0.933
1.50	295.06	319.41	3.37	3.01	2.67	2.49	0.00516	88.6	1.259
1.74	295.08	319.43	3.63	3.19	2.77	2.51	0.00514	95.9	1.629
2.00	295.19	319.38	3.85	3.34	2.84	2.55	0.00514	104.4	1.997

Table F.16 Raw and reduced data associated with Coil 6 at $\alpha = 60°$ with air flow $\perp$ to the tube passes

V [m/s]	$T_{a,in}$ [K]	$T_{r,in}$ [K]	ΔT_4 [K]	ΔT_3 [K]	ΔT_2 [K]	ΔT_1 [K]	$\dot{m}_r$ [kg/s]	Avg. h_w [W/m^2-K]	$\Delta p / N_L$ [Pa]
0.21	295.39	319.61	1.08	1.12	1.33	1.63	0.00534	30.6	0.040
0.25	295.37	319.65	1.23	1.26	1.46	1.71	0.00534	34.4	0.058
0.35	295.22	319.52	1.57	1.54	1.71	1.89	0.00531	42.1	0.116
0.49	295.18	319.60	1.94	1.84	1.95	2.05	0.00531	50.4	0.199
0.75	295.20	319.54	2.51	2.27	2.26	2.23	0.00529	64.5	0.419
1.00	295.21	319.52	2.93	2.57	2.47	2.33	0.00529	75.8	0.691
1.25	295.20	319.51	3.31	2.84	2.64	2.41	0.00529	87.0	1.016
1.50	295.23	319.46	3.61	3.04	2.76	2.46	0.00529	96.4	1.381
1.74	295.19	319.45	3.92	3.23	2.87	2.50	0.00527	106.3	1.785
2.00	295.20	319.42	4.14	3.38	2.94	2.52	0.00527	114.2	2.177

Table F.17 Raw and reduced data associated with Coil 6 at $\alpha = 75°$ with air flow $\perp$ to the tube passes

V [m/s]	$T_{a,in}$ [K]	$T_{r,in}$ [K]	ΔT_4 [K]	ΔT_3 [K]	ΔT_2 [K]	ΔT_1 [K]	$\dot{m}_r$ [kg/s]	Avg. h_w [W/m^2-K]	$\Delta p / N_L$ [Pa]
0.21	295.61	319.61	1.09	1.16	1.34	1.66	0.00541	32.9	0.036
0.25	295.61	319.62	1.21	1.28	1.44	1.75	0.00541	35.8	0.053
0.35	295.60	319.64	1.54	1.57	1.68	1.92	0.00540	44.0	0.105
0.49	295.55	319.60	1.91	1.87	1.90	2.07	0.00540	52.5	0.182
0.75	295.46	319.56	2.47	2.31	2.22	2.24	0.00541	67.1	0.374
1.00	295.46	319.56	2.90	2.63	2.44	2.35	0.00541	79.6	0.614
1.25	295.45	319.56	3.29	2.90	2.62	2.43	0.00540	91.5	0.922
1.50	295.43	319.55	3.60	3.12	2.76	2.48	0.00540	101.8	1.265
1.75	295.44	319.53	3.85	3.28	2.85	2.51	0.00535	108.9	1.602
2.00	295.41	319.51	4.12	3.45	2.95	2.54	0.00535	118.9	1.992

Table F.18 Raw and reduced data associated with Coil 8 at $\alpha = 90°$

V [m/s]	$T_{a,in}$ [K]	$T_{r,in}$ [K]	ΔT_2 [K]	ΔT_1 [K]	$\dot{m}_r$ [kg/s]	Avg. h_w [W/m^2-K]	$\Delta p / N_L$ [Pa]
0.21	296.09	319.75	2.55	2.76	0.00547	31.7	0.043
0.25	296.04	319.74	2.71	2.88	0.00547	33.9	0.073
0.35	295.99	319.68	2.98	3.08	0.00549	38.5	0.135
0.50	295.97	319.70	3.36	3.37	0.00549	45.8	0.238
0.76	295.97	319.67	4.15	3.64	0.00549	60.3	0.432
1.01	296.01	319.66	4.60	3.86	0.00547	70.6	0.655
1.26	296.06	319.66	4.95	4.02	0.00547	80.2	0.907
1.51	296.09	319.66	5.26	4.17	0.00547	89.7	1.187
1.77	296.11	319.68	5.55	4.30	0.00546	98.7	1.496
2.02	296.14	319.67	5.79	4.39	0.00546	107.2	1.833

Table F.19 Raw and reduced data associated with Coil 8 at $\alpha = 45°$ with air flow $\perp$ to the wires

V [m/s]	$T_{a,in}$ [K]	$T_{r,in}$ [K]	ΔT_1 [K]	$\dot{m}_r$ [kg/s]	Avg. h_w [W/m^2-K]	$\Delta p / N_L$ [Pa]
0.20	296.95	319.95	2.88	0.00616	36.2	0.083
0.25	296.81	319.96	3.07	0.00616	40.1	0.109
0.35	296.72	319.95	3.44	0.00614	48.9	0.205
0.50	296.65	319.97	3.86	0.00614	60.1	0.378
0.75	296.61	319.98	4.34	0.00611	75.1	0.746
1.00	296.56	319.90	4.68	0.00611	88	1.185
1.25	296.48	319.84	4.97	0.00610	99.9	1.758
1.50	296.47	319.87	5.23	0.00610	111.4	2.439
1.75	296.41	319.79	5.44	0.00607	121	3.196
2.00	296.39	319.82	5.62	0.00607	129.9	3.967

Table F.20 Raw and reduced data associated with Coil 8 at $\alpha = 60°$ with air flow $\perp$ to the wires

V [m/s]	$T_{a,in}$ [K]	$T_{r,in}$ [K]	ΔT_1 [K]	$\dot{m}_r$ [kg/s]	Avg. h_w [W/m^2-K]	$\Delta p / N_L$ [Pa]
0.20	297.88	320.06	2.82	0.00619	35.7	0.135
0.25	297.90	320.09	2.99	0.00619	39.3	0.170
0.35	297.95	320.04	3.32	0.00617	47.4	0.300
0.50	297.98	320.02	3.67	0.00617	57.1	0.524
0.75	298.09	320.04	4.08	0.00614	70.1	0.984
1.01	298.17	319.98	4.40	0.00614	82.1	1.569
1.25	298.15	320.04	4.69	0.00611	92.1	2.295
1.50	298.09	319.96	4.93	0.00611	102.2	3.149
1.75	297.79	319.84	5.17	0.00612	111.4	4.057
2.00	297.57	319.78	5.39	0.00612	120.2	5.037

Table F.21 Raw and reduced data associated with Coil 8 at $\alpha = 75°$ with air flow $\perp$ to the wires

V [m/s]	$T_{a,in}$ [K]	$T_{r,in}$ [K]	ΔT_1 [K]	$\dot{m}_r$ [kg/s]	Avg. h_w [W/m^2-K]	$\Delta p / N_L$ [Pa]
0.20	297.21	320.03	2.79	0.00631	33.7	0.109
0.25	297.22	320.05	3.00	0.00631	38	0.161
0.35	297.27	320.13	3.30	0.00627	44.1	0.283
0.50	297.35	320.02	3.67	0.00627	53.9	0.498
0.75	297.41	320.00	4.08	0.00624	65.6	0.924
1.00	297.40	319.98	4.46	0.00624	77.3	1.477
1.25	297.57	320.01	4.70	0.00624	86.8	2.133
1.50	297.64	319.97	4.94	0.00624	96.6	2.907
1.75	297.75	319.89	5.07	0.00620	102.9	3.741
2.00	297.88	319.88	5.27	0.00620	112.9	4.626

Table F.22 Raw and reduced data associated with Coil 8 at $\alpha = 45°$ with air flow $\perp$ to the tube passes

V [m/s]	$T_{a,in}$ [K]	$T_{r,in}$ [K]	ΔT_4 [K]	ΔT_3 [K]	ΔT_2 [K]	ΔT_1 [K]	$\dot{m}_r$ [kg/s]	Avg. h_w [W/m^2-K]	$\Delta p / N_L$ [Pa]
0.20	295.17	319.72	1.86	1.91	2.05	2.28	0.00549	27.5	0.029
0.24	295.18	319.73	2.06	2.07	2.15	2.33	0.00549	29.5	0.047
0.34	295.18	319.69	2.48	2.39	2.35	2.40	0.00550	34.1	0.086
0.49	295.19	319.72	2.99	2.78	2.57	2.48	0.00550	40.9	0.159
0.74	295.23	319.66	3.56	3.18	2.78	2.54	0.00550	49.8	0.309
0.99	295.28	319.67	4.04	3.51	2.99	2.57	0.00550	59.2	0.505
1.25	295.40	319.65	4.42	3.73	3.13	2.57	0.00550	67.9	0.740
1.50	295.42	319.62	4.75	3.92	3.22	2.58	0.00550	76.0	1.035
1.75	295.44	319.58	5.05	4.09	3.29	2.57	0.00549	84.2	1.343
2.00	295.50	319.58	5.24	4.18	3.32	2.57	0.00549	89.5	1.652

Table F.23 Raw and reduced data associated with Coil 8 at $\alpha = 60°$ with air flow $\perp$ to the tube passes

V [m/s]	$T_{a,in}$ [K]	$T_{r,in}$ [K]	ΔT_4 [K]	ΔT_3 [K]	ΔT_2 [K]	ΔT_1 [K]	$\dot{m}_r$ [kg/s]	Avg. h_w [W/m^2-K]	$\Delta p / N_L$ [Pa]
0.21	295.28	319.69	1.99	2.06	2.05	2.18	0.00590	31.1	0.042
0.26	295.24	319.78	2.19	2.22	2.15	2.24	0.00590	33.0	0.060
0.35	295.22	319.84	2.55	2.53	2.32	2.34	0.00590	37.7	0.099
0.49	295.21	319.82	2.98	2.85	2.51	2.42	0.00590	43.8	0.174
0.74	295.23	319.80	3.57	3.27	2.75	2.49	0.00591	54.4	0.336
1.00	295.23	319.77	4.04	3.60	2.96	2.51	0.00591	64.6	0.562
1.24	295.27	319.71	4.43	3.81	3.09	2.54	0.00590	74.1	0.838
1.50	295.32	319.70	4.76	4.01	3.18	2.56	0.00590	83.2	1.164
1.75	295.42	319.68	5.00	4.15	3.25	2.56	0.00590	91.3	1.488
2.00	295.43	319.68	5.22	4.30	3.30	2.57	0.00590	98.7	1.848

Table F.24 Raw and reduced data associated with Coil 8 at $\alpha = 75°$ with air flow $\perp$ to the tube passes

V [m/s]	$T_{a,in}$ [K]	$T_{r,in}$ [K]	ΔT_4 [K]	ΔT_3 [K]	ΔT_2 [K]	ΔT_1 [K]	$\dot{m}_r$ [kg/s]	Avg. h_w [W/m^2-K]	$\Delta p / N_L$ [Pa]
0.20	295.37	319.76	1.90	1.92	2.00	2.21	0.00598	29.8	---
0.24	295.27	319.79	2.11	2.09	2.13	2.28	0.00598	32.7	---
0.35	295.22	319.71	2.57	2.44	2.32	2.38	0.00599	39.1	---
0.49	295.24	319.75	3.06	2.81	2.48	2.45	0.00599	46.0	---
0.74	295.28	319.75	3.65	3.23	2.83	2.52	0.00606	58.9	---
1.00	295.32	319.74	4.09	3.50	3.00	2.54	0.00606	68.4	---
1.24	295.35	319.71	4.43	3.70	3.10	2.57	0.00616	78.9	---
1.49	295.45	319.69	4.71	3.85	3.17	2.57	0.00616	87.1	---
1.74	295.48	319.65	4.93	3.98	3.25	2.56	0.00620	95.3	---
1.99	295.48	319.63	5.15	4.09	3.30	2.57	0.00620	102.9	---

Table F.25 Raw and reduced data associated with Coil 9 at $\alpha = 90°$

V [m/s]	$T_{a,in}$ [K]	$T_{r,in}$ [K]	ΔT_3 [K]	ΔT_2 [K]	ΔT_1 [K]	$\dot{m}_r$ [kg/s]	Avg. h_w [W/m^2-K]	$\Delta p / N_L$ [Pa]
0.21	295.91	319.78	0.96	1.04	1.42	0.00603	29.4	0.051
0.25	295.86	319.83	1.08	1.14	1.51	0.00608	32.8	0.065
0.34	295.82	319.87	1.29	1.30	1.68	0.00608	38.1	0.111
0.50	295.77	319.88	1.67	1.53	1.86	0.00606	47.2	0.206
0.75	295.73	319.86	2.16	1.94	2.09	0.00606	62.4	0.426
1.00	295.73	319.76	2.50	2.22	2.21	0.00606	74.1	0.703
1.25	295.74	319.74	2.79	2.45	2.33	0.00606	85.2	1.032
1.51	295.72	319.71	3.05	2.67	2.44	0.00607	96.5	1.434
1.75	295.69	319.72	3.29	2.86	2.54	0.00603	106.6	1.869
2.00	295.68	319.68	3.46	3.00	2.62	0.00604	115.6	2.300

Table F.26 Raw and reduced data associated with Coil 9 at $\alpha = 45°$ with air flow $\perp$ to the wires

V [m/s]	$T_{a,in}$ [K]	$T_{r,in}$ [K]	ΔT_1 [K]	$\dot{m}_r$ [kg/s]	Avg. h_w [W/m^2-K]	$\Delta p / N_L$ [Pa]
0.20	295.60	319.68	1.81	0.00557	36.2	0.100
0.25	295.54	319.72	2.01	0.00557	41.8	0.179
0.35	295.44	319.69	2.25	0.00554	49.2	0.291
0.50	295.43	319.68	2.59	0.00554	61.3	0.550
0.75	295.38	319.69	2.99	0.00553	77	1.059
1.00	295.37	319.64	3.31	0.00553	91.1	1.717
1.25	295.41	319.62	3.59	0.00552	105.1	2.559
1.50	295.31	319.65	3.85	0.00552	117.8	3.550
1.75	295.33	319.60	4.04	0.00551	128.9	4.596
2.00	295.30	319.60	4.23	0.00551	140.2	5.746

Table F.27 Raw and reduced data associated with Coil 9 at $\alpha = 60°$ with air flow $\perp$ to the wires

V [m/s]	$T_{a,in}$ [K]	$T_{r,in}$ [K]	ΔT_1 [K]	$\dot{m}_r$ [kg/s]	Avg. h_w [W/m^2-K]	$\Delta p / N_L$ [Pa]
0.20	295.63	319.87	1.75	0.00591	35.9	0.109
0.25	295.53	319.83	1.93	0.00591	41.2	0.170
0.35	295.48	319.86	2.18	0.00591	49	0.291
0.50	295.40	319.82	2.50	0.00591	60.3	0.541
0.75	295.41	319.78	2.88	0.00591	75.1	1.059
1.00	295.36	319.78	3.17	0.00591	87.2	1.717
1.25	295.38	319.76	3.45	0.00587	99.4	2.559
1.50	295.35	319.75	3.69	0.00587	111.3	3.566
1.75	295.37	319.72	3.90	0.00586	122.5	4.633
2.00	295.31	319.68	4.08	0.00586	132.3	5.767

Table F.28 Raw and reduced data associated with Coil 9 at $\alpha = 75°$ with air flow $\perp$ to the wires

V [m/s]	$T_{a,in}$ [K]	$T_{r,in}$ [K]	ΔT_1 [K]	$\dot{m}_r$ [kg/s]	Avg. h_w [W/m^2-K]	$\Delta p / N_L$ [Pa]
0.20	295.38	319.91	1.67	0.00615	34.2	---
0.24	295.38	319.89	1.82	0.00615	38.7	---
0.35	295.34	319.89	2.08	0.00609	46.1	---
0.50	295.33	319.94	2.31	0.00609	53.6	---
0.75	295.33	319.88	2.68	0.00620	68.9	---
1.00	295.35	319.87	2.96	0.00620	80.1	---
1.25	295.30	319.90	3.24	0.00618	91.6	---
1.49	295.36	319.86	3.44	0.00618	101.2	---
1.75	295.31	319.85	3.67	0.00616	111.8	---
2.00	295.27	319.82	3.85	0.00616	121.5	---

Table F.29 Raw and reduced data associated with Coil 9 at $\alpha = 45°$ with air flow $\perp$ to the tube passes

V [m/s]	$T_{a,in}$ [K]	$T_{r,in}$ [K]	ΔT_3 [K]	ΔT_2 [K]	ΔT_1 [K]	$\dot{m}_r$ [kg/s]	Avg. h_w [W/m^2-K]	$\Delta p / N_L$ [Pa]
0.21	295.80	319.60	1.00	1.17	1.46	0.00507	25.0	0.041
0.25	295.70	319.55	1.12	1.31	1.55	0.00507	28.6	0.058
0.35	295.60	319.51	1.38	1.54	1.71	0.00503	33.7	0.112
0.49	295.55	319.50	1.71	1.81	1.91	0.00503	41.6	0.202
0.75	295.54	319.49	2.13	2.15	2.13	0.00501	52.2	0.405
0.99	295.52	319.46	2.50	2.43	2.32	0.00501	62.7	0.653
1.25	295.51	319.45	2.81	2.66	2.46	0.00498	72.0	0.962
1.50	295.52	319.44	3.07	2.85	2.58	0.00498	80.7	1.320
1.74	295.53	319.42	3.35	3.03	2.68	0.00495	89.8	1.720
2.00	295.53	319.39	3.51	3.15	2.74	0.00495	96.1	2.103

Table F.30 Raw and reduced data associated with Coil 9 at $\alpha = 60°$ with air flow $\perp$ to the tube passes

V [m/s]	$T_{a,in}$ [K]	$T_{r,in}$ [K]	ΔT_3 [K]	ΔT_2 [K]	ΔT_1 [K]	$\dot{m}_r$ [kg/s]	Avg. h_w [W/m^2-K]	$\Delta p / N_L$ [Pa]
0.20	294.79	319.48	1.18	1.41	1.60	0.00503	29.5	0.039
0.24	294.81	319.49	1.34	1.54	1.70	0.00503	33.4	0.056
0.34	294.85	319.52	1.64	1.80	1.89	0.00501	40.1	0.115
0.50	294.91	319.48	1.99	2.07	2.08	0.00501	48.2	0.216
0.75	294.96	319.46	2.47	2.44	2.31	0.00498	60.7	0.444
0.99	294.97	319.47	2.83	2.73	2.46	0.00498	71.1	0.702
1.25	295.03	319.40	3.16	2.97	2.60	0.00497	82.2	1.064
1.50	295.12	319.41	3.47	3.19	2.72	0.00497	93.6	1.492
1.74	295.05	319.36	3.70	3.34	2.80	0.00496	101.7	1.896
2.00	295.09	319.38	3.91	3.48	2.88	0.00496	110.3	2.339

Table F.31 Raw and reduced data associated with Coil 9 at $\alpha = 75°$ with air flow $\perp$ to the tube passes

V [m/s]	$T_{a,in}$ [K]	$T_{r,in}$ [K]	ΔT_3 [K]	ΔT_2 [K]	ΔT_1 [K]	$\dot{m}_r$ [kg/s]	Avg. h_w [W/m^2-K]	$\Delta p / N_L$ [Pa]
0.20	295.74	319.64	1.13	1.33	1.54	0.00527	31.0	0.036
0.25	295.69	319.69	1.24	1.44	1.61	0.00527	33.3	0.044
0.35	295.64	319.65	1.52	1.65	1.80	0.00528	39.7	0.089
0.50	295.63	319.63	1.87	1.90	1.99	0.00528	48.2	0.179
0.75	295.60	319.54	2.37	2.29	2.23	0.00527	62.6	0.366
1.00	295.55	319.63	2.74	2.61	2.40	0.00527	74.3	0.623
1.25	295.60	319.59	3.06	2.85	2.53	0.00528	85.9	0.905
1.50	295.58	319.54	3.35	3.05	2.65	0.00528	97.3	1.265
1.75	295.59	319.47	3.55	3.20	2.72	0.00526	105.8	1.616
2.00	295.62	319.45	3.78	3.35	2.80	0.00526	115.9	2.015

Table F.32 Raw and reduced data associated with Coil 10 at $\alpha = 90°$

V [m/s]	$T_{a,in}$ [K]	$T_{r,in}$ [K]	ΔT_4 [K]	ΔT_3 [K]	ΔT_2 [K]	ΔT_1 [K]	$\dot{m}_r$ [kg/s]	Avg. h_w [W/m^2-K]	$\Delta p / N_L$ [Pa]
0.22	295.65	319.78	2.69	2.65	2.81	3.07	0.00629	32.3	0.079
0.25	295.64	319.77	2.95	2.83	2.91	3.10	0.00629	34.2	0.094
0.35	295.64	319.72	4.04	3.51	3.11	3.03	0.00625	43.0	0.197
0.49	295.67	319.71	4.91	4.19	3.33	2.91	0.00625	52.5	0.307
0.75	295.65	319.74	6.16	4.84	3.68	2.72	0.00622	67.9	0.610
1.00	295.64	319.75	7.04	5.20	3.74	2.55	0.00622	79.3	0.956
1.25	295.82	320.33	5.45	4.46	3.62	2.72	0.00949	90.1	1.400
1.51	295.94	320.28	5.94	4.69	3.67	2.63	0.00828	---	1.891
1.75	296.04	320.18	6.30	4.85	3.68	2.56	0.00953	110.5	2.329
2.00	296.14	320.21	6.64	5.00	3.72	2.50	0.00942	117.8	2.789

Table F.33 Raw and reduced data associated with Coil 10 at $\alpha = 45°$ with air flow $\perp$ to the wires

V [m/s]	$T_{a,in}$ [K]	$T_{r,in}$ [K]	ΔT_1 [K]	$\dot{m}_r$ [kg/s]	Avg. h_w [W/m^2-K]	$\Delta p / N_L$ [Pa]
0.21	295.84	320.42	3.58	0.00899	34.9	0.170
0.25	295.81	320.40	3.90	0.00899	39.6	0.231
0.35	295.77	320.41	4.47	0.00895	48.8	0.378
0.49	295.76	320.40	5.08	0.00895	59.9	0.669
0.75	295.76	320.37	5.85	0.00894	76	1.269
1.00	295.76	320.35	6.42	0.00894	89.8	2.036
1.26	295.78	320.57	3.42	0.02037	100.3	2.985
1.50	295.80	320.47	3.64	0.02035	112	4.065
1.75	295.83	320.47	3.82	0.02038	121.8	5.165
2.00	295.91	320.36	3.95	0.02040	131.1	6.316

Table F.34 Raw and reduced data associated with Coil 10 at $\alpha = 60°$ with air flow $\perp$ to the wires

V [m/s]	$T_{a,in}$ [K]	$T_{r,in}$ [K]	ΔT_1 [K]	$\dot{m}_r$ [kg/s]	Avg. h_w [W/m^2-K]	$\Delta p / N_L$ [Pa]
0.21	295.92	320.52	3.31	0.01018	35.4	0.187
0.25	295.87	320.53	3.52	0.01018	38.7	0.222
0.35	295.81	320.52	4.06	0.01015	47.4	0.386
0.49	295.74	320.49	4.63	0.01015	58.1	0.669
0.75	295.74	320.48	5.36	0.01014	73.3	1.303
1.00	295.71	320.53	5.91	0.01014	85.5	2.044
1.26	295.74	320.45	3.44	0.02049	96.9	3.048
1.50	295.79	320.39	3.66	0.02050	107.4	4.102
1.75	295.85	320.41	3.85	0.02051	116.9	5.243
2.00	295.95	320.35	4.00	0.02050	125.7	6.443

Table F.35 Raw and reduced data associated with Coil 10 at $\alpha = 75°$ with air flow $\perp$ to the wires

V [m/s]	$T_{a,in}$ [K]	$T_{r,in}$ [K]	ΔT_1 [K]	$\dot{m}_r$ [kg/s]	Avg. h_w [W/m^2-K]	$\Delta p / N_L$ [Pa]
0.21	295.56	320.61	3.30	0.01034	34.5	0.109
0.25	295.56	320.52	3.50	0.01034	37.7	0.153
0.35	295.56	320.56	4.00	0.01030	45.5	0.283
0.49	295.55	320.55	4.53	0.01030	55	0.498
0.75	295.57	320.54	5.26	0.01029	69.3	1.009
1.00	295.54	320.45	5.79	0.01029	81.3	1.618
1.25	295.57	320.49	3.38	0.02075	91.7	2.447
1.50	295.62	320.48	3.60	0.02076	101.6	3.343
1.75	295.68	320.45	3.80	0.02077	111.2	4.354
2.01	295.80	320.36	3.97	0.02076	120.6	5.503

Table F.36 Raw and reduced data associated with Coil 10 at $\alpha = 45°$ with air flow $\perp$ to the tube passes

V [m/s]	$T_{a,in}$ [K]	$T_{r,in}$ [K]	ΔT_4 [K]	ΔT_3 [K]	ΔT_2 [K]	ΔT_1 [K]	$\dot{m}_r$ [kg/s]	Avg. h_w [W/m^2-K]	$\Delta p / N_L$ [Pa]
0.19	295.14	319.86	2.09	2.32	2.54	3.03	0.00656	29.1	0.049
0.25	295.14	319.89	2.50	2.64	2.76	3.08	0.00656	31.0	0.079
0.35	295.17	319.93	3.16	3.16	3.05	3.13	0.00655	36.8	0.142
0.50	295.21	319.86	3.96	3.69	3.28	3.10	0.00655	43.5	0.250
0.75	295.33	319.90	5.06	4.36	3.54	3.02	0.00655	55.4	0.487
1.00	295.39	319.91	5.91	4.79	3.66	2.89	0.00655	65.6	0.785
1.25	295.47	319.85	6.60	5.10	3.70	2.76	0.00654	75.6	1.144
1.49	295.52	319.85	7.18	5.34	3.70	2.64	0.00654	84.7	1.544
1.75	295.58	319.83	7.69	5.52	3.69	2.52	0.00654	93.6	1.980
2.00	295.65	319.75	8.08	5.63	3.64	2.40	0.00654	101.4	2.371

Table F.37 Raw and reduced data associated with Coil 10 at $\alpha = 60°$ with air flow $\perp$ to the tube passes

V [m/s]	$T_{a,in}$ [K]	$T_{r,in}$ [K]	ΔT_4 [K]	ΔT_3 [K]	ΔT_2 [K]	ΔT_1 [K]	$\dot{m}_r$ [kg/s]	Avg. h_w [W/m^2-K]	$\Delta p / N_L$ [Pa]
0.20	295.43	319.73	2.70	2.76	2.85	3.14	0.00588	30.8	0.060
0.25	295.30	319.71	3.09	3.04	3.01	3.13	0.00588	32.4	0.086
0.35	295.24	319.71	3.89	3.59	3.32	3.16	0.00586	39.5	0.146
0.50	295.19	319.60	4.86	4.20	3.55	3.01	0.00586	47.8	0.265
0.75	295.20	319.65	6.08	4.83	3.74	2.81	0.00585	60.0	0.527
1.01	295.22	319.56	7.03	5.22	3.76	2.59	0.00585	71.4	0.861
1.25	295.30	319.54	7.83	5.51	3.75	2.43	0.00585	84.2	1.259
1.50	295.32	319.56	8.51	5.72	3.69	2.27	0.00585	95.1	1.712
1.75	295.40	319.60	9.03	5.85	3.64	2.15	0.00585	104.6	2.147
2.00	295.49	319.61	9.51	5.94	3.55	2.02	0.00585	115.0	2.587

Table F.38 Raw and reduced data associated with Coil 10 at $\alpha = 75°$ with air flow $\perp$ to the tube passes

V [m/s]	$T_{a,in}$ [K]	$T_{r,in}$ [K]	ΔT_4 [K]	ΔT_3 [K]	ΔT_2 [K]	ΔT_1 [K]	$\dot{m}_r$ [kg/s]	Avg. h_w [W/m^2-K]	$\Delta p / N_L$ [Pa]
0.21	295.39	319.97	2.67	2.72	2.87	3.15	0.00633	33.1	0.053
0.25	295.44	319.87	3.06	3.02	3.04	3.16	0.00622	35.7	0.071
0.35	295.51	319.99	3.86	3.55	3.30	3.16	0.00622	42.0	0.129
0.50	295.52	319.93	4.88	4.14	3.49	3.04	0.00624	51.6	0.240
0.75	295.46	320.34	4.06	3.66	3.30	2.87	0.00957	64.7	0.466
1.01	295.49	320.22	4.78	4.10	3.49	2.84	0.00956	77.1	0.772
1.25	295.64	320.21	5.39	4.46	3.61	2.79	0.00953	89.7	1.142
1.50	295.67	320.29	5.95	4.76	3.69	2.75	0.00949	100.8	1.535
1.75	295.56	320.29	6.41	4.99	3.77	2.70	0.00952	111.3	1.942
2.00	295.68	320.27	6.69	5.10	3.77	2.65	0.00953	118.5	2.338

APPENDIX G: ADDITIONAL HEAT TRANSFER & PRESSURE DROP PLOTS

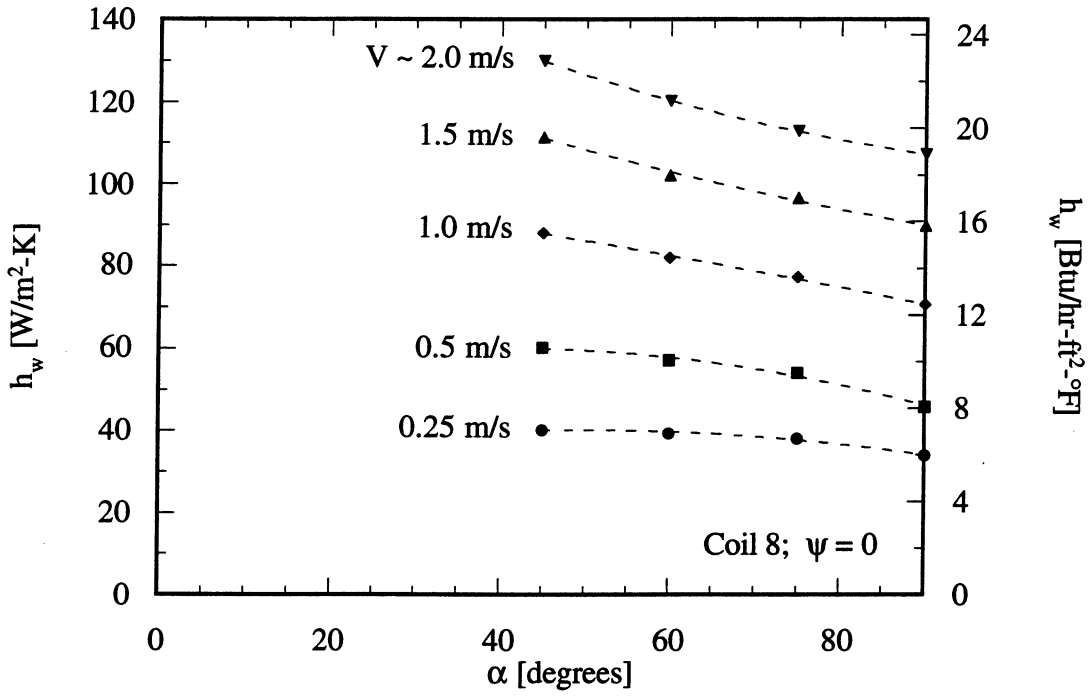

Figure G.1 Effect of α on h_w for Coil 8 with air flow $\perp$ to the wires

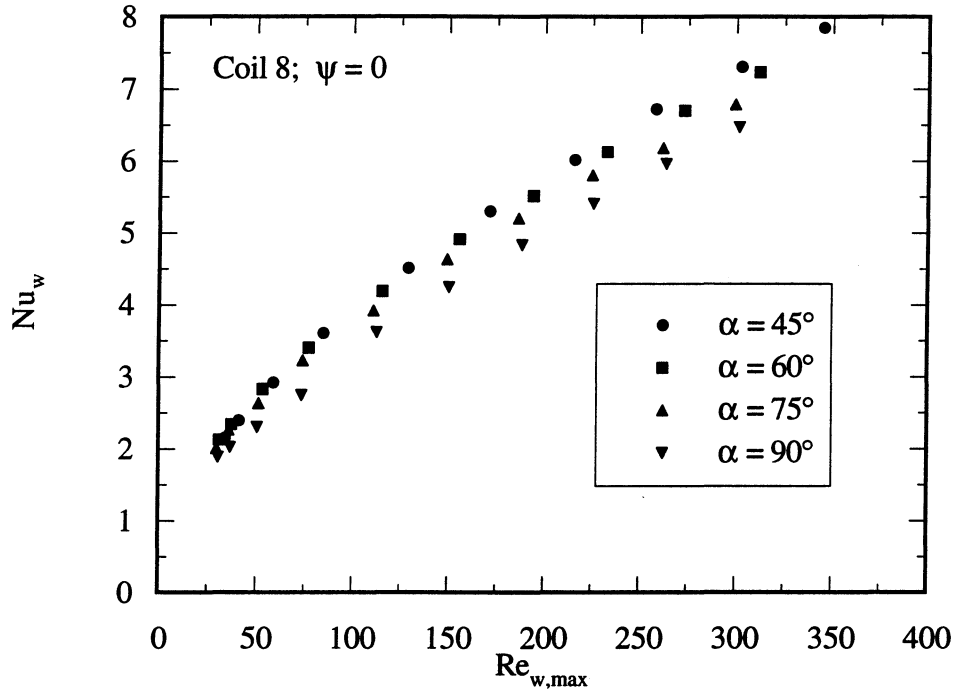

Figure G.2 Nu_w vs. $Re_{w,max}$ for Coil 8 with air flow ⊥ to the wires

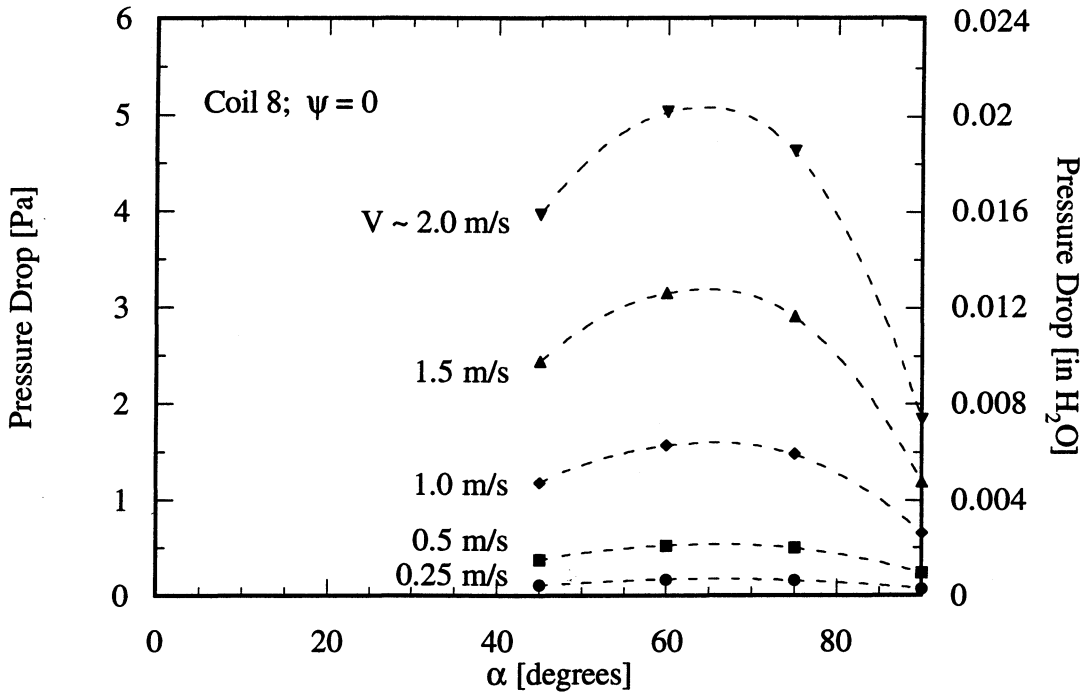

Figure G.3 Δp per layer vs. α for Coil 8 with air flow ⊥ to the wires

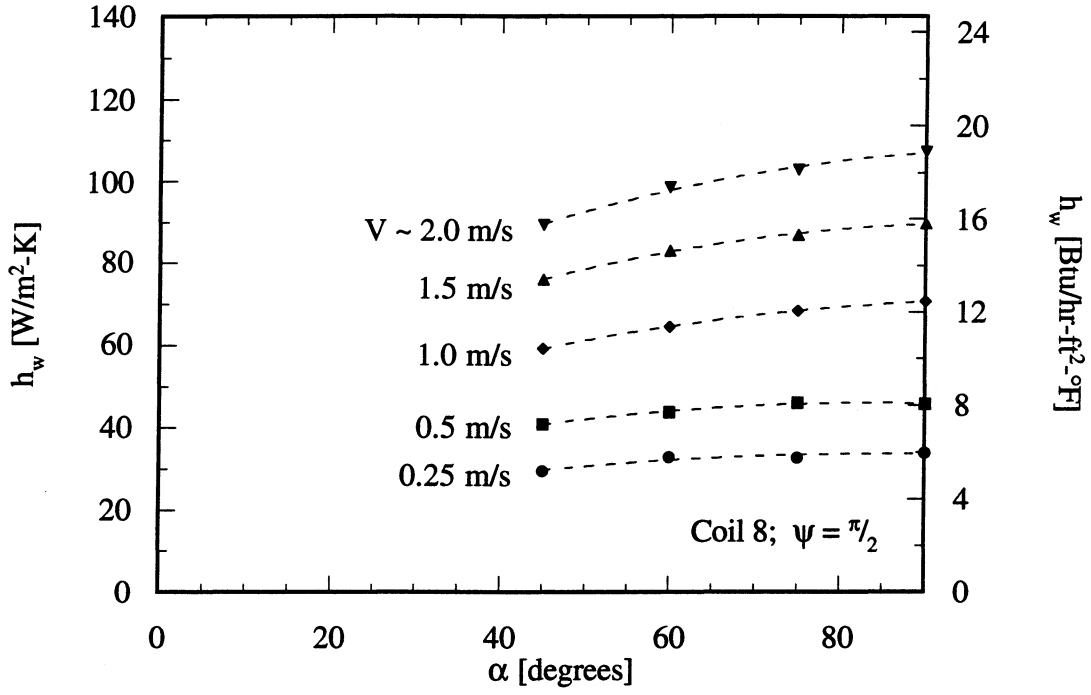

Figure G.4 Effect of α on h_w for Coil 8 with air flow $\perp$ to the tube passes

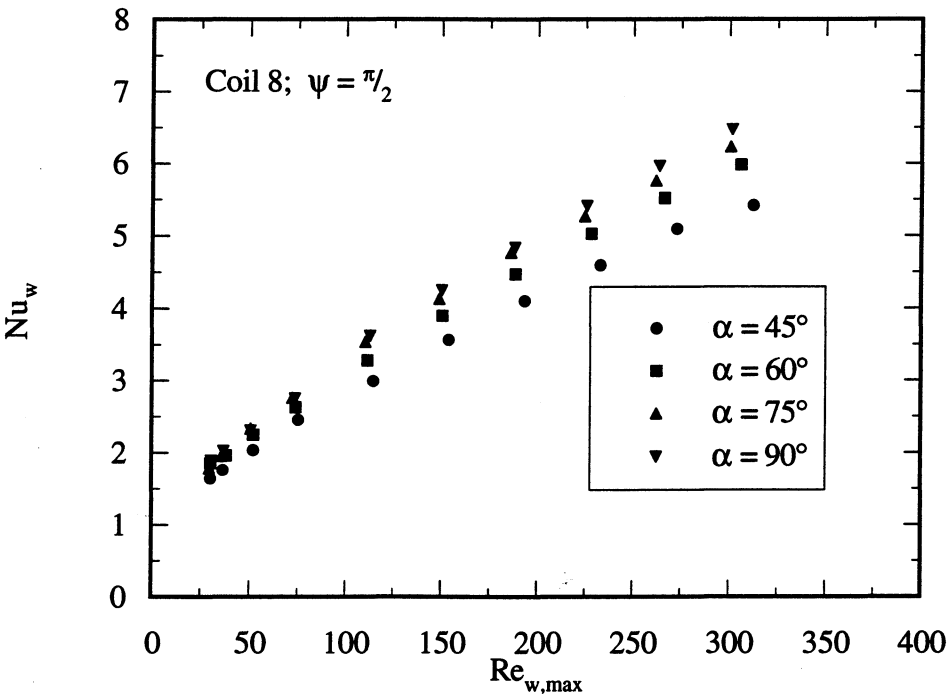

Figure G.5 Nu_w vs. $Re_{w,max}$ for Coil 8 with air flow $\perp$ to the tube passes

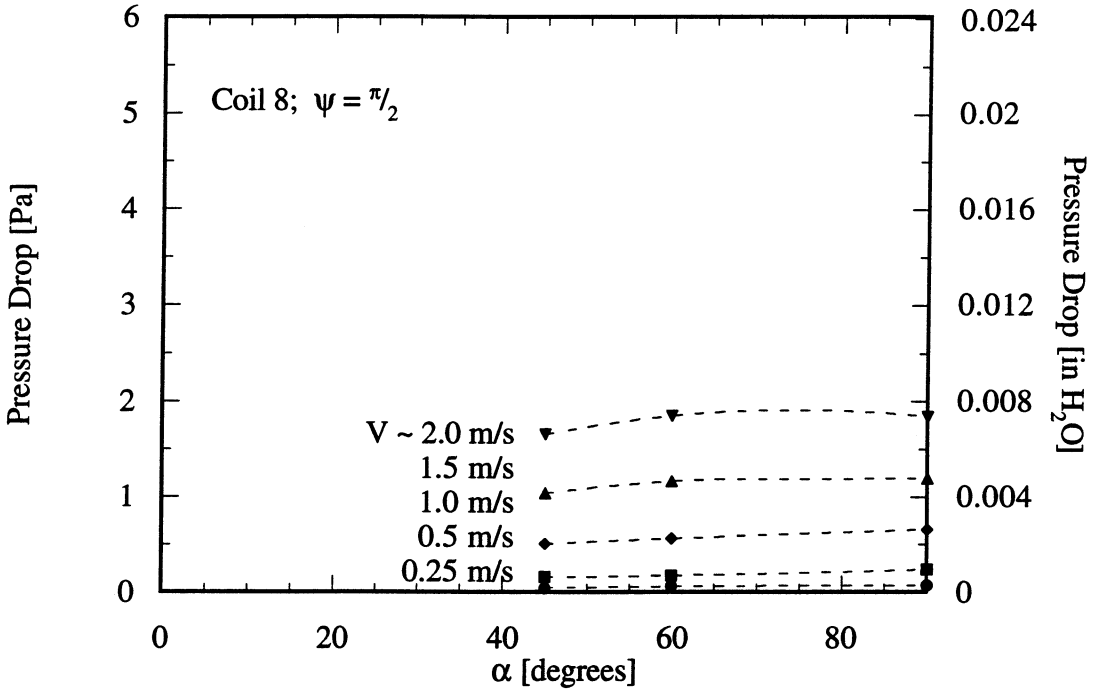

Figure G.6 Δp per layer vs. α for Coil 8 with air flow ⊥ to the tube passes

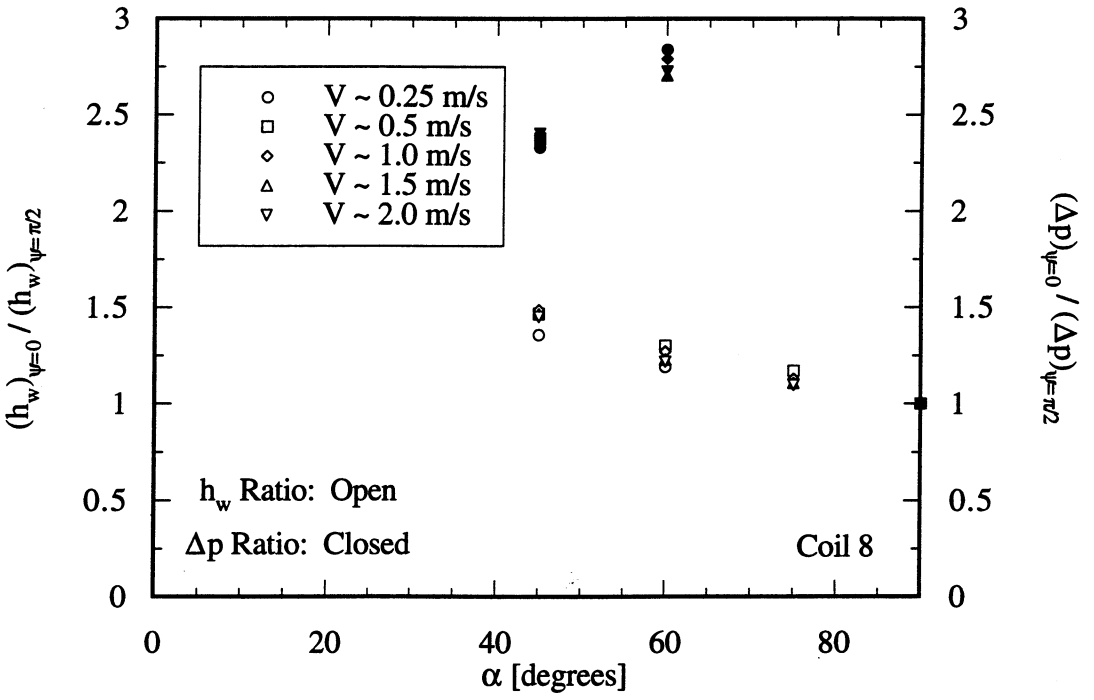

Figure G.7 Comparison of the h_w and Δp per layer of Coil 8 at $\psi = 0$ and $\psi = \pi/2$

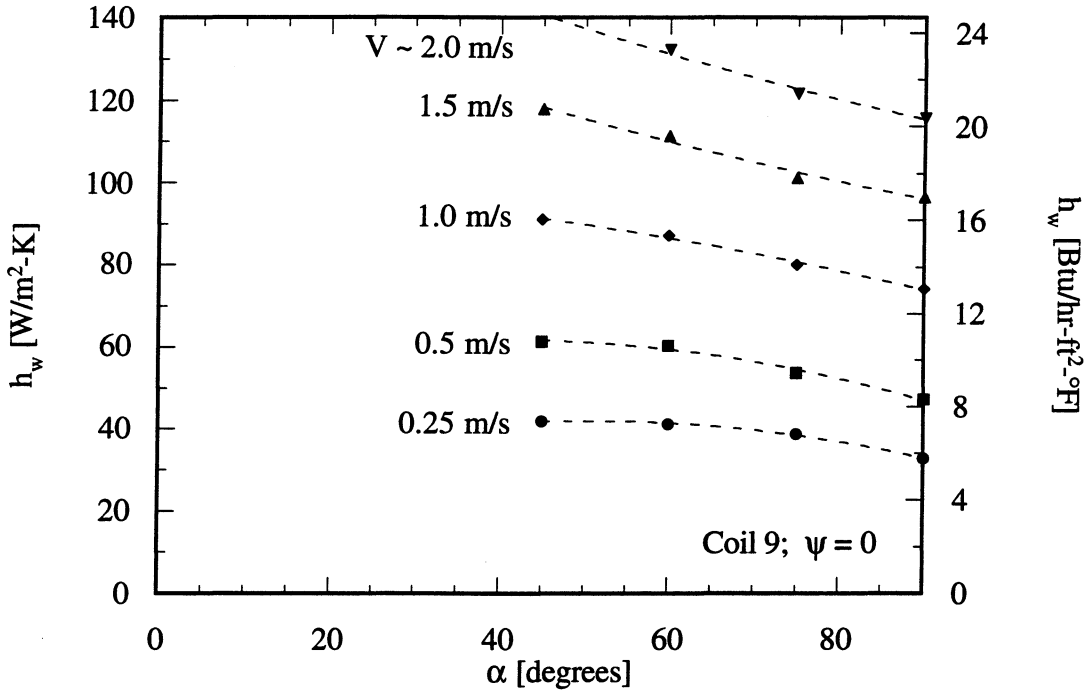

Figure G.8 Effect of α on h_w for Coil 9 with air flow $\perp$ to the wires

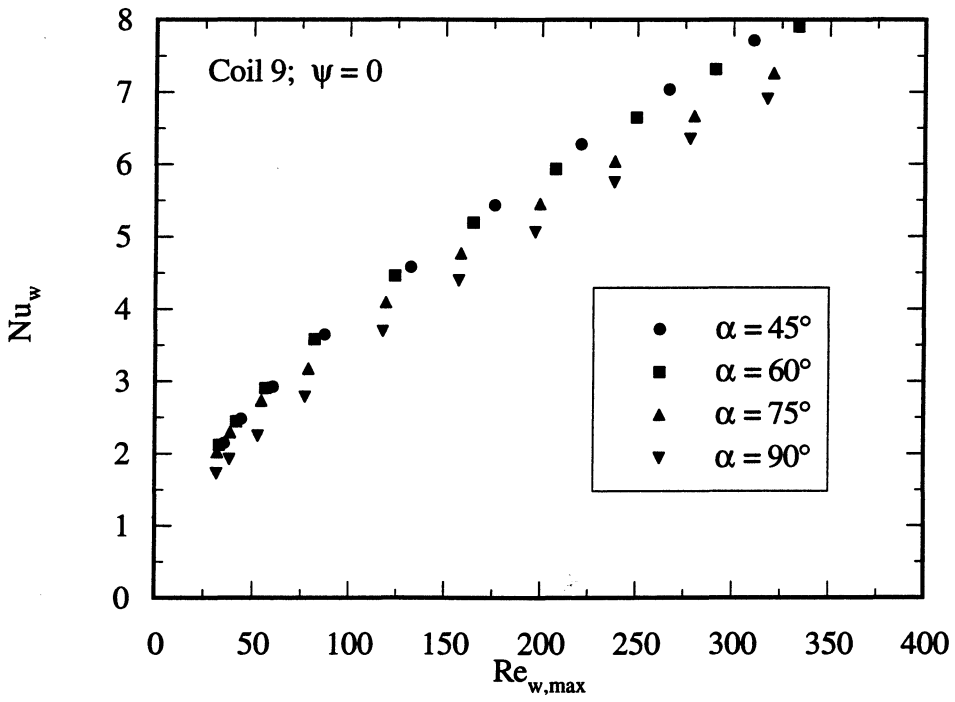

Figure G.9 Nu_w vs. $Re_{w,max}$ for Coil 9 with air flow $\perp$ to the wires

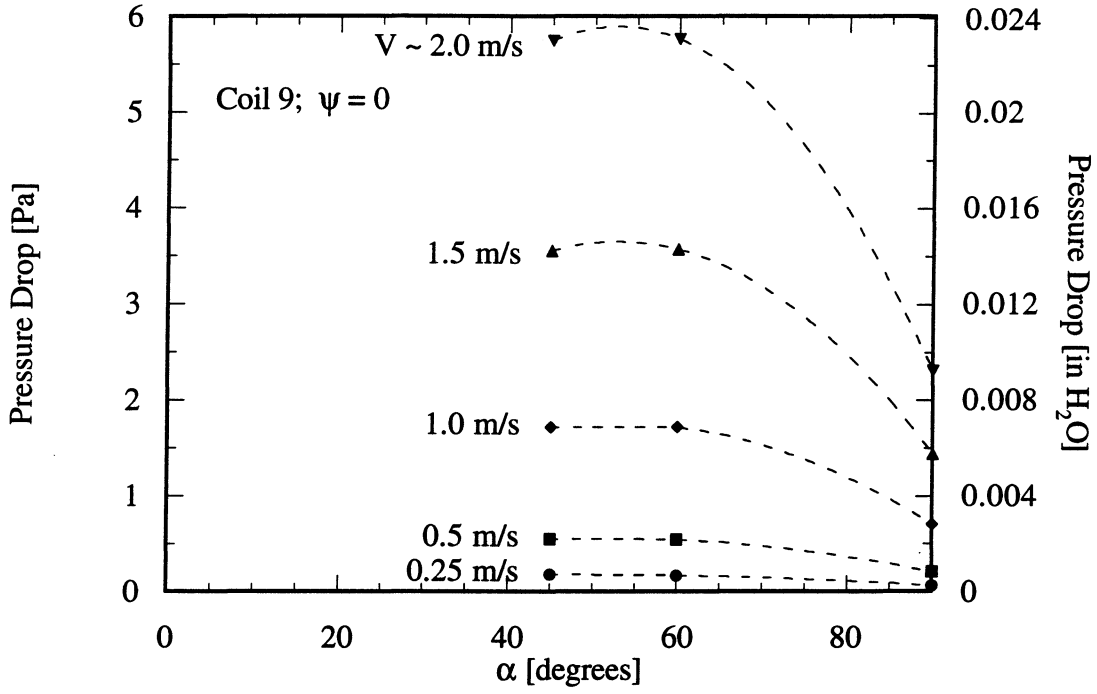

Figure G.10 Δp per layer vs. α for Coil 9 with air flow ⊥ to the wires

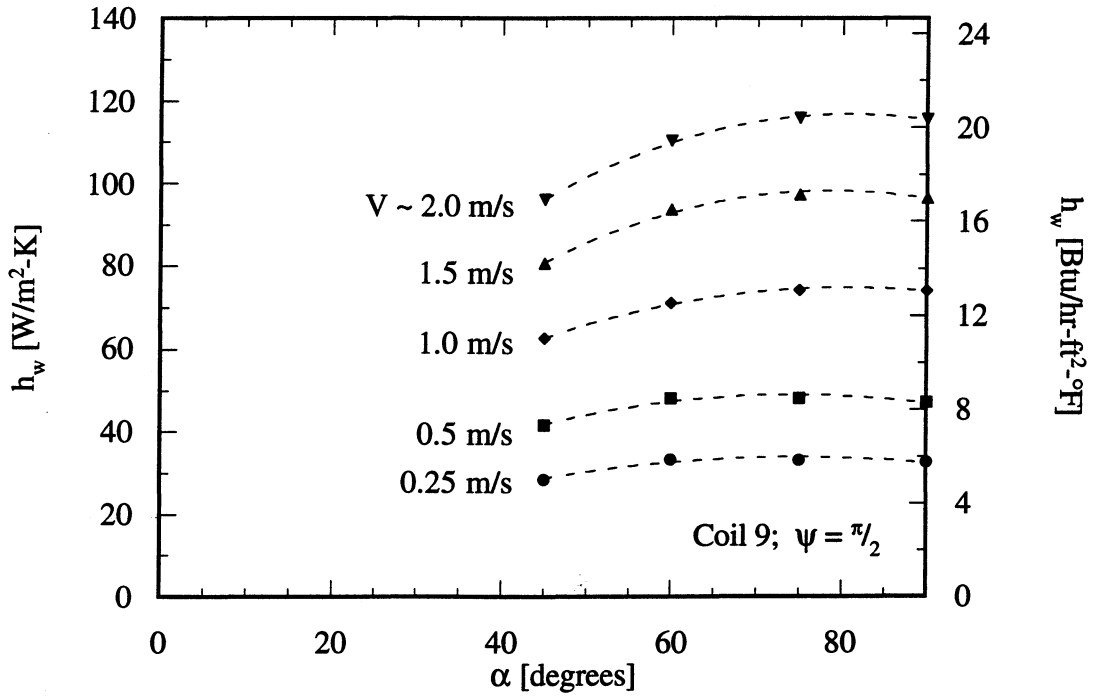

Figure G.11 Effect of α on h_w for Coil 9 with air flow ⊥ to the tube passes

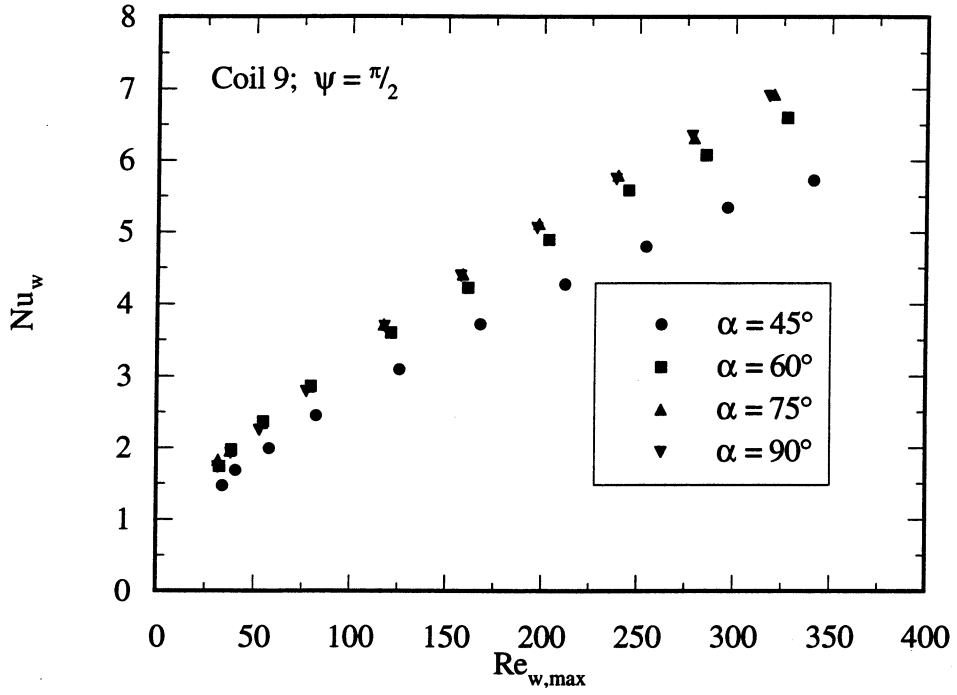

Figure G.12 Nu_w vs. $Re_{w,max}$ for Coil 9 with air flow ⊥ to the tube passes

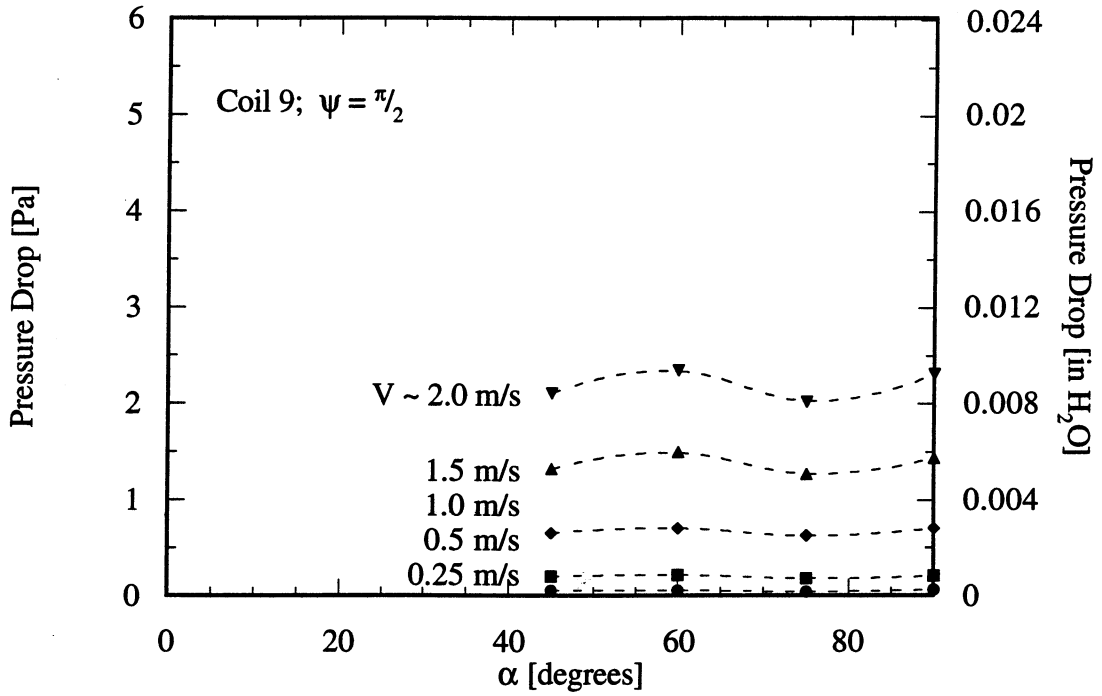

Figure G.13 Δp per layer vs. α for Coil 9 with air flow ⊥ to the tube passes

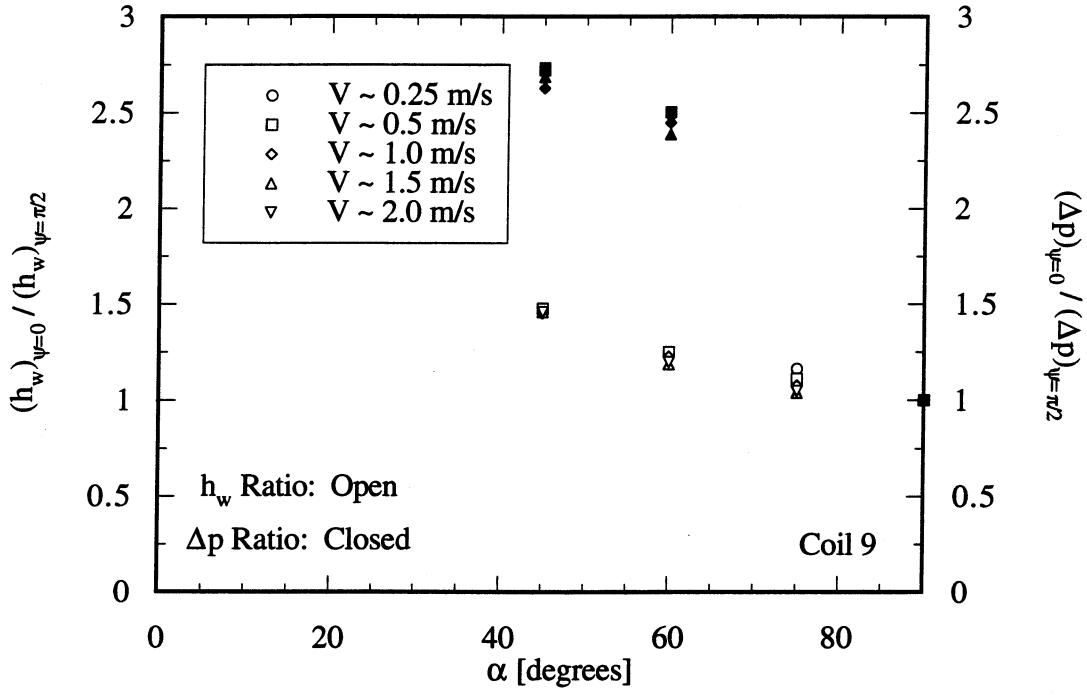

Figure G.14 Comparison of the h_w and Δp per layer of Coil 9 at $\psi = 0$ and $\psi = \pi/2$

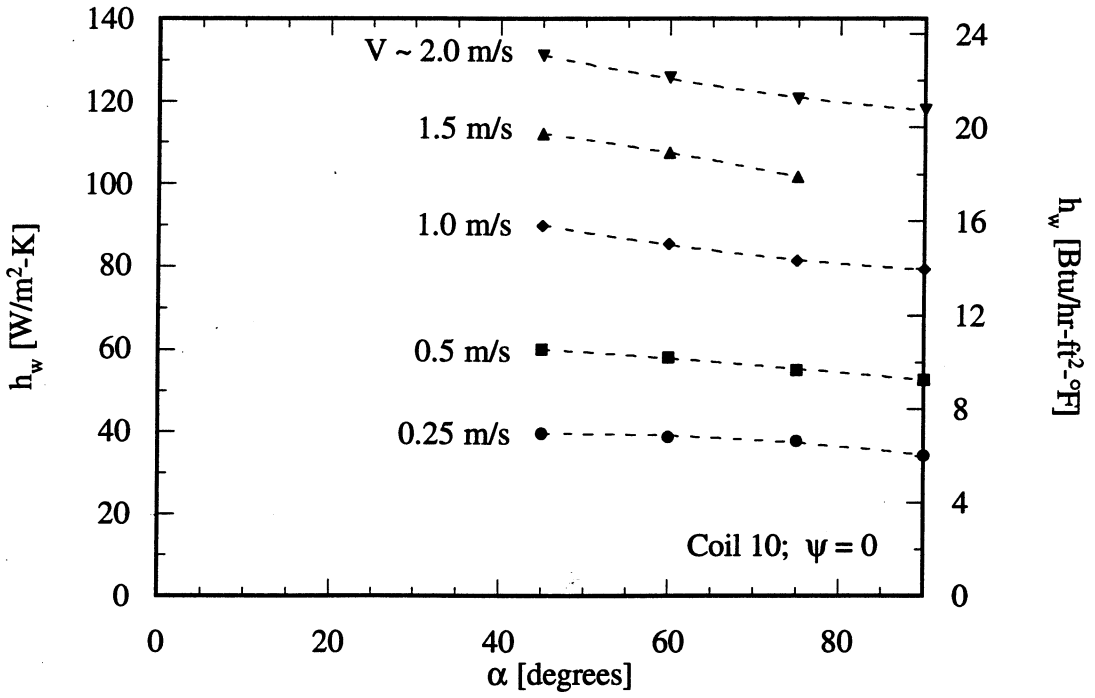

Figure G.15 Effect of α on h_w for Coil 10 with air flow $\perp$ to the wires

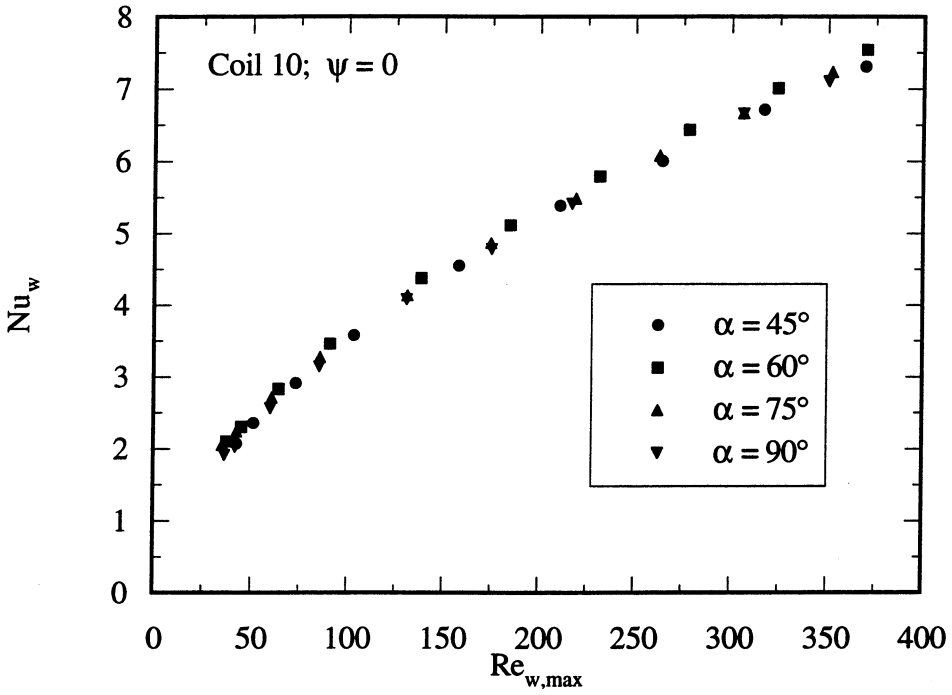

Figure G.16 Nu_w vs. $Re_{w,max}$ for Coil 10 with air flow ⊥ to the wires

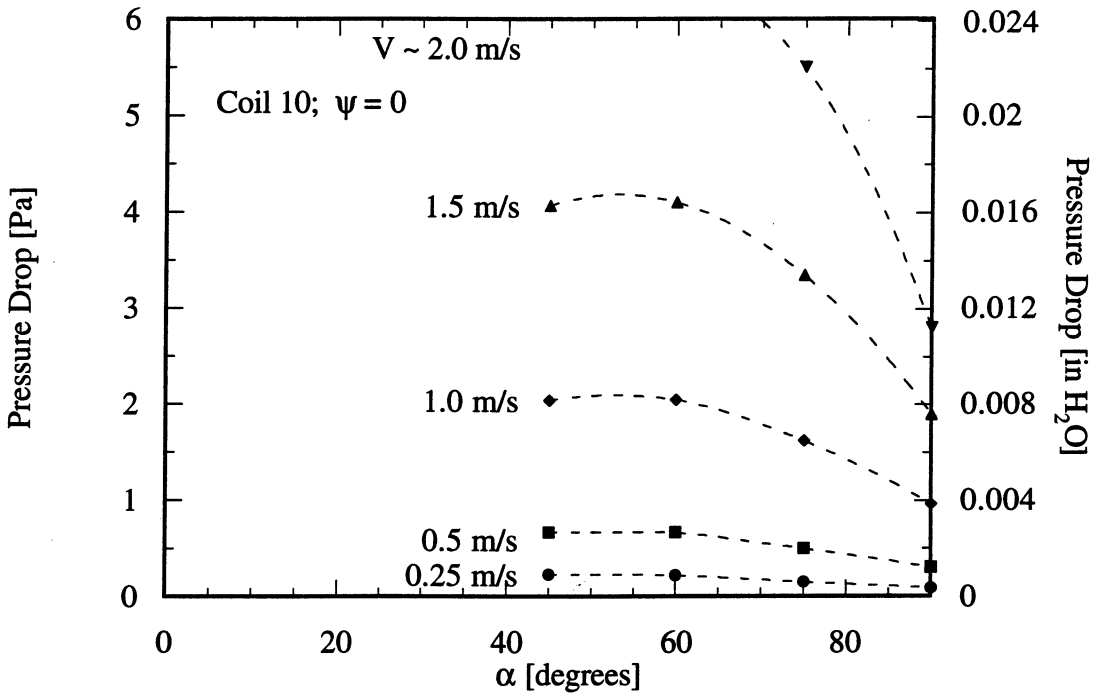

Figure G.17 Δp per layer vs. α for Coil 10 with air flow ⊥ to the wires

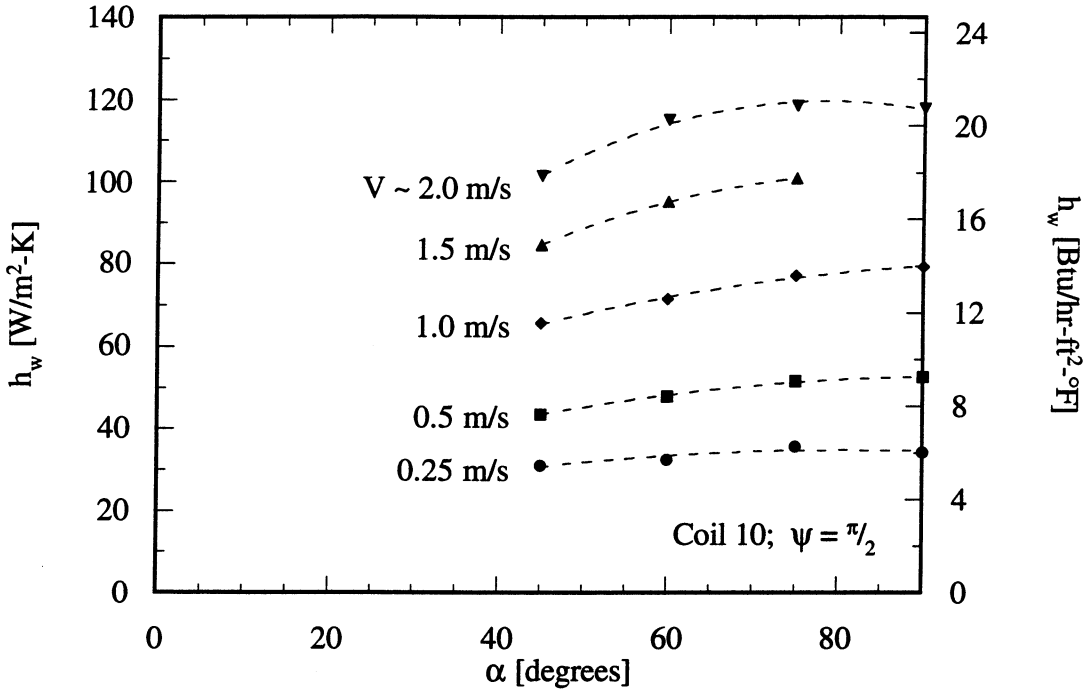

Figure G.18 Effect of α on h_w for Coil 10 with air flow ⊥ to the tube passes

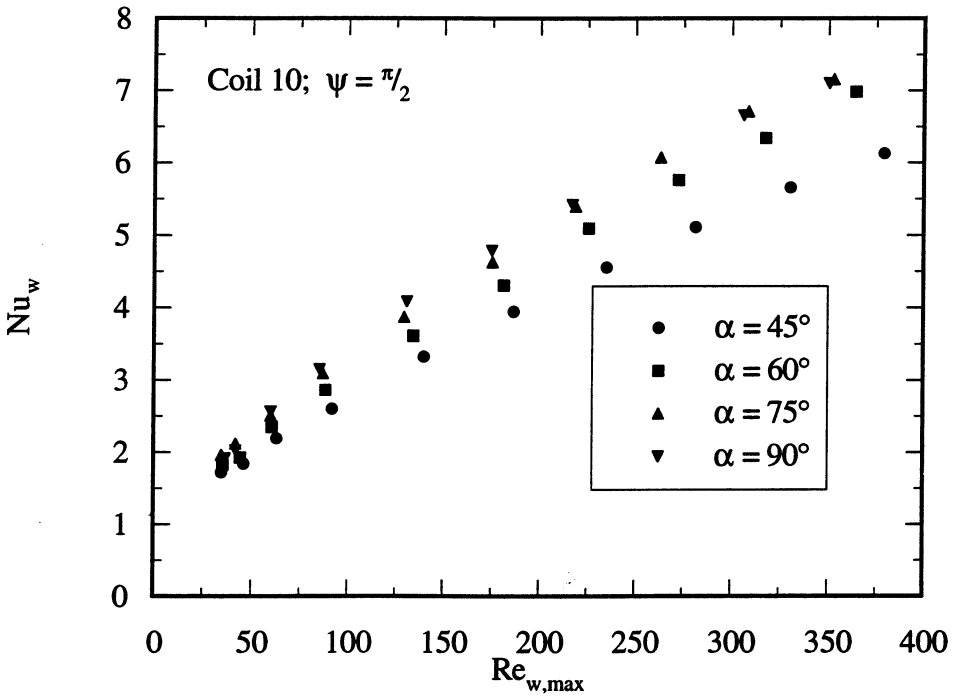

Figure G.19 Nu_w vs. $Re_{w,max}$ for Coil 10 with air-flow ⊥ to the tube passes

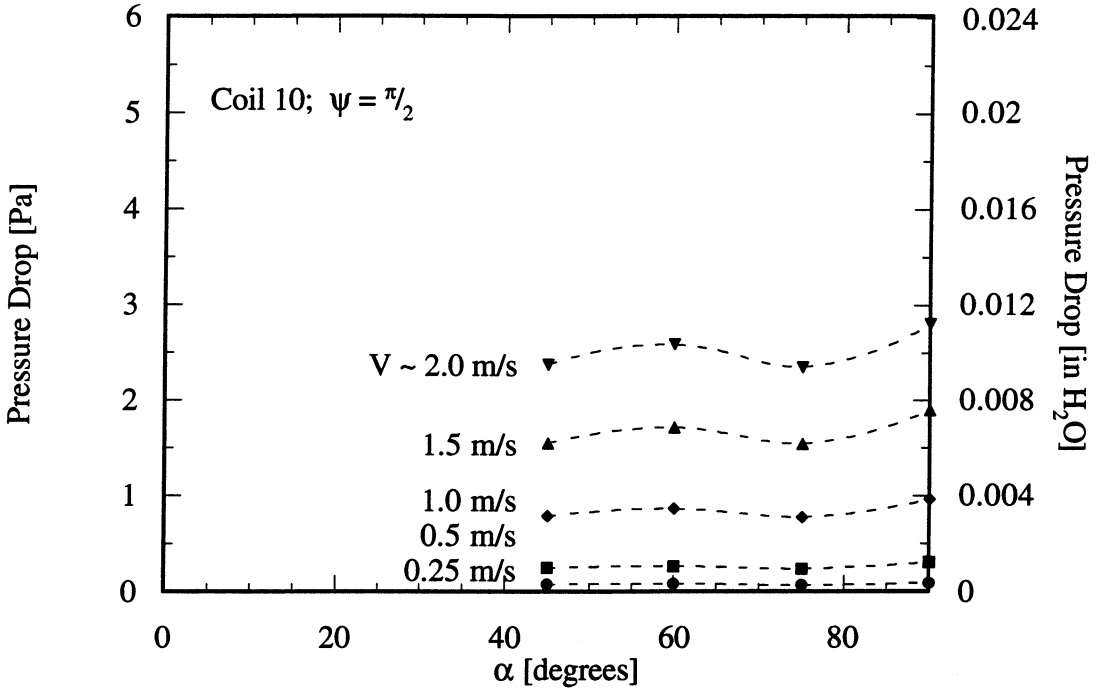

Figure G.20 Δp per layer vs. α for Coil 10 with air flow ⊥ to the tube passes

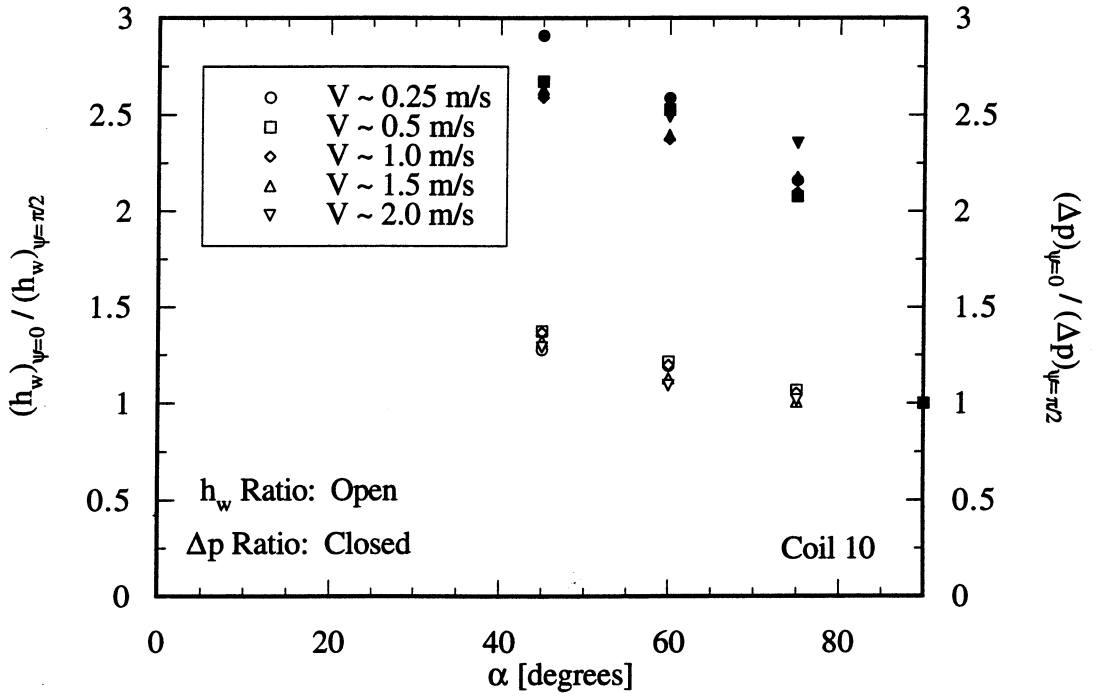

Figure G.21 Comparison of the h_w and Δp per layer of Coil 10 at $\psi = 0$ and $\psi = \pi/2$

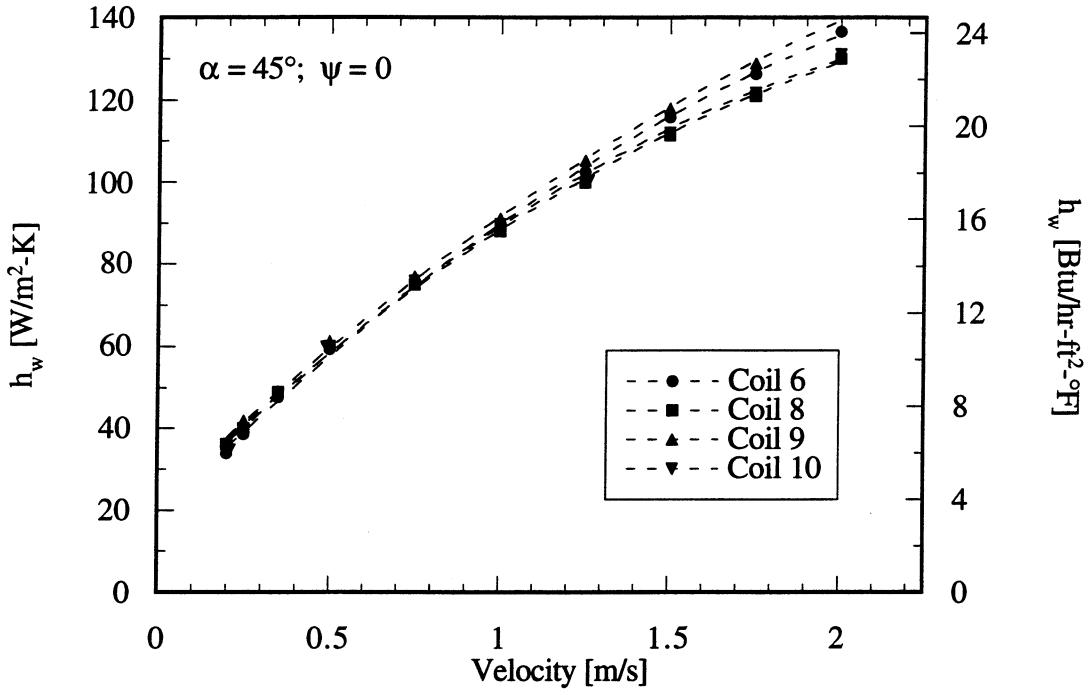

Figure G.22 h_w vs. V for condensers at $\alpha = 45°$ with air flow $\perp$ to the wires

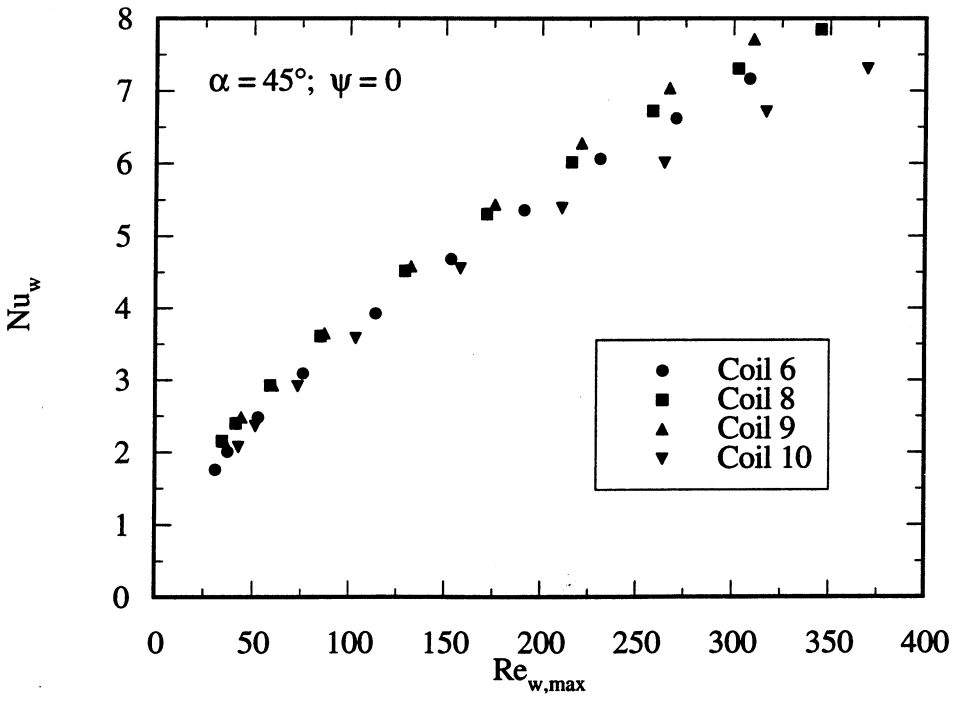

Figure G.23 Nu_w vs. $Re_{w,max}$ for condensers at $\alpha = 45°$ with air flow $\perp$ to the wires

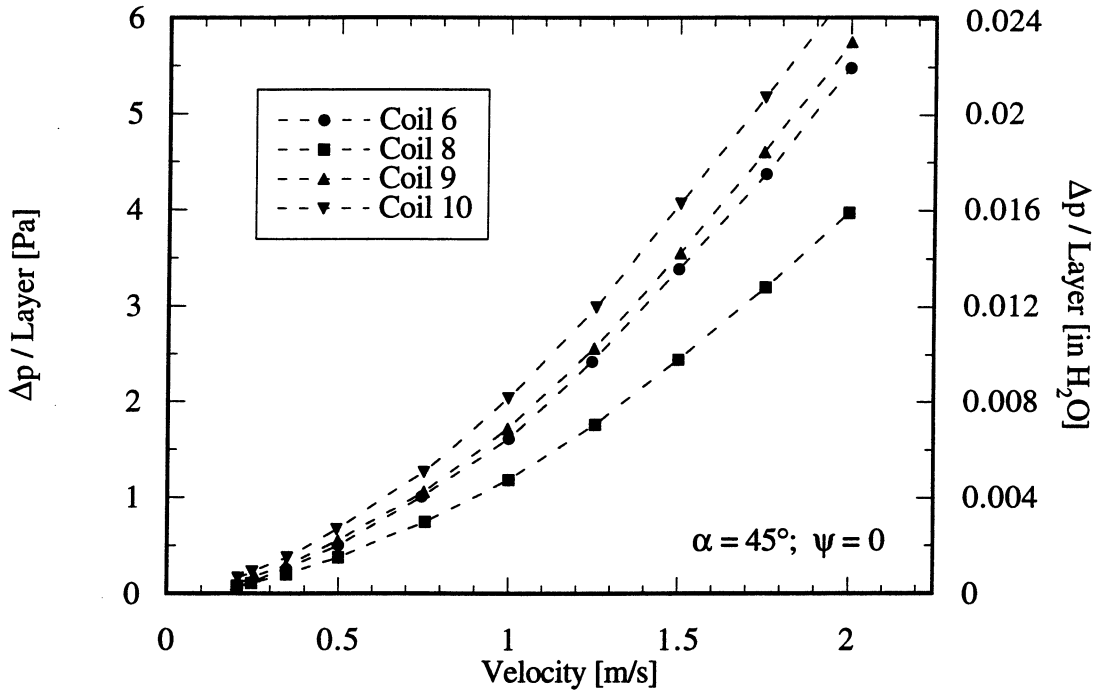

Figure G.24 Δp per layer vs. V for condensers at α = 45° with air flow ⊥ to the wires

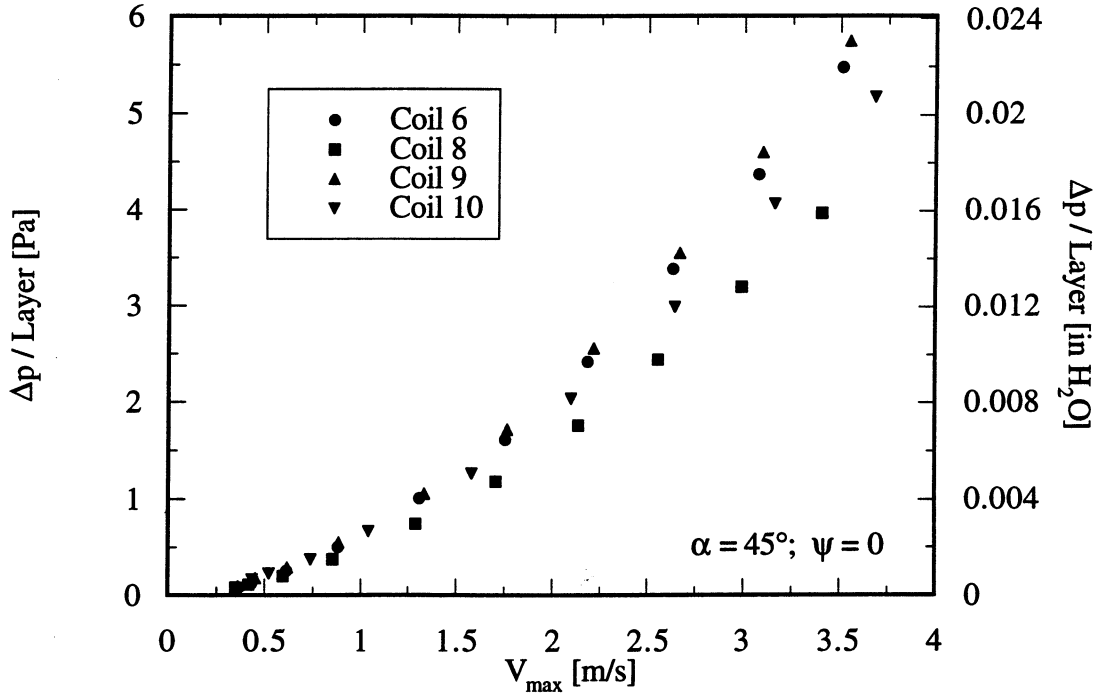

Figure G.25 Δp per layer vs. V_{max} for condensers at α = 45° with air flow ⊥ to the wires

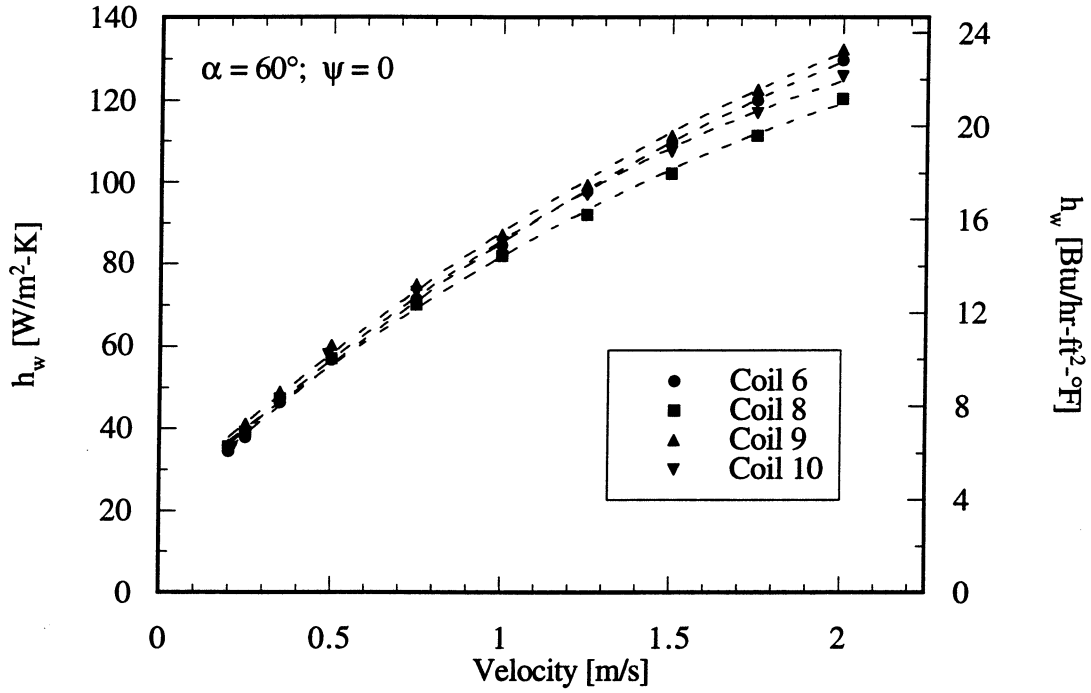

Figure G.26 h_w vs. V for condensers at $\alpha = 60°$ with air flow $\perp$ to the wires

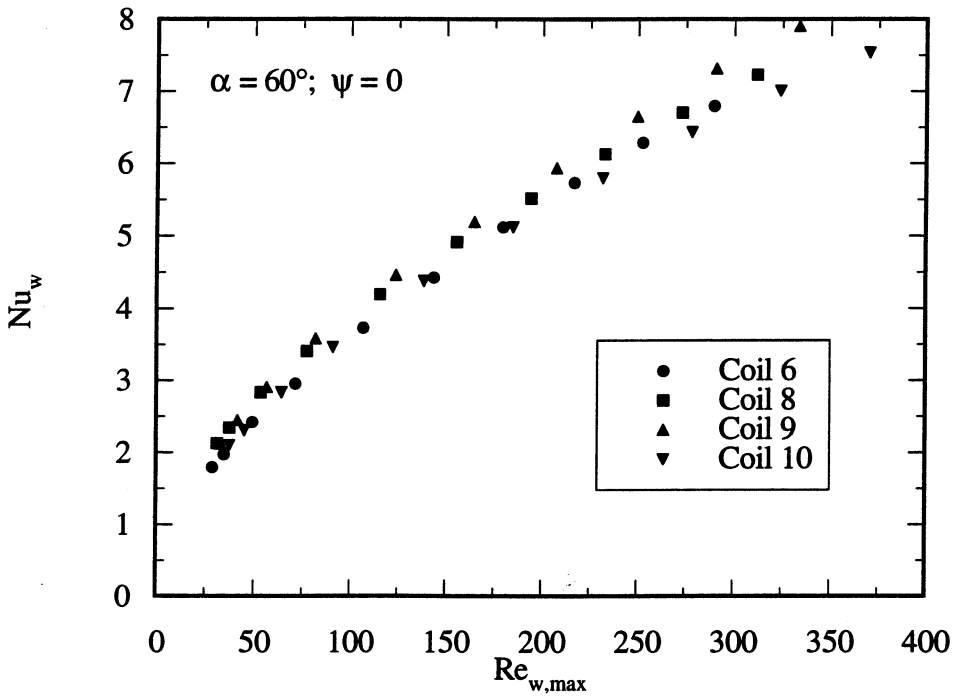

Figure G.27 Nu_w vs. $Re_{w,max}$ for condensers at $\alpha = 60°$ with air flow $\perp$ to the wires

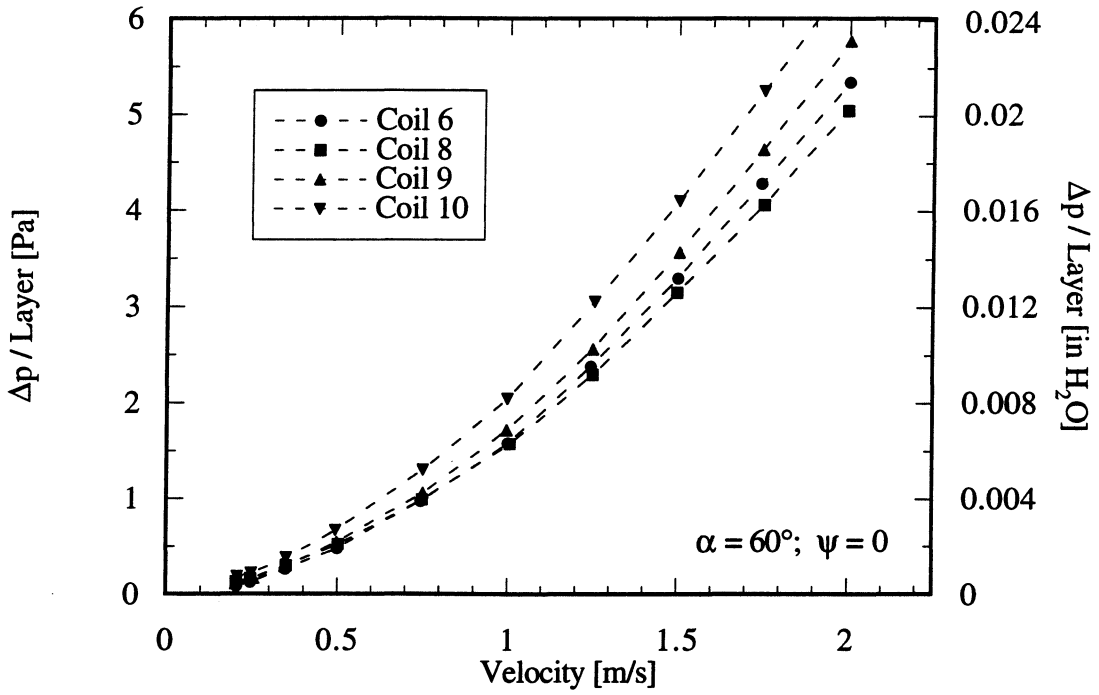

Figure G28 Δp per layer vs. V for condensers at α = 60° with air flow ⊥ to the wires

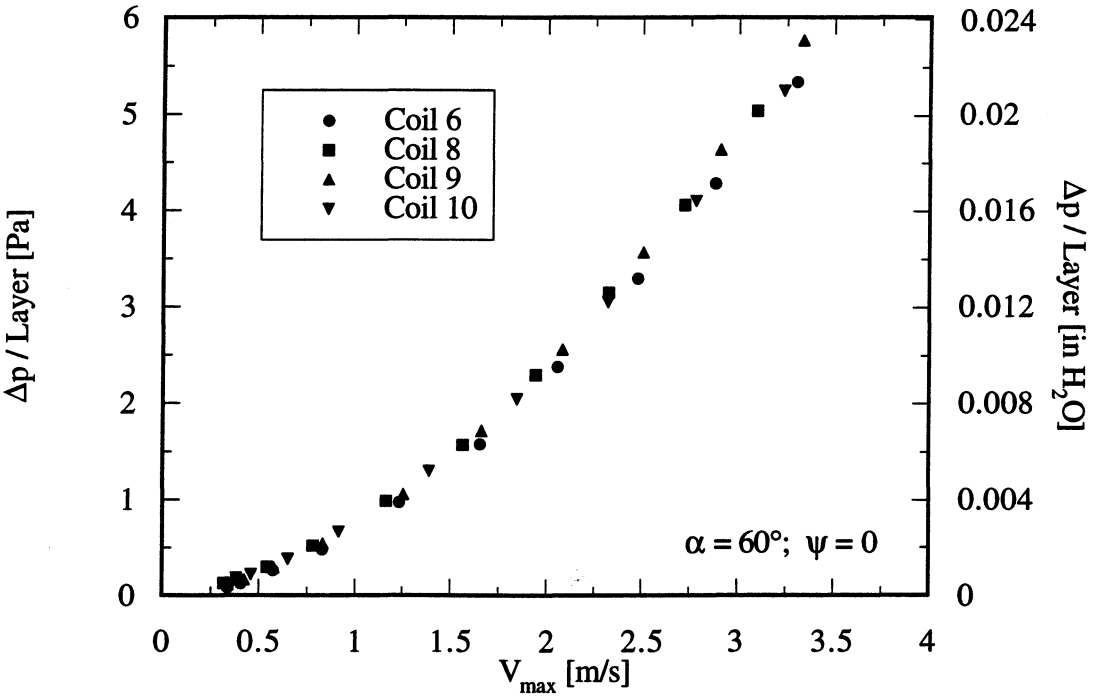

Figure G.29 Δp per layer vs. V_{max} for condensers at α = 60° with air flow ⊥ to the wires

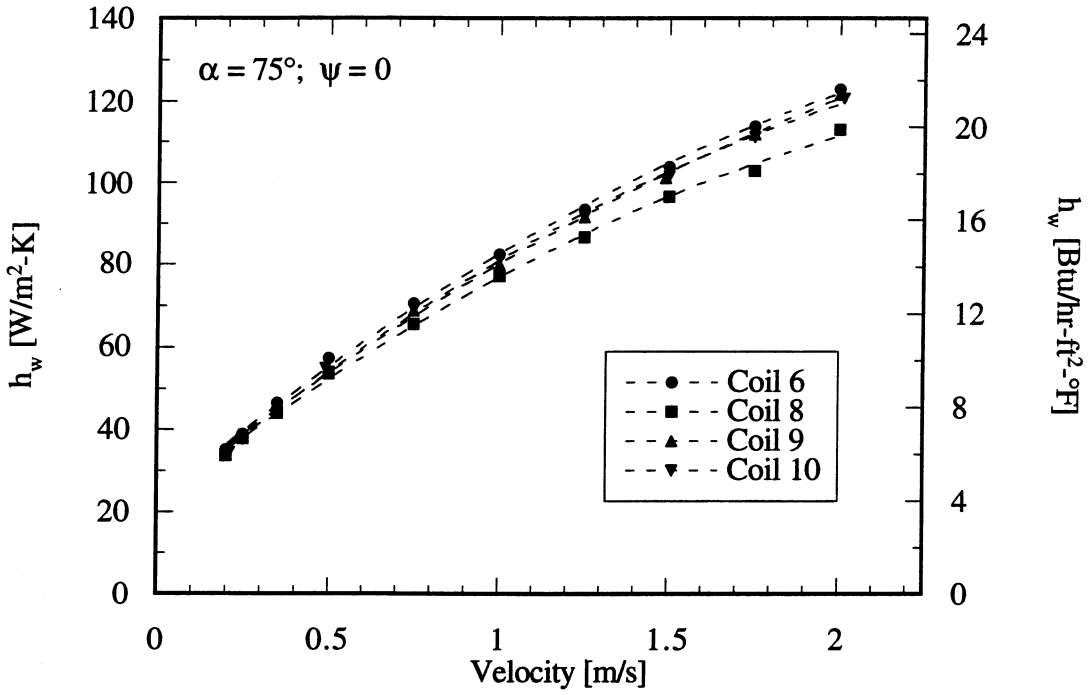

Figure G.30 h_w vs. V for condensers at $\alpha = 75°$ with air flow $\perp$ to the wires

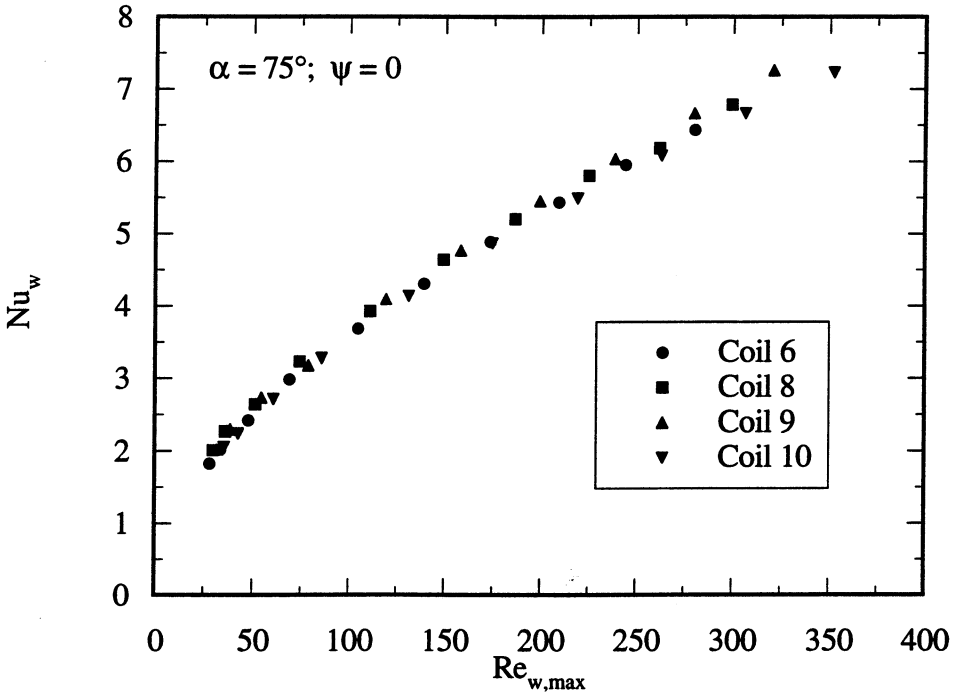

Figure G.31 Nu_w vs. $Re_{w,max}$ for condensers at $\alpha = 75°$ with air flow $\perp$ to the wires

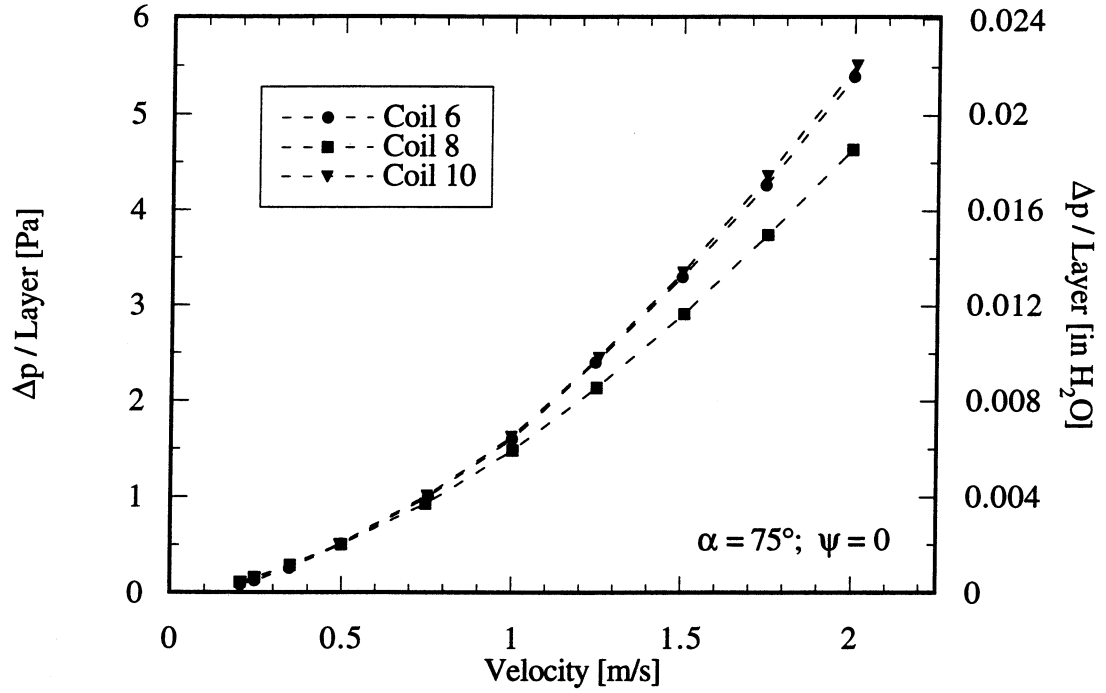

Figure G.32 Δp per layer vs. V for condensers at α = 75° with air flow ⊥ to the wires

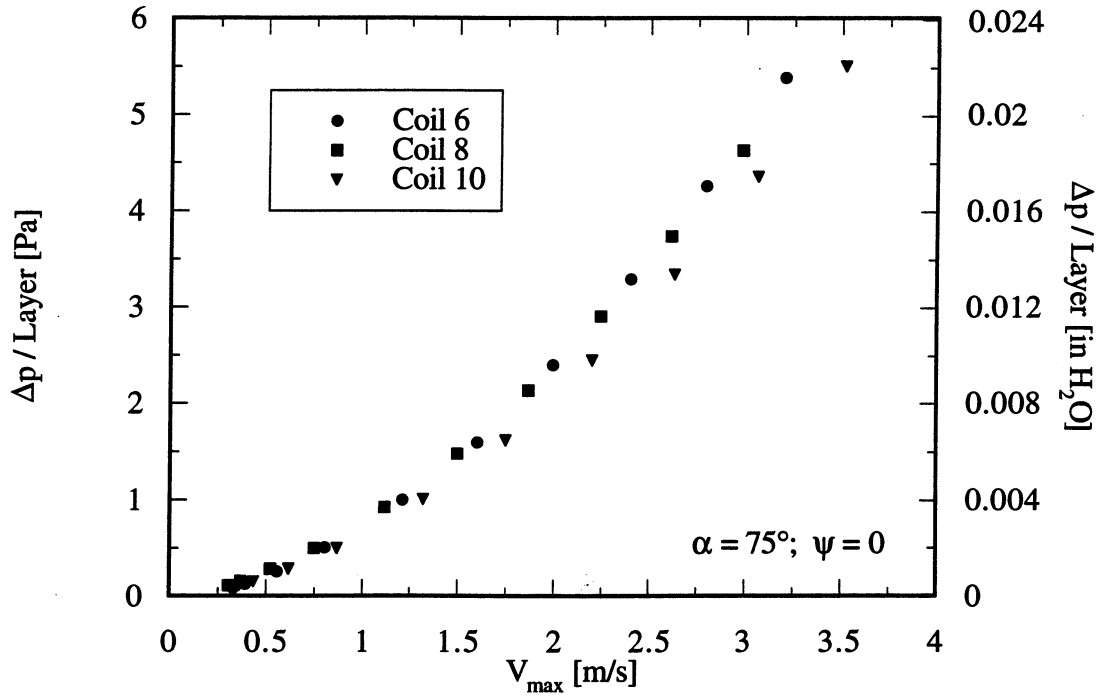

Figure G.33 Δp per layer vs. V_{max} for condensers at α = 75° with air flow ⊥ to the wires

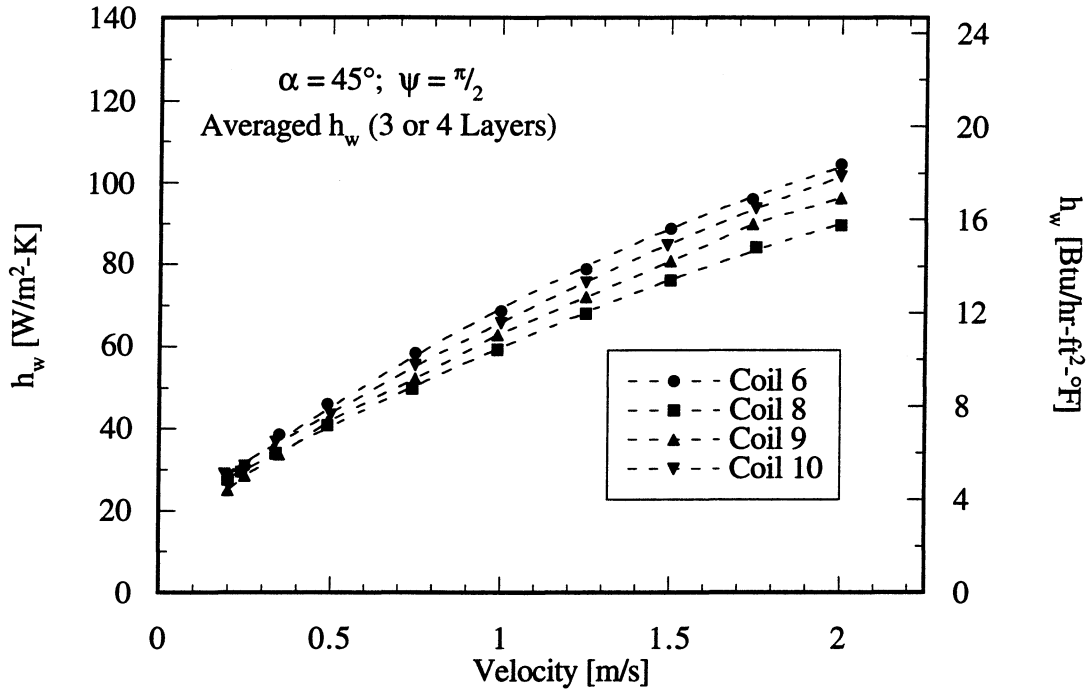

Figure G.34 h_w vs. V for condensers at $\alpha = 45°$ with air flow $\perp$ to the tube passes

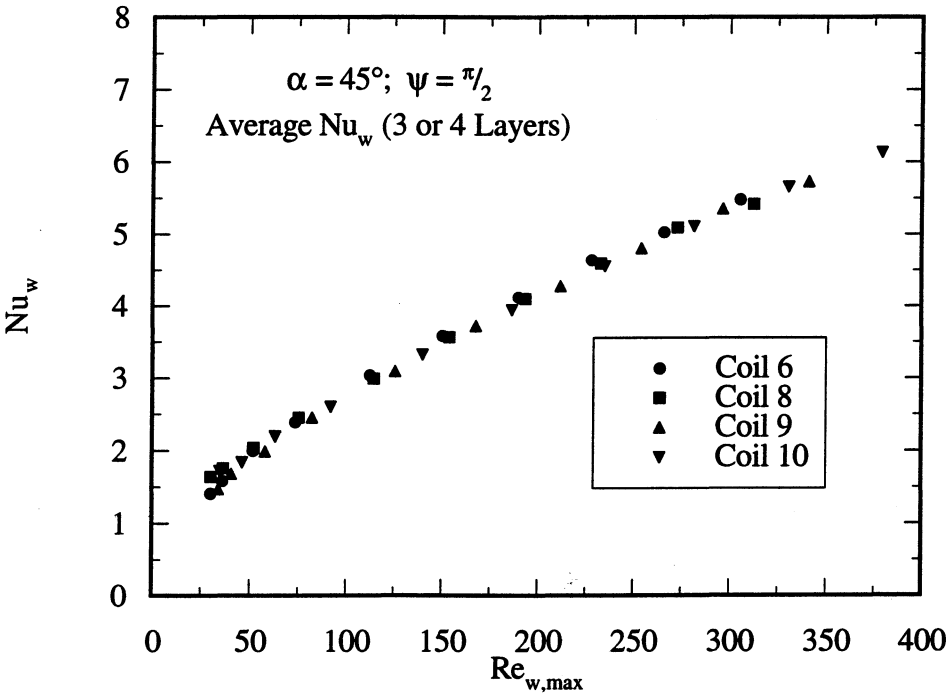

Figure G.35 Nu_w vs. $Re_{w,max}$ for condensers at $\alpha = 45°$ with air flow $\perp$ to the tube passes

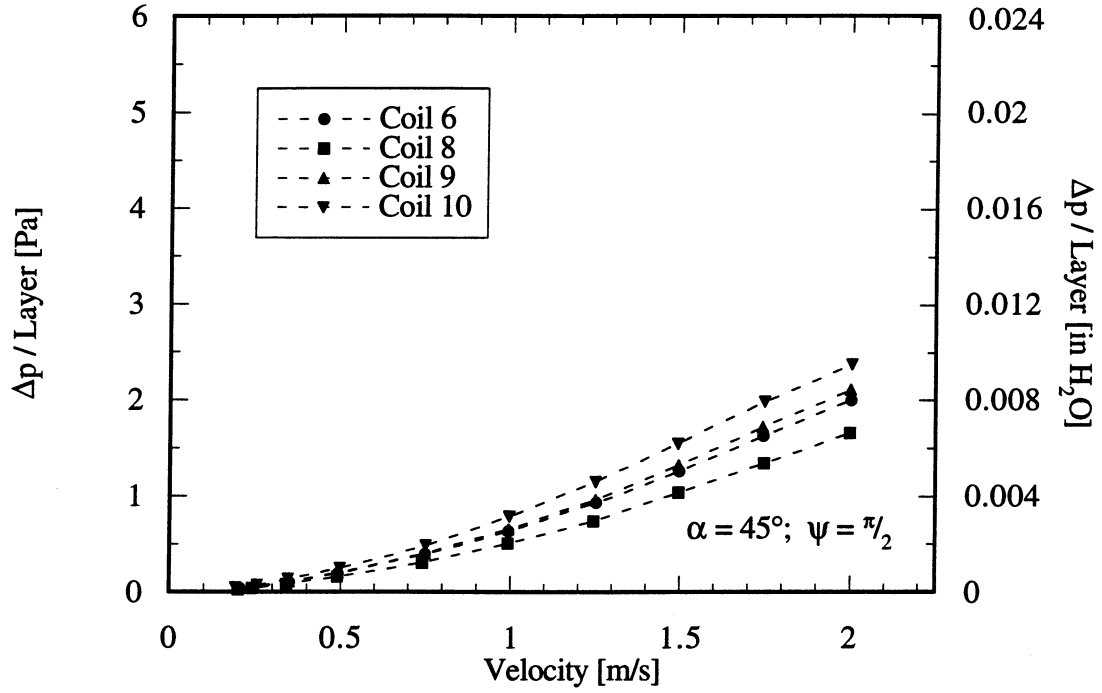

Figure G.36 Δp per layer vs. V for condensers at α = 45° with air flow ⊥ to the tube passes

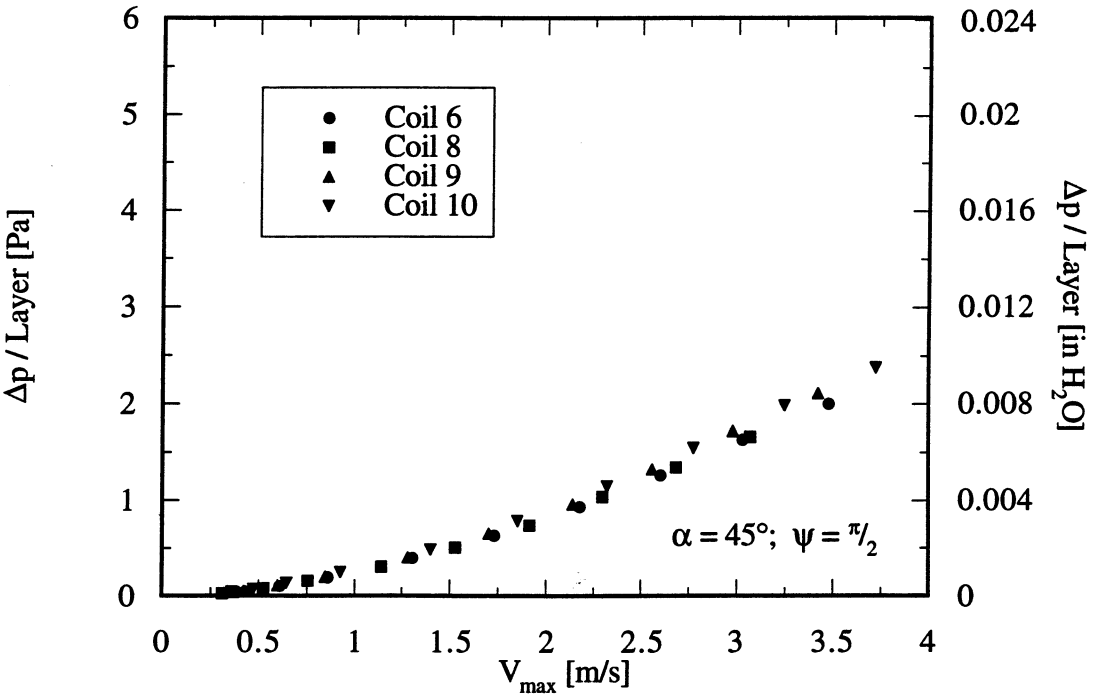

Figure G.37 Δp per layer vs. V_{max} for condensers at α = 45° with air flow ⊥ to the tube passes

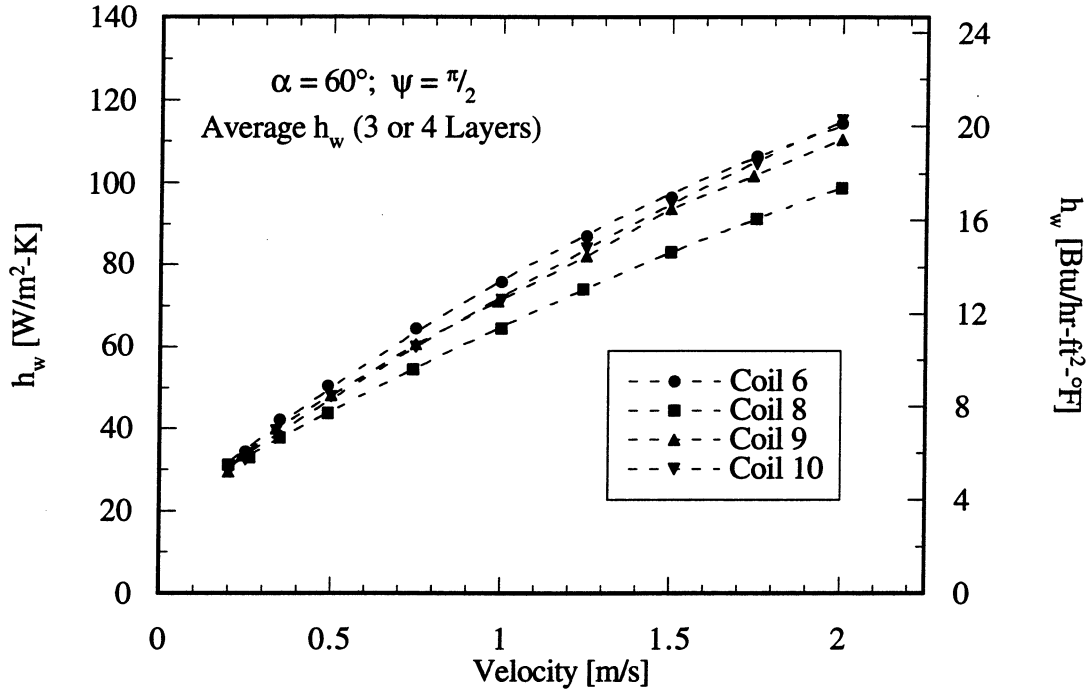

Figure G.38 h_w vs. V for condensers at $\alpha = 60°$ with air flow $\perp$ to the tube passes

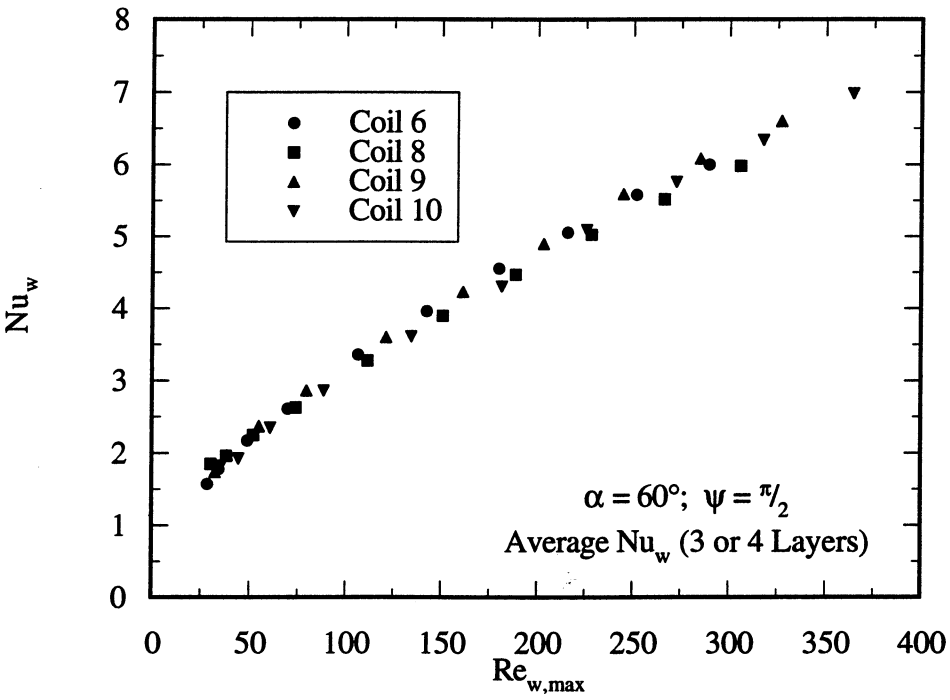

Figure G.39 Nu_w vs. $Re_{w,max}$ for condensers at $\alpha = 60°$ with air flow $\perp$ to the tube passes

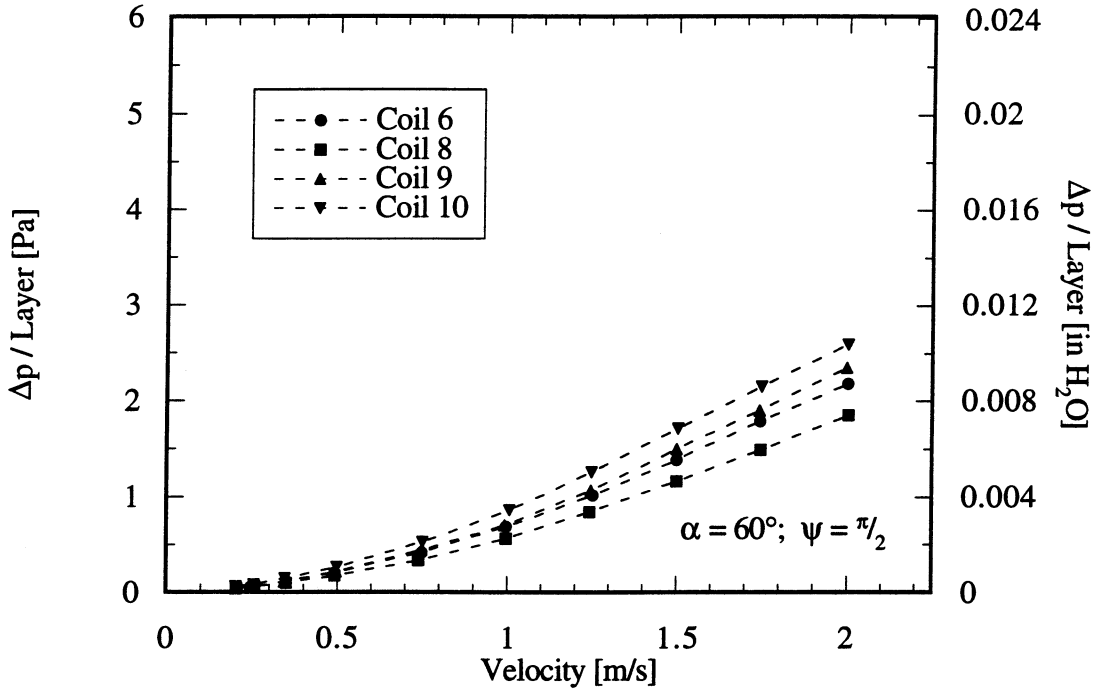

Figure G.40 Δp per layer vs. V for condensers at α = 60° with air flow ⊥ to the tube passes

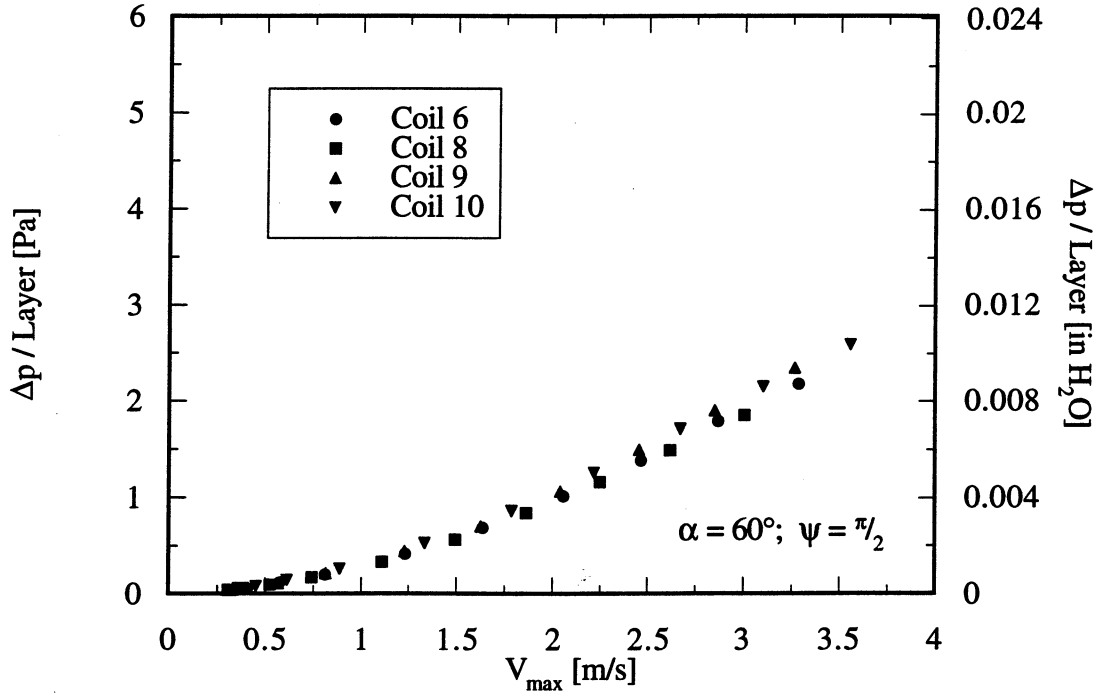

Figure G.41 Δp per layer vs. V_{max} for condensers at α = 60° with air flow ⊥ to the tube passes

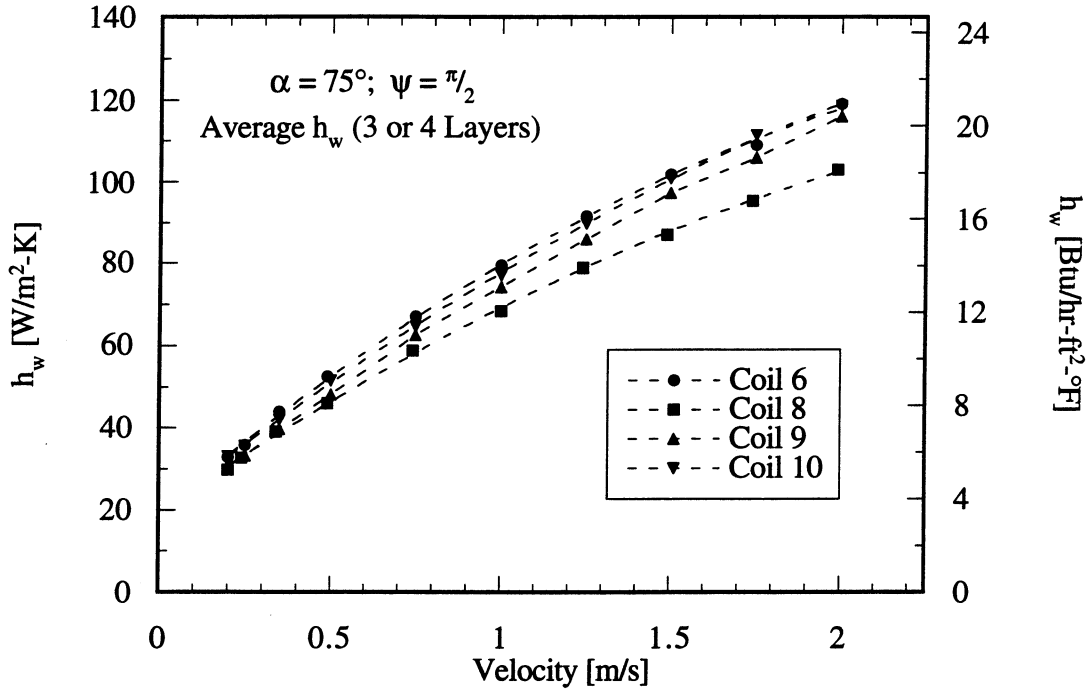

Figure G.42 h_w vs. V for condensers at $\alpha = 75°$ with air flow $\perp$ to the tube passes

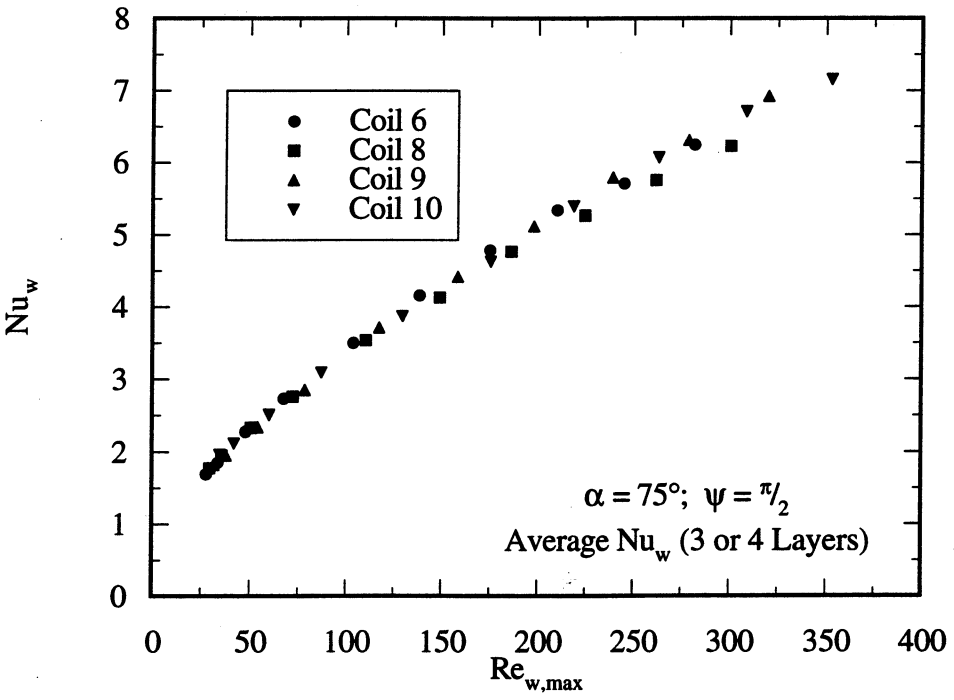

Figure G.43 Nu_w vs. $Re_{w,max}$ for condensers at $\alpha = 75°$ with air flow $\perp$ to the tube passes

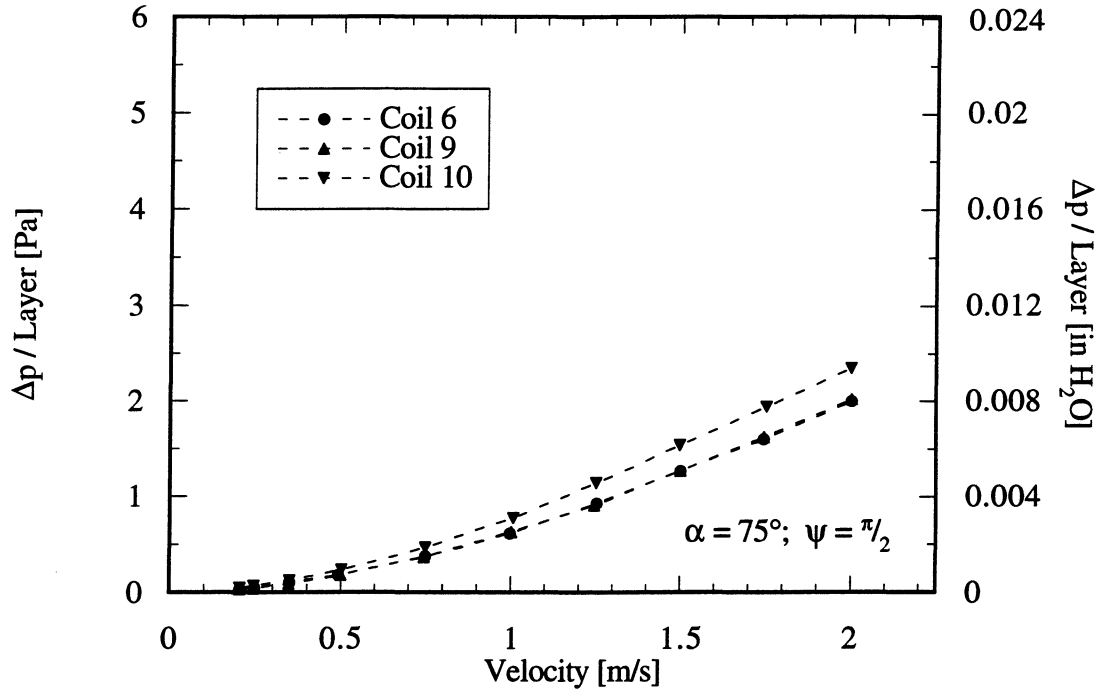

Figure G.44 Δp per layer vs. V for condensers at α = 75° with air flow ⊥ to the tube passes

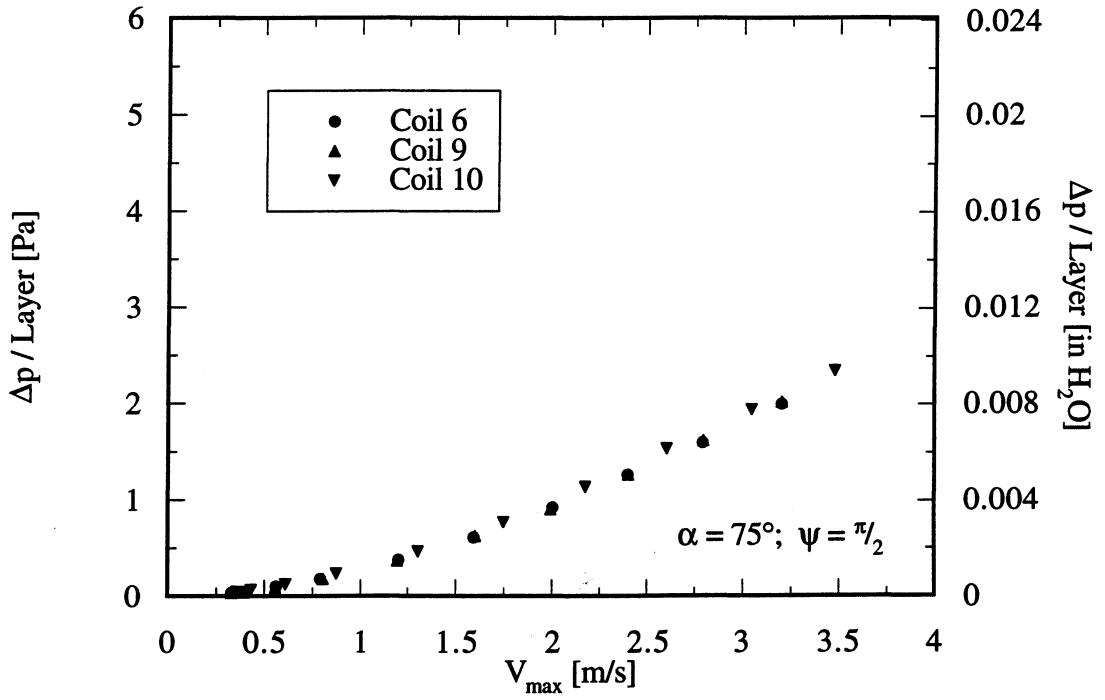

Figure G.45 Δp per layer vs. V_{max} for condensers at α = 75° with air flow ⊥ to the tube passes